Study of methylglyoxal induced proteome in muscle cells

by

Shakuntala Bai
10BB13A26037

A thesis submitted to the
Academy of Scientific & Innovative Research
for the award of the degree of
DOCTOR OF PHILOSOPHY
in
SCIENCE

Under the supervision of
Dr. Mahesh J. Kulkarni

CSIR-National Chemical Laboratory, Pune

Academy of Scientific and Innovative Research
AcSIR Headquarters, CSIR-HRDC campus
Sector 19, Kamla Nehru Nagar,
Ghaziabad, U.P. – 201 002, India

February 2021

Certificate

This is to certify that the work incorporated in this Ph.D. thesis entitled "*Study of methylglyoxal induced proteome in muscle cells*" submitted by *Ms. Shakuntala Bai* to Academy of Scientific and Innovative Research (AcSIR) in fulfilment of the requirements for the award of the degree of *Doctor of Philosophy in Sciences*, embodies original research work carried-out by the student. We further certify that this work has not been submitted to any other University or Institution in part or full for the award of any degree or diploma. Research materials obtained from other sources and used in this research work have been duly acknowledged in the thesis. Images, illustrations, figures, tables, etc., used in the thesis from other sources have also been duly cited and acknowledged.

Shakuntala Bai
(Student)
Date: 12-02-2021

Dr. Mahesh J. Kulkarni
(Research supervisor)
Date: 12-02-2021

Statements of academic integrity

I, Shakuntala Bai, a Ph.D. student of the Academy of Scientific and Innovative Research (AcSIR) with Registration No. 10BB13A26037 hereby undertake that, the thesis entitled "Study of methylglyoxal induced proteome in muscle cells" has been prepared by me and that the document reports original work carried out by me and is free of any plagiarism in compliance with the UGC Regulations on "*Promotion of Academic Integrity and Prevention of Plagiarism in Higher Educational Institutions (2018)*" and the CSIR Guidelines for "*Ethics in Research and in Governance (2020)*".

Signature of the Student
(Shakuntala Bai)
Date: 12-02-2021
Place: CSIR-NCL, Pune.

It is hereby certified that the work done by the student, under my supervision, is plagiarism-free in accordance with the UGC Regulations on "*Promotion of Academic Integrity and Prevention of Plagiarism in Higher Educational Institutions (2018)*" and the CSIR Guidelines for "*Ethics in Research and in Governance (2020)*".

Signature of the Supervisor
(Dr. Mahesh J. Kulkarni)
Date: 12-02-2021
Place: CSIR-NCL, Pune.

Laughter is the best medicine- unless you're diabetic, then insulin comes pretty high on the list.

-Jasper Carrott

Table of Contents

Acknowledgements

During my journey as a Ph.D. student, I have come across a world of excitement, joy, surprises, and difficulties. It was not easy to grow alone and make a place for oneself in this expedition. This was made possible with the continuous support of several people. First and foremost, I would like to express my sincerest gratitude to my research guide ***Dr. Mahesh Kulkarni****, for his valuable guidance, tremendous support, and scientific inputs. I consider myself fortunate to be able to work in his group and learn from his experiences.*

I am very thankful to all my DAC members, ***Dr. Anu Raghunathan****,* ***Dr. Kiran A. Kulkarni,*** *and* ***Dr. H.V. Thulasiram****, for their encouragement, insightful comments, valuable suggestions, and precious time they spared for me during the DAC meetings.*

I acknowledge the ***University Grants Commission*** *(UGC) for Research Fellowship, which enabled me to accomplish my research. I thank the past and the present Director, CSIR-NCL and HOD, Biochemical Sciences Division, for providing infrastructure and lab facilities to carry out my work. I am grateful to the Students Academic office and AcSIR staff for their sustained support. Also, I am thankful to the library staff and administrative staff of CSIR-NCL for their co-operation.*

I want to thank ***Dr. B. Santhakumari*** *for her guidance and support for the mass spectrometry facility. A special mention to* ***Dr. Faraz Rashid****, Sciex Ltd, India, who taught and helped me run mass spectrometry experiments in their facility. I would also like to thank Deo Sir and Shashikala mam. I also thank* ***Dr. A.G Unnikrishnan*** *for supporting us with clinical plasma samples. I also would like to express my warm gratitude to the volunteer diabetic and non-diabetic individuals for donating blood samples for the study.*

I would like to thank ***Dr. Sachin Agawane*** *for his immense support during Animal experiments. I also thank Dr. Santosh Koratkar for providing us the experimental animal facility at Symbiosis School of Biological Sciences. I also extend my thanks to Dr. Chandrashekhar Mote for*

supporting in histopathology studies of diabetic tissue samples. I also thank ***Gouri*** *and* ***Arvindkumar*** *for their help during animal experiments.*

I would take this opportunity to sincerely thank Dr. H.V. Thulasiram, Dr. Mughda Gadgil, Dr. Dhanasekaran Shanmugam, Dr. Kiran A. Kulkarni, Dr. Subashchandrabose Chinnathambi, Dr. Narendra Kadoo, and Dr. Ashok Giri for allowing me to use the equipment available in their group.

I would like to extend my gratitude for the extended support I have received from members of many research groups; specifically, Dr. Vishwanath, Dr. Rupa, Dr. Avinash, Dr. Tejas, Dr. Anurag, Dr. Rahul, Dr. Parag, Dr. Anand, Tanaya, Tejal, Jyoti, Anuja, Nimisha, Fayaz, Zenia, Sneha, Sindoori, Nalini, Shweta, Abhishek, Tushar, Gauri and many more for your scientific input in my initial learning phase of various techniques, providing the reagents in urgency and your moral support in troubleshooting of technical problem I have faced during my Ph.D.

I extend my deepest appreciation to all the past and present labmates, Dr. Arvind Korwar, Dr. Sandeep, Dr. Suresh, Dr. Yogesh, Dr. Sneha Bansode, Dr. Shweta, Dr. Arati, Dr. Reema, Dr. Rubina, Dr. Kedar, Dr. Jagadeesh, Vinashya, Swamy, Rashmi, Sharda, Amrita, Akshay, Piyush, Bhusan, Arvindkumar, Yugendra, Prachi, Rajeshwari, Gouri, Shabda, Babasaheb, Shiva, Dr. Vaibhav, Dr. Gauri, Dr. Aditi, Meera, Preeti, Nikita, Sneha, Hemlatha, Amreen, Swaraj as well as all trainees and visiting researchers whose presence made the lab a pleasant and joyous place of work. You all have made my journey at NCL more meaningful, beautiful, and filled with memorable moments. Memories of lunch and evening tea time in old canteen will be cherished forever.

It's my pleasure to acknowledge the constant support throughout my research work at NCL I received from ***Reema, Yugendra,*** *and* ***Arati****, who played the role of both labmates and friends, whom I could approach for any help or advice whenever needed. I am grateful to* ***Arvindkumar*** *for his dedicated involvement and association in my work. I am lucky for the beautiful friendship, and good times we have had together in NCL.*

*I would like to mention my special thanks to **Reema** and **Arvindkumar** for taking the time to proofread my thesis and valuable inputs in making it better.*

*I extend my thanks to **Dr. Jyoti Das** from **ICMR-NIMR**, New Delhi, for allowing me to work on my MSc Dissertation under her guidance. I also thank Dr. Rewa, Dr. Praveen, Dr. Vikky for their help during the training period in NIMR. I am incredibly grateful to my teachers and professors for always being inspirational, believing in my potential, and encouraging me to pursue a research career during my bachelors and masters.*

*I am thankful to my childhood friends **Priti** and **Jyoti,** who were always there in all my good and bad times. You both are the source of my happiness and motivation.*

*I owe a lot to my family, who encouraged and helped me at every stage of my personal and academic life, the immense support, motivation, and judicious guidance from my father **Shri SiyaRam Kolewar,** immensurate love from my mother **Smt. Shanti Devi** has brought me to this stage. I thank my parents for giving me the freedom and courage to pursue my dreams. They are and will always be the pillars of my strength and my motivation to succeed.*

*I am blessed to have brothers **Shailendra, Arun**, **Makhan**, who stood by me at every stage. I thank my sweet niece **Aanya**, sister-in-laws **Mamta** and **Jyoti,** for bestowing their affection for me and being my strength.*

*I feel fortunate to have **Manish** in my life, who is the best ever thing that happened to me and turned out to be a Bestfriend for a lifetime. His broad interests, may it be gardening, traveling, movies, or cooking, and his wit and wisdom have fascinated me. I am thankful to him for being there for me always. I owe my deepest gratitude to my father-in-law **Shri Bhikam Singh**, mother-in-law **Smt. Lalita Singh,** sister-in-law **Dr. Manisha** and brother-in-law **Mayank** for having faith in me and being understanding and supportive towards me. I love you all dearly!*

There are several people who have supported me in many ways during my Ph.D. work; I am greatly indebted to everyone who helped me unconditionally to achieve this important milestone. Above all, I owe it all to God for granting me the wisdom, health, and strength to undertake this research task and enabling me to its completion.

List of Figures

List of Tables

List of Appendix

Abbreviations

ACN	Acetonitrile
ADA	American Diabetes Association
AGEs	Advanced glycation end products
ANOVA	Analysis of Variance
BSA	Bovine Serum Albumin
CDI	Chellaram Diabetes Institute
CEL	Carboxyethyllysine
CML	Carboxymethyllysine
DCFH-DA	2',7'- dichlorodihydrofluorescein diacetate
DCCT	Diabetes Control and Complications Trial
DHAP	Dihydroxy-Acetone phosphate
DMEM	Dulbecco's Modified Eagle's medium
ELISA	Enzyme-linked immunosorbent assay
ERK	Extracellular signal-regulated kinase
FBS	Fetal bovine serum
FDR	False Determination Rate
FITC	Fluorescein Isothiocyanate

FPG	Fasting plasma glucose
G3P	Glyceraldehyde-3-Phosphate
GDM	Gestational Diabetes Mellitus
GLO1	Glyoxalase 1
GLO2	Glyoxalase 2
GLUT1	Glucose Transporter 1
GLUT4	Glucose Transporter 4
GSH	Glutathione
GSVs	GLUT4 storage vesicles
HSA	Human serum albumin
IDA	Information dependent acquisition
IDDM	Insulin-dependent diabetes mellitus
IDF	International Diabetes Federation
IGT	Impaired glucose tolerance
IR	Insulin Receptor
IRS	Insulin Receptor Substrate
JAK	Janus activated kinase
JNK	c-Jun N-terminal Kinase
LC	Liquid chromatography

LADA	Latent autoimmune diabetes in adults
MAPK	Mitogen-activated protein kinase
MG	Methylglyoxal
MODY	Maturity-onset diabetes of the young
MS	Mass spectrometry
MS/MS	Tandem mass spectrometry
mTOR	Mammalian target of rapamycin
2-NBDG	2-(N-(7-Nitrobenz-2-oxa-1,3-diazol-4-yl)Amino)-2-Deoxyglucose
NF-κB	Nuclear factor-kappa B
NCD	Non-communicable diseases
NIDDM	Non-insulin-dependent diabetes mellitus
NRF1	Nuclear Respiratory Factor 1
OGTT	Oral glucose tolerance test
PBS	Phosphate Buffered Saline
PCA	Principal Component Analysis
PI3K	Phosphoinositide 3-kinase
PPG	Postprandial plasma glucose
RAGE	Receptor for advanced glycation end products
STAT	Signal transducers and activators of transcription

STZ	Streptozotocin
SWATH	Sequential Window Acquisition of all Theoretical mass spectra
T1D	Type 2 Diabetes
T2D	Type 2 Diabetes
TNFα	Tumor necrosis factor-alpha
WHO	World Health Organization

Dedicated To My Parents
& to everyone who
motivated me

Chapter 1

Introduction

Chapter 1 Introduction

1.1 Diabetes

Diabetes mellitus, also called diabetes, is a chronic condition that occurs when there are high glucose levels in the blood as the body cannot produce any or enough of the hormone insulin or use insulin effectively. Both the conditions eventually lead to persistent hyperglycemia that elevated blood sugar levels[1]. Typical symptoms of diabetes are polyphagia (increased hunger), polyuria (frequent urination), and polydipsia (increased thirst) [2]. Unexplained weight loss, frequent infections, weakness, or tiredness are also associated with a diabetic condition. Apart from these, blurred vision, numbness or tingling in hands or feet, slow healing of sores or cuts are signs of chronic disease condition [3][4]. Chronic hyperglycemia may lead to several diabetic complications. Two major subdivisions of diabetic complications are microvascular and macrovascular. Microvascular complications are specific to diabetes and can damage the eye, kidney, and nervous system by causing retinopathy, nephropathy, and neuropathy, respectively. Macrovascular complications are not unique to diabetes but occur commonly in diabetic conditions. The main large vessels involved are those supplying the heart, the brain, and the legs. Thus, macrovascular disease gives rise to heart attack, stroke, and gangrene[3].

1.1.1 History of diabetes

The history of diabetes dates back to ancient times. In the first documented reference, an Egyptian Papyrus, in 1500 BC describes diabetes as a rare disease that causes the patients to suffer from excessive thirst, plenteous urination, and treated by 'plant's extracts[5]. In 500 century BC, Indian surgeon Sushruta, in his work, also developed a clinical test for diabetes by observing the urine from diabetic people that attracted ants and flies and named it "madhumeha" or "honey urine" [6]. Additionally, he had mentioned that primarily rich people were affected by the illness and were related to excessive food consumption like sweets, rice, and cereals. The Chinese Hippocrates, in ancient China, described symptoms of a specific disease as polyuria, polydipsia, and loss of weight. At the same time, in the 7th century AD, Chen Chuan recorded the

sweet urine in diabetes mellitus and mentioned its characteristic symptoms, excessive thirst, plenteous urine, which tasted sweet. In an attempt to treat that disease, his colleague Li Hsuan proposed abstinence from wine, salt, and sex[7].

In 200 AD, Aretaeus of Cappadocia coined the term "'diabetes' originated from the Greek word 'diabaino', meaning that the fluid runs through. Later in 1675, Thomas Willis added the Latin term 'Mellitus' (meaning honey-sweet) as a suffix to the word 'diabetes' to describe the extremely sweet taste of the urine [8]. Four years later, Frank classified the diabetes types based on sugar-like substance into diabetes *insipidus*(tasteless urine) and diabetes *vera* (sweet urine). In 1869, Paul Langerhans discovered that the human pancreas contained two kinds of cells, although he was unaware of their function. In 1889, Mering and Minkowski performed a pancreatectomy and found the pancreas' role in the pathogenesis of diabetes, suggesting that this organ was somehow central to blood sugar regulation. The important milestone in the history of diabetes is insulin isolation and its clinical use by Banting and Best in 1921 [8]. In January 1922, insulin was first administered to a 14-year-old boy, and results were excellent, his blood glucose fell from 520 mg/dL to 120 mg/dL in 24 h, and urinary ketones disappeared. This anti-diabetic substance was named 'insulin,' for which Banting and Macleod were awarded a Nobel Prize for discovering insulin in 1923. Lilly Pharmaceutical Company collaborated with the two scientists and in 1923 introduced Iletin, the 'world's first commercially available insulin product[9].

1.1.2 **Classification of Diabetes**

A heterogeneous group of disorders represents diabetes mellitus. Some distinct diabetic phenotypes can be characterized in terms of specific etiology or pathogenesis, but in many cases, etiological and pathogenetic classification has become difficult due to overlapping phenotypes. Three significant categories of diabetes mellitus : (a) type 1 diabetes, which results from a failure in insulin secretion, (b) type 2 diabetes, which is a result of insulin resistance; and (c) gestational diabetes, which is observed among the women who are pregnant have a high glucose level but never had diabetes.

1.1.2.1 Type 1 diabetes

Earlier, Type 1 diabetes was known as insulin-dependent diabetes mellitus (IDDM). It is characterized by autoimmune destruction of the β-cells of the pancreas' islets, with consequent insulin deficiency. It is often associated with elevated blood glucose levels, including polyuria, polydipsia, and unexplained weight loss [10]. Type 1 diabetes can be further classified as idiopathic or immune-mediated. Idiopathic refers to rare forms of diabetes with an unknown cause. The majority of type 1 diabetes cases are of the immune-mediated nature, where β-cell loss is through T-cell mediated autoimmune attack destroying the cells in the pancreas that produce insulin [10]. The autoantibodies for glutamic acid carboxylase (anti-GAD) serve as an autoimmune marker in 85-90 % of type 1 diabetes [11]. Type 1 diabetes, key symptoms include high blood glucose levels, frequent urination, blurred vision, unusual thirst, and extreme hunger but a loss of weight, irritability, nausea, and fatigue. The causes of these destructive processes are not fully understood, but environmental triggers like dietary factors, viral infection or toxins, and genetic susceptibility combinedly have been involved.[12]

1.1.2.2 Type 2 diabetes

Type 2 diabetes (T2DM) or non-insulin-dependent diabetes mellitus (NIDDM) caused by insulin resistance is often connected to reduced insulin secretion. Patients with Type 2 diabetes develop significantly reduced responsiveness to secrete insulin, which leads to diminished glucose uptake in peripheral tissues and potentiates the metabolic effects of glucose resultant of hyperglycemia[13]. It is also characterized by the failure to inhibit hepatic glucose production by insulin and dysregulated insulin secretion[14]. T2DM accounts for about 90-95 % of the diagnosed cases of diabetes all over the world[15]. Some of the crucial variable risk factors include prediabetes or impaired glucose tolerance (IGT), lack of physical inactivity, obesity, smoking, history of gestational diabetes with subjection to high blood glucose to an unborn child during pregnancy, and less nutritious food. Studies have also shown a relation between high intake of sweetened beverages and increased risk of type 2 diabetes [16][17][18].

1.1.2.3 Gestational diabetes

Gestational diabetes occurs in approximately ~5% of women during pregnancy, but the condition may improve or disappear after delivery, 30-40% percent of women experiencing gestational diabetes develop type 2 diabetes within five to ten years. It is fully treatable only if critical medical supervision is achieved effectively throughout the pregnancy[19]. Weight gain and production of hormone resistine are the two main factors responsible for the onset of gestational diabetes[20][21].

Other types of diabetes are less common such as monogenic forms of diabetes, which include latent autoimmune diabetes in adults (LADA), and maturity-onset diabetes of the young (MODY).

1.1.3 Global Burden of Diabetes

People having diabetes are increasing due to urbanization, population growth, increasing prevalence of obesity and physical inactivity, and aging[22]. Globally, it has become a severe threat to human health as the incidences of diabetes, and the number of patients with diabetes is jumping up sharply, which has emerged as a worldwide public health problem. As stated by the International Diabetes Federation (IDF), there are nearly 500 million people with diabetes globally, and approximately 80% of people with diabetes live in low-income and middle-income countries. People with diabetes in the group of the ages of 20 and 79 years, in the world, were 425 million in 2017, and this number is expected to grow up to 629 million by 2045. In young people, the occurrence of type 2 diabetes is remarkably lesser than in elderly people. In 2017, there were less people within 20-79 years of age with diabetes in rural (145.7 million) versus urban (279.2 million) settings, and the incidence is lower in rural versus urban areas. In urban areas, the number of diabetic people is anticipated to increase to 472.6 million in 2045 because of development and expansion, which leads to a sedentary life style[23][24]. Diabetes ranks 5th among diseases based on burden in disability-adjusted life in developing countries [25] [26]. In 21st century one of the largest global health emergency is diabetes. The major non-communicable

diseases (NCDs) are respiratory disease, cardiovascular disease, and cancer, along with diabetes. Diabetes accounts for over 80% of deaths in the category of all premature NCD deaths and comes under the top 10 causes of mortality. In 2015, globally, 39.5 million of the 56.4 million deaths were due to NCDs[27]. Almost 30-80% of people with diabetes remain undiagnosed, which is a significant contributor to diabetes[28]. The top ten countries for people with diabetes (20-79 years) in 2017 and 2045 are shown in Table 1.1.

Table 1.1 Top ten countries/territories for the number of people with diabetes (20-79 years), 2017 and 2045 (adapted from IDF atlas, 2017)

2017			2045		
Rank	Country/territory	Number of people with diabetes	Rank	Country/ territory	Number of people with diabetes
1	China	114.4 million (104.1-146.3)	1	India	134.3 million (103.4-165.2)
2	India	72.9 million (55.5-90.2)	2	China	119.8 million (86.3-149.7)
3	United States	30.2 million (28.8-31.8)	3	United States	35.6million (33.9-37.9)
4	Brazil	12.5 million (11.4-13.5)	4	Mexico	21.8 million (11.0-26.2)
5	Mexico	12.0 million (6.0-14.3)	5	Brazil	20.3 million (18.6-22.1)
6	Indonesia	10.3 million (8.9-11.1)	6	Egypt	16.7million (9.0-19.1)
7	Russian Federation	8.5 million (6.7-11.0)	7	Indonesia	16.7million (14.6-18.2)
8	Egypt	8.2million (4.4-9.4)	8	Pakistan	16.1 million (11.5-23.2)
9	Germany	7.5 million (6.1-8.3)	9	Bangladesh	13.7 million (11.3-18.6)
10	Pakistan	7.5 million (5.3-10.9)	10	Turkey	11.2 million (10.1-13.3)

1.1.4 **Diagnosis of Diabetes**

Diabetes mellitus is a common and severe disease that has widely affected the global population. About 30% of the affected population is unaware of being affected[29]. According to the

American Diabetes Association (ADA) standard guidelines, early diagnosis and monitoring of diabetes after treatment are crucial for preventing or delaying the onset of long-term diabetes-associated complications[30]. The Diabetes diagnostic and prognostic strategies of diabetes are mainly based on HbA_{1c} measurement or plasma glucose measurement, including either the fasting plasma glucose (FPG) and postprandial plasma glucose (PPG) or oral glucose tolerance test (OGTT). These tests are recommended by Diabetes Control and Complications Trial (DCCT), World Health Organisation (WHO), International Diabetes Federation (IDF), and American Diabetes Association (ADA)[31][32]. For oral glucose tolerance test (OGTT), the person fasts overnight (at least 8 hours, but not more than 16 hours), and the fasting plasma glucose is measured. Post fasting, the person receives 75 g of glucose orally; after 2 hours of the glucose intake, a glucose tolerance test is measured[30]. Glucose reacts non-enzymatically with NH_2-terminal Valine of the β-chain hemoglobin to initiate a glycation process and forms Glycated hemoglobin (HbA1c)[33][34]. Thus, the assumption that the rate of HbA1c is directly proportional to the glycemic status drifting the bloodstream in the past 120 days. Hemoglobin A1c is a measure of the degree to which hemoglobin is glycated in erythrocytes and is expressed as a percentage of total hemoglobin concentration. It reflects erythrocyte exposure to glucose in an irreversible time and concentration-dependent manner[34].

Revised criteria for diagnosing diabetes Mellitus recommended by The World Health Organization (WHO) is as follows:

1. Fasting plasma glucose (FPG) concentration is greater than or equal to 7 mmol/L (140mg/dL), wherein fasting is defined as no caloric intake for at least 8 h.
2. Postprandial 2 h plasma glucose concentration is greater than or equal to 11.1 mmol/L (200mg/dL) during an oral glucose tolerance test (OGTT) (Alberti et al., 1998) wherein blood glucose level is measured after 2 hours of meal in the individuals fasting between 8-16 hours.
3. Diabetes symptoms and a casual (i.e., any time of day without regard to time since the previous meal) plasma glucose concentration greater than 11.1 mmol/L (200 mg/dL) [35].

4. HbA_{1c} equal to or greater than 6.5% (48 mmol/mol).

1.2 Insulin signaling

Insulin is a dipeptide containing A and B chains linked by a disulfide bond. The A and B chain comprises 21 and 30 amino acids, respectively. The molecular weight of insulin is 5808 Da[36][37]. When there is a rise in the extracellular glucose levels, the glucose enters β-cell via glucose transporter GLUT2, localized at the cell surface. To capitulate a net rise in the ATP: ADP ratio, intracellular glucose is swiftly metabolized to trigger the closure of ATP-sensitive K^+ channels (K_{ATP}) and cell depolarization.Membrane depolarization induces the opening of voltage-gated Ca^{2+} channels to increase the intracellular Ca^{2+} concentration leading to exocytosis of the insulin-containing granules and insulin secretion[38][39][40]. Insulin plays an important role in regulating glucose homeostasis by acting at multiple sites. In the liver, it reduces hepatic glucose output via decreased glycogenolysis and gluconeogenesis. In muscle cells and adipose tissue, it increases the glucose uptake rate by stimulating the process where glucose transporter GLUT4 translocation takes place from intracellular sites to the cell surface. In liver and fat cells by enhancing lipid synthesis and in muscle and fat cells by decreasing fatty acid delivery from triglycerides, insulin also has a great impact on lipid metabolismi[40][41][42]. Around 75% of insulin-dependent glucose disposal takes place in skeletal muscle, whereas adipose tissue is responsible for only a minimal part[43][44]. At the cellular level, the actions of insulin are initiated by insulin binding to its plasma membrane receptor. Insulin binds to the extracellular α subunits, transmitting a signal across the plasma membrane that activates the intracellular tyrosine kinase domain of the β subunit leading to autophosphorylation of insulin receptor (IR) and the tyrosine phosphorylation by the insulin receptor tyrosine kinase of insulin receptor substrates (IRS-1, IRS-2, and IRS-3). This grant the association of IRSs with the regulatory subunit (p85) of phosphoinositide 3-kinase (PI3K) through its SRC homology 2 (SH2) domains [45][46]. Once activated, the catalytic subunit of PI3K (p110) phosphorylates phosphoinositides at the '3'position of the inositol ring of proteins at serine residues. PI3K phosphorylatesPtdIns(3,4)P_2 to PtdIns(3,4,5)P_3. A key downstream effector of PIP_3 is AKT. Activation of AKT also requires 3-phosphoinositide-dependent kinase 1 (PDK1).

In turn, AKT deactivates glycogen synthase kinase 3 (GSK-3), leading to glycogen synthase activation and thus glycogen synthesis in muscle cells. Phosphorylation of AKT also results in the translocation of GLUT-4 vesicles from their intracellular site to the plasma membrane, where

they let uptake of glucose into the cell[45][47]. GLUT4 is a glucose transporter regulated by insulin and responsible for glucose uptake into muscle and fat cells. In insulin absence, GLUT4 is mainly found in intracellular vesicles known as GLUT4 storage vesicles (GSVs). Insulin-stimulated activation of AKT leads to inhibitory phosphorylation of AS160, which is Rab GTPase activating protein. Inhibition of AS160 favors the GTP-loaded state of Rab and relieves an inhibitory effect towards GLUT4 translocation from an intracellular pool to the plasma membrane[48]. Thus insulin via targeted exocytosis triggers the GLUT4 translocation to the plasma membrane. In GLUT4 trafficking, the actin cytoskeleton and microtubule network act as essential members. They initiate the process, either by connecting signaling components or by administering the movement of vesicles from the perinuclear region to the plasma membrane in response to insulin. Glucose uptake takes place when the GLUT4 vesicles dock and fuse at the plasma membrane and allows extracellular exposure of the transporter[49] [50].

A brief representation of the insulin signaling pathway is shown in Figure 1.1

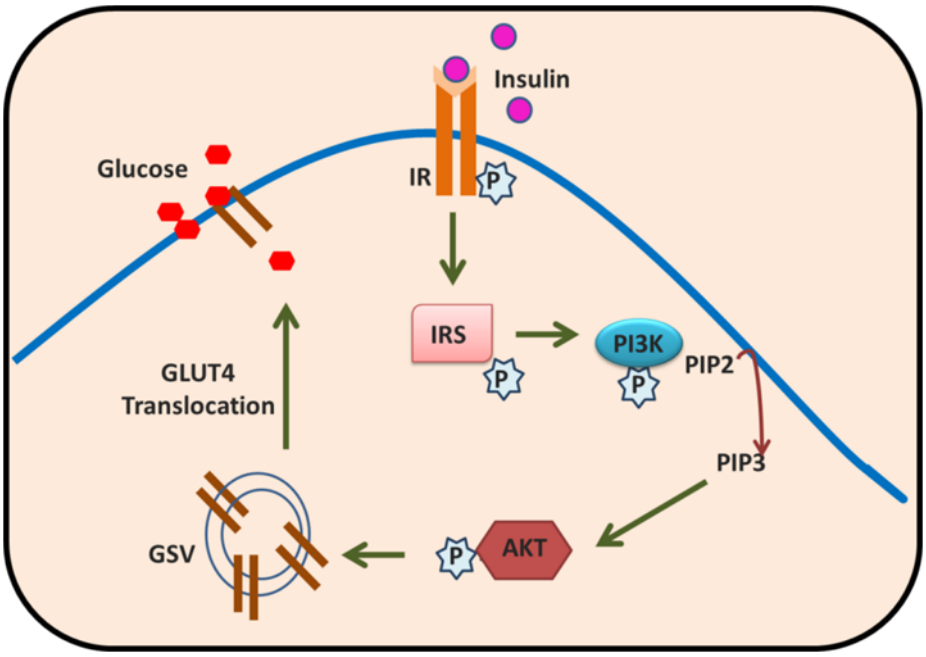

Figure 1.1 Insulin signaling cascade

1.2.1 **Insulin resistance**

Insulin resistance refers to the inadequate response of a cell, tissue, or organism to insulin. It's the condition when insulin is unable to increase the glucose uptake into muscle and adipose tissues and unable to decrease the glucose production in the liver. Insulin resistance is an essential hallmark of type 2 diabetes [51][52]. IRS proteins lose their affinity to PI 3-kinase after serine phosphorylation; as a result, PI 3-kinase activation is minimized, that further leads to expedite degradation of IRS-1 protein.

Hence, extravagant serine phosphorylation of IRS proteins, in contrast to a signal encouraging tyrosine phosphorylation, could be harmful for average communication of the metabolic downstream insulin signaling, causing insulin resistance[53]. Disturbance in the balance between the amounts of the PI 3-kinase subunits leads to insulin resistance. PI3-kinase exists as a heterodimer and is a part of the class 1a PI3-kinases, and has a regulatory subunit (p85), closely bound with a catalytic subunit, p110[53].

For PI 3-kinase activity, the p85-p110 heterodimer plays an important role. In general, as compared to the catalytic subunit, there is stoichiometric excess of the regulatory subunit, emanating in a large amount of free p85 monomers, which are not bound with the p110 catalytic subunit. Tyrosine-phosphorylated IRS proteins have binding sites for which both p85 and p85-110 heterodimer competes, so when the expression of p85 increases or decreases, that shifts the equilibrium in support of either free p85 or p85-p110 complexes. Disproportion in binding could alter PI 3-kinase activity [54]. Causes reported for this imbalance are steroids[55], excess growth hormones[56], human placental growth hormone[57], short-term overfeeding[58], and obesity.

Recent studies have shown that MG has a role in insulin resistance[59]. MG may modify the insulin molecule and can cause functional and structural changes, which contribute to the pathogenesis of insulin resistance[60]. Apart from that, MG impedes downstream insulin signaling in muscle cells[61], endothelial cells[62], and β-cells[63], and is straightly connected to insulin resistance. Therefore, MG not only contributes to hyperglycemia but it also initiates insulin resistance and β-cell dysfunction, and hence lead to T2D[64].

1.3 Diabetes and Glycation

In all types of diabetes, the primary hallmark of the disease is constant higher levels of glucose, which have an impact on various metabolic processes[65]. Prolonged plasma proteins exposure to high blood glucose has been observed in diabetic patients with poor glycemic control. Various plasma proteins, such as hemoglobin, serum albumin, and transferrin, have been found to be modified by glycation, a post-translational modification (PTM) caused by a non-enzymatic reaction between glucose and protein[66]. Glycation leads to the formation of heterogeneously modified proteins called advanced glycation end products (AGEs). Glycation was first reported by Louis Camille Maillard when he heated the mixture of amino acids and reducing sugars together and observed the characteristic brown color[67]. Hence, the reaction was also termed as 'Maillard's reaction or Browning. Glycation reaction starts with the condensation reaction among the carbonyl group of glucose and the free amino group of protein, leading to the formation of 'Schiff's base. This is the first step of glycation reaction and is reversible. This Schiff's base is thermodynamically unstable, forms a stable Amadori product. Several carbonyl compounds such as methylglyoxal, glyoxal, glucosones, and 3-deoxyglucosone (3-DG)forms are formed when Amadori product under autooxidation and glycoxidation goes through a series of fragmentation and dehydration reactions [68]. Autoxidation of the Amadori products results in the formation of AGEs, which is also termed as Hodge-pathway. Furthermore, the development of AGEs can result from degradation of lipids and amino acids, autoxidation of monosaccharides (Wolff pathway), and the cleavage of dicarbonyl compounds from aldimines (Namiki pathway)(Figure 1.2)[69][68][70]. Most predominant and well-characterized AGEs involved in the development of diabetic complications include mainly fructosyl-lysine (FL), N-ε-carboxymethyl lysine (CML), N-ε-carboxyethyl lysine (CEL), argpyrimidine, pyralline, methylglyoxal derived hydroimidazolone (MG-H1), and imidazolones, which are non-fluorescent, and pentosidine, crossline, vesperlysine, alkyl formyl glucosyl pyrrole (AFGP), methylglyoxal lysine dimer(MOLD), glyoxal lysine dimer (GOLD) and so on, which are fluorescent[68][71][72]. In addition to the accelerated formation of AGEs *in vivo* due to longstanding hyperglycemia of diabetes, AGEs can also get elevated in the body by consuming dietary AGEs and aggravating

the situation. AGEs are reported to be present naturally in uncooked foods of animal origin. Besides, thermal processing associated with different cooking methods of modern diet such as roasting, grilling, broiling, searing, and frying induces and also accelerates the formation of newer AGEs[73][74] [75]. Oral AGEs have been implicated in mounting chronic risk for renal vascular lesion since excretion of orally absorbed glycotoxins is mostly suppressed in diabetic nephropathy conditions[76]. A pronounced acute postprandial vascular dysfunction post-consumption of a meal with high AGE compared to that of low AGE diet in T2DM patients was also reported [77].

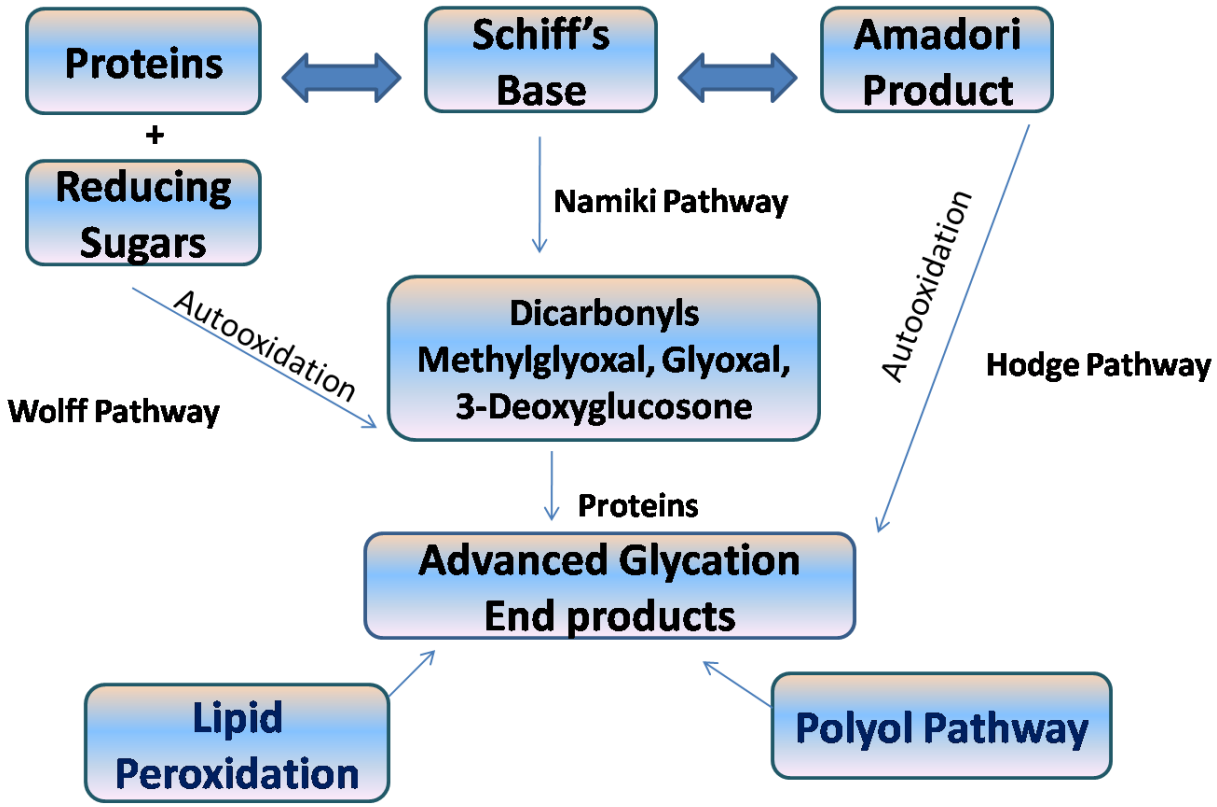

Figure 1.2 Formation of Advanced glycation end products

1.4 Methylglyoxal

Consumption of fast food, thermally processed food, a diet rich in sugar and excess saturated fats, and physical inactivity are modern lifestyle hallmarks. Dramatically increased prevalence of insulin resistance is attributed to the contemporary lifestyle. Hyperglycemia is the primary manifestation of diabetes. Indeed, the formation of AGEs results mainly from the action of various reactive metabolites other than glucose[78], with MG as a significant precursor in the formation of AGEs[79]. In diabetes, levels of dicarbonyls and AGEs are high. The most studied and well-researched dicarbonyl is MG, as a series of MG derived intracellular AGEs are formed in diabetes. Proteins modified from MG are correlated to various disease pathologies. Interestingly, being having a highly permeable nature, MG is expected to have higher intracellular levels (1-2μM)[80].

In the plasma, the concentration of MG is close to 25,000-fold lesser than glucose; despite that, it contributes more to glycation because it is 50,000-fold higher reactive than glucose[81]. Thus, MG causes the swift generation of glycation adducts on cellular and extracellular proteins[82][83][84], lipids[85], and DNA[86], potentially modifying their function. Its molecular formula is $C_3H_4O_2$ (MW 72.06) (Figure 1.3)

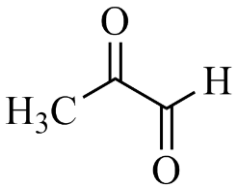

Figure 1.3 Structure of methylglyoxal

1.4.1 **Formation of Methylglyoxal**

Methylglyoxal is primarily formed as a byproduct of glucose metabolism by the non-enzymatic degradation of the glycolytic triose phosphates, glyceraldehyde-3-phosphate (G3P), and dihydroxyacetone-phosphate (DHAP)[87] [88]. An increase in various metabolic pathways such as glucose metabolism in diabetes, glyceroneogenesis, and gluconeogenesis with high levels of trioses leads to enhanced MG formation[89]. MG can be formed from other sources via glycated proteins degradation[68], during ketoacidosis metabolism of ketone bodies where acetone oxidation is involved[90], catabolism of threonine[91], and lipid peroxidation[92](Figure 1.4). MG is also present in several daily consumed products[93]. Apart from the endogenous sources, there are also exogenous sources, and their intake can lead to a higher amount of MG in blood. These sources can be processed foods that go through thermal degradation or oxidation of glucose during sterilization, culinary, or at the time of commercial processing. But before absorption in the gastrointestinal tract, the MG in food items either gets metabolized or reacts and modifies the proteins. Hence, MG from these exogenous sources contributes negligibly to the plasma MG levels[94]. Since MG gets metabolized or reacts, most of the MG remains reversibly bound to amino acids, peptides, proteins, and the free form of MG such as unhydrated, monohydrated, or dihydrated, exists is only 1%[83]. Quantification of MG is difficult in the plasma and tissues of control subjects. It requires different processing levels during sample preparation; because of that, reversibly bound fraction and free MG concentration obtained were with significant variation from 60 nM to 400 μM[95][96][97][98][99][100][101]. Due to its highly reactive nature, MG predominantly reacts with protein's arginine residues and form various MG-derived AGEs[102]. MG modifies proteins and genomic DNA and adds different complications at secreted and cellular protein levels, like creating an imbalance in cells' functioning and instability at genetic levels[103][104].

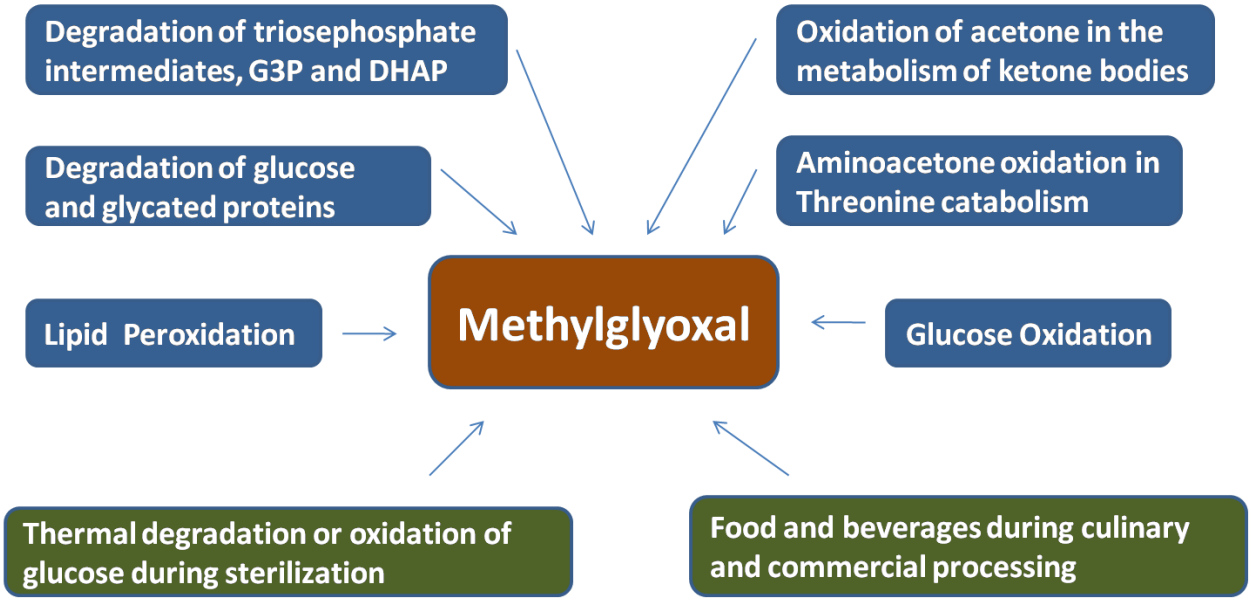

Figure 1.4 Sources of Methylglyoxal

1.4.2 **Detoxification of methylglyoxal**

For the detoxification of MG, there are several mechanisms present in the body, and the glyoxalase system is the primary and central system that remains active in mammalian cell's cytoplasm and detoxifies the maximum amount of MG to D-lactate. In 1913, Dakin and Dudley brought to light that the glyoxalase system, which is glutathione-dependent, was distinctly particular and evolutionary conserved. The system comprised two significant enzymes, glyoxalase 1 (Glo1), glyoxalase 2 (Glo2), and glutathione (GSH)[105]. Hemithioacetal acted as a primary substrate for Glo1 and formed impulsively from MG and GSH. Glo1 catalyzes hemithioacetal isomerization and converts it to S-D-lactoylglutathione. Glo2, which is a thiolesterase, catalyzes S-D-lactoylglutathione hydrolysis and finally converts it to D-lactate and GSH[106][107]. Without depleting its cofactor GSH, the glyoxalase system has a limited substrate specificity. For the detoxification of MG, the rate-limiting step is represented by Glo1[108]. More than 99% of MG is metabolized under normal conditions via the glyoxalase

system inside cells[109]. The increase in the enzymatic MG detoxification leads to reduced MG concentration, both intra and extracellularly[110]. In Glo1 knockout animal models, it had been observed that the ability to detoxify MG was preserved, which indicated that other detoxifying mechanisms exist[111][112]. It had been shown aldehyde dehydrogenases (ALDHs), Aldo-ketoreductases (AKRs), and the DJ-1 protein helps in the removal of MG[113][114][115]. Apart from these enzymatic detoxification systems, some metabolites, for example, acetoacetate and creatine reaction with α-dicarbonyls, leads to the formation of less harmful products formation[116][117][118].

1.4.3 **Methylglyoxal in diabetes**

After discovering that high glucose concentrations result in MG formation [119] [79] [120] and higher levels of MG and MG derived AGEs are present in the plasma of diabetic subjects[95] [121], further studies strengthened the significance of MG and its role in diabetes and various diabetes-related complications. The vascular endothelium is the main mediator that helps in maintaining vascular homeostasis. It forms a barrier and allows only selective molecules to pass across. When there is a reduction in the endothelium-mediated vasodilation and an increase in the pro-coagulant nature, the condition is called endothelial dysfunction. It is an unsuitable situation for organs to preserve their function[121]. The characteristic changes for diabetes-related endothelial dysfunction are inflammation, high oxidative stress, and vasoregulation changes[121] [122] [123]. In endothelial cells, MG is a certain AGE precursor as the Formation of significant AGEs induced due to hyperglycemia was utterly prevented by Glo1 overexpression in endothelial cells[79].

Along with the MG formation, various other pathways conciliate the hyperglycemia effect on the kidney, which ultimately lead to diabetic complication nephropathy[124] [125]. In diabetes, the predominance of chronic kidney disease was found to be correlated to the levels of MG in the plasma[126][127][128]. Also, in both T1D and T2D patient's plasma, the increased MG levels were correlated with the higher risk for lower eGFR and albuminuria[129] [129] [130]. In diabetic nephropathy, the presence of various MG-induced AGEs indicates an increase in the

development of lesions, and MG-H1 can significantly predict the growth in the glomerular basement membrane. [131]. MG-H1 levels were higher and, increased MG-H1 levels were found in proliferative retinopathy patients as compared to non-proliferative retinopathy patients, which suggests an essential role of MG in the retinopathy progression. This observation was further confirmed in a study where within 24 weeks of diabetes, retinal levels of MG-H1 were found with an increase of 3-fold in diabetic rats[132]. MG plays a key role in the pathogenesis of diabetic neuropathy, as shown by and studied in various mammalian systems and animal subjects. In Schwann cells, activation of p38 MAPK by MG leads to induction of apoptosis[133]. In addition, cells viability gets affected in neuronal cells because of MG's deleterious repercussion on signal transducer and activator of transcription 3 (STAT3) signaling, which ultimately emerges in the suppression of anti-apoptotic protein Bcl-2[134]. Diabetic patients have higher MG concentration in their plasma that results in depolarization of sensory neurons and induction of post-translational modifications of arginine residues inside the voltage-gated sodium channel. Hence MG gives rise to enhanced intensity of pain sensation by increasing blood flow towards brain regions[135].

In atherosclerosis, higher levels of MG-H1 can be a result of impaired Glo1 function in MG detoxification, and these MG-H1 levels co-localize with different markers of inflammation, hypoxia, apoptosis, and oxidative stress in the atherosclerotic plaque, indicating that increase of MG-H1 in the plaque consequent leads to macrophage death and grant to the conversion of stable plaques to rupture-prone plaques[136]. Atherosclerosis is a leading cause of various cardiovascular health events; furthermore, for cardiovascular morbidity and mortality in diabetic patients, a significant grantor is heart failure[137]. In the hearts of type 1 diabetic rats, increased levels of MG modifications have been reported on RyR2 and SERCA2a, which led to improper functions about Ca^{2+} cycling; hence it can be a likely molecular mechanism where MG plays a role in heart failure [138][139][140].

1.4.4 **Methylglyoxal and Insulin resistance**

It had observed that in the β-cells, secretion of insulin deteriorated after the incorporation of elevated concentrations of MG. At average concentrations of glucose, a fast depolarization of rat

pancreatic β-cells persuaded by MG developing in higher cytosolic $Ca^{2+}$and transient stimulation of insulin secretion. In contradiction, insulin secretion was notably inhibited by MG at higher glucose concentrations [141][63]. Glycolytic rates are relatively higher in Pancreatic β-cells, and thus MG formation occurs during glycolysis leading to an increase in the intracellular concentrations of MG [142]. MG decreased insulin secretion in acetylcholine presence but intensified in potassium and epinephrine presence [143]. When MG modified insulin, it hindered control of an autocrine function in β-cells for insulin secretion. As compared to native insulin, MG-modified insulin reduced glucose uptake in adipocytes and skeletal muscle cells, which are primary insulin-sensitive cells [144].

Skeletal muscle cells are insulin sensitive cells and play a significant role in the insulin signaling pathway. The treatment of MG or MG-modified proteins to skeletal muscle cells can alter the action of the insulin signaling pathway and decreases the glucose uptake without influencing IR tyrosine phosphorylation but via deterioration of insulin-stimulated phosphorylation of protein kinase B (PKB) and extracellular signal-regulated protein kinases 1/2 (ERK1/2)[145] [61]. In metabolically healthy muscle cells, despite increased MG flux, an increase in MG stimulated Glo1 protein expression results inefficient detoxification of MG [146]. Nonetheless, in the case of T2D, decreased expression of Glo1 results in the accumulation of MG in metabolically impaired muscles[147]. Nrf2 is an important transcription factor that regulates Glo1. Kelch-like ECH-associating protein 1 (Keap1) binds to Nrf2, which results in its degradation. In T2D, increased Keap1 expression and decreased Nrf2 protein expression is related to reduced expression of Glo1 protein in skeletal muscle cells[147].

1.4.5 **Skeletal muscle MG-GLO1 physiology**

Metabolically, skeletal muscles are the essential tissues in the body. Muscle tissue accounts for greater than 40% of total body protein and has a significant role in the disposal of glucose, accounting for greater than 80% of insulin-mediated glucose uptake[148]. Reduced glucose uptake in response to insulin is known as insulin resistance and is implicated in many disease pathogenesis, most prominently T2DM. MG induces pathways that are responsible for insulin resistance and also oxidative stress, which is caused by mitochondrial damage[149] and

mitochondrial DNA[150], generation of AGEs [151], and Receptor for Advanced Glycation End Products (RAGE) signaling mediated inflammation [152][153][154]. RAGE is highly expressed in skeletal muscle [155] [156], and upon binding of RAGE-ligands (e.g., MG-H1), a well-characterized inflammatory signaling cascade ensues [157] [158][159]. Additionally, in L6 myotubes *in vitro* experiments showed that treatment of MG or MG-modified proteins inhibited insulin-triggered glucose uptake.phosphorylation of phosphatidylinositol-4,5-bisphosphate 3-kinase (P13K) and extracellular-signal-regulated kinase 1 and 2 (ERK1/2) [160][61][161]. It further showed that binding of insulin signaling protein, IRS-1, to MG might be important for induction of insulin resistance, not the oxidative stress generated by MG.

MG-GLO1 physiology in skeletal muscle in the context of diabetes is shown in figure 1.5. In healthy state physiology, in the skeletal muscle, MG is formed as a byproduct of glycolysis from dihydroxyacetone phosphate, DHAP, and glyceraldehyde-3-phosphate, G3P. Glyoxalase-1 (Glo1) efficiently detoxifies this MG to D-lactate. However, in metabolically compromised states, such as type 2 diabetes mellitus (T2DM), high-fat diet feeding, and insulin resistance, there is a reduction in the expression of GLO1 protein. From glycolysis, the production of MG occurs at a higher rate. Consequently, through multiple pathways, it leads to poor skeletal muscle metabolic health. An increased amount of MG damages mitochondria and gives rise to oxidative stress, lipid peroxidation, and ultimately the generation of more MG. This extra MG can also impair insulin signaling directly by attaching to insulin present in the circulation or by binding to insulin receptor substrate-1 within the skeletal muscle.

Also, excessive MG can activate the RAGE-mediated inflammatory signaling cascade by binding to proteins present in circulation as MG-H1 adducts or MG-modified proteins. Dicarbonyl stress can be managed by different targeted therapeutic strategies like exercise, metformin, and GLO1-inducers, which increase the Glo1 protein expression.

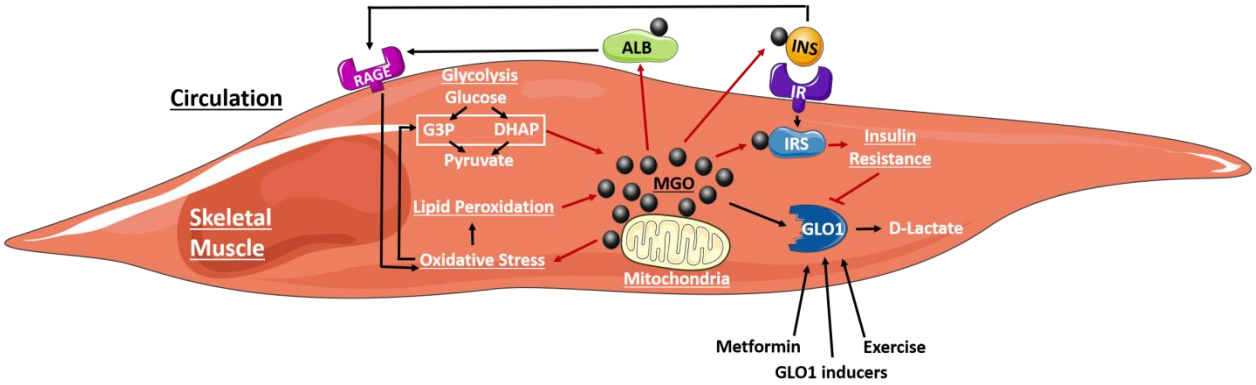

Figure 1.5 Skeletal muscle MG-GLO1 physiology in the context of diabetes

1.5 Skeletal muscle and secretome

Recent studies have indicated that apart from being the largest organ, skeletal muscles also have an endocrine function, producing a large number of proteins called myokines. These proteins have been reported to have widespread action on different organs and tissues.[162] A number of tissues are reported to be regulated by myokines, and the synthesis and secretion of myokines are controlled by several factors, including differentiation, exercise[163], and *in vitro* electrical stimulation[164]. Apart from these factors, insulin resistance, affects the secretion of myokines[162]. Various factors including oxidative stress, palmitic acid, TNF-α are known to induce insulin resistance and affect the myokine secretion in muscle cells[165][166][167]. Similarly, it has been shown that MG induces insulin resistance in muscle cells[168]; however, MG induced changes in myokine secretion are not yet studied. Characterization of skeletal muscle secretome is still not complete even after the identification of numerous myokines in recent profiling studies, which is evident from the amount of overlap seen among these studies. The pathogenesis of Type 2 diabetes affects the functioning of all major organs that govern metabolic control, including skeletal muscles. Since myokines influence a number of different organs, any alteration of the skeletal muscle secretome can have wide and detrimental effects.

1.6 Objectives

Based on this literature survey, we designed our objectives as

1. Study of methylglyoxal induced secretome in L6 rat skeletal muscle cells

2. Study of methylglyoxal induced secretome in clinical samples

3. Total cell proteomics of skeletal muscles to understand the role of methylglyoxal in the development of insulin resistance

4. Study of methylglyoxal induced proteins in animal plasma

Chapter 2

Study of methylglyoxal induced secretome in L6 rat skeletal muscle cells

Content of this chapter are published as research article in *ACS omega* 5, no. 39 (2020): 25016-25028. https://doi.org/10.1021/acsomega.0c01318

Chapter 2 Study of methylglyoxal induced secretome in L6 Rat skeletal muscle cells

2.1 Background

Methylglyoxal (MG) is produced as a minor by-product of various metabolic processes[169]. However, in insulin-resistant states like obesity and type 2 diabetes, MG levels are known to increase due to altered glucose metabolism. The concentration of MG in the plasma of diabetic patients is associated with the level of blood glucose[99]. The intracellularly produced MG can readily diffuse into the extracellular matrix. Since MG is highly reactive, it readily reacts with and modifies proteins, lipids, and DNA and can affect their normal structure and function[170][171]. It is also a major precursor of advanced glycation end products which are reported to be involved in the development of diabetes and diabetic complications and whose detrimental effects have been widely reported[172][173][174][175]. Therefore, various detoxification mechanisms are present in the body, one of them being the glyoxalase system. This system comprises glutathione and two enzymes, viz., glyoxalase I and II. MG first reacts with glutathione to form a hemithioacetal, which is metabolized by glyoxalase I into S-D-lactoyl-glutathione. This intermediate is further metabolized into D-lactate by glyoxalase II, and glutathione is regenerated[176]. However, in diabetes, because of higher levels of MG, it can modify proteins from several tissues, including vascular endothelium and smooth muscles[177][178]. MG-induced modification in proteins may have adverse effects on cellular processes, and therefore such proteins are removed by exocytosis or secretion into the extracellular matrix[179].

Secreted proteins comprise an important class of biomolecules that include a wide array of proteins such as serum proteins, matrix proteins as well as hormones, and growth factors. It is believed that approximately 10% of the human genome encodes for secreted proteins[180]. Quintessential examples of secreted proteins include serum albumin, immunoglobulins, and enzymes of the digestive tract[181]. Even in the regulation of cell renewal and differentiation, proteins secreted in low abundance but that are highly bioactive, such as cytokines, and growth factors contribute significantly[182].

Recent studies have indicated that apart from being the largest organ, skeletal muscles also have an endocrine function, producing a large number of proteins called myokines. These proteins have been reported to have widespread action on different organs and tissues[162]. A number of tissues are reported to be regulated by myokines, and the synthesis and secretion of myokines are controlled by several factors, including differentiation, exercise[163], and *in vitro* electrical stimulation[164]. Apart from these factors, insulin resistance, affects the secretion of myokines[162]. Various factors including oxidative stress, palmitic acid, TNF-α are known to induce insulin resistance and affect the myokine secretion in muscle cells[165][166][167]. Similarly, it has been shown that MG induces insulin resistance in muscle cells[168]; however, MG induced changes in myokine secretion are not yet studied. Characterization of skeletal muscle secretome is still not complete even after the identification of numerous myokines in recent profiling studies, which is evident from the amount of overlap seen among these studies. The pathogenesis of Type 2 diabetes affects the functioning of all major organs that govern metabolic control including skeletal muscles. Since myokines influence a number of different organs, any alteration of the skeletal muscle secretome can have wide and detrimental effects. Herein, we sought to identify the MG induced secretome of rat muscle cells and its validation in clinical plasma samples to identify potential biomarkers for diabetes.

2.2 Material and Methods

2.2.1 **Chemicals**

All fine chemicals and reagents were obtained from Sigma-Aldrich (St. Louis, MO, USA). Dulbecco's Modified Eagle Medium (DMEM) for cell culture was procured from HiMedia. Fetal bovine serum (US origin) and trypsin were purchased from Invitrogen (Carlsbad, CA, USA). Plasticware for tissue culture was procured from Nunc (Rochester, NY, USA). Bradford protein estimation kit was purchased from Bio-Rad Laboratories, USA. 3 kDa cut-off centrifugal filters and C18 Zip-Tip® desalting columns were procured from Millipore (Millipore, Billerica, MA, USA). Liquid chromatography columns Eskigent C18-RP HPLC column (100×0.3mm, 3µm,

120 Å) were procured from Sciex (Sciex, Framingham, MA, USA). RapiGest™ SF surfactant was purchased from Waters (#186001860, Waters Corporation, MA, USA). All solvents were for LC-MS procured from J.T. Baker (J T. Baker, PA, USA). ELISA kit sCD44std Instant ELISA was procured from Thermo (#BMS209INST, eBioscience, Vienna, Austria).

2.2.2 **Research design**

The schematic of the complete experimental design adopted in this study is depicted in (Figure 2.1). The study was conducted to characterize the methylglyoxal induced secretome of muscle cells and identify the presence of methylglyoxal induced secreted proteins in the diabetic plasma. The conditioned media from three individual experiments, each of control cells and methylglyoxal treated cells, were used for the identification of secretome by SWATH-MS. The mass spectrometric acquisition was performed for three different experiments in technical triplicates. The presence of methylglyoxal induced secreted proteins was evaluated by performing proteomics analysis of 10 plasma samples each of healthy control and diabetic subjects by SWATH-MS in technical triplicates. CD44, one of the predominant methylglyoxal-induced secreted proteins, was evaluated for its presence in the same set of clinical samples in technical duplicates. Since this was a pilot study, the sample size was limited to a maximum of 20 samples.

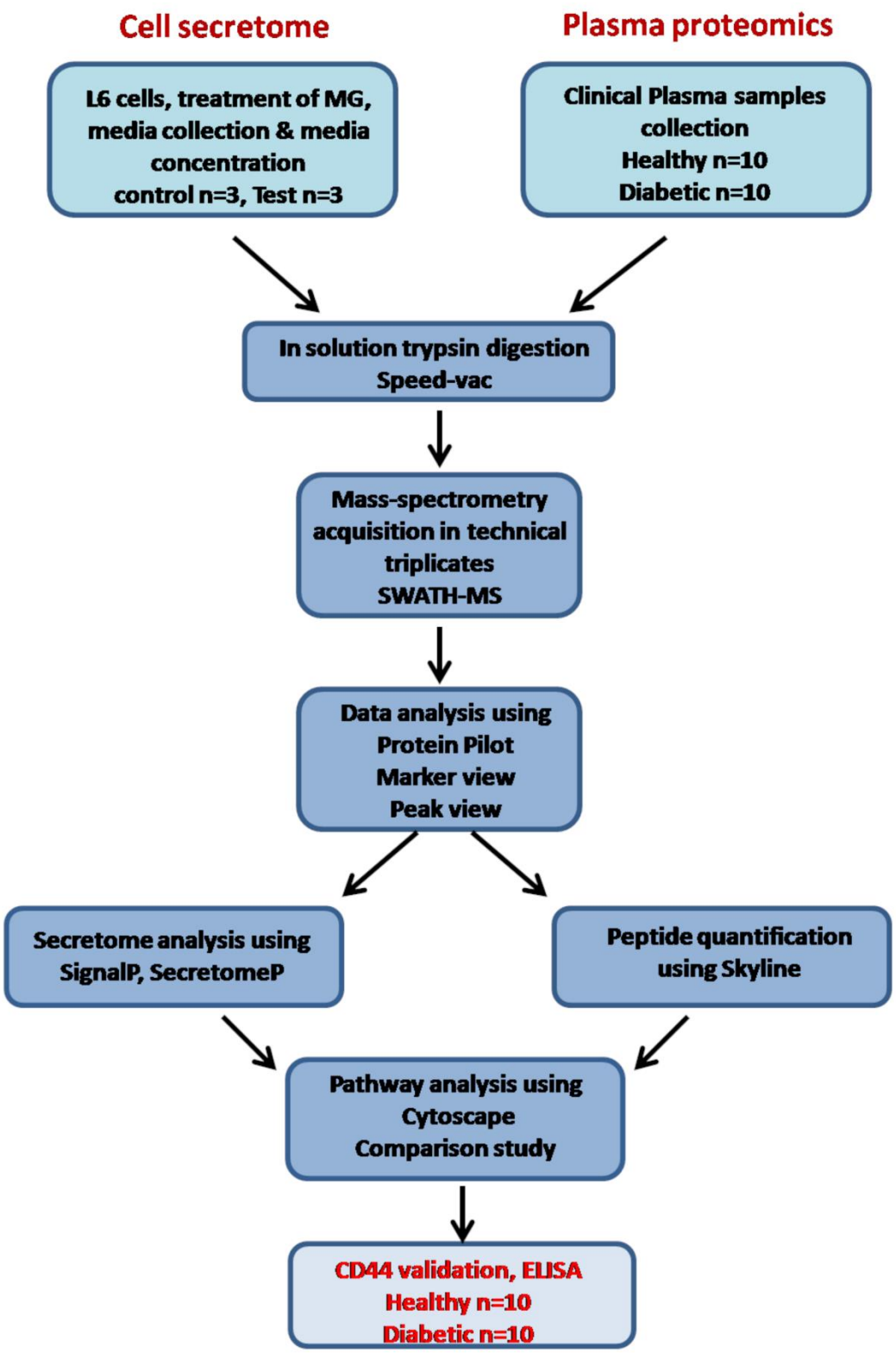

Figure 2.1 Overview of the complete experimental design

2.2.3 Cell culture and Differentiation

Rat L6 muscle cells were procured from the National Centre for Cell Sciences, Pune. They were grown in DMEM media supplemented with 10% (v/v) heat-inactivated fetal bovine serum (FBS). The cells were maintained at 37°C in a humidified atmosphere containing 5% (v/v) CO_2. Cells were differentiated in DMEM media supplemented with 2% FBS for 6 days, and the progress of differentiation was monitored microscopically.

2.2.4 Cell viability assay

The cytotoxicity of methylglyoxal on L6 cells was assessed using the trypan blue (0.5%) dye exclusion test. Cells were seeded into 24-well culture plates and were grown for 24 h. Further cells were serum-starved for 4 h in serum-free DMEM and treated with methylglyoxal at different concentrations for 3 h. After treatment, cells were washed twice with Dulbecco's phosphate-buffered saline, harvested using trypsin, and trypan blue staining was performed for assessing cell viability. Viable cells were counted using a hemocytometer.

2.2.5 Collection and preparation of conditioned media

Differentiated and confluent cells were washed thrice with completely DMEM with no supplements, including phenol red, serum, or antibiotics, and were kept for serum starvation for 4 h. After treatment with methylglyoxal for 3 h, the conditioned media containing secretory proteins were collected and centrifuged twice at 4,018 ×g, for 15 min at 4 °C to pellet down the detached cells and debris. The supernatant was collected and concentrated by passing through Amicon 15 ml 3kDa cut-off filters (Millipore). The final secreted proteins were then dissolved in RapiGest. Protein concentration was estimated colorimetrically by Bradford's assay.

2.2.6 In-solution Trypsin Digestion

100 µg of total protein in 0.1% RapiGest for each plasma sample was used for digestion. Before reduction and alkylation, proteins were denatured by incubating at 80 °C for 15 min. Further, proteins were reduced using 100 mM dithiothreitol for 15 min at 60 °C and then alkylated by treating with 200 mM iodoacetamide for 30 min in the dark at room temperature. Trypsin was

added at 1:25 (w/w) enzyme to protein ratio and incubated at 37°C for 18 h, 2 µl formic acid was added to inactivate trypsin and stop the digestion. For desalting of the digested peptides, C18 Zip tips were used, and the desalted peptides were concentrated using Speed vac. For LC-MS analysis, peptides were reconstituted in 3% acetonitrile with 0.1% formic acid.

2.2.7 Liquid Chromatography-Mass Spectrometry Analysis

2.2.7.1 SWATH-MS Analysis for Secretome

SWATH analysis was performed on a Triple-TOF 5600 (AB Sciex; Concord, Canada) mass spectrometer coupled with Micro LC 200 (Eksigent; Dublin, CA) in high-sensitivity mode. A spectral library was generated by pooling equal amounts of peptide samples from each treatment and analyzing them by Information dependent acquisition (IDA). Briefly, peptides were separated on an Eksigent C18-RP HPLC column (100×0.3mm, 3µm, 120 Å) using a 95 min gradient of 3% to 35% mobile phase B at a flow rate of 8 µL/min (mobile phase A: water with 0.1% formic acid mobile phase B: acetonitrile with 0.1% formic acid). Accumulation time for MS was 250 ms and for MS/MS was 100 ms. Fragmentation was done using rolling collision energy. For SWATH-MS acquisition, the precursor mass range of 400–1250 m/z was divided into a set of 34 overlapping windows of 25 m/z each. For MS/MS, collision energy was optimized for each window, and spectra were collected from 100 to 2000 m/z. Fragment ion scans were performed over an accumulation time of 70 ms, while for the precursor survey scan, it was 100 ms. All samples were acquired in biological and technical triplicates.

To get spectral library from IDA run, data was analyzed by ProteinPilot™ software version 5.0 using UniProt *Rattus norvegicus* database updated with Uniprot release 2019_02; 8,060 reviewed protein entries. The enzyme used for digestion was set to trypsin, and carbamidomethylation of cysteine residues was set as a fixed modification. The search was performed using a False Discovery Rate (FDR) of 1%. The resultant spectral library was imported into PeakView v2.2 software, and SWATH runs for all samples were processed using 50 ppm mass error, 5 min RT window, and 99% confidence, and 1% FDR. The peak areas thus generated in PeakView were imported into MarkerView™ v1.2.1, wherein statistical analysis using t-test was performed.

Normalization across the runs was performed using total area sum. All the raw mass spectrometric data has been deposited at the public repository PeptideAtlas (PASS01477).

2.2.8 **Bioinformatic analysis**

The differentially secreted proteins were analyzed for protein-protein interactions and pathways using the STRING 11.0 database (Search Tool for the Retrieval of Interacting Genes), and the protein-protein interaction (PPI) network was imported into Cytoscape 3.2, an open-source network visualization software. The clustering of proteins was performed using the clusterMaker plugin in Cytoscape. The identification of secretory proteins was made by using both classical and non-classical secretion prediction tools. The web-based SignalP 5.0 server (http://www.cbs.dtu.dk/services/SignalP/) was used for predicting classically secreted proteins, and the data was processed using the "eukarya" option. For the prediction of non-classically secreted proteins, SecretomeP 2.0 (http://www.cbs.dtu.dk/services/SecretomeP/) was used.

2.2.9 **Statistical analysis**

Mass spectrometry acquisition for cell secretome experiments was performed for three individual cell culture experiments in technical triplicates. Statistical analysis was performed by Student's t-test for quantitation of proteomic data, and one-way ANOVA was performed for cell viability assay. Data were expressed as mean ± SEM. A p-value ≤ 0.05 was considered statistically significant. For proteomic analysis, the proteins with more than 2 matching peptides and fold change difference of ≥ 1.3 in protein expression were assessed.

2.3 Results and Discussion

2.3.1 **Methylglyoxal does not affect cell viability up to 3mM concentration**

Methylglyoxal, a highly reactive dicarbonyl compound, is reported to induce oxidative stress in cells[173]. Therefore, we have evaluated its cytotoxicity on L6 rat skeletal muscle cells. MG concentration above 3 mM reduced the cell viability, as observed by trypan blue staining (Figure 2.2), and therefore, 3 mM MG treatment was used for all secretome experiments.

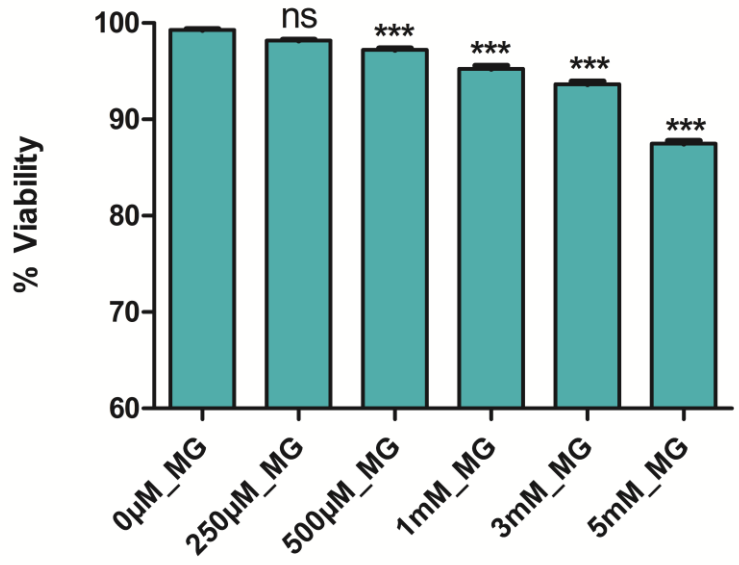

Figure 2.2 Effect of methylglyoxal (MG) on cell viability

Cytotoxicity of L6 cells was evaluated after treatment with different concentrations of MG as indicated using trypan blue exclusion test. Values represent mean ± SEM from three biological replicates. (*** indicates p-value < 0.0001) Statistical significance was calculated by One way of ANOVA.

2.3.2 **Methylglyoxal induced secretome**

Methylglyoxal induced secretome was tryptically digested, and SWATH-MS analysis was carried out for three individual experiments in technical triplicates for identification and expression analysis. Figure 2.3 shows the PCA plot. The volcano plot indicates the proteins with differential abundance > 1.3 fold and p-value < 0.05 in pink (Figure 2.4A). The IDA spectral library had 643 proteins (Appendix 2), and 82 of those were upregulated while 99 were downregulated by more than 1.3 fold in MG induced secretome in SWATH analysis (Figure 2.4B). All the differential expressed proteins (Appendix 3) were significant at p-value <0.05. Secretory proteins from classical secretory pathway and non-classical secretory pathway were determined using SignalP and SecretomeP, respectively[183, 184]. Out of the total identified proteins, 180 proteins were identified with SignalP, and 113 proteins were identified with SecretomeP (Figure 2.4C). KEGG Pathway analysis was done using Cytoscape software with

plugin clusterMaker[185]. Differentially expressed proteins were found to be involved in various pathways like ECM-receptor interaction (Figure 2.5A), leukocyte transendothelial migration (Figure 2.5B), fluid shear stress and atherosclerosis (Figure 2.5C), complement and coagulation cascades (Figure 2.5D), and lysosome (Figure 2.5E). ECM-receptor interaction is known to contribute to histopathological lesions in diabetic nephropathy. Previously, methylglyoxal was found to inhibit endothelial cell adhesion to type IV collagen of renal glomerular cells, podocytes, and mesangial cells leading to the development of diabetic nephropathy[186]. In this study, the extracellular matrix (ECM) proteins such as Integrin beta-1, Fibronectin, and CD44 antigen were upregulated in methylglyoxal induced secretome and may induce insulin resistance. Aberrant regulation of ECM components is observed in obesity associated with insulin resistance[187]. MG induced upregulation of key proteins such as Ezrin, Integrin beta-1, Ras-related protein Rap-1b, Transforming protein RhoA, Thy-1 membrane glycoprotein and Vascular cell adhesion protein 1; and downregulation of 72 kDa type IV collagenase, which are involved in leukocyte transendothelial migration, an important step in eliciting inflammatory immune response[188]. MT1-MMP-dependent shedding of CD44 plays a key role in the regulation of leukocyte adhesion to the pancreatic blood vessels and the transendothelial migration of diabetogenic, cytotoxic, T cells into the islet cells[189]. This was also associated with enrichment of proteins involved in complement and coagulation cascades such as Complement C3, Alpha-2-macroglobulin, and Urokinase-type plasminogen activator were upregulated, and proteins such as Complement C1s subcomponent, Clusterin, Vitamin K-dependent protein S, and Plasminogen activator inhibitor 1 were downregulated in MG induced secretome. Complement and coagulation system has been implicated in the pathogenesis of metabolic disorders including, insulin resistance, non-alcoholicfatty liver disease and type 2 diabetes[190]. In obesity and type 2 diabetes, adipocytes are actively involved in production of complement components such C3 factor. Higher levels of serum C3 are correlated with insulin resistance, endothelial dysfunction and progression of diabetic nephropathy[191]. C3 is also associated with cardiovascular diseases, as it interacts with the coagulation system. Similarly, proteins involved in fluid shear stress and atherosclerosis such as Endoplasmin, Heat shock protein HSP 90-beta, Heat shock protein HSP 90-alpha, Transforming protein RhoA, Vascular cell adhesion protein 1, NAD(P)H dehydrogenase [quinone] 1, Glutathione S-transferase Mu 2, were upregulated and proteins such as Platelet-derived growth factor subunit A, Vascular endothelial growth factor A, 72 kDa type

IV collagenase, C-C motif chemokine 2 were downregulated in response to MG treatment. People with diabetes tend to develop accelerated atherosclerosis[192]. Glycation of extracellular matrix proteins such as glycated collagen alters endothelial cell function and could contribute to the development of atherosclerotic plaques. In this study, ECM proteins were differentially regulated in response to MG treatment. Protein such as Vascular cell adhesion protein 1, Transforming protein RhoA were upregulated[193]. NAD(P)H dehydrogenase [quinone] 1 and its homolog NADPH oxidase act downstream to the AGE-RAGE axis, is involved in the production of ROS and inflammatory response[194]. Another important pathway that was enriched in the MG induced secretome was the lysosomal pathway. MG is a highly reactive dicarbonyl responsible for the formation of diverse AGEs, which are implicated in the pathogenesis of diabetes. Cells have evolved combat mechanisms to degrade AGEs via lysosome mediated autophagy pathways. In a recent study, it has been demonstrated that modulation of lysosome biogenesis leading to autophagy was responsible for the degradation of AGEs in the diabetic kidney. In case of autophagy deficient mutant cells, lysosomal biogenesis was not observed,resulting in the accumulation of AGEs in the glomeruli and renal vasculature, which was associated with enhanced inflammation and fibrosis[195]. However, MG induced secretome, showed down regulation of various proteins such as N(4)-(Beta-N-acetylglucosaminyl)-L-asparaginase, Acid ceramidase, V-type proton ATPase subunit S1, Cathepsin B, Cathepsin D, Pro-cathepsin H, Cathepsin L1, Deoxyribonuclease-2-alpha, Tissue alpha-L-fucosidase, N-acetylgalactosamine-6-sulfatase, Beta-glucuronidase, Beta-hexosaminidase subunit alpha, Beta-hexosaminidase subunit beta, Hyaluronidase-1, Legumain, Alpha-N-acetylgalactosaminidase, Palmitoyl-protein thioesterase 1, Prosaposin and Tripeptidyl-peptidase 1, that are involved in lysosomal degradation pathway. Impaired lysosomal degradation system is associated with aging and diabetes. Accumulated AGEs exacerbates diabetes and its diabetic complications[196].

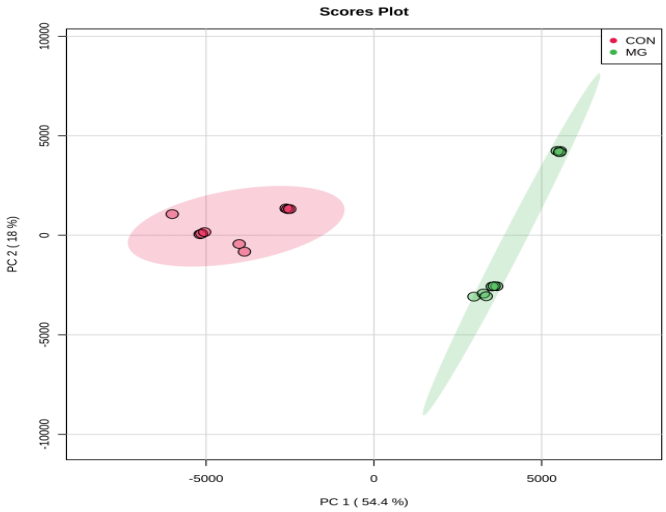

Figure 2.3 PCA plot suggesting the reproducibility of replicate acquisition

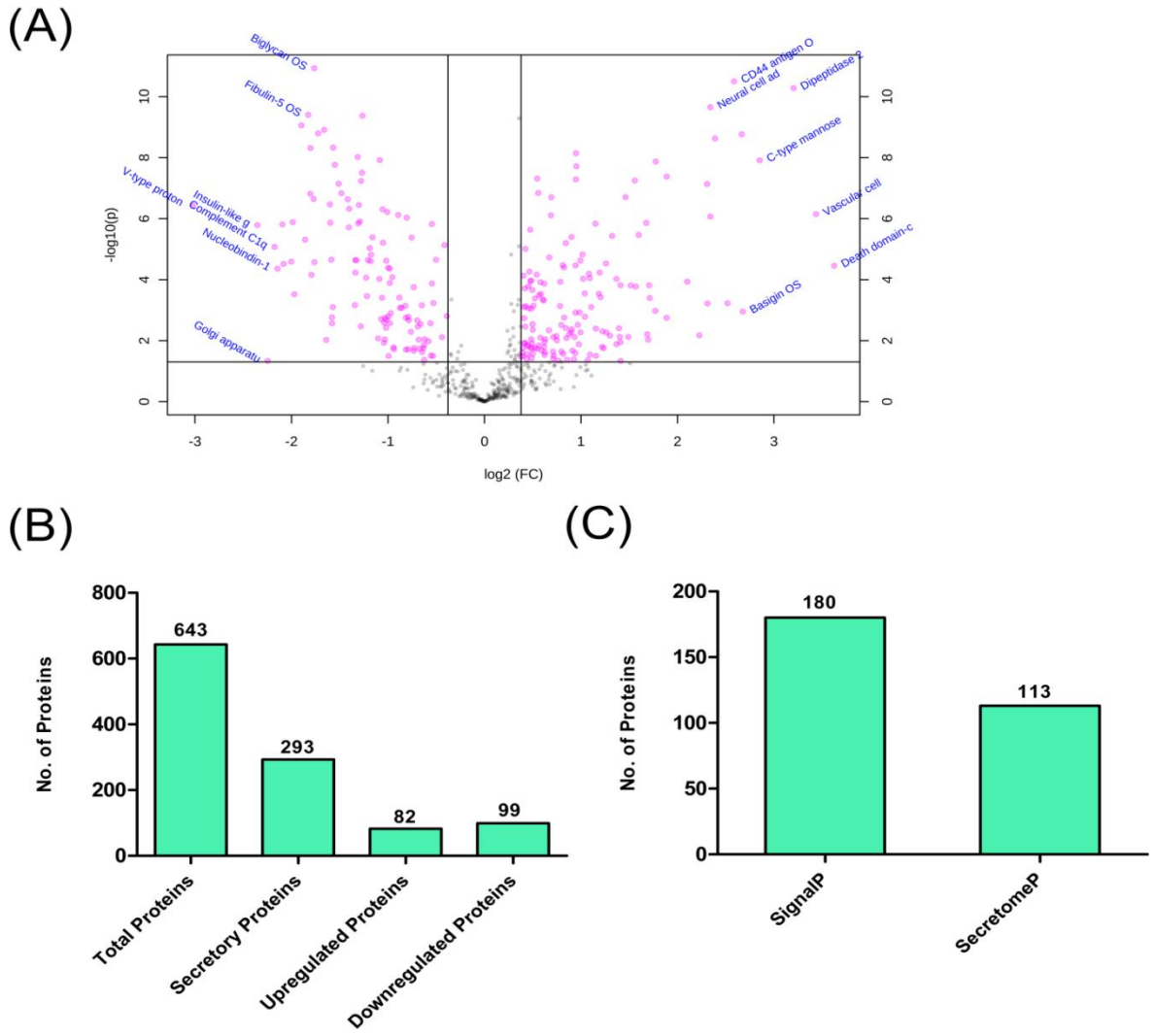

Figure 2.4 Proteomic Analysis for Secretome

Differential proteomics analysis was done by SWATH-MS. (A) The volcano plot, made using Metaboanalyst 4.0 online analytical tool, indicates the proteins with differential abundance > 1.3 fold and p-value < 0.05 in pink. (B) The number of differentially expressed proteins in MG vs. Control. (C) The number of secretory proteins obtained through SignalP and SecretomeP.

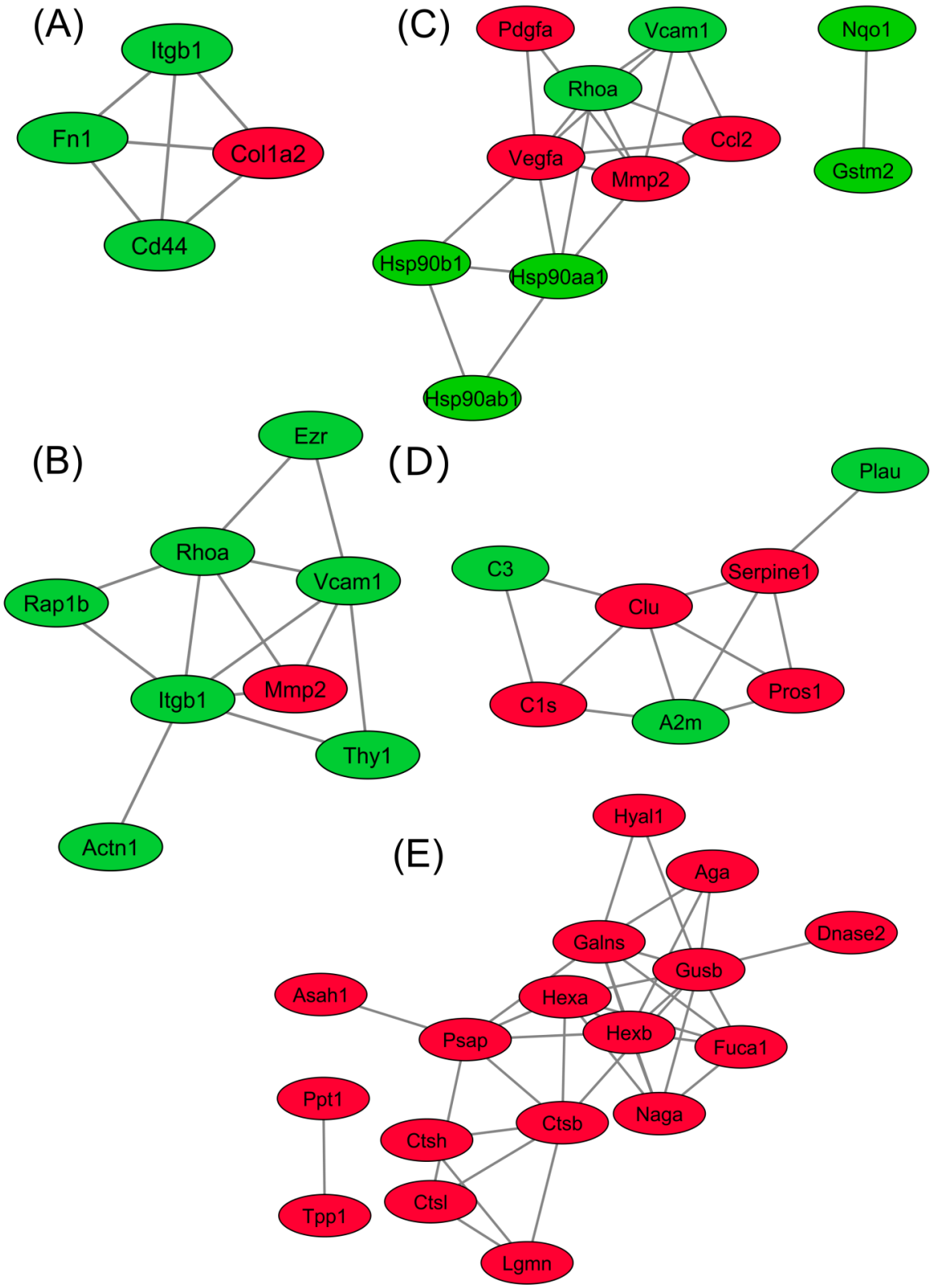
(A)
Itgb1
Fn1
Col1a2
Cd44
(C)
Pdgfa
Vcam1
Nqo1
Rhoa
Ccl2
Vegfa
Mmp2
Gstm2
Hsp90b1
Hsp90aa1
Hsp90ab1
(B)
Ezr
Rhoa
Vcam1
Rap1b
Itgb1
Mmp2
Thy1
Actn1
(D)
Plau
C3
Serpine1
Clu
Pros1
C1s
A2m
(E)
Hyal1
Aga
Galns
Dnase2
Gusb
Asah1
Hexa
Psap
Hexb
Fuca1
Ppt1
Ctsb
Naga
Ctsh
Ctsl
Tpp1
Lgmn

Figure 2.5 Bioinformatic analysis

PPI network clusters showing differentially abundant proteins involved in (A) ECM-receptor interaction, (B) Leukocyte transendothelial migration, (C) Fluid shear stress and atherosclerosis, (D) Complement and coagulation cascades, (E) Lysosome; green indicates > 1.3 fold higher abundance and red indicates > 1.3 fold lesser abundance in MG treated cells**.**

Apart from the above pathways, MG induced secretome had several proteins related to insulin resistance, obesity, and metabolic syndrome. Table 2.1 provides information on these essential proteins. Proteins such as Vascular cell adhesion protein 1, Cell adhesion molecule 1, CD44 antigen, Atrial natriuretic peptide receptor 3, Alpha-2-macroglobulin, Monocyte differentiation antigen CD14, Annexin A2, Complement C3, and C4 proteins, Calreticulinm, Urotensin-2B, Protein S100-A4, Galectin 3 were upregulated, and similarly, some of the downregulated proteins included were Lanosterol synthase, Acid ceramidase, Cathepsin D, Cathepsin L1, Carboxypeptidase E, Metalloproteinase inhibitor 2, Meteorin- like protein, etc. In our previous study, we have shown that MG downregulates enzymes such as lanosterol synthase involved in cholesterol biosynthesis.[197]

Table 2.1 Differentially expressed secretory proteins involved in insulin resistance

Accession Number	Gene Name	Protein Name	p-value	Fold change	Reference
UPregulated proteins					
P29534	**Vcam1**	**Vascular cell adhesion protein 1**	**7.13E-07**	**10.82**	**[198]**
P26051	**Cd44**	**CD44 antigen**	**3.15E-11**	**6**	**[199]**
Q6AYP5	**Cadm1**	**Cell adhesion molecule 1**	**0.00059**	**5.73**	**[200]**
P41740	**Npr3**	**Atrial natriuretic peptide receptor 3**	**8.55E-07**	**5.06**	**[201]**
P01946	**Hba1**	**Hemoglobin subunit alpha-1/2**	**0.0006**	**4.96**	**[202]**
Q63691	**Cd14**	**Monocyte differentiation antigen CD14**	**0.00015**	**3.26**	**[203]**

P06238	**A2m**	**Alpha-2-macroglobulin**	**0.00919**	**3.24**	**[204]**
Q07936	**Anxa2**	**Annexin A2**	**1.38E-06**	**3.19**	**[205]**
P24090	**Ahsg**	**Alpha-2-HS-glycoprotein**	**0.04601**	**2.65**	**[206]**
P08649	**C4**	**Complement C4**	**0.00393**	**2.62**	**[207]**
P0C5H9	**Manf**	**Mesencephalic astrocyte-derived neurotrophic factor**	**0.00685**	**2.46**	**[208]**
P18418	**Calr**	**Calreticulin**	**1.45E-06**	**2.21**	**[209]**
P01026	**C3**	**Complement C3**	**0.02878**	**2.13**	**[210]**
Q765I2	**Uts2b**	**Urotensin-2B**	**0.04336**	**2.09**	**[211]**
P38659	**Pdia4**	**Protein disulfide-isomerase A4**	**0.00165**	**2.05**	**[212]**
P05942	**S100a4**	**Protein S100-A4**	**0.00119**	**1.98**	**[213]**
P08699	**Lgals3**	**Galectin-3**	**3.99E-05**	**1.77**	**[214]**
P13084	**Npm1**	**Nucleophosmin**	**0.04491**	**1.69**	**[215]**
P62963	**Pfn1**	**Profilin-1**	**6.86E-05**	**1.45**	**[216]**
Downregulated proteins					
P05371	**Clu**	**Clusterin**	**4.84E-09**	**3.48**	**[217]**
P51886	**Lum**	**Lumican**	**2.68E-05**	**3.39**	**[218]**
Q9WV75	**Spon2**	**Spondin-2**	**1.61E-09**	**3.3**	**[219]**
P53813	**Pros**	**Vitamin K-dependent protein S**	**0.00271**	**2.99**	**[220]**
P42930	**Hspb1**	**Heat shock protein beta-1**	**4.73E-07**	**2.64**	**[221]**
P16612	**Vegfa**	**Vascular endothelial growth factor A**	**5.86E-05**	**2.52**	**[222]**
Q5RJL6	**Metrnl**	**Meteorin-like protein**	**1.43E-06**	**2.47**	**[223]**
P30121	**Timp2**	**Metalloproteinase inhibitor 2**	**4.21E-10**	**2.4**	**[224]**

P02466	**Col1a2**	**Collagen alpha-2(I) chain**	**2.4E-05**	**2.02**	**[225]**
P15087	**Cpe**	**Carboxypeptidase E**	**4.05E-05**	**1.99**	**[226]**
P07154	**Ctsl**	**Cathepsin L1**	**4.38E-05**	**1.97**	**[227]**
P24268	**Ctsd**	**Cathepsin D**	**0.00269**	**1.97**	**[228]**
Q6P7S1	**Asah1**	**Acid ceramidase**	**0.0174**	**1.65**	**[229]**
P48450	**Lss**	**Lanosterol synthase**	**0.03092**	**1.46**	**[197]**

2.3.3 **Conclusion**

This is the first study that describes the secretome of muscle cells in response to methylglyoxal treatment in muscle cells. About 180 proteins were identified to be secretory proteins either with SignalP or SecretomeP. The differentially expressed secretory proteins were involved in various pathways like ECM-receptor interaction, leukocyte transendothelial migration, fluid shear stress and atherosclerosis, complement and coagulation cascades, and lysosomal pathway.

Chapter 3

Study of methylglyoxal induced secretome in clinical samples

Content of this chapter are published as research article in *ACS omega* 5, no. 39 (2020): 25016-25028. https://doi.org/10.1021/acsomega.0c01318

Chapter 3 Study of methylglyoxal induced secretome in clinical subjects

3.1 Background

Hyperglycemic condition in diabetes promotes glycation and formation of reactive carbonyls such as glyoxal, methylglyoxal, which can, in turn, modify proteins leading to the formation of carboxyethyllysine (CEL) and Argpyrimidines (ARGPYR)[89, 230]. In severe diabetes, due to elevated levels of MG, it is expected that MG associated modifications such as CEL and ARGPYR can be observed in plasma proteins. Human Serum albumin has been considered as a primary target for glycation due to its abundance, many lysine and arginine residues, and relatively long half-life[231, 232]. We, therefore, studied MG associated modification of HSA, which could reflect elevated levels of MG. Label-free SWATH-MS approach was used for the quantification of MG modified peptides.

3.2 Material and Methods

3.2.1 **Chemicals**

All fine chemicals and reagents were obtained from Sigma-Aldrich (St. Louis, MO, USA). Bradford protein estimation kit was purchased from Bio-Rad Laboratories, USA. 3 kDa cut-off centrifugal filters and C18 Zip-Tip® desalting columns were procured from Millipore (Millipore, Billerica, MA, USA). Liquid chromatography columns EksigentTrap (ChromXP C-18-CL – 0.35 x 0.5 mm, 3 µm, 120 Å) and analytical Nano column (ChromXP3C-18-CL– 0.075 x 15mm, 3 µm, 120 Å) were procured from Sciex (Sciex, Framingham, MA, USA). RapiGest™ SF surfactant was purchased from Waters (#186001860, Waters Corporation, MA, USA). All solvents were for LC-MS procured from J.T. Baker (J T. Baker, PA, USA). ELISA kit sCD44std Instant ELISA was procured from Thermo (#BMS209INST, eBioscience, Vienna, Austria).

3.2.2 **Clinical sample details**

Clinical plasma proteomics was performed to validate the results of methylglyoxal induced L6 cell secretome. Clinical plasma samples were collected from Chellaram Diabetes Institute, Pune, India, as per the guidelines of the Indian Council of Medical Research. The approval of the Institutional Ethics committee was taken for the study, and informed consent was obtained from all the subjects before the blood collection. Only subjects with no history of other chronic clinical disorders such as liver or kidney disease, thyroid disorders, or pregnancy were included in the study. Proteomics study and ELISA study both comprised of Healthy subjects (n=10) and diabetic subjects (n=10). Plasma preparation was done by collecting peripheral venous blood in EDTA vacutainers (BD Biosciences). After the sample collection, biochemical parameters such as fasting blood glucose, glycated hemoglobin (HbA_{1c}) were analyzed immediately. Details of patients are given in (Appendix 1). Erythrocytes were separated from plasma by centrifugation at 200 ×g for 5 min. Next, the supernatant was centrifuged at 9,300 ×g for 15 min, and plasma was carefully separated plasma and stored at -80 °C until use.

3.2.3 **In-solution Trypsin Digestion**

100 µg of total protein in 0.1% RapiGest for each plasma sample was used for digestion. Before reduction and alkylation, proteins were denatured by incubating at 80 °C for 15 min. Further, proteins were reduced using 100 mM dithiothreitol for 15 min at 60 °C and then alkylated by treating with 200 mM iodoacetamide for 30 min in the dark at room temperature. Trypsin was added at 1:25 (w/w) enzyme to protein ratio and incubated at 37°C for 18 h, 2 µl formic acid was added to inactivate trypsin and stop the digestion. For desalting of the digested peptides, C18 Zip tips were used, and the desalted peptides were concentrated using Speed vac. For LC-MS analysis, peptides were reconstituted in 3% acetonitrile with 0.1% formic acid.

3.2.4 SWATH-MS Analysis for Clinical Plasma

3.2.4.1 LC-MS Conditions

The trypsin digested samples (healthy and diabetic) were desalted offline by ZipTip (Millipore, USA) and loaded on to an EksigentTrap (ChromXP C-18-CL – 0.35 x 0.5 mm, 3 µm, 120 Å) and analytical Nano column (ChromXP3C-18-CL– 0.075 x 15mm, 3 µm, 120 Å) fitted with Eksigent nano-LC-Ultra® 2D System, which was connected to a Triple TOF 6600 mass spectrometer (Sciex, Ontario, Canada). Peptides were separated on nanoLC using the following mobile phase composition: water/acetonitrile/formic acid (A, 98/2/0.2%; B, 2/98/0.2%). The flow rate was kept at 300 nl/min, and 2000 ng of each sample was injected on the column. An overall 3.5 h gradient run was used for separation, which started with 5 min of 5% B, followed by a linear increase of B to 35% in 80 min and further increase to 50% B in 90 min. In the end, mobile phase B was increased to 90% in 1 min and maintained for 13 min after which the gradient was brought back to the initial 5% B in 1 min and held for 6 min.

3.2.4.2 MS/MS Conditions

The sample data was acquired in information-dependent acquisition (IDA) mode using an ESI ion source. The ESI source was maintained at a voltage of 2300 V, and a temperature of 130 °C, with curtain gas of 25 psi, nebulizer gas of 20 psi, and heater gas of 10 psi. For MS survey scan, mass range m/z 350-1250 was scanned with a resolution ≥ 30,000 FWHM (Full Width at Half Maxima) with an accumulation time of 250 ms. For MS/MS, 35 product ion scans over the mass range m/z 100–1600 were collected in high sensitivity mode. The criteria for precursor selection for MS/MS were set at a threshold of more than 120 counts per second and charge state of 2+ to 5+. Also, the dynamic exclusion for precursor selection was set for 3 s. Collision energy (CE) for fragmentation was optimized for each precursor using an IDA CE parameter script, and collision energy spread (CES) was set at 5 eV. The total cycle time for the survey scan and product ion scan was set at 2.35 s.

3.2.4.3 Label-Free Quantitation

Label-free quantification was performed using SWATH-MS, wherein the mass range of 350-1250 Da was divided into a set of 75 overlapping windows of 12 Da each with 1 Da overlap between each window. The CE for each window was optimized, and a CES of 5 eV was set. MS/MS scans were acquired in high sensitivity mode with a mass resolution of 15,000. The total duty cycle comprised of one MS survey scan of 50 ms and 75 MS/MS scans of 50 ms each. Each sample was acquired in triplicate runs for quantification. The raw mass spectrometric data for all IDA and SWATH runs is deposited at the public repository PeptideAtlas (PASS01478).

3.2.4.4 SWATH Data processing

The IDA runs were searched against the UniProt protein database (release 2018_04; 20,341 reviewed protein entries) limited to *Homo sapiens* taxonomy with ProteinPilot™ v5.0 software. For the analysis, cysteine alkylation was set to iodoacetamide and digestion to trypsin. The search was performed using biological modifications as ID focus and thorough ID as a search effort. FDR for peptide identification was set to 1%. Proteins having at least two unique peptides with a minimum 95% confidence and detected with less than 1% FDR were considered for relative quantitation analysis.

The result of the IDA analysis was used as a reference spectral library for SWATH processing using PeakView® v2.2 software. The spectral library was imported and filtered by setting the mass tolerance to 50 ppm, peptide confidence to 99%, number of peptides to 5, and number of transitions to 6. Peptides shared between 2 or more protein families were excluded from quantitation. Further, the proteins whose peptides passed the 1% FDR criteria set in the SWATH™ 2.0 plugin of PeakView were exported to MarkerView™ v 1.2.1. Statistical analysis was performed in MarkerView using a t-test, and those proteins with a p-value ≤ 0.05 were considered for quantitation. The proteins having fold change ≥ 1.3 or ≤ 1.3 were considered as differentially expressed in our experiment.

3.2.5 **Data analysis for Quantification of methylglyoxal modified peptides**

Skyline (version4.1.0 , MacCoss lab) was used for the quantification of peptides using SWATH .wiff files. FASTA file of human serum albumin was used for theoretical mass spectral library generation. Unmodified peptides and corresponding carboxyethyl modified peptides of albumin were specified for the targeted quantification of peptides. Retention times of precursors were manually corrected wherever required. Only intense and co-eluting fragment ions of a particular precursor were considered for quantification. The Sum of the area under the curve of these selected fragment ions was used for the quantification of the precursor. Digestion enzyme was specified as trypsin. The maximum missed cleavage was set to 1. Carbamidomethylation at cysteine (57.021464 Da), MG-H1 at arginine (54.01565 Da), and carboxyethyl modification at lysine and arginine (72.021126 Da) were specified as methylglyoxal associated modifications. Precursor ion charge states were specified as +2 and +3, whereas fragment ion charge states were specified as +1 and +2. Fragment ion mass tolerance was set to 0.5 Da. The acquisition method was selected as DIA, and the product mass analyzer was set as TOF. The isolation scheme was selected as SWATH (15 m/z) at resolving power of 15,000. The peak area of the modified peptide was normalized with the peak area of its corresponding unmodified peptide. CEL modified peptide content in diabetic plasma was expressed as a fold change ratio of the normalized peak area of CEL modified peptide of diabetic plasma to the normalized peak area of CEL modified peptide of healthy plasma.

3.2.6 **ELISA**

20 µl of the prediluted human plasma samples (1:60) were added to each well, and the volume was made up with 130 µl distilled water. The plate was covered and incubated for 3 h at room temperature with intermittent agitation on a microplate shaker. The plate was washed thrice with 400 µl per well wash buffer. After the washes, the excess wash buffer was removed by tapping the plate on an absorbent pad. 100 µl of TMB substrate solution was added to all wells, including the blank wells, and incubated at room temperature for about 10 min. The enzyme reaction was stopped by adding 100 µl of stop solution into each well, and the absorbance of each microwell was recorded at 450 nm. The standard curve of CD44 was plotted in the concentration range of 62.5 pg/ml to 4000 pg/ml, and CD44 concentration in the plasma was calculated by

elisaanalysis.com online software using 4-Parameter Logistic Regression algorithm. Box plot of CD44 concentration was plotted for healthy and diabetic subjects using a web app PlotsOfData[233].

3.2.7 Statistical analysis

The clinical plasma proteomic analysis was performed for 10 plasma samples each of healthy control and diabetic subjects in technical triplicates for each sample, and ELISA was performed in duplicates for the same set of plasma samples. Statistical analysis was performed by Student's t-test for quantitation of proteomic data, peptide quantification in clinical plasma, and for ELISA. Data were expressed as mean ± SEM. A p-value ≤ 0.05 was considered statistically significant. For proteomic analysis, the proteins with more than 2 matching peptides and fold change difference of ≥ 1.3 in protein expression were assessed.

3.3 Results and Discussion

3.3.1 Elevated levels of methylglyoxal modified serum albumin peptides in diabetic plasma

Hyperglycemic condition in diabetes promotes glycation and formation of reactive carbonyls such as glyoxal, methylglyoxal, which can, in turn, modify proteins leading to the formation of carboxyethyllysine (CEL) and Argpyrimidines (ARGPYR)[89, 230]. In severe diabetes, due to elevated levels of MG, it is expected that MG associated modifications such as CEL and ARGPYR can be observed in plasma proteins. Human Serum albumin has been considered as a primary target for glycation due to its abundance, many lysine and arginine residues, and relatively long half-life[231, 232]. We, therefore, studied MG associated modification of HSA, which could reflect elevated levels of MG. Label-free SWATH-MS approach was used for the quantification of MG modified peptides. The peptides and their fragments that are consistently observed in all the samples were considered for analysis (Figure 3.1A,3.1B). The y ions were considered for peptide quantification as they were more intense than b ions[234]. Sum of the area under the curve (AUC) of selected y ions were used for peptide quantification. Two peptides,

F**K**DLGEENFK and **K**VPQVSTPTLVEVSR, showed CEL modification of lysine residues, and their intensities were found to be high in diabetic plasma. The peak area of CEL modified peptides in healthy and diabetic plasma samples was normalized with the peak area of their corresponding unmodified peptide. The increase in CEL modification in diabetes was expressed as a fold change over healthy control (Figure 3.1C). The level of CEL modified peptide FK*(CEL)*DLGEENFK in diabetic subjects was 1.31 fold higher than in healthy subjects. Similarly, the level of CEL modified albumin peptide K*(CEL)*VPQVSTPTLVEVSR in diabetic subjects was 1.47 fold higher as compared to healthy subjects. Details of precursor and fragment ions used for quantification are summarized in (Table 3.1), The retention time of quantified peptides has shown in (Figure 3.2), The normalized CEL-modified area for both peptides is shown in (Figure 3.3).

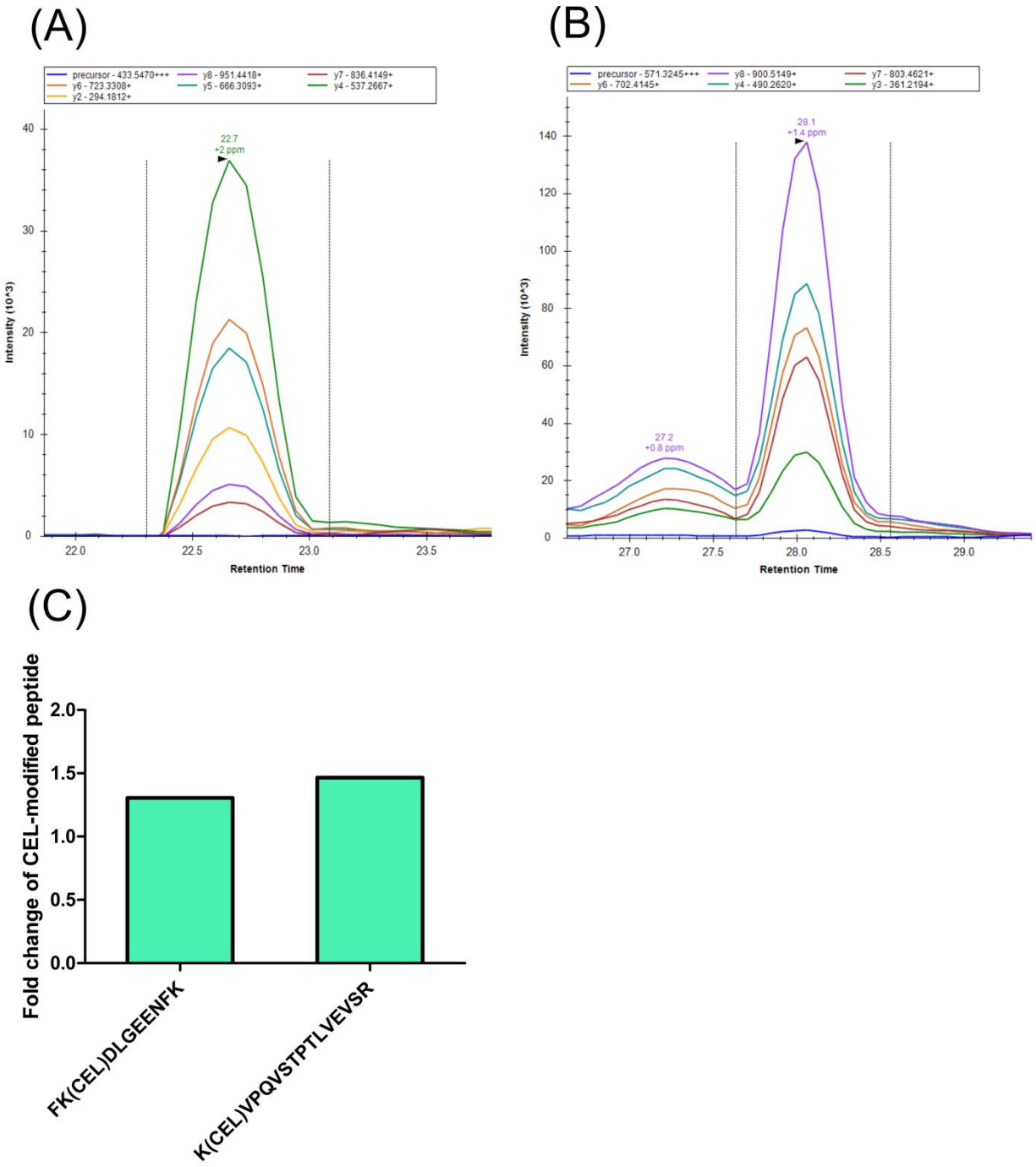

Figure 3.1 Quantification of CEL-modified peptides

Representative extracted ion chromatograms showing co-elution of y fragment ions of CEL-modified peptides (A) FK*(CEL)*DLGEENFK and (B) K*(CEL)*VPQVSTPTLVEVSR of human serum albumin in diabetic plasma (C) Fold change in expression of CEL-modified albumin

peptides FK*(CEL)*DLGEENFK and K*(CEL)*VPQVSTPTLVEVSR in plasma sample of diabetic subjects compared to healthy subjects.

Table 3.1 Details of precursors and fragments used in quantification

Sr. No	Modification site	Peptide sequence	Charge state	Modification	Monoisotopic m/z	Fragments ion (m/z) used for quantification
1	K36	FKDLGEENFK	+3	Unmodified	409.5399	$y2^+$ (294.1812)
						$y4^+$ (537.2667)
						$y5^+$ (666.3093)
						$y6^+$ (723.3308)
						$y7^+$ (836.4149)
						$y8^+$ (951.4418)
2	K36	FKDLGEENFK	+3	CEL	433.547	$y2^+$ (294.1812)
						$y4^+$ (537.2667)
						$y5^+$ (666.3093)
						$y6^+$ (723.3308)
						$y7^+$ (836.4149)
						$y8^+$ (951.4418)
3	K438	KVPQVSTPTLVEVSR	+3	Unmodified	547.3174	$y3^+$ (361.2194)
						$y4^+$ (490.262)
						$y6^+$ (702.4145)
						$y7^+$ (803.4621)

						$y8^+$ (900.5149)
4	K438	KVPQVSTPTLVEVSR	+3	CEL	571.3245	$y3^+$ (361.2194) $y4^+$ (490.262) $y6^+$ (702.4145) $y7^+$ (803.4621) $y8^+$ (900.5149)

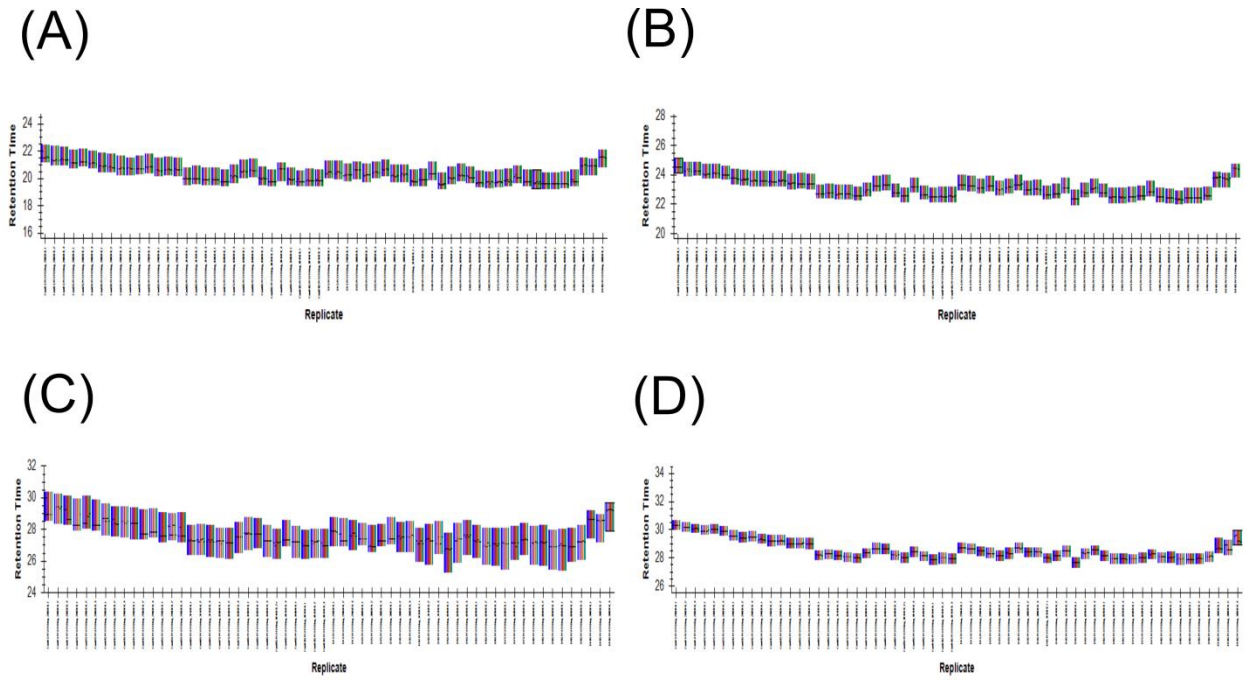

Figure 3.2 Retention time of quantified peptides

(A) Unmodified FKDLGEENFK (B) CEL modified FK*(CEL)*DLGEENFK (C) Unmodified KVPQVSTPTLVEVSR (D) CEL modified K*(CEL)*VPQVSTPTLVEVSR

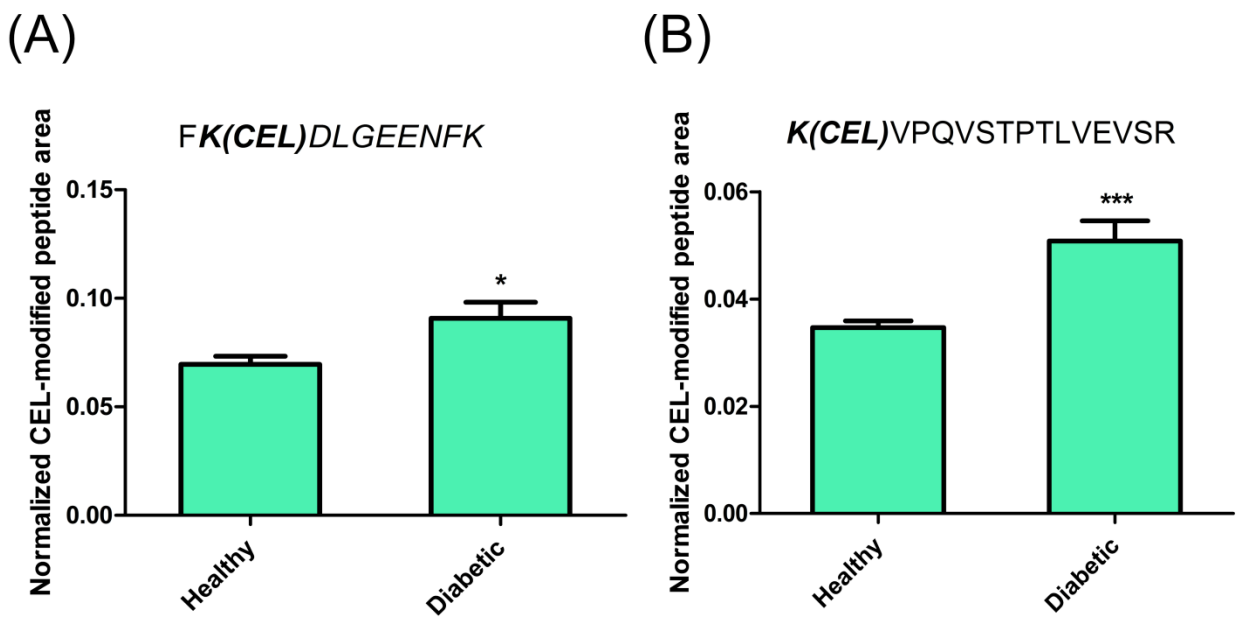

Figure 3.3 Normalized CEL-modified peptide area

(A) and (B) show significant increase in CEL-modification of peptides F***K(CEL)***DLGEENFK (p-value ≤ 0.0141) and ***K(CEL)***VPQVSTPTLVEVSR (p-value ≤ 0.0001), respectively from albumin in plasma of diabetic subjects as compared to healthy subjects.

3.3.2 **Proteomic Analysis of Clinical Plasma**

The usefulness of MG-induced secretome was studied in clinical plasma. Since MG levels increase in diabetes, it is expected that some of the secreted proteins observed in cell culture may also be found in clinical plasma. Therefore, to identify such proteins, SWATH-MS was performed to identify and quantify MG associated secreted proteins in the plasma. Tryptic digest of clinical plasma was subjected to expression analysis using SWATH-MS workflow. A total of 238 proteins were identified in the spectral library obtained from IDA (Appendix 4), out of which 37 proteins were upregulated, and 13 proteins were downregulated by more than 1.3 fold (Figure 3.4A). All the differentially expressed proteins (Appendix 5) were significant at p-value

< 0.05. Out of the total identified proteins, 189 proteins were identified with SignalP and 24 proteins with SecretomeP (Figure 3.4B). KEGG Pathway analysis was done using Cytoscape software with a plugin clusterMaker. The differentially expressed proteins were found to be involved in pathway Complement and coagulation cascades (Figure 3.4C). Among differentially expressed proteins, upregulated proteins were Complement C1r subcomponent, Complement C1s subcomponent, Vitronectin, Complement C5, Complement component C7, Fibrinogen alpha chain, Coagulation factor XIII A chain, Vitamin K-dependent protein S, Plasma kallikrein, Plasma serine protease inhibitor; while downregulated proteins included Complement C3, Antithrombin-III, Plasma protease C1 inhibitor, and Complement C4-A. Interestingly, two pathways, mainly complement system and ECM receptor interaction, were shared between MG induced secretome and diabetic plasma.

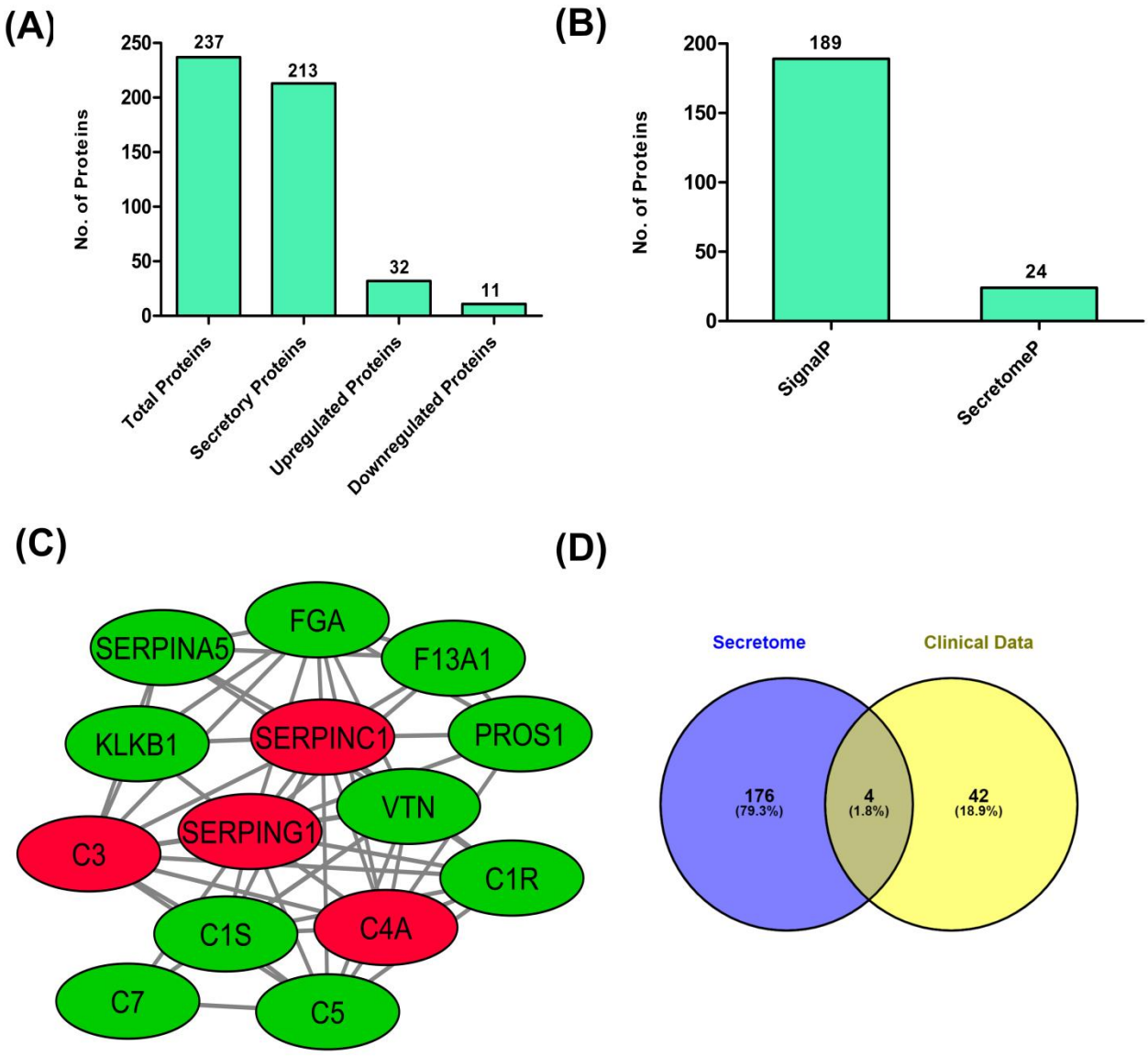

Figure 3.4 Proteomic Analysis for Clinical Plasma

Differential proteomics analysis was done by SWATH-MS. (A) The number of differentially expressed proteins in Diabetic-Healthy Control. (B) The number of secretory proteins obtained through SignalP and SecretomeP. (C) PPI network cluster showing proteins involved in complement and coagulation cascades; green indicates > 1.3 fold higher abundance, and red indicates > 1.3 fold lesser abundance in diabetic subjects. (D) Venn diagram showing the common proteins in secretome and clinical data.

3.3.3 CD44 antigen protein was found common among secretome and clinical data

To identify MG induced secreted proteins in the clinical plasma, the differentially expressed proteins from secretome and clinical plasma were analyzed for the presence of common proteins. There was a scarce overlap between MG-induced secretome and plasma proteins since plasma is a heterogeneous matrix that represents proteins secreted from various tissues, including muscle cells, liver, adipose, and nervous tissue. Amongst 189 proteins identified, only four proteins were observed to be common between MG induced secretome and clinical plasma (Figure 3.4D); however, only one protein, particularly CD44 antigen protein, showed a common trend in both the groups (Table 3.2). CD44 antigen protein was found to be upregulated with a six-fold change in MG induced secretome and 1.89 fold in diabetic plasma.

Table 3.2 Common proteins between cell secretome and clinical plasma proteome

Sr. No	Protein name	fold change (Secretome)	fold change(Clinical plasma proteomics)
1	Complement C1s subcomponent	3.02 Down	2.48 Up
2	Vitamin K-dependent protein S	2.99 Down	2.09 Up
3	**CD44 antigen**	**6** Up	**1.88** Up
4	Complement C3	2.13 Up	1.71 Down

3.3.4 Validation of CD44 antigen protein by ELISA in Clinical subjects

To validate CD44, an MG induced secreted protein upregulated in diabetes, ELISA was performed in duplicates in the plasma from healthy and diabetic subjects (n=10 from each group). The CD44 median for healthy and diabetic subjects was 1321 pg/mL and 1840 pg/mL, respectively (Figure 3.5A). Fold change was calculated, which showed a similar trend as that of

proteomics data, and the protein was found to be 1.6 fold upregulated in diabetic plasma (Figure 3.5B).

CD44 is a multifunctional cell surface receptor molecule. It interacts with hyaluronan and osteopontin and regulates inflammatory and proinflammatory responses. It exists in several isoforms due to alternate splicing mechanisms[235]. The protein is expressed in several cell types and is involved in various disease conditions, including insulin resistance, obesity, metabolic syndrome, diabetes, and cancer[236][237][238]. The levels of CD44 were found to be significantly increased in insulin-resistance conditions (IR) in a study involving 58 healthy, overweight, and moderately obese white adult participants. The elevated level of CD44 gene was accompanied with increased expression of OPN, CD68 and IL6[199]. In another study, CD44 protein levels were positively correlated with insulin resistance as measured by HbA_{1c} ($n = 55$, $r = 0.49$, p-value < 0.001) and HOMA-IR ($n = 55$, $r = 0.29$, p-value < 0.03). Similarly, genome-wide association studies, as well as computational biology studies involving analysis of microarray data, suggested that CD44 plays an important role in the pathogenesis of adipose tissue inflammation and insulin resistance[239]. Further studies are required to develop CD44 as a molecular marker for dysregulated methylglyoxal metabolism.

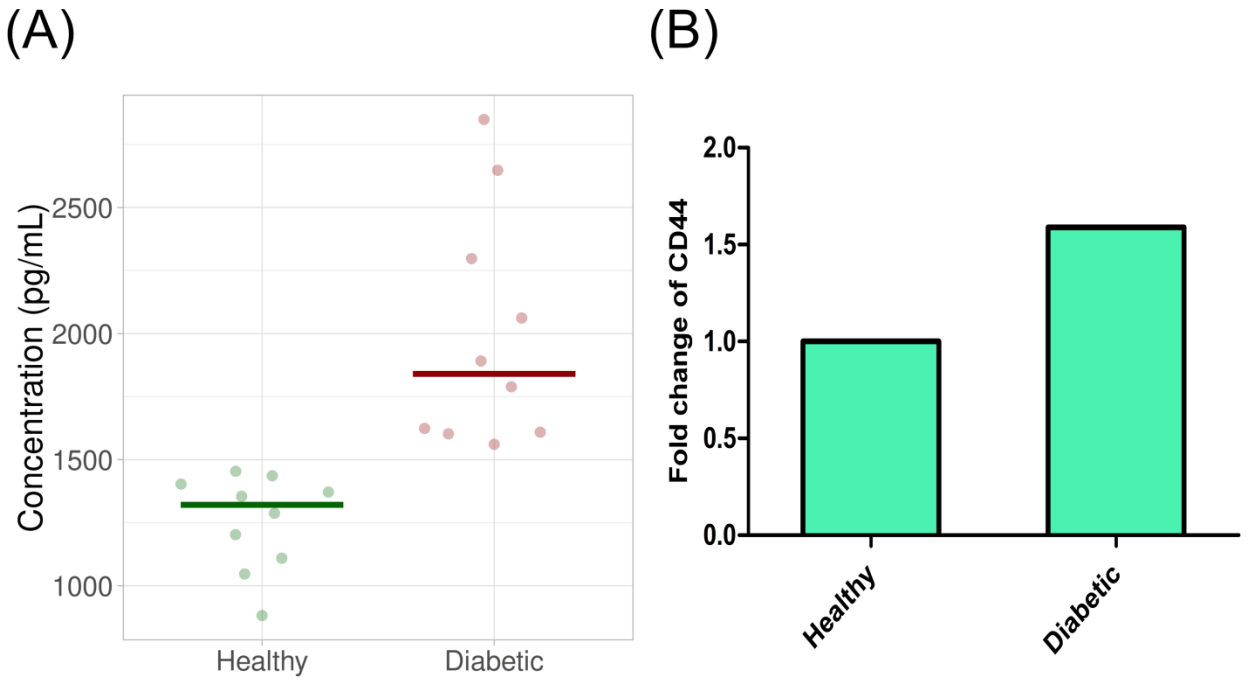

Figure 3.5 Validation of CD44 antigen protein by ELISA in Clinical plasma

(A) Box plot of CD44 concentration was plotted for healthy and diabetic subjects (n=10 each group). The CD44 median for healthy and diabetic subjects was 1321 pg/mL and 1840 pg/mL, respectively. (B) Fold change bar graph showing a higher abundance of CD44 in diabetic subjects. (p-value < 0.0002)

3.4 Conclusion

To identify the MG induced secreted proteins in the clinical plasma, the proteins identified in the plasma were compared with the MG induced secreted proteins in the muscle cells. CD44 was found to be a common protein between MG induced secretome and clinical plasma proteome. It was found to be upregulated in the diabetic plasma as measured by ELISA and has a role in the development of insulin resistance. The elevated levels of CD44 were accompanied by an increase in MG induced CEL modifications of two HSA peptides, FKDLGEENFK and KVPQVSTPTLVEVSR, suggesting that the high levels of CD44 could be associated with an increase in the levels of MG in diabetes. The graphical abstract for secretome and clinical plasma proteomics is shown in (Figure 3.6).

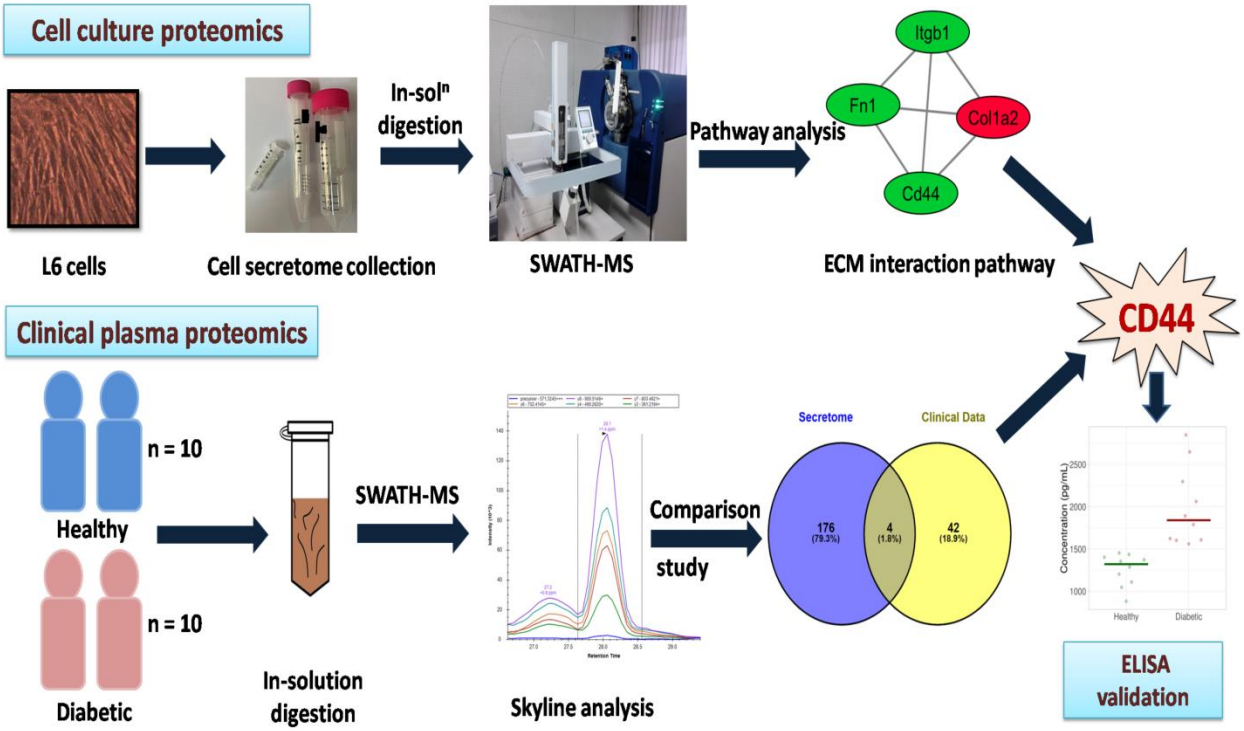

Figure 3.6 Graphical abstract for secretome and clinical plasma proteomics

Chapter 4

Total cell proteomics of skeletal muscles to understand the role of methylglyoxal in the development of insulin resistance

Chapter 4 Total cell proteomics of skeletal muscles to understand the role of methylglyoxal in the development of insulin resistance

4.1 Background

Insulin resistance is an essential hallmark of type 2 diabetes, where it is a driver of hyperglycemia. Insulin resistance is a condition when cells fail to respond appropriately to insulin. Molecular mechanisms known are serine phosphorylation of IRS, which weakens signal transduction, and increased expression of P85α, which decreases the activity of PI3K[53]. Hyperglycemia also leads to excess formation of toxic glycolytic intermediates like methylglyoxal. Additionally, lack of exercise, sedentary lifestyle, and contemporary eating habits involve consuming carbohydrate-rich, thermally processed, and fermented food items, which further elevate exposure to MG [197]. MG not only induces various diabetic complications but it also aggravates insulin resistance To maintain whole-body glucose, the insulin-sensitive cells such as skeletal muscles and adipose tissues are involved in glucose homeostasis.

Various studies have shown that in skeletal muscle cells and adipocytes, insulin-induces glucose uptake occurs via glucose transporter 4 (GLUT4) translocation to the membrane place[240]. While insulin resistance results from impairment in glucose transport efficiency and GLUT4 activity [241]. Skeletal muscles are responsible for up to 75% of insulin-dependent glucose disposal. Chronic MG has accounted for inducing type 2 diabetes and causing pancreatic β-cell dysfunction. However, the mechanisms of MG induced insulin resistance is still not entirely known. Since altered insulin signaling underlies the final manifestation of the syndrome, we have analyzed MG's effect on total cell proteomics of skeletal muscles.

4.2 Materials and methods

4.2.1 Chemicals

All fine chemicals and reagents were obtained from Sigma-Aldrich (St. Louis, MO, USA). Dulbecco's Modified Eagle Medium (DMEM) for cell culture was procured from HiMedia. Fetal bovine serum (US origin), 2-NBDG (2-(N-(7-Nitrobenz-2-oxa-1,3-diazol-4-yl)Amino)-2-Deoxyglucose), and trypsin were purchased from Invitrogen (Carlsbad, CA, USA). Plasticware for tissue culture was procured from Nunc (Rochester, NY, USA). Bradford protein estimation kit was purchased from Bio-Rad Laboratories, USA. Liquid chromatography columns Eskigent C18-RP HPLC column (100×0.3mm, 3µm, 120 Å) were procured from Sciex (Sciex, Framingham, MA, USA). RapiGest™ SF surfactant was purchased from Waters (#186001860, Waters Corporation, MA, USA). All LC-MS grade solvents were procured from J.T. Baker (J T. Baker, PA, USA).

4.2.2 Cell culture and Differentiation

Rat L6 muscle cells were procured from the National Centre for Cell Sciences, Pune. They were grown in DMEM media supplemented with 10% (v/v) heat-inactivated fetal bovine serum (FBS). The cells were maintained at 37°C in a humidified atmosphere containing 5% (v/v) CO_2. Cells were differentiated in DMEM media supplemented with 2% FBS for 6 days, and the progress of differentiation was monitored microscopically.

4.2.3 Apoptosis assay

Oxidative stress and apoptosis are initial signs of diabetic complications. Translocation of phosphatidylserine (PS) to the external cell membrane is an early indicator of apoptosis, and since annexins have a high affinity for PS, Annexin V conjugated to fluorescent tags can be used for the detection of apoptotic cells. Propidium iodide is a fluorescent DNA binding dye that does not enter live cells and hence, was used to detect dead cells. Thus, simultaneous staining with Annexin V-FITC and PI can be used to differentiate early and late apoptotic cells from necrotic dead cells. L6 Rat muscle cells were seeded on 6-well plates and allowed to grow up to 80% confluence, followed by 4 h serum starvation. Cells were then treated with methylglyoxal and

harvested using trypsin after 3 h. The percentage of apoptotic cells was determined using Annexin V-FITC Apoptosis Detection Kit (Sigma) as per the manufacturer's instructions. Briefly, the harvested cells were resuspended in 1X Annexin Binding Buffer and incubated with Annexin V-FITC and Propidium iodide followed by flow cytometry acquisition on BDAccuri C6 Cytometer using 488 nm excitation laser. For each treatment, 10,000 cells were analyzed, and Annexin V-FITC and PI staining were monitored on the green channel (530/30nm) and red channel (585/40 nm), respectively. Appropriate quadrants were set to detect viable cells (negative for both dyes), early apoptotic cells (positive for Annexin V), late apoptotic cells (positive for both dyes), and necrotic cells (positive for PI).

4.2.4 **2-NBDG Glucose uptake study**

To test the effect of MG on glucose uptake in L6 cells, we performed 2-NBDG based glucose uptake assay. 2-NBDG is a fluorescent glucose analog that has been used to monitor glucose uptake in live cells as an indicator of cell viability. Although sensitive to its environment,2-NBDG fluorescence typically displays excitation/emission maxima of ~465/540 nm and can be visualized using optical filters designed for fluorescein. Briefly, L6 cells were seeded in Dulbecco's Modified Eagle's Medium (DMEM) supplemented with 10% (v/v) heat-inactivated FBS (Fetal Bovine Serum) at a density of 10^3 cells per well into a 96-well culture plate and were grown for 24 h. Cells were kept in 2% FBS medium for 6 days for differentiation of myoblasts into myotubes. Differentiated cells were starved for 4 h in serum-free DMEM; medium was then replaced with serum-free medium, and the cells were treated with methylglyoxal at 37°C in a humidified atmosphere containing 5% (v/v) CO_2. 100 µM 2-NBDG was added to the cells, simultaneously, with 100 nM insulin after 30 min; then, the reaction was stopped using chilled PBS. After two PBS washes, fluorescence was read on a Varioscan plate reader using excitation/emission maxima of ~465/540 nm.

4.2.5 **Protein extraction**

After serum starvation, the differentiated L6 cells were treated with MG for 3 h, followed by treatment with 100nM insulin for 30 min, washing with Dulbecco's phosphate-buffered saline

and harvesting with trypsin. The action of trypsin was stopped by the addition of DMEM containing 10% FBS. Cells were pelleted by centrifuging at 2000 rpm, for 5 min. The cell pellet was washed twice with ice-cold PBS; protease and phosphatase inhibitor cocktail were added, and protein extraction was carried out. Cells treated with insulin were used as a control for the experiment. Cells were solubilized in 50 mM ammonium bicarbonate buffer containing 0.1% Rapigest SF(Waters), a mass spectrometry compatible detergent. Cells were incubated in lysis buffer for 30 min on ice with brief vortexing after every five minutes. Whole-cell lysates were cleared by centrifugation at 25,000×*g* for 50 min at 4 °C. Bradford's assay was used for protein quantification.

4.2.6 **In-solution Trypsin Digestion**

100 µg of total protein in 0.1% RapiGest SF was used for digestion. Before reduction and alkylation, proteins were denatured by incubating at 80 °C for 15 min. Further, proteins were reduced using 100 mM dithiothreitol for 15 min at 60 °C and then alkylated by treating with 200 mM iodoacetamide for 30 min in the dark at room temperature. Trypsin was added at 1:25 (w/w) enzyme to protein ratio and incubated at 37°C for 18 h, 2 µl formic acid was added to inactivate trypsin and stop the digestion, and the surfactant RapiGest was precipitated by incubating at 37 °C for 45 min followed by centrifugation at 14000 g for 15 min. The precipitated surfactant was discarded, and the digested peptide supernatant was collected.

4.2.6.1 Desalting of peptides

Desalting of the digested peptides was done through C18 chromatography using Zip tips (miniature C18 columns) (Millipore, Billerica, MA). Zip tips were activated and equilibrated with acetonitrile and 0.1% formic acid, respectively, followed by sample binding and desalting using 0.1% formic acid. Then peptides were eluted in 50% acetonitrile with 0.1% formic acid. Eluate was concentrated using a vacuum concentrator. For LC-MS analysis, peptides were reconstituted in 3% acetonitrile with 0.1% formic acid.

4.2.7 Liquid Chromatography-Mass Spectrometry Analysis

4.2.7.1 SWATH-MS Analysis

SWATH analysis was performed on a Triple-TOF 5600 (AB Sciex; Concord, Canada) mass spectrometer coupled with Micro LC 200 (Eksigent; Dublin, CA) in high-sensitivity mode. A spectral library was generated by pooling equal amounts of peptide samples from each treatment and analyzing them by Information dependent acquisition (IDA). Briefly, peptides were separated on an Eksigent C18-RP HPLC column (100×0.3mm, 3µm, 120 Å) using a 95 min gradient of 3% to 35% mobile phase B at a flow rate of 8 µL/min (mobile phase A: water with 0.1% formic acid mobile phase B: acetonitrile with 0.1% formic acid). Accumulation time for MS was 250 ms and for MS/MS was 100 ms. Fragmentation was done using rolling collision energy. For SWATH-MS acquisition, the precursor mass range of 400–1250 m/z was divided into a set of 34 overlapping windows of 25 m/z each. For MS/MS, collision energy was optimized for each window, and spectra were collected from 100 to 2000 m/z. Fragment ion scans were performed over an accumulation time of 70 ms, while for the precursor survey scan, it was 100 ms. All samples were acquired in biological and technical triplicates.

To get spectral library from IDA run, data was analyzed by ProteinPilot™ software version 5.0 using UniProt *Rattus norvegicus* database updated with Uniprot release 2019_12; 8086 reviewed protein entries. The enzyme used for digestion was set to trypsin, and carbamidomethylation of cysteine residues was selected as a fixed modification. The search was performed using a False Discovery Rate (FDR) of 1%. The resultant spectral library was imported into PeakView v2.2 software, and SWATH runs for all samples were processed using 50 ppm mass error, 5 min RT window, and 99% confidence, and 1% FDR. Thus the peak areas generated in PeakViewv2.2 were imported into MarkerView™ v1.2.1, wherein statistical analysis using t-test was performed. Normalization across the runs was performed using the total area sum. The data set containing mass spectrometry results from the analysis of 3 biological and 3 technical replicates per treatment leading to 18 raw files were considered for statistical analysis. For each analyzed sample, the values of the technical replicates were averaged and subjected to statistical analysis. The proteins with a minimum 2 fold change (normalized with total intensity) and p values below 0.05 were considered significantly deregulated.

4.2.8 **Bioinformatic analysis**

The differentially expressed proteins were analyzed for protein-protein interactions and Gene ontology using Cytoscape 3.2, an open-source network visualization software using the clueGO plugin. Transcription factor prediction was performed using the iRegulon plug-in of Cytoscape.

4.2.9 **Statistical analysis**

Mass spectrometry acquisition for the total cell proteomic analysis was performed for 3 biological and 3 technical replicates for each sample. Student's t-test performed statistical analysis for quantitation of proteomic data. For proteomic analysis, the proteins with more than 2 matching peptides and fold change difference of ≥ 1.3 in protein expression were considered. Data were expressed as mean ± SEM. A p-value ≤ 0.05 was considered statistically significant.

4.3 Results and Discussion

4.3.1 **Apoptosis Assay**

To detect apoptotic cells after methylglyoxal treatment in L6 cells, we performed Annexin V and propidium iodide (PI) staining. Translocation of phosphatidylserine (PS) to the external cell membrane is an early indicator of apoptosis. After treatment with methylglyoxal, there was an increase in the number of both early and late apoptotic cells as compared to control cells, as seen by flow cytometry (Figure 4.1).

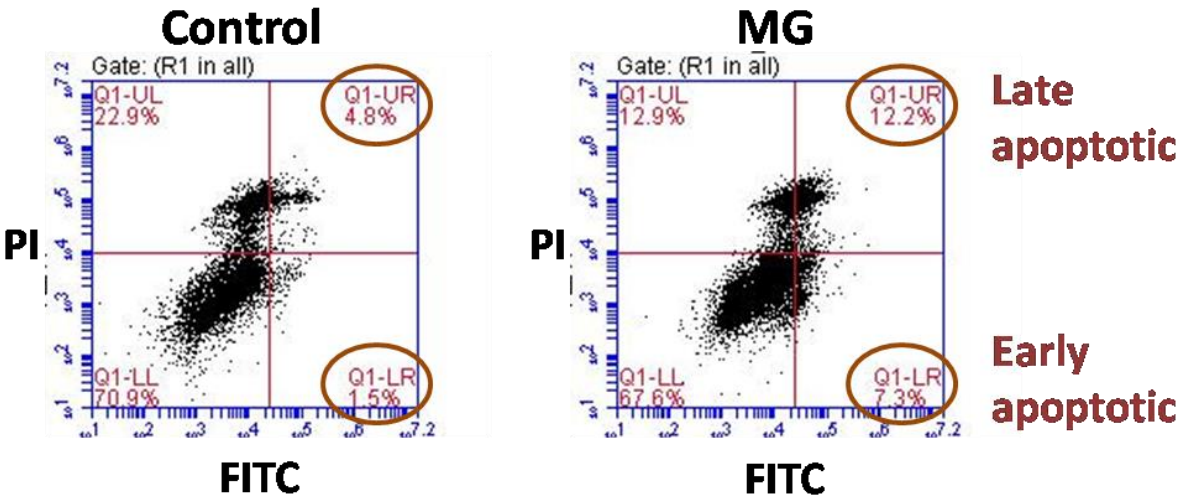

Figure 4.1 Apoptosis assay by flow cytometry

Scatter plots show an increase in the number of cells in the early apoptotic phase (lower right quadrant: LR) and late apoptotic (upper right quadrant: UR) phase after methylglyoxal treatment as compared to control.

4.3.2 Glucose Uptake Assay

To test the methylglyoxal effect on glucose uptake in L6 cells, we performed 2-NBDG based Glucose uptake assay. MG treatment to L6 cells showed a decrease in glucose consumption (Figure 4.2)

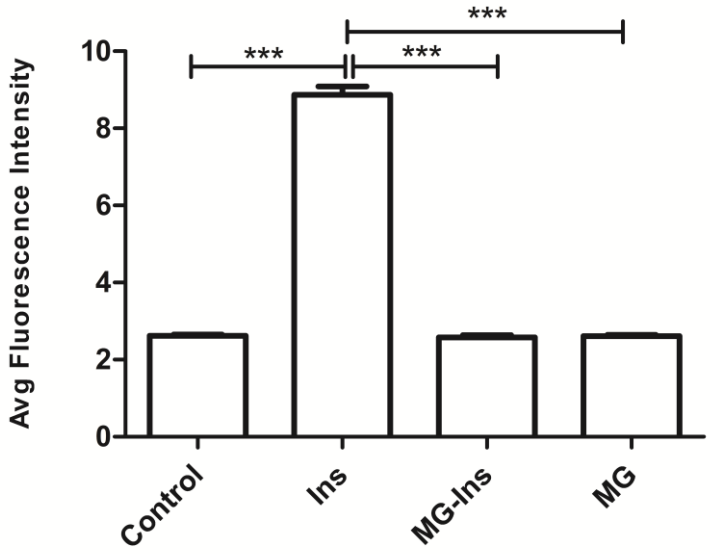

Figure 4.2 Glucose uptake assay

MG treated L6 cells showed a decrease in 2-NBDG uptake. Values represent mean ±SEM. (*** indicates p-value < 0.0001) Statistical significance was calculated by One way of ANOVA.

4.3.3 **Differential Proteomics of L6 muscle cells treated with Methylglyoxal**

Tryptic digest of total cell lysate was subjected to SWATH-MS analysis. The spectral library obtained from information-dependent acquisition (IDA) had 1963 proteins; out of these, 214 proteins were upregulated, and 59 proteins were downregulated by more than 2 fold in MG-Ins treated cells as compared to cells treated with Insulin (Figure 4.3)

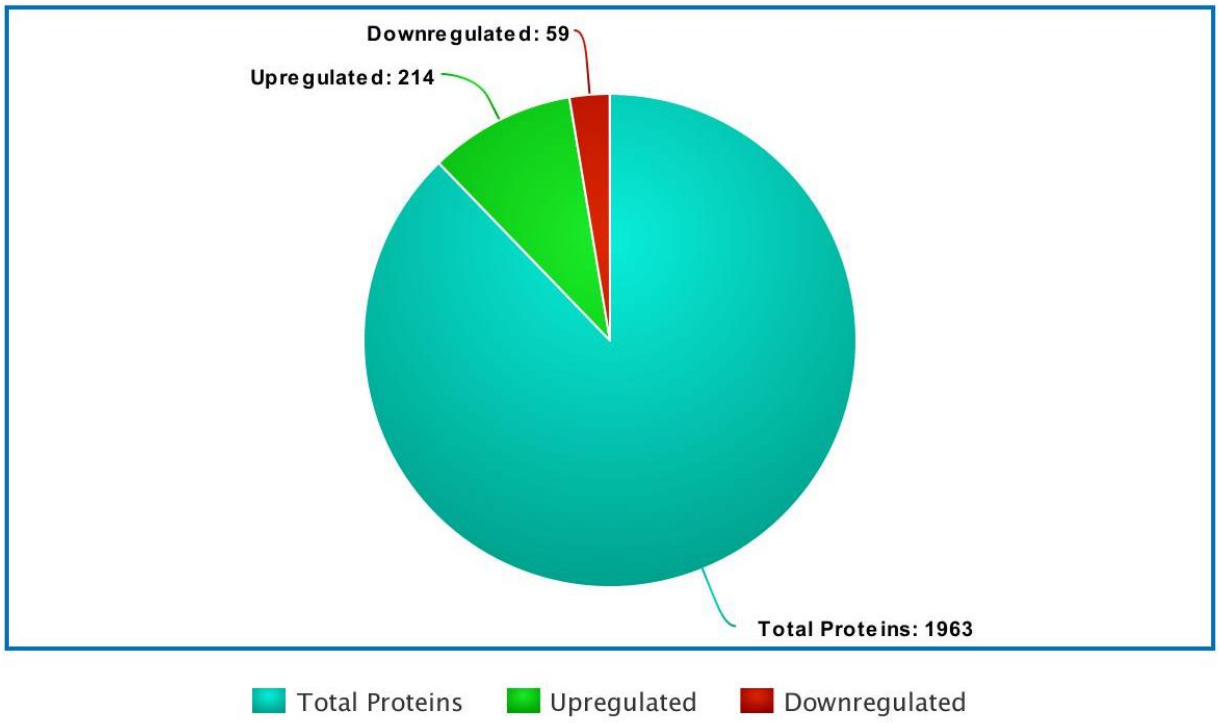

Figure 4.3 Piechart for number of deregulated proteins

Number of differentially expressed proteins in MG-Ins treated cells as compared to cells treated with Insulin

4.3.4 **Transcription Factor Prediction**

The iRegulon plugin in the Cytoscape determines the transcription factors that are associated with the proteins by exploring their binding motifs in the gene promoter regions. Analysis of the differentially expressed proteins in this study suggested that many of them are regulated by ATF4 (Figure 4.4). ATF4 is a stress-inducible bZIP transcription factor subunit. In mammalian cells, it is associated with a wide range of stress responses, including ER stress, which plays a vital role in metabolic homeostasis. It had reported that in stress conditions, ATF4 expression could induce muscle fiber atrophy. It helps in the expression of Gadd45a and p21, where Gadd45a activates the protein kinase MEKK4 and encourages muscle fiber atrophy, and p21

reduces expression of spermine oxidase and encourages atrophy. Spermine oxidase is a metabolic enzyme, and in normal, non-stressed situations, it helps maintain muscle fiber size[242]. Skeletal muscles play an essential role in regulating glucose disposal and maintaining glucose homeostasis. Insulin resistance in T2DM impairs skeletal muscle mass and causes muscle atrophy[243]. In T2DM model mice, it had shown the activation of the ubiquitin-proteasome system in skeletal muscle, leading to augmentation of protein degradation, hence to muscle atrophy.

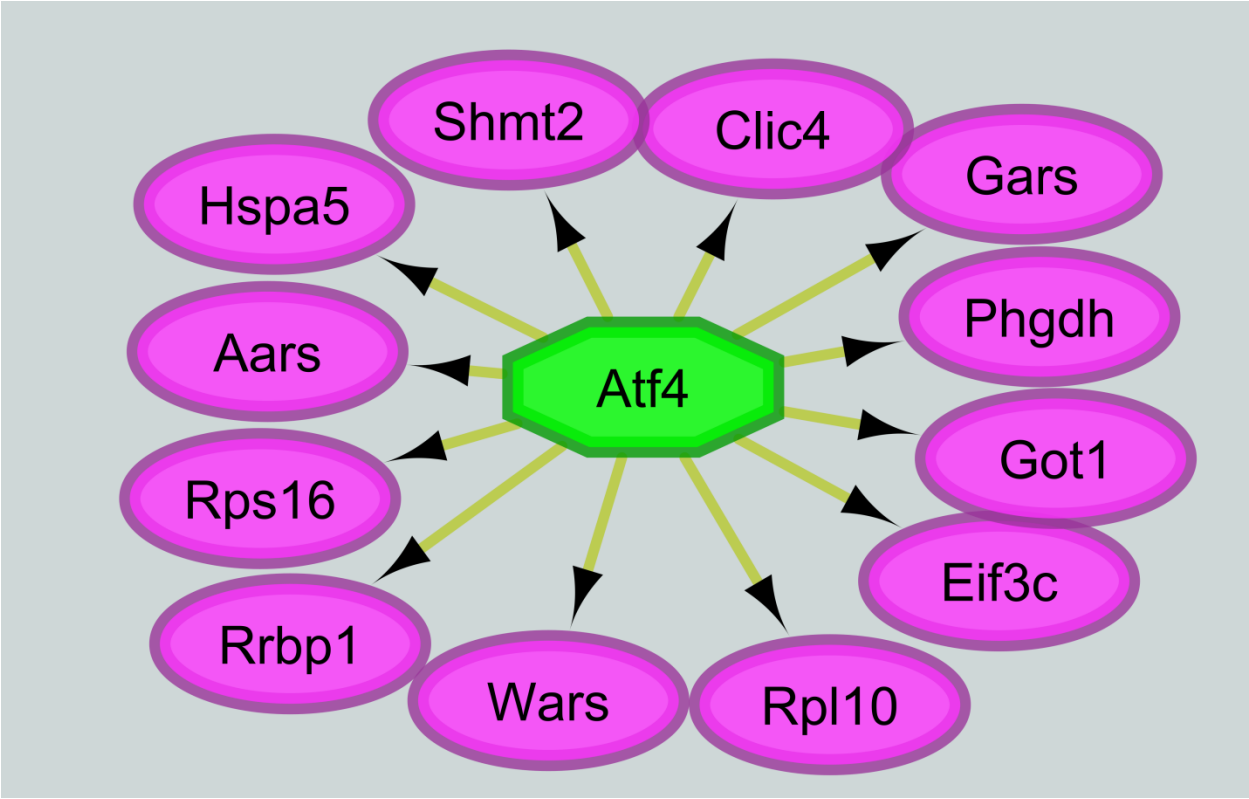

Figure 4.4 Transcription factor ATF4 , and it's target genes as predicted by iRegulon

Another key transcription factor observed to be involved was NFE2 (Figure 4.5). It was shown when hepatic NFE2 was overexpressed in mice, it increased miR-423-5p, leading to the suppression of the FAM3A-ATP-Akt signaling pathway. The impaired hepatic NFE2/miR-423-

5p axis promotes gluconeogenesis, lipid deposition, and hyperglycemia that can result in type 2 diabetes and non-alcoholic fatty liver disease (NAFLD)[244].

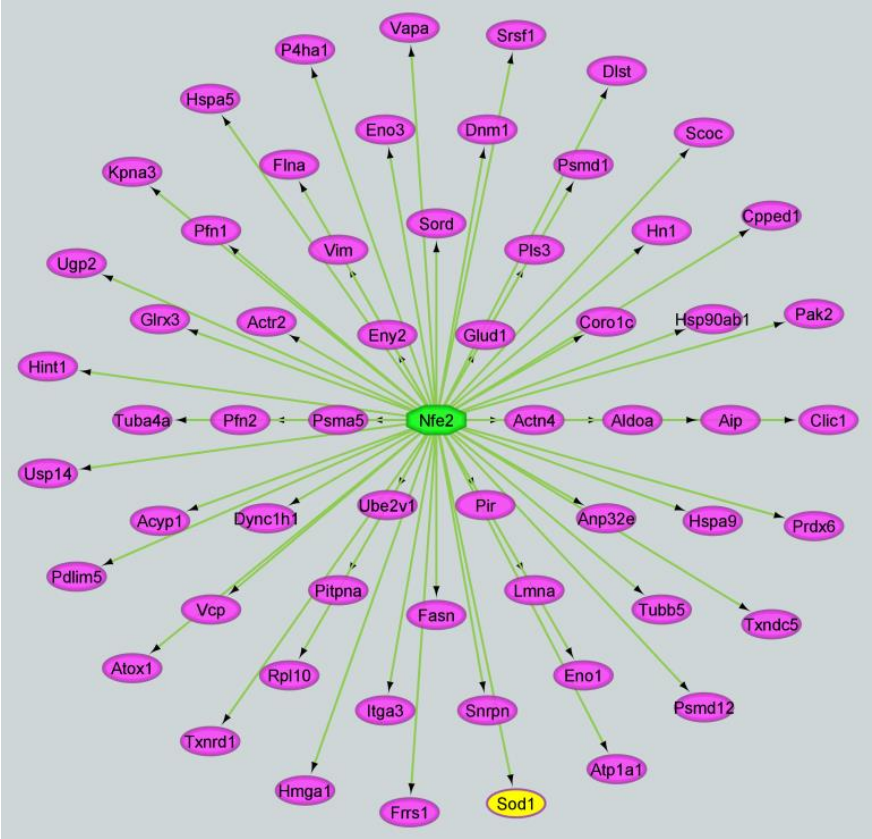

Figure 4.5 Transcription factor NFE2 , and it's target genes as predicted by iRegulon

Another key transcription factor observed to be involved was Nrf1 (Figure 4.6), which regulates many mitochondrial genes. Nuclear Respiratory Factor (Nrf1) is a transcription factor involved in expressing respiratory subunits and mitochondrial transcription factors. Nrf1 regulates an essential protein nuclear-encoded transcription factor TFAM, which controls the transcription of mitochondrial proteins. Nrf1 regulates various genes, which encodes for different vital enzymes involved in oxidative metabolism and mitochondrial function, and reduction in expression of these enzymes had observed in insulin resistance and diabetes mellitus [245]. Nrf1 also regulates glyoxalase 1, which plays a vital role in the detoxification process of methylglyoxal. Cellular dicarbonyl stress is a significant outcome of decreased Glo1 protein expression and is high in metabolic diseases such as T2DM, insulin resistance, and obesity(T2DM)[59].

Figure 4.6 Transcription factor Nrf1, and it's target genes as predicted by iRegulon

Another key transcription factor observed to be involved was Myc (Figure 4.7). The transcription factor c-Myc induces hepatic glucose uptake and utilization and blocks gluconeogenesis[246]. The Myc network coordinates cellular utilization of glucose and glutamine in biosynthetic pathways by directly regulating mitochondrial mass and activity. MondoA (Transcription factor of Myc network) senses glutaminolytic flux into the tricarboxylic acid cycle and appears to coordinate the utilization of glucose and glutamine by regulating the expression of thioredoxin interacting protein[247].

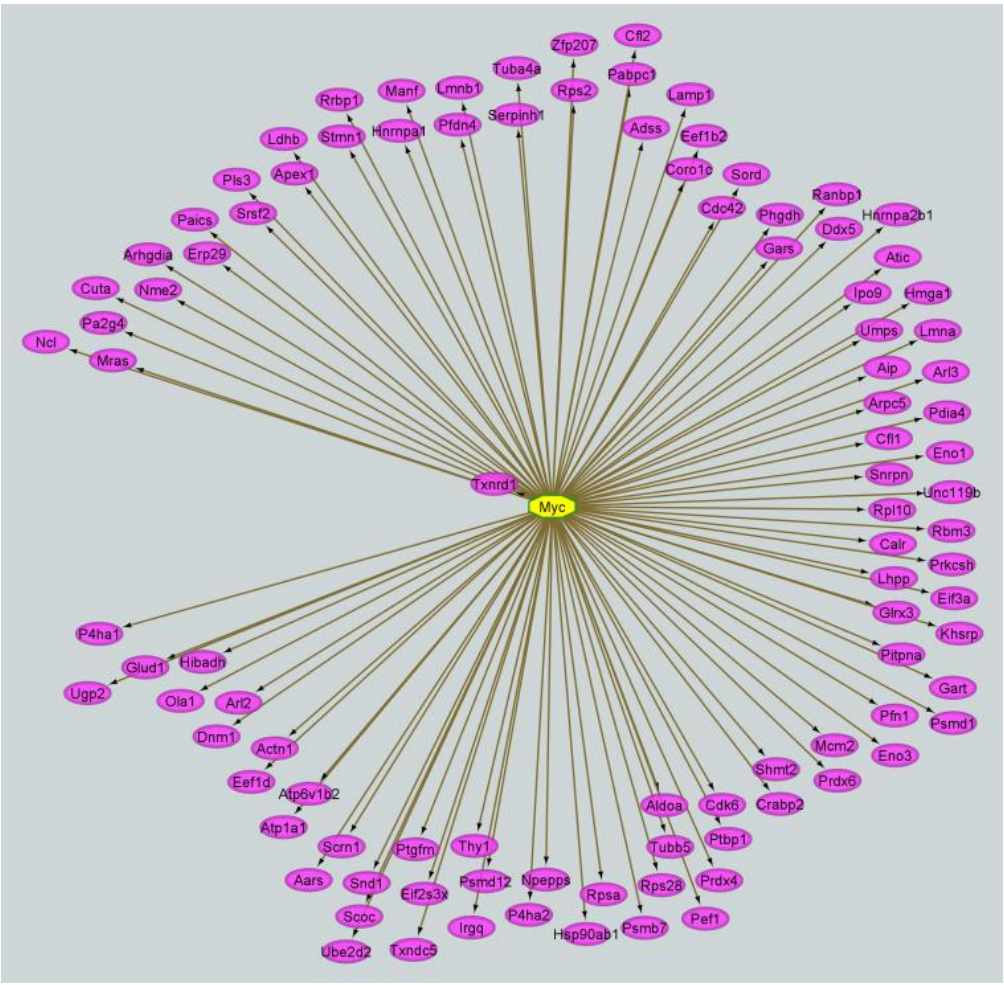

Figure 4.7 Transcription factor Myc, and it's target genes as predicted by iRegulon

4.3.5 **Functional annotation**

Gene Ontology analysis was performed by Cytoscape using the ClueGo plugin; protein-protein interaction network shows the processes which involve the proteins differentially expressed in MG-Ins treatment as compared to Ins. Proteins deregulated in MG treated cells were mainly involved in metabolic processes like citrate cycle (TCA cycle), glycolysis/gluconeogenesis, glyoxylate, and dicarboxylate metabolism(Figure 4.8). Proteins such as citrate synthase, dihydrolipoamide S-succinyltransferase, and isocitrate dehydrogenase [NAD] subunit alpha were found to be deregulated in the TCA cycle.

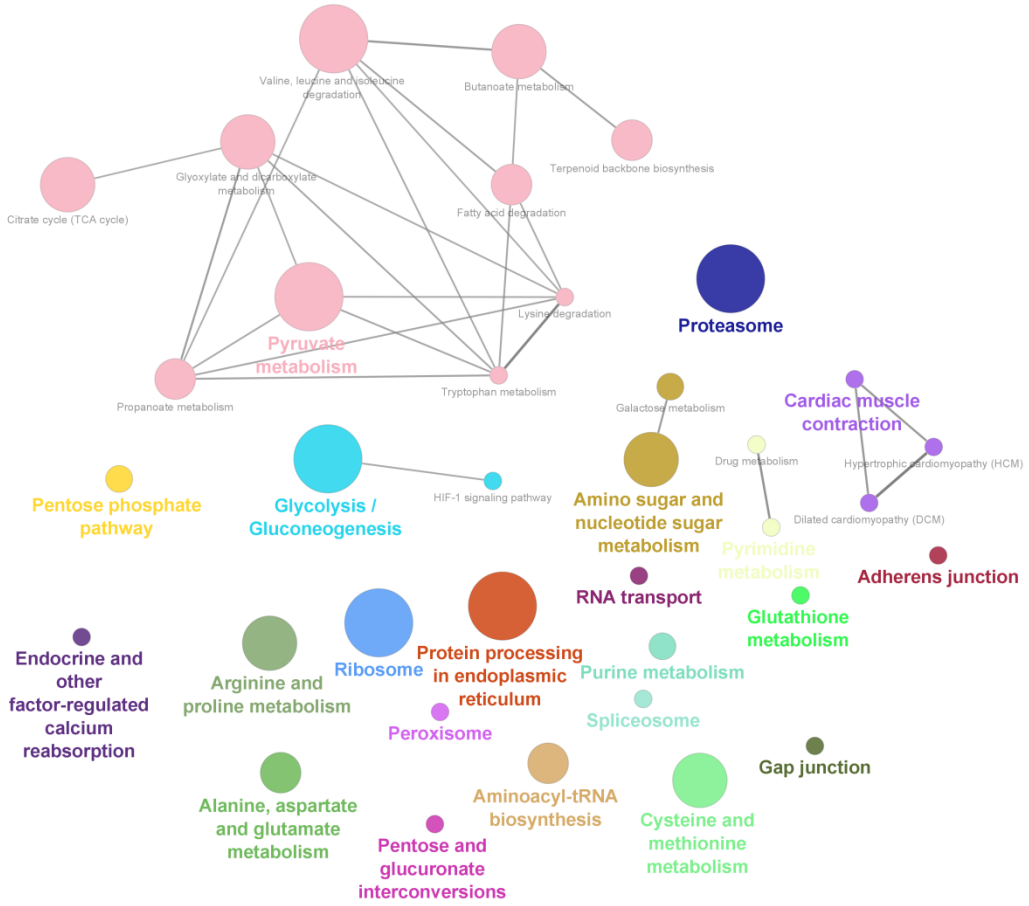

Figure 4.8 Bioinformatic analysis

Gene ontology analysis showing biological process in which the differentially abundant proteins are involved.

TFAM elevated the muscle tricarboxylic acid cycle and citrate synthase, facilitating energy expenditure. A study also suggests that TFAM increased the aspartate-malate shuttle to increase NAD+ import into the mitochondrial matrix [248]. The gluconeogenic pathway and Krebs cycle play an essential role in maintaining glucose homeostasis; imbalance in these pathways can be seen in diabetes. The Krebs cycle uses substrates obtained by fatty acids, carbohydrates, and amino acids and plays a quintessential role in aerobic metabolism. A metabolomics study

showed that treatment with Coreopsis *tinctoria* (CT) flowering tops notably enhanced glucose homeostasis. It targeted essential proteins of the gluconeogenic pathway by reducing the expression of glucose-6-phosphatase and phosphoenolpyruvate carboxykinase. Regulation of the Krebs cycle's few necessary enzymes was also observed, such as dihydrolipoamide S-succinyltransferase, citrate synthase, flavoprotein, and succinate dehydrogenase complex, subunit A[249][250]. Hyperglycemia is the primary manifestation of diabetes, and dysfunction of mitochondria is a significant result of hyperglycemia, which can further lead to dysfunction and pathology at cellular levels and tissue levels, ultimately resulting in severe complications; hence mitochondrial metabolism plays an essential role. In our data, we found pyruvate kinase downregulated, which shows MG can induce mitochondrial dysfunction. There are reports that PKM2 activation not only enhances but even alters mitochondrial dysfunction. PKM2 increases mitochondrial mass and also levels of MMP and PGC-1α; therefore, mitochondrial metabolism is also increased[251][252][253][254]. Several studies showed that PKM2 activators could reverse the mitochondrial dysfunctions arising from hyperglycemia and diabetes; research further indicates in diabetes, epigenetic factors that cause neurological changes and metabolic memory could be reversed[251][255][252][253][254]. Aldehyde dehydrogenase was deregulated in glycolysis, which plays an essential role in the detoxification of MG.

4.4 Conclusion

Since skeletal cells are the major cell type involved in glucose homeostasis, we have analyzed MG's effect on total cell proteomics of skeletal muscles. Methylglyoxal treatment reduces glucose uptake in muscle cells and induces apoptosis. The IDA spectral library had 1963 proteins, and 214 of those were upregulated while 59 were downregulated by more than 2 fold in MG treated cells in SWATH analysis. Pathway analysis shows deregulation of various metabolic processes like citrate cycle (TCA cycle), glycolysis/gluconeogenesis, glyoxylate, and dicarboxylate metabolism. Transcription factors Nrf1, Atf4, Nfe2, myc were found to regulate many deregulated proteins and have a role in insulin resistance. Further, the effect of MG can be analyzed by overexpression or knock-out of the proteins involved in the glyoxalase system in mammalian cells.

Chapter 5

Study of methylglyoxal induced proteins in animal plasma

Chapter 5 Study of methylglyoxal induced proteins in animal plasma

5.1 Background

For a better understanding of the molecular mechanisms of disease, appropriate experimental models are necessary. In biomedical research, animal models have been extensively used since research on human beings is impeded mainly by ethical restrictions. Also, the pathogenesis of the disease and therapeutic intervention strategies can be conveniently studied in animal models. Especially among the animal models being used, rodent models have extensively been used since the inducible pathology resembles that of humans, as well as due to their short generation time, economic considerations, and small size, they are convenient for experimental use. Further, STZ is a toxic glucose analog extensively used in diabetes research owing to its diabetogenic property. It is taken up by the pancreatic beta cells by glucose transporter GLUT 2 [256], and inside the cells, it alkylates deoxyribonucleic acid (DNA) and destroys the beta cells causing decreased or absolute inhibition of insulin production [257] which leads to persistent hyperglycemia mimicking conditions of diabetes.

Following our initial observations in the cell secretome and clinical experiments, in this study, animal experiments were carried out to study the effect of methylglyoxal induced proteins *in-vivo*. Since MG levels increase in diabetes, it is expected that some of the secreted proteins observed in cell culture or clinical plasma may also be found in animal plasma. Therefore, to identify such proteins, SWATH-MS was performed to identify and quantify MG induced proteins in the animal plasma. Hyperglycemic condition in diabetes promotes glycation and formation of reactive carbonyls such as glyoxal, methylglyoxal, which can, in turn, modify proteins. We, therefore, studied MG associated modification of Rat serum albumin, which could reflect elevated levels of MG.

5.2 Materials and methods

5.2.1 Chemicals

All the reagent materials were procured from Sigma-Aldrich if not mentioned otherwise.

5.2.2 Rat sample details

To check methylglyoxal induced changes in plasma proteins *in-vivo*, animal experiments were carried out at the experimental animal facility, Symbiosis Institute of Technology, Pune, India. Experiments were carried out following the guidelines of the Committee for Control and Supervision of Experiments on Animals, India, and approved by the Institutional Animal Ethics committee. Sprague Dawley rats were taken from Nutrivet life sciences. The study was carried out in four groups, Control, STZ, MG, and STZ-MG. Diabetes was induced in rats by injecting them intraperitoneally with 55 mg/kg body weight of STZ in 50 mM citrate buffer, pH 4.5, to induce hyperglycemia, whereas control rats were injected with 50 mM citrate buffer. The induction of diabetes was confirmed by measuring the blood glucose levels with a glucometer. The rats with a blood glucose of 200 mg/dl were considered diabetic. The glycation was monitored by glycated hemoglobin (HbA_{1c}) measurement (Nycocard HbA_{1c}analyzer). Further, rats were given MG at a dose of 50 mg/kg by oral gavage method for about 60 days after induction of diabetes. The rats were recorded for body weight, blood glucose, and HbA_{1c}. At the end of the study, blood samples were collected in sterile tubes containing EDTA, and plasma was obtained by centrifugation at 1500 g for 10 min. Rats were sacrificed by using carbon dioxide, and the organs were collected in liquid nitrogen by snap freezing after a brief washing with PBS and then stored at -80 °C.

Plasma proteins were quantified, and in-solution trypsin digestion was performed. Mass spectrometric Acquisition (Both IDA and SWATH) was done on Triple ToF5600. Data analysis was done, and differentially expressed proteins were compared with the previously acquired skeletal muscle cell line secretome data and diabetic plasma Clinical Data.

5.2.3 **Histopathological evaluation of kidney**

The animals were sacrificed group-wise at the end of the test study, and detailed necropsy of all animals was carried out, and gross pathological changes, if any, were recorded. All the animals were sacrificed using carbon dioxide. The whole kidney tissue from all the experimental animals was collected group-wise in 10% neutral buffered formalin in a labeled plastic container for fixation immediately after necropsy.

The collected tissues were grossed, kept in cassette, and then processed using an automated tissue processor using an alcohol-xylene protocol for dehydration and clearing of tissues. The processed tissues, embedded in paraffin, were sectioned at 4-5 µ using an automated microtome (*Leica*, Germany). The cut tissue sections were stained by routine Haematoxylin and Eosin protocol [258]. Histopathological evaluation was performed by the expert qualified veterinary pathologist, who was blinded to the group codes[259]. The microphotographs were taken using a microphotography unit with a microscope (*Nikon*, Japan).

5.2.4 **In-solution Trypsin Digestion**

100 µg of total protein in 0.1% RapiGest for each plasma sample was used for digestion. Before reduction and alkylation, proteins were denatured by incubating at 80 °C for 15 min. Further, proteins were reduced using 100 mM dithiothreitol for 15 min at 60 °C and then alkylated by treating with 200 mM iodoacetamide for 30 min in the dark at room temperature. Trypsin was added at 1:25 (w/w) enzyme to protein ratio and incubated at 37°C for 18 h, 2 µl formic acid was added to inactivate trypsin and stop the digestion, and the surfactant RapiGest was precipitated by incubating with acidic pH at 37 °C for 45 min followed by centrifugation at 14000 ×g for 15 min. The precipitated surfactant was discarded, and the digested peptide supernatant was collected. For desalting of the digested peptides, C18 Zip tips were used, and the desalted peptides were concentrated using Speed vac. For LC-MS analysis, peptides were reconstituted in 3% acetonitrile with 0.1% formic acid.

5.2.5 Liquid Chromatography-Mass Spectrometry Analysis

5.2.5.1 SWATH-MS Analysis

SWATH analysis was performed on a Triple-TOF 5600 (AB Sciex; Concord, Canada) mass spectrometer coupled with Micro LC 200 (Eksigent; Dublin, CA) in high-sensitivity mode. A spectral library was generated by pooling equal amounts of peptide samples from each treatment and analyzing them by Information dependent acquisition (IDA). Briefly, peptides were separated on an Eksigent C18-RP HPLC column (100×0.3mm, 3µm, 120 Å) using a 95 min gradient of 3% to 35% mobile phase B at a flow rate of 8 µL/min (mobile phase A: water with 0.1% formic acid mobile phase B: acetonitrile with 0.1% formic acid). Accumulation time for MS was 250 ms and for MS/MS was 100 ms. Fragmentation was done using rolling collision energy. For SWATH-MS acquisition, the precursor mass range of 400–1250 m/z was divided into a set of 34 overlapping windows of 25 m/z each. For MS/MS, collision energy was optimized for each window, and spectra were collected from 100 to 2000 m/z. Fragment ion scans were performed over an accumulation time of 70 ms, while for the precursor survey scan, it was 100 ms. All samples were acquired in biological and technical triplicates.

To get spectral library from IDA run, data was analyzed by ProteinPilot™ software version 5.0 using UniProt *Rattus norvegicus* database updated with Uniprot release 2018_06; 8027 reviewed protein entries. The enzyme used for digestion was set to trypsin, and carbamidomethylation of cysteine residues was selected as a fixed modification. The search was performed using a False Discovery Rate (FDR) of 1%. The resultant spectral library was imported into PeakView v2.2 software, and SWATH runs for all samples were processed using 50 ppm mass error, 5 min RT window, and 99% confidence, and 1% FDR. The peak areas thus generated in PeakView v2.2 were imported into MarkerView™ v1.2.1, wherein statistical analysis using t-test was performed. Normalization across the runs was performed using the total area sum.

5.2.6 **Bioinformatic analysis**

The differentially expressed proteins were analyzed for protein-protein interactions and Gene ontology using Cytoscape 3.2, an open-source network visualization software using the clueGO plugin.

5.2.7 **Data analysis for Quantification of methylglyoxal modified peptides**

Skyline (version4.1.0, MacCoss lab) was used for the quantification of peptides using SWATH .wiff files. FASTA file of rat serum albumin was used for theoretical mass spectral library generation. Unmodified peptides and corresponding carboxyethyl and argpyrimidine modified peptides of albumin were specified for the targeted quantification of peptides. Retention times of precursors were manually corrected wherever required. Only intense and co-eluting fragment ions of a particular precursor were considered for quantification. The sum of the area under the curve of these selected fragment ions was used for the quantification of the precursor. Digestion enzyme was specified as trypsin. The maximum missed cleavage was set to 1. Carbamidomethylation at cysteine (57.021464 Da), MG-H1 at arginine (54.01565 Da), argpyrimidine at arginine (80.026), and carboxyethyl modification at lysine and arginine (72.021126 Da) were specified as methylglyoxal associated modifications. Precursor ion charge states were specified as +2 and +3, whereas fragment ion charge states were specified as +1 and +2. Fragment ion mass tolerance was set to 0.5 Da. The acquisition method was selected as DIA, and the product mass analyzer was set as TOF. The isolation scheme was selected as SWATH (15 m/z) at a resolving power of 15,000. The peak area of the modified peptide was normalized with the peak area of its corresponding unmodified peptide. CEL modified peptide content in diabetic plasma was expressed as a fold change ratio of the normalized peak area of CEL modified peptide of diabetic plasma to the normalized peak area of CEL modified peptide of control rat plasma. Argpyrimidine modified peptide content in diabetic rat plasma was expressed as a fold change ratio of the normalized peak area of argpyr modified peptide of diabetic rat plasma to the normalized peak area of argpyr modified peptide of control rat plasma.

5.2.8 Statistical analysis

Mass spectrometry acquisition for the rat plasma proteomic analysis was performed for 3 plasma samples each of healthy control and diabetic rat subjects from each group in technical triplicates for each sample. Statistical analysis was performed by Student's t-test for quantitation of both proteomic data and peptide quantification in rat plasma. Data were expressed as mean ± SEM. A p-value ≤ 0.05 was considered statistically significant. For proteomic analysis, the proteins with more than 2 matching peptides and fold change difference of ≥ 1.3 in protein expression were considered.

5.3 Results and Discussion

5.3.1 Physiological data

Diabetic animals showed a marked increase in the level of blood glucose and HbA1c in comparison to control animals. Besides, polydipsia and polyuria were developed in diabetic animals, which was evident by the observation of water cans and the visible cage wetting. Diabetic animals also showed a decrease in body weight compared to the control animals. The physiological data at the end of the study are shown in Table 5.1.

Table 5.1 The physiological data

Group (n=3)	Blood Glucose (mg/dL)
Control	87 ± 15.59
MG	82.67 ±10.26
STZ	426.67 ±152.53
STZ+MG	310 ±127.39

5.3.2 Elevated levels of methylglyoxal modified rat serum albumin peptides in diabetic rat plasma

Hyperglycemic condition in diabetes promotes glycation and formation of reactive carbonyls such as glyoxal, methylglyoxal, which can, in turn, modify proteins leading to the formation of carboxyethyllysine (CEL) and Argpyrimidines (ARGPYR). In severe diabetes, due to elevated levels of MG, it is expected that MG associated modifications such as CEL and ARGPYR can be observed in plasma proteins. Rat serum albumin (RSA) has been considered as a primary target for glycation due to its abundance, many lysines, and arginine residues, and relatively long half-life. We, therefore, studied MG associated modification of RSA, which could reflect elevated levels of MG. Label-free SWATH-MS approach was used for the quantification of MG modified peptides. Two peptides, RPCFSALTVDETYVPK and LVQEVTDFAKTCVADENAENCDK, showed ARGPYR and CEL modification of arginine and lysine residues, respectively, and their intensities were found to be high in diabetic rat plasma. Details of precursor and fragment ions used for quantification are summarized in (Table 5.2). For RPCFSALTVDETYVPK, the peptide and their fragments that are consistently observed in all the samples were considered for analysis (Figure 5.1A, B). The normalized ARGPYR-modified area for unmodified RPCFSALTVDETYVPK and modified peptide R(ARGPYR)PCFSALTVDETYVPK is shown in (Figure 5.2A). The Sum of the area under the curve (AUC) of selected fragment ions was used for peptide quantification. The peak area of ARGPYR-modified peptides in control and other groups of rat plasma samples were normalized with the peak area of their corresponding unmodified peptide. The increase in Argpyr- modification in MG, STZ, and STZ-MG group was expressed as a fold change over the healthy control group (Figure 5.2B). The level of ARGPYR-modified peptide R(Argpyr)PCFSALTVDETYVPKin in the MG group was 1.76 fold, in the STZ group was 1.96 fold, and in the STZ-MG group was 2.65 fold higher than in the healthy control group. The retention time of quantified peptides has shown in (Figure 5.3A, B).

Table 5.2 Details of precursor and fragment ions used for quantification

Sr. No	Modification site	Peptide sequence	Charge state	Modification	Monoisotopic m/z	Fragments ion (m/z) used for quantification
1	K509	RPCFSALTV DETYVPK	+2	Argpyr	941.9720	$b4^{+}$ (561.2602)
						$b10^{+}$ (1147.5565)
						$b10^{++}$(574.2819)
						$b12^{++}$(689.3270)
						$y9^{+}$ (1051.5306)
						$y7^{+}$ (851.4145)
						$y14^{++}$(815.3951)
						$y11^{++}$(618.3295)
2	K509	RPCFSALTV DETYVPK	+2	Argpyr	981.9851	$b4^{+}$ (641.2863)
						$b10^{+}$ (1227.5826)
						$b10^{++}$(614.2949)
						$b12^{++}$(729.3401)
						$y9^{+}$ (1051.5306)
						$y7^{+}$ (851.4145)
						$y14^{++}$(815.3951)
						$y11^{++}$(618.3295)
3	K75	LVQEVTDF AKTCVADE NAENCDK	+3	Unmodified	886.0670	$b15^{++}$(839.4113)
						$b18^{++}$(996.4726)
						$y18^{++}$(1044.4359)
						$y12^{++}$(712.7745)

4	K75	LVQEVTDF AKTCVADE NAENCDK	+3	CEL	910.0741	$b15^{++}$(875.4218) $b18^{++}$(1032.4831) $y18^{++}$(1080.4464) $y12^{++}$(712.7745)

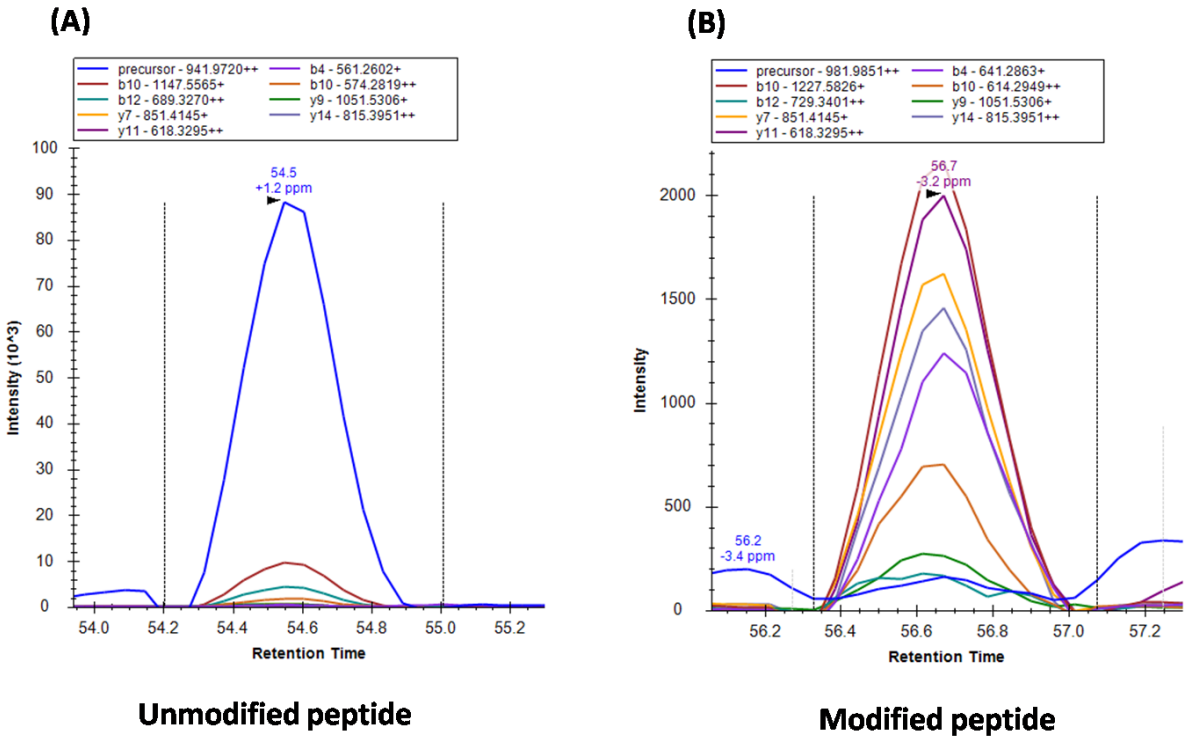

Figure 5.1 Representative extracted ion chromatograms showing co-elution of fragment ions of ARGPYR modified peptide

(A) unmodified peptide RPCFSALTVDETYVPK and (B) modified peptide R(Argpyr)PCFSALTVDETYVPK of rat serum albumin in diabetic plasma.

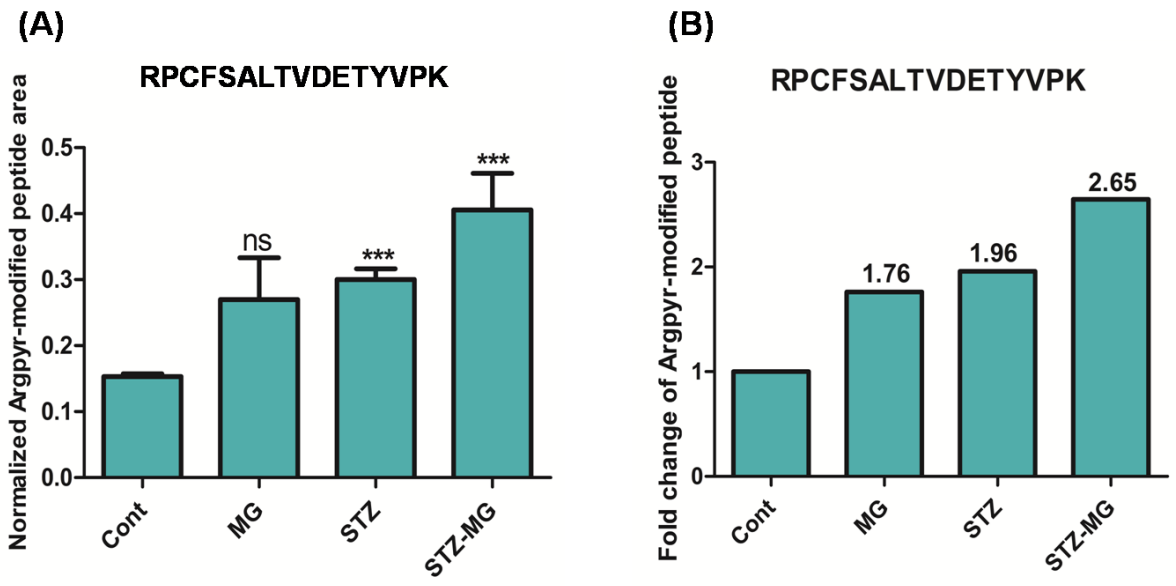

Figure 5.2 Normalized Argpyr-modified peptide area and Fold change in expression of Argpyr-modified albumin peptides

(A) Normalized Argpyr-modified peptide area shows a significant increase in Argpyr-modification of peptide R(Argpyr)PCFSALTVDETYVPK from albumin in plasma of STZ and STZ-MG group subjects as compared to a healthy control subject. (B) Fold change in expression of Argpyr-modified albumin peptides R(Argpyr)PCFSALTVDETYVPK in plasma sample of MG, STZ, and STZ-MG group rats compared to healthy control rats.

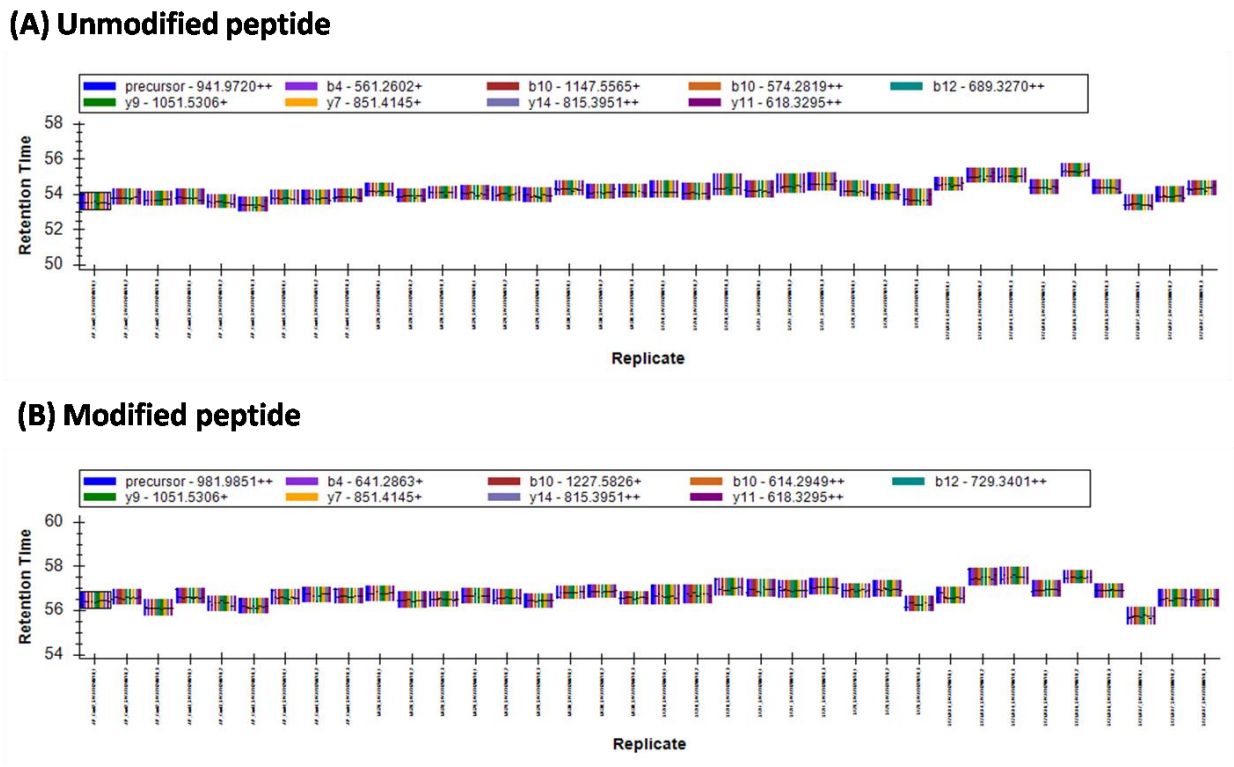

Figure 5.3 Retention time of quantified peptides

(A) Unmodified peptide RPCFSALTVDETYVPK (B) ARGPYR modified R(Argpyr)PCFSALTVDETYVPK

Similarly, for LVQEVTDFAKTCVADENAENCDK, the peptide and their fragments that are consistently observed in all the samples were considered for analysis (Figure 5.4A, B). The normalized CEL-modified area for unmodified LVQEVTDFAKTCVADENAENCDK and modified peptide LVQEVTDFAK(CEL)TCVADENAENCDK is shown in (Figure 5.5A). The Sum of the area under the curve (AUC) of selected fragment ions was used for peptide quantification. The peak area of CEL-modified peptides in control and other groups of rat plasma samples were normalized with the peak area of their corresponding unmodified peptide. The increase in CEL-modification in MG, STZ, and STZ-MG group was expressed as a fold change over the healthy control group (Figure 5.5B). The level of CEL-modified peptide LVQEVTDFAK(CEL)TCVADENAENCDKin in the MG group was 1.43 fold, and in the STZ

group was 1.48 fold higher than in the healthy control group. The retention time of quantified peptides is shown in (Figure 5.6A, B).

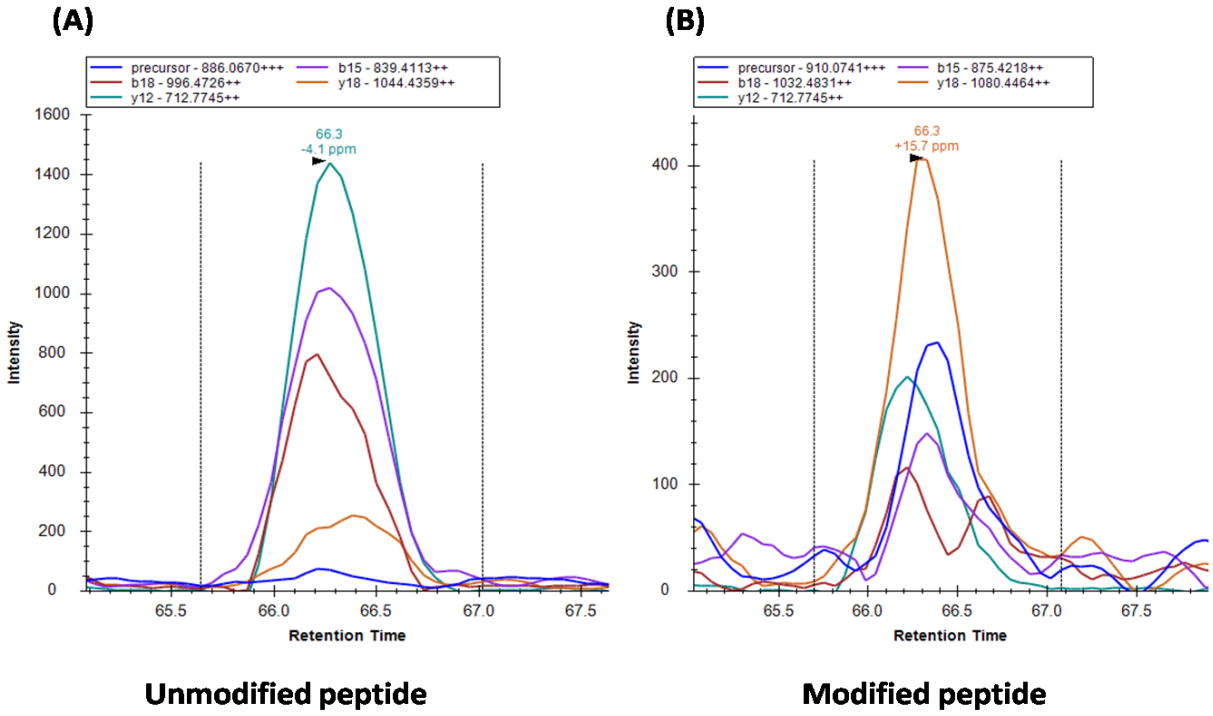

Figure 5.4 Representative extracted ion chromatograms showing co-elution of fragment ions of CEL-modified peptide

(A) unmodified peptide LVQEVTDFAKTCVADENAENCDKand (B) modified peptide LVQEVTDFAK(CEL)TCVADENAENCDKof rat serum albumin in diabetic plasma.

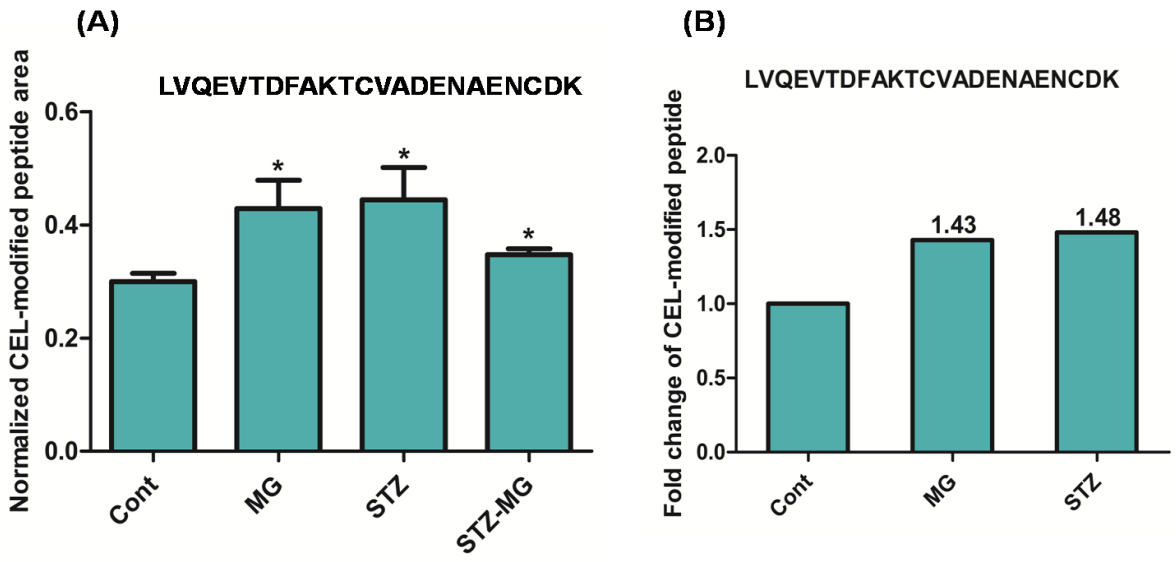

Figure 5.5 Normalized CEL-modified peptide area and Fold change in expression of CEL-modified albumin peptides

(A) Normalized CEL-modified peptide area shows a significant increase in CEL-modification of peptide LVQEVTDFAK(CEL)TCVADENAENCDK from albumin in plasma of MG, STZ, and STZ-MG group subjects as compared to a healthy control subject. (B) Fold change in expression of CEL-modified albumin peptides LVQEVTDFAK(CEL)TCVADENAENCDK in plasma sample of MG and STZ group rats compared to healthy control rats.

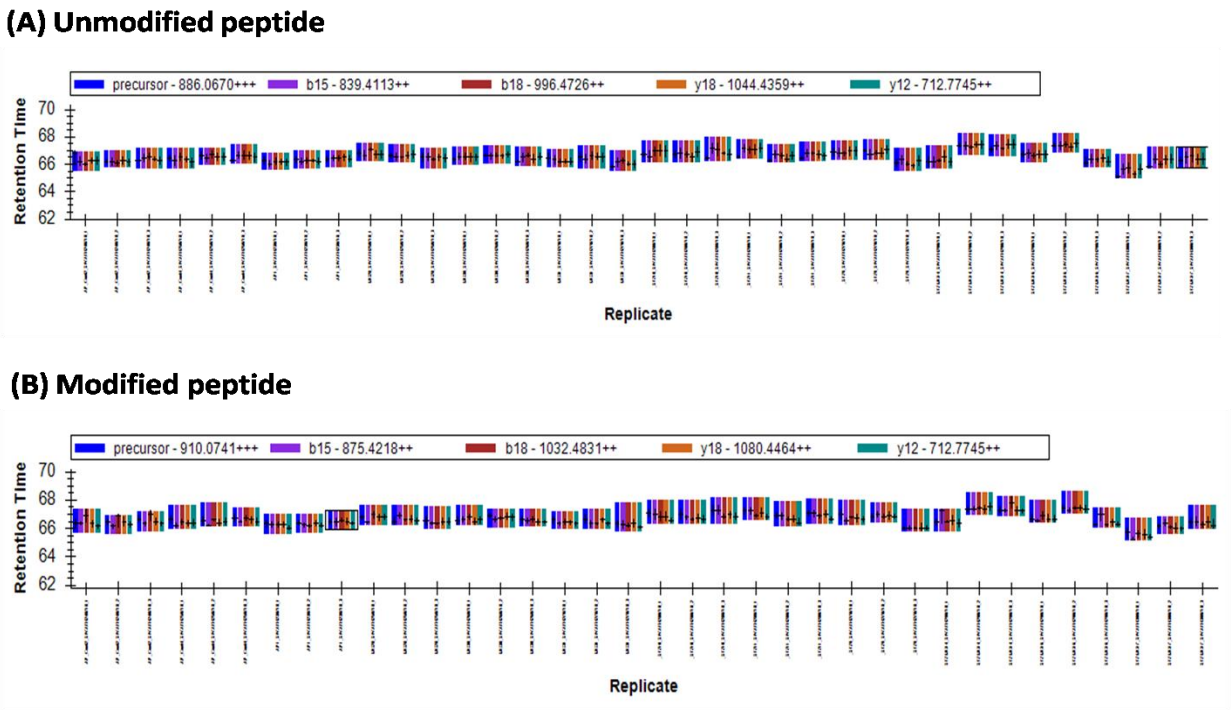

Figure 5.6 Retention time of quantified peptides

(A)Unmodified peptide LVQEVTDFAKTCVADENAENCDK (B) CEL modified LVQEVTDFAK(CEL)TCVADENAENCDK

5.3.3 **Hyperglycemia induced cataract**

In this study, we observed a change in the color of the eyes of Diabetic rats (Figure 5.7). In the development of cataract, the polyol pathway has an important role. In the hyperglycemic condition, the reduction of glucose takes place, and it got converted to sorbitol. The reaction is catalyzed by the aldose reductase enzyme. Intracellularly, when a high amount of sorbitol accumulated, it further leads to a hyperosmotic effect, which results in degeneration of hydroponic lens fibers and hence in cataract[260].

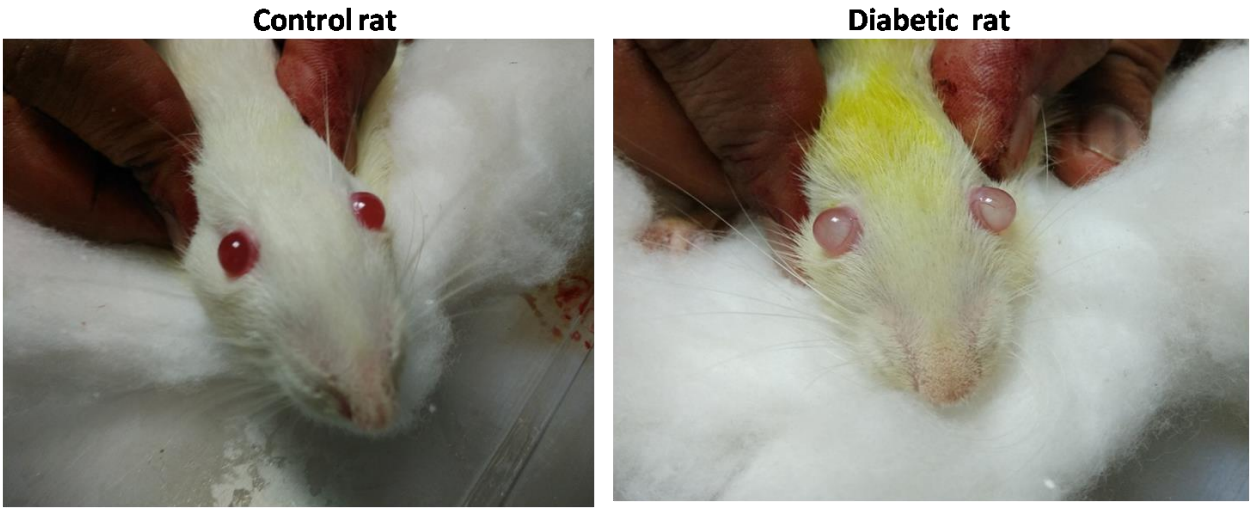

Figure 5.7 Change observed in color of eyes of diabetic rat

5.3.4 **Histopathological observation**

The overall pathological grade was measured as minimal (focal and very less degree of pathological changes which may be non-significant, Less than 10% of the tissue is affected/showing lesions), mild (lesions observed at multiple foci of tissue/organ, and showing prominent/pathological cellular changes in tissues, Approx. 10 to 30% of the tissue is affected/showing cellular lesions), moderate (lesions observed at DIFFUSE of tissue/organ and showing prominent/pathological cellular changes in tissues, Approx. 30 to 60% of the tissue is affected/showing cellular lesions) to severe (DIFFUSE and prominent/pathological cellular changes in tissues, More than 60% of the tissue is affected/showing cellular lesions). Histopathological observations such as degenerative, vacuolar, and cellular swelling changes of renal tubules, necrobiotic changes of renal tubular epithelial tissue, presence of eosinophilic debris in the lumen of renal tubules with degenerative changes of tubules, glomerular pathology, swelling of glomeruli, loss of glomerular tuft/tissue, inflammatory cellular infiltration in the renal parenchyma, vascular changes, and congestion and interstitial hemorrhages in renal parenchyma were monitored. There was no detection of any pathology in the control group of rats; in the MG group of rats, it was minimal to mild, while in the STZ and STZ-MG group of rats, it was moderate to severe (Figure 5.8).

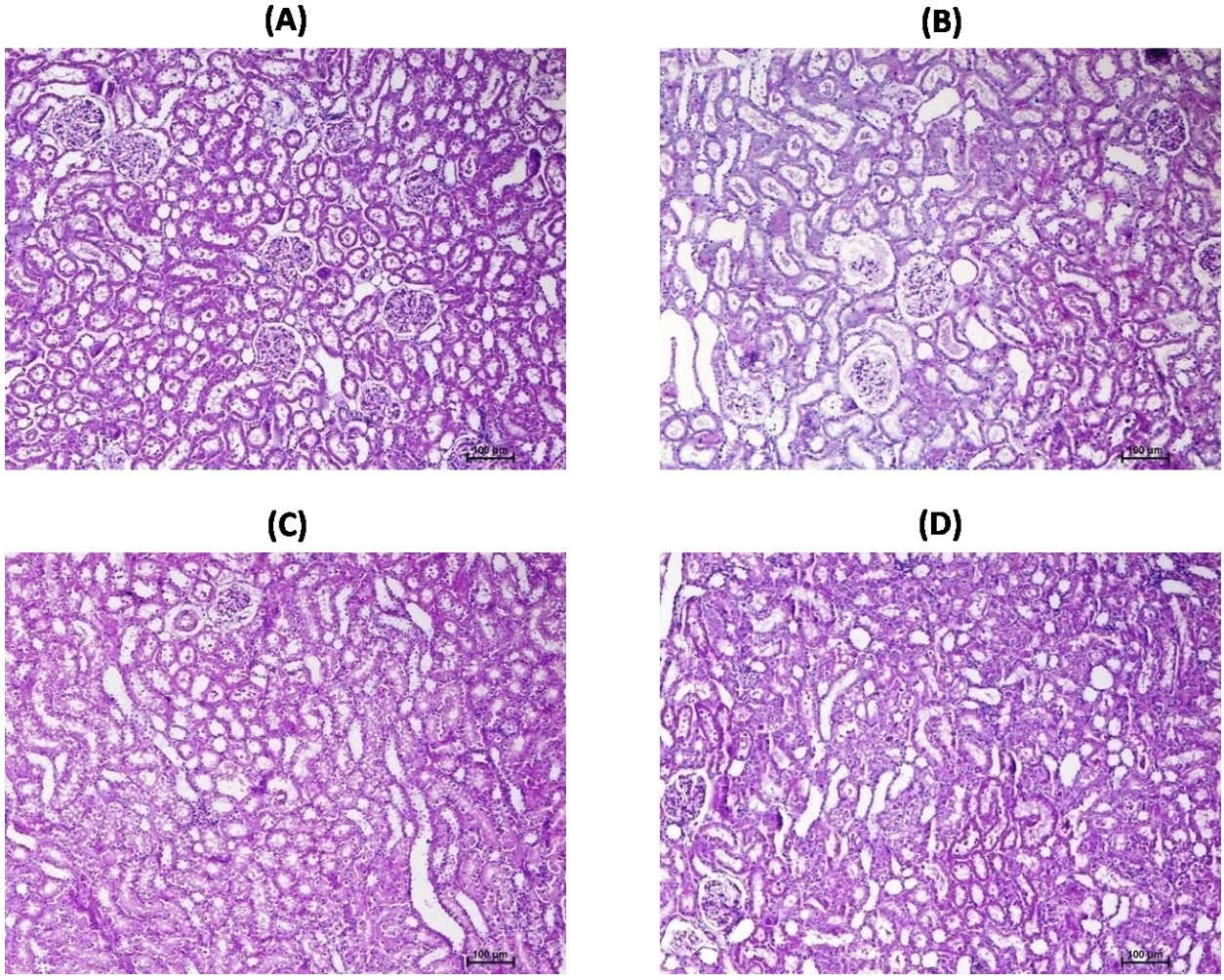

Figure 5.8 Histopathological observation in all rat groups (A) Control, (B) STZ, (C) MG, (D) STZ-MG

5.3.5 **Proteomic Analysis of Rat Plasma**

The usefulness of MG-induced secretome was studied in rat plasma. Since MG levels increase in diabetes, it is expected that some of the secreted proteins observed in cell culture may also be found in plasma. Therefore, to identify such proteins, SWATH-MS was performed to identify and quantify MG associated proteins in the plasma. Tryptic digest of rat plasma was subjected to

expression analysis using SWATH-MS workflow. PCA of all replicate runs showed good reproducibility between the replicate runs of each treatment (Figure 5.9)

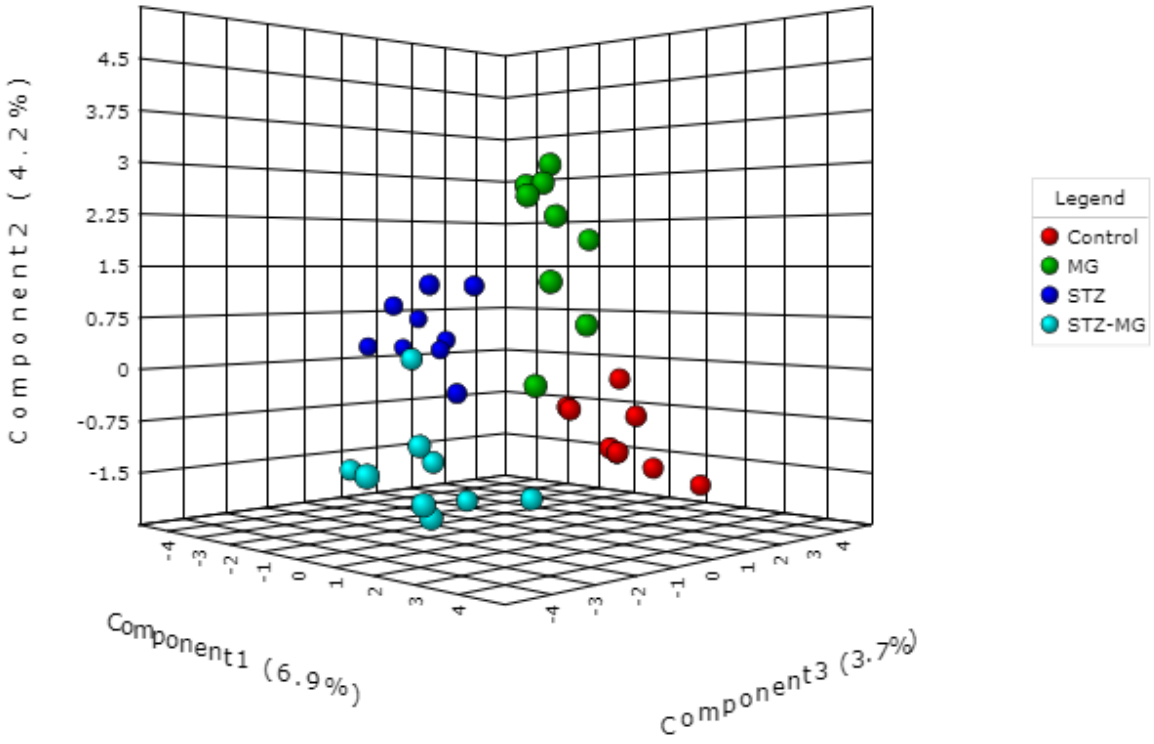

Figure 5.9 PCA plot shows reproducibility among replicate runs of each treatment

5.3.5.1 Methylglyoxal induces altered expression of different proteins in animal plasma

Tryptic digest of animal plasma was subjected to expression analysis using SWATH-MS workflow. A total of 132 proteins were identified in the spectral library obtained from the combined IDA of all groups. All the differentially expressed proteins were significant at p-value < 0.05. Differential proteomics analysis of all groups is shown in (Figure 5.10). In MG to Control group comparison, 13 proteins were upregulated, and 34 proteins were downregulated by more than 1.3 fold. In STZ to Control group comparison, 28 proteins were upregulated, and 17 proteins were downregulated by more than 1.3 fold. In STZ-MG to Control group comparison, 14 proteins were upregulated, and 20 proteins were downregulated by more than 1.3 fold. Gene Ontology analysis was performed by Cytoscape using the ClueGo plugin; the protein-protein

interaction network shows the processes in which the differentially expressed proteins of MG to Control comparison (Figure 5.11) and STZ to control comparison (Figure 5.12) are involved. For MG to control comparison group, the differentially expressed proteins were found to be involved in biological processes such as proteasomal ubiquitin-independent protein catabolic process, collagen fibril organization, response to epidermal growth factor, and bone resorption. For STZ to control the comparison group, the differentially expressed proteins were found to be involved in biological processes such as positive regulation of receptor-mediated endocytosis, collagen fibril organization, and positive regulation of reactive oxygen species metabolic process.

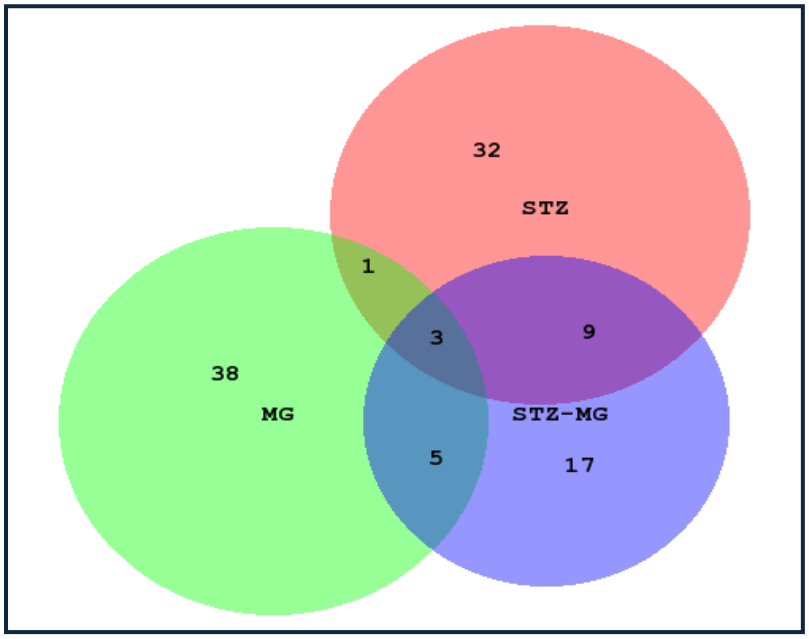

Figure 5.10 Proteomic Analysis of Rat Plasma

Differential proteomics analysis was done by SWATH-MS. The total number of differentially expressed proteins in all groups

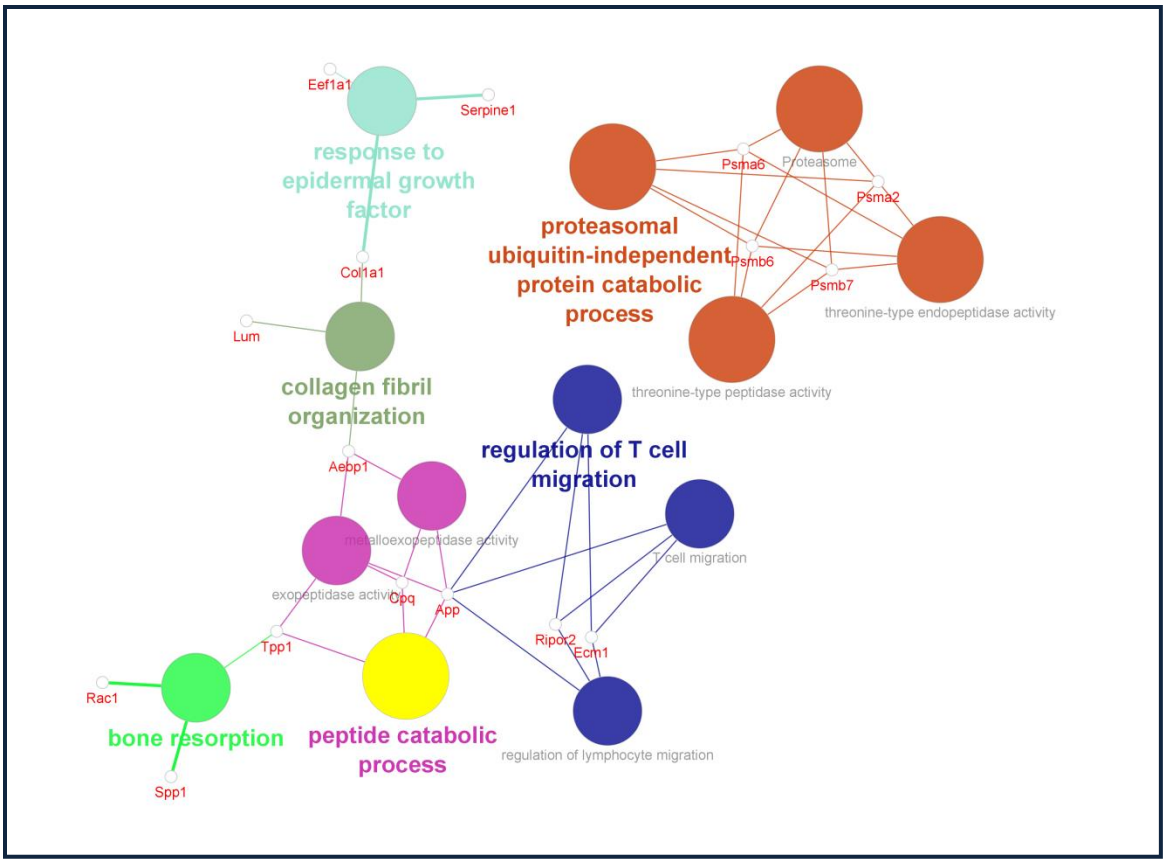

Figure 5.11 Bioinformatic analysis

PPI network for MG to control group comparison showing differentially abundant proteins Gene ontology (biological process)

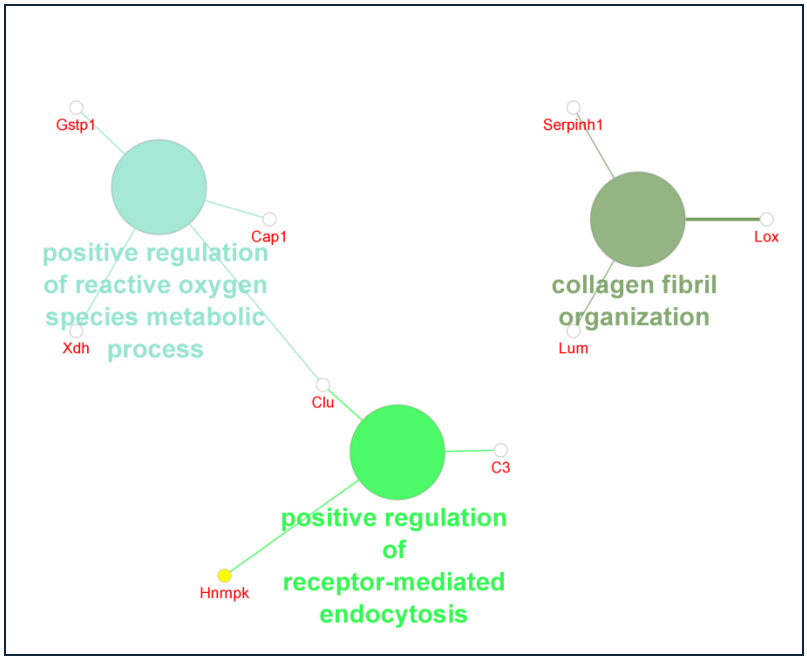

Figure 5.12 Bioinformatic analysis

PPI network for STZ to control group comparison showing differentially abundant proteins Gene ontology (biological process)

5.3.6 **Comparison of Animal plasma and Secretome**

Proteins from secretome and animal plasma proteome were compared, and Carboxypeptidase Q was found to be common and downregulated between both the groups as well as among animal groups(Table 5.3). Carboxypeptidase has been localized to the endothelial and epithelial cells of the heart and kidney, where at the cell surface, it may hydrolyze bioactive peptides present in the circulation. It has a vital role in heart function, in regulating blood pressure, and in diabetes[261].

Table 5.3 Comparison of secretome and animal plasma proteins

Protein Name	MG-Control (Fold change)	STZ-Control (Fold change)	STZ-MG-Control (Fold change)	Secretome (Fold change)
Carboxypeptidase Q	**0.71**	**0.67**	**0.33**	**0.41**

5.3.7 **Comparison of Animal plasma and Clinical plasma**

Proteins from clinical plasma and animal plasma proteome were compared, and Vitamin K-dependent protein S protein was found to be common between both the groups (Table 5.4). It was upregulated in the STZ-control group and in clinical plasma by 1.64 fold and 1.99 fold, respectively. Vitamin K-dependent protein S (PROS1 or protein S) is an essential anticoagulant and multifunctional protein, and it also regulates inflammation and cell apoptosis[262].

Table 5.4 Comparison of Animal plasma and Clinical plasma proteins

Protein Name	Fold change (STZ-Control)	Fold change (Clinical Plasma)
Vitamin K-dependent protein S	**1.64**	**1.99**

5.4 Conclusion

In this chapter, we discussed animal experiments, which were performed in 4 groups, control, MG, STZ, and STZ-MG. We did the animal plasma proteomics study where 132 proteins were obtained through IDA spectral library. We studied MG-induced modifications in rat serum albumin. An increase in MG-induced modifications of two Rat Serum Albumin peptides, R(Argpyr)PCFSALTVDETYVPK and LVQEVTDFAK(CEL)TCVADENAENCDK, could be associated with an increase in the levels of MG in diabetes. Kidney histopathology studies have shown moderate to severe changes in STZ and STZ-MG groups. Changes in Rat's eyes were observed, which indicates the onset of diabetic complications.

Deregulated proteins of the MG-control group were found to be involved in the Proteasomal ubiquitin-independent protein catabolic process and collagen fibril organization. Deregulated proteins of the STZ-control group were found to be involved in positive regulation of reactive oxygen species metabolic process and positive regulation of receptor-mediated endocytosis.

References

1. Expert Committee on the, D. and M. Classification of Diabetes, *Follow-up report on the diagnosis of diabetes mellitus.* Diabetes care, 2003. **26**(11): p. 3160-3167.
2. Colberg, S.R., et al., *Exercise and type 2 diabetes: the American College of Sports Medicine and the American Diabetes Association: joint position statement.* Diabetes care, 2010. **33**(12): p. e147-e167.
3. Campbell, I.W., *Epidemiology and clinical presentation of type 2 diabetes.* Value in Health, 2000. **3**: p. S3-S6.
4. Zhao, Y., et al., *Type 2 diabetes mellitus-disease, diagnosis and treatment.* J Diabetes Metab, 2015. **6**(533): p. 2.
5. Karamanou, M., et al., *Milestones in the history of diabetes mellitus: The main contributors.* World journal of diabetes, 2016. **7**(1): p. 1.
6. Eknoyan, G. and J. Nagy, *A history of diabetes mellitus or how a disease of the kidneys evolved into a kidney disease.* Advances in chronic kidney disease, 2005. **12**(2): p. 223-229.
7. Peumery, J.-J., *Histoire illustrée du diabète: de l'antiquité à nos jours*. 1987: Dacosta.
8. Ahmed, A.M., *History of diabetes mellitus.* Saudi medical journal, 2002. **23**(4): p. 373-378.
9. Marín-Peñalver, J.J., et al., *Update on the treatment of type 2 diabetes mellitus.* World journal of diabetes, 2016. **7**(17): p. 354.
10. Rother, K.I., *Diabetes treatment-bridging the divide.* The New England journal of medicine, 2007. **356**(15): p. 1499.
11. Verge, C.F., et al., *Prediction of type I diabetes in first-degree relatives using a combination of insulin, GAD, and ICA512bdc/IA-2 autoantibodies.* Diabetes, 1996. **45**(7): p. 926-933.
12. You, W.-P. and M. Henneberg, *Type 1 diabetes prevalence increasing globally and regionally: the role of natural selection and life expectancy at birth.* BMJ open diabetes research and care, 2016. **4**(1).

13. Ward, W.K., et al., *Diminished B cell secretory capacity in patients with noninsulin-dependent diabetes mellitus.* The Journal of clinical investigation, 1984. **74**(4): p. 1318-1328.
14. Defronzo, R.A., *Pathogenesis of type 2 diabetes: metabolic and molecular implications for identifying diabetes genes.* Diabetes reviews, 1997. **5**: p. 177-266.
15. Evans, J.M.M., et al., *Socio-economic status, obesity and prevalence of Type 1 and Type 2 diabetes mellitus.* Diabetic Medicine, 2000. **17**(6): p. 478-480.
16. Imamura, F., et al., *Consumption of sugar sweetened beverages, artificially sweetened beverages, and fruit juice and incidence of type 2 diabetes: systematic review, meta-analysis, and estimation of population attributable fraction.* Bmj, 2015. **351**: p. h3576.
17. InterAct, C., *Consumption of sweet beverages and type 2 diabetes incidence in European adults: results from EPIC-InterAct.* Diabetologia, 2013. **56**(7): p. 1520-1530.
18. Malik, V.S., et al., *Sugar-sweetened beverages and risk of metabolic syndrome and type 2 diabetes: a meta-analysis.* Diabetes care, 2010. **33**(11): p. 2477-2483.
19. Homko, C.J. and M. Khandelwal, *Glucose monitoring and insulin therapy during pregnancy.* Obstetrics and Gynecology Clinics, 1996. **23**(1): p. 47-74.
20. Saldana, T.M., et al., *The relationship between pregnancy weight gain and glucose tolerance status among black and white women in central North Carolina.* American journal of obstetrics and gynecology, 2006. **195**(6): p. 1629-1635.
21. Kuzmicki, M., et al., *High resistin and interleukin-6 levels are associated with gestational diabetes mellitus.* Gynecological endocrinology, 2009. **25**(4): p. 258-263.
22. Wild, S., et al., *Global prevalence of diabetes: estimates for the year 2000 and projections for 2030.* Diabetes care, 2004. **27**(5): p. 1047-1053.
23. Saeedi, P., et al., *Global and regional diabetes prevalence estimates for 2019 and projections for 2030 and 2045: Results from the International Diabetes Federation Diabetes Atlas.* Diabetes Research and Clinical Practice, 2019. **157**: p. 107843.
24. Cowie, C.C., et al., *Full accounting of diabetes and pre-diabetes in the US population in 1988-1994 and 2005-2006.* Diabetes care, 2009. **32**(2): p. 287-294.
25. Mathers, C.D. and D. Loncar, *Projections of global mortality and burden of disease from 2002 to 2030.* PLoS medicine, 2006. **3**(11): p. e442.

26. Murray, C.J.L., A.D. Lopez, and O. World Health, *The global burden of disease: a comprehensive assessment of mortality and disability from diseases, injuries, and risk factors in 1990 and projected to 2020: summary*. 1996: World Health Organization.
27. DeFronzo, R.A., et al., *International textbook of diabetes mellitus*. 2015: John Wiley & Sons.
28. Fendler, W., et al., *Prevalence of monogenic diabetes amongst Polish children after a nationwide genetic screening campaign.* Diabetologia, 2012. **55**(10): p. 2631-2635.
29. Gavin Iii, J.R., et al., *Report of the expert committee on the diagnosis and classification of diabetes mellitus.* Diabetes care, 1997. **20**(7): p. 1183.
30. American Diabetes, A., *Standards of medical care in diabetes-2010.* Diabetes care, 2010. **33**(Supplement 1): p. S11-S61.
31. Goldstein, D.E., et al., *Tests of Glycemia in Diabetes.* Diabetes care, 2004. **27**(7): p. 1761-1773.
32. Higgins, T., *HbA 1c for screening and diagnosis of diabetes mellitus.* Endocrine, 2013. **43**(2): p. 266-273.
33. Sacks, D.B., *Measurement of hemoglobin A1c: a new twist on the path to harmony.* Diabetes care, 2012. **35**(12): p. 2674-2680.
34. Rahbar, S., *The Discovery of Glycated Hemoglobin: A Major Event in the Study of Nonenzymatic Chemistry in Biological Systems.* Annals of the New York Academy of Sciences, 2005. **1043**.
35. Sacks, D.B., et al., *Guidelines and Recommendations for Laboratory Analysis in the Diagnosis and Management of Diabetes Mellitus.* Diabetes care, 2011. **34**(6): p. e61-e99.
36. Wilcox, G., *Insulin and insulin resistance.* Clinical biochemist reviews, 2005. **26**(2): p. 19.
37. Mayer, J.P., F. Zhang, and R.D. DiMarchi, *Insulin structure and function.* Peptide Science: Original Research on Biomolecules, 2007. **88**(5): p. 687-713.
38. Rorsman, P. and M. Braun, *Regulation of insulin secretion in human pancreatic islets.* Annual review of physiology, 2013. **75**: p. 155-179.
39. Wang, Z. and D.C. Thurmond, *Mechanisms of biphasic insulin-granule exocytosis-roles of the cytoskeleton, small GTPases and SNARE proteins.* Journal of cell science, 2009. **122**(7): p. 893-903.

40. Röder, P.V., et al., *Pancreatic regulation of glucose homeostasis.* Experimental & molecular medicine, 2016. **48**(3): p. e219-e219.
41. Hers, H.G., *Mechanisms of blood glucose homeostasis.* Journal of inherited metabolic disease, 1990. **13**(4): p. 395-410.
42. Qaid, M.M. and M.M. Abdelrahman, *Role of insulin and other related hormones in energy metabolismâ€"A review.* Cogent Food & Agriculture, 2016. **2**(1): p. 1267691.
43. Klip, A. and M.R. PÃ¢quet, *Glucose transport and glucose transporters in muscle and their metabolic regulation.* Diabetes care, 1990. **13**(3): p. 228-243.
44. Pessin, J.E. and A.R. Saltiel, *Signaling pathways in insulin action: molecular targets of insulin resistance.* The Journal of clinical investigation, 2000. **106**(2): p. 165-169.
45. Bevan, P., *Insulin signalling.* Journal of cell science, 2001. **114**(8): p. 1429-1430.
46. Kahn, C.R. and M. White, *The insulin receptor and the molecular mechanism of insulin action.* The Journal of clinical investigation, 1988. **82**(4): p. 1151-1156.
47. Fröjdö, S., H. Vidal, and L. Pirola, *Alterations of insulin signaling in type 2 diabetes: a review of the current evidence from humans.* Biochimica et Biophysica Acta (BBA)-Molecular Basis of Disease, 2009. **1792**(2): p. 83-92.
48. Stöckli, J., D.J. Fazakerley, and D.E. James, *GLUT4 exocytosis.* Journal of cell science, 2011. **124**(24): p. 4147-4159.
49. Chang, L., S.-H. Chiang, and A.R. Saltiel, *Insulin signaling and the regulation of glucose transport.* Molecular medicine, 2004. **10**(7-12): p. 65-71.
50. Foley, K., S. Boguslavsky, and A. Klip, *Endocytosis, recycling, and regulated exocytosis of glucose transporter 4.* Biochemistry, 2011. **50**(15): p. 3048-3061.
51. Hesselink, M.K.C., V. Schrauwen-Hinderling, and P. Schrauwen, *Skeletal muscle mitochondria as a target to prevent or treat type 2 diabetes mellitus.* Nature Reviews Endocrinology, 2016. **12**(11): p. 633.
52. Kang, S., L.T.Y. Tsai, and E.D. Rosen, *Nuclear mechanisms of insulin resistance.* Trends in cell biology, 2016. **26**(5): p. 341-351.
53. Draznin, B., *Molecular mechanisms of insulin resistance: serine phosphorylation of insulin receptor substrate-1 and increased expression of p85Î±: the two sides of a coin.* Diabetes, 2006. **55**(8): p. 2392-2397.

54. Bandyopadhyay, G.K., et al., *Increased p85/55/50 expression and decreased phosphotidylinositol 3-kinase activity in insulin-resistant human skeletal muscle.* Diabetes, 2005. **54**(8): p. 2351-2359.

55. Giorgino, F., et al., *Specific increase in p85α expression in response to dexamethasone is associated with inhibition of insulin-like growth factor-I stimulated phosphatidylinositol 3-kinase activity in cultured muscle cells.* Journal of Biological Chemistry, 1997. **272**(11): p. 7455-7463.

56. Barbour, L.A., et al., *Increased P85α is a potent negative regulator of skeletal muscle insulin signaling and induces in vivo insulin resistance associated with growth hormone excess.* Journal of Biological Chemistry, 2005. **280**(45): p. 37489-37494.

57. Barbour, L.A., et al., *Human placental growth hormone increases expression of the p85 regulatory unit of phosphatidylinositol 3-kinase and triggers severe insulin resistance in skeletal muscle.* Endocrinology, 2004. **145**(3): p. 1144-1150.

58. Cornier, M.A., et al., *Nutritional upregulation of p85α expression is an early molecular manifestation of insulin resistance.* Diabetologia, 2006. **49**(4): p. 748-754.

59. Mey, J.T. and J.M. Haus, *Dicarbonyl stress and Glyoxalase-1 in skeletal muscle: implications for insulin resistance and type 2 diabetes.* Frontiers in cardiovascular medicine, 2018. **5**: p. 117.

60. Schalkwijk, C.G., O. Brouwers, and C.D.A. Stehouwer, *Modulation of insulin action by advanced glycation endproducts: a new player in the field.* Hormone and Metabolic Research, 2008. **40**(09): p. 614-619.

61. Riboulet-Chavey, A., et al., *Methylglyoxal impairs the insulin signaling pathways independently of the formation of intracellular reactive oxygen species.* Diabetes, 2006. **55**(5): p. 1289-1299.

62. Nigro, C., et al., *Methylglyoxal impairs endothelial insulin sensitivity both in vitro and in vivo.* Diabetologia, 2014. **57**(7): p. 1485-1494.

63. Fiory, F., et al., *Methylglyoxal impairs insulin signalling and insulin action on glucose-induced insulin secretion in the pancreatic beta cell line INS-1E.* Diabetologia, 2011. **54**(11): p. 2941.

64. Moraru, A., et al., *Elevated levels of the reactive metabolite methylglyoxal recapitulate progression of type 2 diabetes.* Cell metabolism, 2018. **27**(4): p. 926-934. e8.

65. Michael Brownlee, M.D., *Advanced Protein Glycosylation In Diabetes And Aging.* Annual Review of Medicine, 1995. **46**(1): p. 223-234.
66. Ulrich, P. and A. Cerami, *Protein glycation, diabetes, and aging.* Recent progress in hormone research, 2001. **56**(1): p. 1-22.
67. Baynes, J.W. and S.R. Thorpe, *Role of oxidative stress in diabetic complications: a new perspective on an old paradigm.* Diabetes, 1999. **48**(1): p. 1-9.
68. Thornalley, P.J., A. Langborg, and H.S. Minhas, *Formation of glyoxal, methylglyoxal and 3-deoxyglucosone in the glycation of proteins by glucose.* Biochemical Journal, 1999. **344**(1): p. 109-116.
69. Thornalley, P.J., *Pharmacology of methylglyoxal: formation, modification of proteins and nucleic acids, and enzymatic detoxification-a role in pathogenesis and antiproliferative chemotherapy.* General Pharmacology: The Vascular System, 1996. **27**(4): p. 565-573.
70. Ott, C., et al., *Role of advanced glycation end products in cellular signaling.* Redox biology, 2014. **2**: p. 411-429.
71. Kalousova, M., et al., *Advanced glycation end products in clinical nephrology.* Kidney and Blood Pressure Research, 2004. **27**(1): p. 18-28.
72. Lieuw-A-Fa, M.L.M., et al., *Increased levels of N e-(carboxymethyl) lysine and N e-(carboxyethyl) lysine in type 1 diabetic patients with impaired renal function: correlation with markers of endothelial dysfunction.* Nephrology Dialysis Transplantation, 2004. **19**(3): p. 631-636.
73. O'Brien, J., P.A. Morrissey, and J.M. Ames, *Nutritional and toxicological aspects of the Maillard browning reaction in foods.* Critical Reviews in Food Science & Nutrition, 1989. **28**(3): p. 211-248.
74. Goldberg, T., et al., *Advanced glycoxidation end products in commonly consumed foods.* Journal of the American Dietetic Association, 2004. **104**(8): p. 1287-1291.
75. Uribarri, J., et al., *Advanced glycation end products in foods and a practical guide to their reduction in the diet.* Journal of the American Dietetic Association, 2010. **110**(6): p. 911-916. e12.
76. Koschinsky, T., et al., *Orally absorbed reactive glycation products (glycotoxins): an environmental risk factor in diabetic nephropathy.* Proceedings of the National Academy of Sciences, 1997. **94**(12): p. 6474-6479.

77. Negrean, M., et al., *Effects of low-and high-advanced glycation endproduct meals on macro-and microvascular endothelial function and oxidative stress in patients with type 2 diabetes mellitus.* The American journal of clinical nutrition, 2007. **85**(5): p. 1236-1243.
78. Brownlee, M., *Biochemistry and molecular cell biology of diabetic complications.* Nature, 2001. **414**(6865): p. 813-820.
79. Shinohara, M., et al., *Overexpression of glyoxalase-I in bovine endothelial cells inhibits intracellular advanced glycation endproduct formation and prevents hyperglycemia-induced increases in macromolecular endocytosis.* The Journal of clinical investigation, 1998. **101**(5): p. 1142-1147.
80. Rabbani, N. and P.J. Thornalley, *Measurement of methylglyoxal by stable isotopic dilution analysis LC-MS/MS with corroborative prediction in physiological samples.* Nature protocols, 2014. **9**(8): p. 1969.
81. Thornalley, P.J., *Dicarbonyl intermediates in the Maillard reaction.* Annals of the New York Academy of Sciences, 2005. **1043**(1): p. 111-117.
82. Degenhardt, T.P., S.R. Thorpe, and J.W. Baynes, *Chemical modification of proteins by methylglyoxal.* Cellular and molecular biology (Noisy-le-Grand, France), 1998. **44**(7): p. 1139.
83. Lo, T.W., et al., *Binding and modification of proteins by methylglyoxal under physiological conditions. A kinetic and mechanistic study with N alpha-acetylarginine, N alpha-acetylcysteine, and N alpha-acetyllysine, and bovine serum albumin.* Journal of Biological Chemistry, 1994. **269**(51): p. 32299-32305.
84. Westwood, M.E. and P.J. Thornalley, *Molecular characteristics of methylglyoxal-modified bovine and human serum albumins. Comparison with glucose-derived advanced glycation endproduct-modified serum albumins.* Journal of protein chemistry, 1995. **14**(5): p. 359-372.
85. Shoji, N., et al., *LC-MS/MS analysis of carboxymethylated and carboxyethylated phosphatidylethanolamines in human erythrocytes and blood plasma.* Journal of lipid research, 2010. **51**(8): p. 2445-2453.
86. Li, Y., et al., *The structural modification of DNA nucleosides by nonenzymatic glycation: an in vitro study based on the reactions of glyoxal and methylglyoxal with 2â€²-deoxyguanosine.* Analytical and bioanalytical chemistry, 2008. **390**(2): p. 679-688.

87. Phillips, s.a. And p.j. Thornalley, *The formation of methylglyoxal from triose phosphates: investigation using a specific assay for methylglyoxal.* European Journal of Biochemistry, 1993. **212**(1): p. 101-105.

88. Sousa Silva, M., et al., *The glyoxalase pathway: the first hundred years... and beyond.* Biochemical Journal, 2013. **453**(1): p. 1-15.

89. Ahmed, N., et al., *Increased formation of methylglyoxal and protein glycation, oxidation and nitrosation in triosephosphate isomerase deficiency.* Biochimica et Biophysica Acta (BBA)-Molecular Basis of Disease, 2003. **1639**(2): p. 121-132.

90. Reichard, G.A., et al., *Acetone metabolism in humans during diabetic ketoacidosis.* Diabetes, 1986. **35**(6): p. 668-674.

91. Lyles, G.A. and J. Chalmers, *The metabolism of aminoacetone to methylglyoxal by semicarbazide-sensitive amine oxidase in human umbilical artery.* Biochemical pharmacology, 1992. **43**(7): p. 1409-1414.

92. Baynes, J.W. and S.R. Thorpe, *Glycoxidation and lipoxidation in atherogenesis.* Free Radical Biology and Medicine, 2000. **28**(12): p. 1708-1716.

93. Degen, J., M. Hellwig, and T. Henle, *1, 2-Dicarbonyl compounds in commonly consumed foods.* Journal of agricultural and food chemistry, 2012. **60**(28): p. 7071-7079.

94. Degen, J., et al., *Metabolic transit of dietary methylglyoxal.* Journal of agricultural and food chemistry, 2013. **61**(43): p. 10253-10260.

95. Beisswenger, P.J., et al., *Metformin reduces systemic methylglyoxal levels in type 2 diabetes.* Diabetes, 1999. **48**(1): p. 198-202.

96. Han, Y., et al., *Plasma methylglyoxal and glyoxal are elevated and related to early membrane alteration in young, complication-free patients with Type 1 diabetes.* Molecular and cellular biochemistry, 2007. **305**(1-2): p. 123-131.

97. Henning, C., et al., *Extending the spectrum of α-dicarbonyl compounds in vivo.* Journal of Biological Chemistry, 2014. **289**(41): p. 28676-28688.

98. Lapolla, A., et al., *Glyoxal and methylglyoxal levels in diabetic patients: quantitative determination by a new GC/MS method.* Clinical Chemistry and Laboratory Medicine, 2003. **41**(9): p. 1166-1173.

99. McLellan, A.C., et al., *Glyoxalase system in clinical diabetes mellitus and correlation with diabetic complications.* Clinical Science, 1994. **87**(1): p. 21-29.

100. Odani, H., et al., *Increase in three α, β-dicarbonyl compound levels in human uremic plasma: Specificin vivodetermination of intermediates in advanced maillard reaction.* Biochemical and biophysical research communications, 1999. **256**(1): p. 89-93.

101. Scheijen, J.L.J.M. and C.G. Schalkwijk, *Quantification of glyoxal, methylglyoxal and 3-deoxyglucosone in blood and plasma by ultra performance liquid chromatography tandem mass spectrometry: evaluation of blood specimen.* Clinical Chemistry and Laboratory Medicine (CCLM), 2014. **52**(1): p. 85-91.

102. Ahmed, N., et al., *Methylglyoxal-derived hydroimidazolone advanced glycation end-products of human lens proteins.* Investigative ophthalmology & visual science, 2003. **44**(12): p. 5287-5292.

103. Tamae, D., et al., *Mutagenesis and repair induced by the DNA advanced glycation end product N 2-1-(carboxyethyl)-2â€²-deoxyguanosine in human cells.* Biochemistry, 2011. **50**(12): p. 2321-2329.

104. Wuenschell, G.E., et al., *Mutagenic potential of DNA glycation: Miscoding by (R)-and (S)-N 2-(1-carboxyethyl)-2'-deoxyguanosine.* Biochemistry, 2010. **49**(9): p. 1814-1821.

105. Racker, E., *The mechanism of action of glyoxalase.* Journal of Biological Chemistry, 1951. **190**(2): p. 685-696.

106. Ekwall, K. and B. Mannervik, *The sterochemical configuration of the lactoyl group of S-lactoylglutathionine formed by the action of glyoxalase I from porcine erythrocytes and yeast.* Biochimica et Biophysica Acta (BBA)-General Subjects, 1973. **297**(2): p. 297-299.

107. Rabbani, N. and P.J. Thornalley. *Glyoxalase in diabetes, obesity and related disorders*. in *Seminars in cell & developmental biology*. 2011: Elsevier.

108. Thornalley, P., *Glyoxalase I–structure, function and a critical role in the enzymatic defence against glycation*. 2003, Portland Press Limited.

109. Rabbani, N. and Paul J. Thornalley, *Dicarbonyl proteome and genome damage in metabolic and vascular disease.* Biochemical Society Transactions, 2014. **42**(2): p. 425-432.

110. Dobler, D., et al., *Increased dicarbonyl metabolism in endothelial cells in hyperglycemia induces anoikis and impairs angiogenesis by RGD and GFOGER motif modification.* Diabetes, 2006. **55**(7): p. 1961-1969.

111. Morgenstern, J., et al., *Loss of glyoxalase 1 induces compensatory mechanism to achieve dicarbonyl detoxification in mammalian Schwann cells.* Journal of Biological Chemistry, 2017. **292**(8): p. 3224-3238.

112. Schumacher, D., et al., *Compensatory mechanisms for methylglyoxal detoxification in experimental & clinical diabetes.* Molecular metabolism, 2018. **18**: p. 143-152.

113. Baba, S.P., et al., *Reductive metabolism of AGE precursors: a metabolic route for preventing AGE accumulation in cardiovascular tissue.* Diabetes, 2009. **58**(11): p. 2486-2497.

114. Lee, J.-y., et al., *Human DJ-1 and its homologs are novel glyoxalases.* Human molecular genetics, 2012. **21**(14): p. 3215-3225.

115. Lodd, E., et al., *The combination of loss of glyoxalase1 and obesity results in hyperglycemia.* JCI insight, 2019. **4**(12).

116. Löbner, J.r., J. Degen, and T. Henle, *Creatine is a scavenger for methylglyoxal under physiological conditions via formation of N-(4-methyl-5-oxo-1-imidazolin-2-yl) sarcosine (MG-HCr).* Journal of agricultural and food chemistry, 2015. **63**(8): p. 2249-2256.

117. Pal, A., A. Roy, and M. Ray, *Creatine supplementation with methylglyoxal: a potent therapy for cancer in experimental models.* Amino acids, 2016. **48**(8): p. 2003-2013.

118. Salomón, T., et al., *Ketone body acetoacetate buffers methylglyoxal via a non-enzymatic conversion during diabetic and dietary ketosis.* Cell Chemical Biology, 2017. **24**(8): p. 935-943. e7.

119. Schalkwijk, C.G., et al., *Heat-shock protein 27 is a major methylglyoxal-modified protein in endothelial cells.* FEBS letters, 2006. **580**(6): p. 1565-1570.

120. Thornalley, P.J., *Modification of the glyoxalase system in human red blood cells by glucose in vitro.* Biochemical Journal, 1988. **254**(3): p. 751-755.

121. Van Eupen, M.G.A., et al., *The methylglyoxal-derived AGE tetrahydropyrimidine is increased in plasma of individuals with type 1 diabetes mellitus and in atherosclerotic lesions and is associated with sVCAM-1.* Diabetologia, 2013. **56**(8): p. 1845-1855.

122. Eringa, E.C., et al., *Endothelial dysfunction in (pre) diabetes: characteristics, causative mechanisms and pathogenic role in type 2 diabetes.* Reviews in Endocrine and Metabolic Disorders, 2013. **14**(1): p. 39-48.

123. Banarjee, R., et al., *Proteomic study of endothelial dysfunction induced by AGEs and its possible role in diabetic cardiovascular complications.* Journal of proteomics, 2018. **187**: p. 69-79.

124. Rabbani, N. and P.J. Thornalley, *Advanced glycation end products in the pathogenesis of chronic kidney disease.* Kidney international, 2018. **93**(4): p. 803-813.

125. Hanssen, N.M.J., C.D.A. Stehouwer, and C.G. Schalkwijk, *Methylglyoxal stress, the glyoxalase system, and diabetic chronic kidney disease.* Current Opinion in Nephrology and Hypertension, 2019. **28**(1): p. 26-33.

126. Beisswenger, P.J., et al., *Susceptibility to diabetic nephropathy is related to dicarbonyl and oxidative stress.* Diabetes, 2005. **54**(11): p. 3274-3281.

127. Lu, J., et al., *Increased plasma methylglyoxal level, inflammation, and vascular endothelial dysfunction in diabetic nephropathy.* Clinical biochemistry, 2011. **44**(4): p. 307-311.

128. Nakayama, K., et al., *Plasma α-oxoaldehyde levels in diabetic and nondiabetic chronic kidney disease patients.* American journal of nephrology, 2008. **28**(6): p. 871-878.

129. Hanssen, N.M.J., et al., *Higher plasma methylglyoxal levels are associated with incident cardiovascular disease in individuals with type 1 diabetes: a 12-year follow-up study.* Diabetes, 2017. **66**(8): p. 2278-2283.

130. Jensen, T.M., et al., *Methylglyoxal is associated with changes in kidney function among individuals with screen-detected Type 2 diabetes mellitus.* Diabetic Medicine, 2016. **33**(12): p. 1625-1631.

131. Beisswenger, P.J., et al., *Early progression of diabetic nephropathy correlates with methylglyoxal-derived advanced glycation end products.* Diabetes care, 2013. **36**(10): p. 3234-3239.

132. Karachalias, N., et al., *Accumulation of fructosyl-lysine and advanced glycation end products in the kidney, retina and peripheral nerve of streptozotocin-induced diabetic rats.* Biochemical Society Transactions, 2003. **31**(6): p. 1423-1425.

133. Fukunaga, M., et al., *Methylglyoxal induces apoptosis through activation of p38 MAPK in rat Schwann cells.* Biochemical and biophysical research communications, 2004. **320**(3): p. 689-695.

134. Lee, H.K., et al., *A novel mechanism of methylglyoxal cytotoxicity in neuroglial cells.* Journal of neurochemistry, 2009. **108**(1): p. 273-284.

135. Bierhaus, A., et al., *Methylglyoxal modification of Na v 1.8 facilitates nociceptive neuron firing and causes hyperalgesia in diabetic neuropathy.* Nature medicine, 2012. **18**(6): p. 926-933.

136. Hanssen, N.M.J., et al., *Higher levels of advanced glycation endproducts in human carotid atherosclerotic plaques are associated with a rupture-prone phenotype.* European heart journal, 2014. **35**(17): p. 1137-1146.

137. Lehrke, M. and N. Marx, *Diabetes mellitus and heart failure.* The American Journal of Cardiology, 2017. **120**(1): p. S37-S47.

138. Shao, C.H., et al., *Carbonylation contributes to SERCA2a activity loss and diastolic dysfunction in a rat model of type 1 diabetes.* Diabetes, 2011. **60**(3): p. 947-959.

139. Shao, C.H., et al., *Carbonylation induces heterogeneity in cardiac ryanodine receptor function in diabetes mellitus.* Molecular pharmacology, 2012. **82**(3): p. 383-399.

140. Tian, C., et al., *Reactive carbonyl species and their roles in sarcoplasmic reticulum Ca 2+ cycling defect in the diabetic heart.* Heart failure reviews, 2014. **19**(1): p. 101-112.

141. Cook, L.J., et al., *Effects of methylglyoxal on rat pancreatic β-cells.* Biochemical pharmacology, 1998. **55**(9): p. 1361-1367.

142. Newgard, C.B. and J.D. McGarry, *Metabolic coupling factors in pancreatic β-cell signal transduction.* Annual review of biochemistry, 1995. **64**(1): p. 689-719.

143. Elmhiri, G., et al., *Acute exposure to a precursor of advanced glycation end products induces a dual effect on the rat pancreatic islet function.* International journal of endocrinology, 2014. **2014**.

144. Jia, X., et al., *Structural and functional changes in human insulin induced by methylglyoxal.* The FASEB Journal, 2006. **20**(9): p. 1555-1557.

145. Miele, C., et al., *Human glycated albumin affects glucose metabolism in L6 skeletal muscle cells by impairing insulin-induced insulin receptor substrate (IRS) signaling through a protein kinase Cα-mediated mechanism.* Journal of Biological Chemistry, 2003. **278**(48): p. 47376-47387.

146. Xue, M., et al., *Transcriptional control of glyoxalase 1 by Nrf2 provides a stress-responsive defence against dicarbonyl glycation.* Biochemical Journal, 2012. **443**(1): p. 213-222.

147. Mey, J.T., et al., *Dicarbonyl stress and glyoxalase enzyme system regulation in human skeletal muscle.* American Journal of Physiology-Regulatory, Integrative and Comparative Physiology, 2018. **314**(2): p. R181-R190.

148. DeFronzo, R.A., et al., *The effect of insulin on the disposal of intravenous glucose: results from indirect calorimetry and hepatic and femoral venous catheterization.* Diabetes, 1981. **30**(12): p. 1000-1007.

149. Amicarelli, F., et al., *Age-dependent ultrastructural alterations and biochemical response of rat skeletal muscle after hypoxic or hyperoxic treatments.* Biochimica et Biophysica Acta (BBA)-Molecular Basis of Disease, 1999. **1453**(1): p. 105-114.

150. Blake, R. and I.A. Trounce, *Mitochondrial dysfunction and complications associated with diabetes.* Biochimica et Biophysica Acta (BBA)-General Subjects, 2014. **1840**(4): p. 1404-1412.

151. Brings, S., et al., *Dicarbonyls and advanced glycation end-products in the development of diabetic complications and targets for intervention.* International journal of molecular sciences, 2017. **18**(5): p. 984.

152. Brouwers, O., et al., *Mild oxidative damage in the diabetic rat heart is attenuated by glyoxalase-1 overexpression.* International journal of molecular sciences, 2013. **14**(8): p. 15724-15739.

153. Brouwers, O., et al., *Overexpression of glyoxalase-I reduces hyperglycemia-induced levels of advanced glycation end products and oxidative stress in diabetic rats.* Journal of Biological Chemistry, 2011. **286**(2): p. 1374-1380.

154. Brouwers, O., et al., *Hyperglycaemia-induced impairment of endothelium-dependent vasorelaxation in rat mesenteric arteries is mediated by intracellular methylglyoxal levels in a pathway dependent on oxidative stress.* Diabetologia, 2010. **53**(5): p. 989-1000.

155. Brett, J., et al., *Survey of the distribution of a newly characterized receptor for advanced glycation end products in tissues.* The American journal of pathology, 1993. **143**(6): p. 1699.

156. López-Díez, R., et al., *Ager deletion enhances ischemic muscle inflammation, angiogenesis, and blood flow recovery in diabetic mice.* Arteriosclerosis, thrombosis, and vascular biology, 2017. **37**(8): p. 1536-1547.

157. Cassese, A., et al., *In skeletal muscle advanced glycation end products (AGEs) inhibit insulin action and induce the formation of multimolecular complexes including the receptor for AGEs.* Journal of Biological Chemistry, 2008. **283**(52): p. 36088-36099.

158. Mahmoud, A.M., et al., *Hyperinsulinemia augments endothelin-1 protein expression and impairs vasodilation of human skeletal muscle arterioles.* Physiological Reports, 2016. **4**(16): p. e12895.

159. Mahmoud, A.M., et al., *Skeletal muscle vascular function: a counterbalance of insulin action.* Microcirculation, 2015. **22**(5): p. 327-347.

160. Miele, C., et al., *Human glycated albumin affects glucose metabolism in L6 skeletal muscle cells by impairing insulin-induced insulin receptor substrate (IRS) signaling through a protein kinase CÎ±-mediated mechanism.* Journal of Biological Chemistry, 2003. **278**(48): p. 47376-47387.

161. Pirola, L., et al., *Phosphoinositide 3-kinase-mediated reduction of insulin receptor substrate-1/2 protein expression via different mechanisms contributes to the insulin-induced desensitization of its signaling pathways in L6 muscle cells.* Journal of Biological Chemistry, 2003. **278**(18): p. 15641-15651.

162. Eckardt, K., et al., *Myokines in insulin resistance and type 2 diabetes.* Diabetologia, 2014. **57**(6): p. 1087-1099.

163. Norheim, F., et al., *Proteomic identification of secreted proteins from human skeletal muscle cells and expression in response to strength training.* American Journal of Physiology-Endocrinology and Metabolism, 2011. **301**(5): p. E1013-E1021.

164. Nikolić, N., et al., *Electrical pulse stimulation of cultured human skeletal muscle cells as an in vitro model of exercise.* PloS one, 2012. **7**(3): p. e33203.

165. Giacco, F. and M. Brownlee, *Oxidative stress and diabetic complications.* Circulation research, 2010. **107**(9): p. 1058-1070.

166. Deshmukh, A.S., et al., *Secretome analysis of lipid-induced insulin resistance in skeletal muscle cells by a combined experimental and bioinformatics workflow.* Journal of proteome research, 2015. **14**(11): p. 4885-4895.

167. Yoon, J.H., et al., *Proteomic analysis of tumor necrosis factor-alpha (TNF-α)-induced L6 myotube secretome reveals novel TNF-α-dependent myokines in diabetic skeletal muscle.* Journal of proteome research, 2011. **10**(12): p. 5315-5325.

168. Ahmad, K., et al., *Consequences of dicarbonyl stress on skeletal muscle proteins and in Type 2 diabetes.* Current protein & peptide science, 2019.

169. Thornalley, P.J., *The glyoxalase system in health and disease.* Molecular aspects of medicine, 1993. **14**(4): p. 287-371.

170. Maessen, D.E.M., C.D.A. Stehouwer, and C.G. Schalkwijk, *The role of methylglyoxal and the glyoxalase system in diabetes and other age-related diseases.* Clinical Science, 2015. **128**(12): p. 839-861.

171. Rabbani, N. and P.J. Thornalley, *Dicarbonyl proteome and genome damage in metabolic and vascular disease*. **2014**, Portland Press Ltd. p. 425-432.

172. Jang, J.H., et al., *Methylglyoxal-induced apoptosis is dependent on the suppression of c-FLIPL expression via down-regulation of p65 in endothelial cells.* Journal of cellular and molecular medicine, 2017. **21**(11): p. 2720-2731.

173. Miyazawa, N., et al., *Methylglyoxal augments intracellular oxidative stress in human aortic endothelial cells.* Free radical research, 2010. **44**(1): p. 101-107.

174. Schalkwijk, C.G., *Vascular AGE-ing by methylglyoxal: the past, the present and the future.* Diabetologia, 2015. **58**(8): p. 1715-1719.

175. Yamawaki, H., et al., *Methylglyoxal mediates vascular inflammation via JNK and p38 in human endothelial cells.* American Journal of Physiology-Cell Physiology, 2008. **295**(6): p. C1510-C1517.

176. Thornalley, P.J., *The glyoxalase system: new developments towards functional characterization of a metabolic pathway fundamental to biological life.* Biochemical Journal, 1990. **269**(1): p. 1.

177. Dhar, A., et al., *Methylglyoxal scavengers attenuate endothelial dysfunction induced by methylglyoxal and high concentrations of glucose.* British journal of pharmacology, 2010. **161**(8): p. 1843-1856.

178. Chang, T., R. Wang, and L. Wu, *Methylglyoxal-induced nitric oxide and peroxynitrite production in vascular smooth muscle cells.* Free Radical Biology and Medicine, 2005. **38**(2): p. 286-293.

179. Thornalley, P.J., *Cell activation by glycated proteins. AGE receptors, receptor recognition factors and functional classification of AGEs.* Cellular and molecular biology (Noisy-le-Grand, France), 1998. **44**(7): p. 1013-1023.

180. Pavlou, M.P. and E.P. Diamandis, *The cancer cell secretome: a good source for discovering biomarkers?* Journal of proteomics, 2010. **73**(10): p. 1896-1906.

181. Lodish, H., et al., *Molecular cell biology 4th edition.* National Center for Biotechnology Information, Bookshelf, 2000. **9**.

182. Skalnikova, H., et al., *Mapping of the secretome of primary isolates of mammalian cells, stem cells and derived cell lines.* Proteomics, 2011. **11**(4): p. 691-708.

183. Armenteros, J.J.A., et al., *SignalP 5.0 improves signal peptide predictions using deep neural networks.* Nature biotechnology, 2019. **37**(4): p. 420.

184. Bendtsen, J.D.v., et al., *Feature-based prediction of non-classical and leaderless protein secretion.* Protein Engineering Design and Selection, 2004. **17**(4): p. 349-356.

185. Morris, J.H., et al., *clusterMaker: a multi-algorithm clustering plugin for Cytoscape.* BMC bioinformatics, 2011. **12**(1): p. 436.

186. Pedchenko, V.K., et al., *Mechanism of perturbation of integrin-mediated cell-matrix interactions by reactive carbonyl compounds and its implication for pathogenesis of diabetic nephropathy.* Diabetes, 2005. **54**(10): p. 2952-2960.

187. Lin, D., T.-H. Chun, and L. Kang, *Adipose extracellular matrix remodelling in obesity and insulin resistance.* Biochemical pharmacology, 2016. **119**: p. 8-16.

188. Getter, T., et al., *Novel inhibitors of leukocyte transendothelial migration.* Bioorganic Chemistry, 2019. **92**: p. 103250.

189. Savinov, A.Y. and A.Y. Strongin, *Defining the roles of T cell membrane proteinase and CD44 in type 1 diabetes.* IUBMB life, 2007. **59**(1): p. 6-13.

190. Phieler, J., et al. *The role of the complement system in metabolic organs and metabolic diseases*. in *Seminars in immunology*. 2013: Elsevier.

191. Morinaga, H., et al., *Increased macrophage migration into adipose tissue in obese mice.* Diabetes, 2012. **61**(2): p. 346-354.

192. Cantero, A.-V., et al., *Methylglyoxal induces advanced glycation end product (AGEs) formation and dysfunction of PDGF receptor-β: implications for diabetic atherosclerosis.* The FASEB Journal, 2007. **21**(12): p. 3096-3106.

193. Kemeny, S.F., et al., *Glycated collagen alters endothelial cell actin alignment and nitric oxide release in response to fluid shear stress.* Journal of biomechanics, 2011. **44**(10): p. 1927-1935.

194. Papadaki, M., et al., *Fluid shear stress as a regulator of gene expression in vascular cells: possible correlations with diabetic abnormalities.* Diabetes Research and Clinical Practice, 1999. **45**(2-3): p. 89-99.

195. Takahashi, A., et al., *Autophagy inhibits the accumulation of advanced glycation end products by promoting lysosomal biogenesis and function in the kidney proximal tubules.* Diabetes, 2017. **66**(5): p. 1359-1372.

196. Grimm, S., et al., *Cathepsins D and L reduce the toxicity of advanced glycation end products.* Free Radical Biology and Medicine, 2012. **52**(6): p. 1011-1023.

197. Deshmukh, A.B., et al., *Methylglyoxal attenuates insulin signaling and downregulates the enzymes involved in cholesterol biosynthesis.* Molecular BioSystems, 2017. **13**(11): p. 2338-2349.

198. Indulekha, K., J. Surendar, and V. Mohan, *High sensitivity C-reactive protein, tumor necrosis factor-α, interleukin-6, and vascular cell adhesion molecule-1 levels in Asian Indians with metabolic syndrome and insulin resistance (CURES-105).* Journal of diabetes science and technology, 2011. **5**(4): p. 982-988.

199. Liu, L.F., et al., *The receptor CD44 is associated with systemic insulin resistance and proinflammatory macrophages in human adipose tissue.* Diabetologia, 2015. **58**(7): p. 1579-1586.

200. Wang, T.-T., X.-M. Wang, and X.-L. Zhang. *Circulating Vascular Cell Adhesion Molecule-1 (VCAM-1) and Intercellular Adhesion Molecule-1 (ICAM-1): Relationship with carotid artery elasticity in patients with impaired glucose regulation (IGR).* in *Annales d'endocrinologie*. 2019: Elsevier.

201. Pivovarova, O., et al., *Insulin up-regulates natriuretic peptide clearance receptor expression in the subcutaneous fat depot in obese subjects: a missing link between CVD risk and obesity?* The Journal of Clinical Endocrinology, 2012. **97**(5): p. E731-E739.

202. Zhang, R., et al., *Mining biomarkers in human sera using proteomic tools.* Proteomics, 2004. **4**(1): p. 244-256.

203. Lim, P.S., Y.-K. Chang, and T.-K. Wu, *Serum Lipopolysaccharide-Binding Protein is Associated with Chronic Inflammation and Metabolic Syndrome in Hemodialysis Patients.* Blood purification, 2019. **47**(1-3): p. 28-36.

204. Cura-Esquivel, I., et al., *Acute phase markers in obese children and adolescents with metabolic disorders.* Arch Argent Pediatr, 2018. **116**(4): p. 275-282.

205. Liu, B., et al., *Altered protein expression in gestational diabetes mellitus placentas provides insight into insulin resistance and coagulation/fibrinolysis pathways.* PloS one, 2012. **7**(9): p. e44701.

206. Wang, Y., et al., *Plasma Fetuin-A Levels and Risk of Type 2 Diabetes Mellitus in A Chinese Population: A Nested Case-Control Study.* Diabetes & metabolism journal, 2019. **43**.

207. Copenhaver, M., C.-Y. Yu, and R.P. Hoffman, *Complement Components, C3 and C4, and the Metabolic Syndrome.* Current diabetes reviews, 2019. **15**(1): p. 44-48.

208. Wu, T., et al., *Circulating mesencephalic astrocyte-derived neurotrophic factor is increased in newly diagnosed prediabetic and diabetic patients, and is associated with insulin resistance.* Endocrine journal, 2017: p. EJ16-0472.

209. Srinivasan, V., et al., *Molecular convergence of hexosamine biosynthetic pathway and ER stress leading to insulin resistance in L6 skeletal muscle cells.* Molecular and cellular biochemistry, 2009. **328**(1-2): p. 217-224.

210. Xin, Y., et al., *Complement C3 and C4, but not their regulators or activated products, are associated with incident metabolic syndrome: the CODAM study.* Endocrine, 2018. **62**(3): p. 617-627.

211. Calan, M., et al., *The relationship between urotensin II and insulin resistance in women with gestational diabetes mellitus.* Hormones, 2019. **18**(1): p. 91-97.

212. Chien, C.-Y., et al., *A novel potential biomarker for metabolic syndrome in Chinese adults: Circulating protein disulfide isomerase family A, member 4.* PloS one, 2017. **12**(6): p. e0179963.

213. Arner, P., et al., *Screening of potential adipokines identifies S100A4 as a marker of pernicious adipose tissue and insulin resistance.* International Journal of Obesity, 2018. **42**(12): p. 2047.

214. Atalar, M.N., et al., *Assessment of serum galectin-3, methylated arginine and Hs-CRP levels in type 2 diabetes and prediabetes.* Life sciences, 2019. **231**: p. 116577.

215. Wang, X., H. Ma, and X. Wang, *Nucleophosmin/B23 contributes to hepatic insulin resistance through the modulation of NF-κB pathway.* Biochemical and biophysical research communications, 2019. **511**(2): p. 214-220.

216. Romeo, G.R., et al., *Profilin-1 haploinsufficiency protects against obesity-associated glucose intolerance and preserves adipose tissue immune homeostasis.* Diabetes, 2013. **62**(11): p. 3718-3726.

217. Hoofnagle, A.N., et al., *Low clusterin levels in high-density lipoprotein associate with insulin resistance, obesity, and dyslipoproteinemia.* Arteriosclerosis, thrombosis, and vascular biology, 2010. **30**(12): p. 2528-2534.

218. Wolff, G., et al., *Diet-dependent function of the extracellular matrix proteoglycan Lumican in obesity and glucose homeostasis.* Molecular metabolism, 2019. **19**: p. 97-106.

219. Zhu, L.-H., et al., *Mindin/Spondin 2 inhibits hepatic steatosis, insulin resistance, and obesity via interaction with peroxisome proliferator-activated receptor α in mice.* Journal of hepatology, 2014. **60**(5): p. 1046-1054.

220. Yasuma, T., et al., *Amelioration of diabetes by protein S.* Diabetes, 2016. **65**(7): p. 1940-1951.

221. Yuan, H., et al., *AMP-activated protein kinase-mediated expression of heat shock protein beta 1 enhanced insulin sensitivity in the skeletal muscle.* FEBS letters, 2017. **591**(1): p. 97-108.

222. Wagner, H., et al., *Improvement of insulin sensitivity in response to exercise training in type 2 diabetes mellitus is associated with vascular endothelial growth factor A expression.* Diabetes and Vascular Disease Research, 2016. **13**(5): p. 361-366.

223. Jung, T.W., et al., *METRNL attenuates lipid-induced inflammation and insulin resistance via AMPK or PPARδ-dependent pathways in skeletal muscle of mice.* Experimental & molecular medicine, 2018. **50**(9): p. 122.

224. Nagareddy, P.R., et al., *Inhibition of matrix metalloproteinase-2 improves endothelial function and prevents hypertension in insulin-resistant rats.* British journal of pharmacology, 2012. **165**(3): p. 705-715.

225. Kang, L., et al., *Diet-induced muscle insulin resistance is associated with extracellular matrix remodeling and interaction with integrin α2β1 in mice.* Diabetes, 2011. **60**(2): p. 416-426.

226. Liew, C.W., et al., *Insulin regulates carboxypeptidase E by modulating translation initiation scaffolding protein eIF4G1 in pancreatic β cells.* Proceedings of the National Academy of Sciences, 2014. **111**(22): p. E2319-E2328.

227. Huang, X., et al., *Impaired cathepsin L gene expression in skeletal muscle is associated with type 2 diabetes.* Diabetes, 2003. **52**(9): p. 2411-2418.

228. Liu, L., et al., *Increased cathepsin D correlates with clinical parameters in newly diagnosed type 2 diabetes.* Disease markers, 2017. **2017**.

229. Chavez, J.A., et al., *Acid ceramidase overexpression prevents the inhibitory effects of saturated fatty acids on insulin signaling.* Journal of Biological Chemistry, 2005. **280**(20): p. 20148-20153.

230. Mir, A.R., et al., *Structural changes in histone H2A by methylglyoxal generate highly immunogenic amorphous aggregates with implications in auto-immune response in cancer.* Glycobiology, 2015. **26**(2): p. 129-141.

231. Bhat, S., et al., *Abundance matters: role of albumin in diabetes, a proteomics perspective.* Expert review of proteomics, 2017. **14**(8): p. 677-689.

232. Jagadeeshaprasad, M.G., et al., *Albumin Abundance and Its Glycation Status Determine Hemoglobin Glycation.* ACS omega, 2018. **3**(10): p. 12999-13008.

233. Postma, M. and J. Goedhart, *PlotsOfData—A web app for visualizing data together with their summaries.* PLoS biology, 2019. **17**(3): p. e3000202.

234. Rathore, R., et al., *Glycation of glucose sensitive lysine residues K36, K438 and K549 of albumin is associated with prediabetes.* Journal of proteomics, 2019. **208**: p. 103481.

235. Nagano, O. and H. Saya, *Mechanism and biological significance of CD44 cleavage.* Cancer science, 2004. **95**(12): p. 930-935.

236. Hasib, A., et al., *CD44 contributes to hyaluronan-mediated insulin resistance in skeletal muscle of high-fat-fed C57BL/6 mice.* American Journal of Physiology-Endocrinology and Metabolism, 2019. **317**(6): p. E973-E983.

237. Nomiyama, T., et al., *Osteopontin mediates obesity-induced adipose tissue macrophage infiltration and insulin resistance in mice.* The Journal of clinical investigation, 2007. **117**(10): p. 2877-2888.

238. Mattheolabakis, G., et al., *Hyaluronic acid targeting of CD44 for cancer therapy: from receptor biology to nanomedicine.* Journal of drug targeting, 2015. **23**(7-8): p. 605-618.

239. Kodama, K., et al., *Expression-based genome-wide association study links the receptor CD44 in adipose tissue with type 2 diabetes.* Proceedings of the National Academy of Sciences, 2012. **109**(18): p. 7049-7054.

240. Ishiki, M. and A. Klip, *Minireview: recent developments in the regulation of glucose transporter-4 traffic: new signals, locations, and partners.* Endocrinology, 2005. **146**(12): p. 5071-5078.

241. Petersen, K.F. and G.I. Shulman, *Etiology of insulin resistance.* The American journal of medicine, 2006. **119**(5): p. S10-S16.

242. Adams, C.M., S.M. Ebert, and M.C. Dyle, *Role of ATF4 in skeletal muscle atrophy.* Current Opinion in Clinical Nutrition & Metabolic Care, 2017. **20**(3): p. 164-168.

243. Wang, X., et al., *Insulin resistance accelerates muscle protein degradation: activation of the ubiquitin-proteasome pathway by defects in muscle cell signaling.* Endocrinology, 2006. **147**(9): p. 4160-4168.

244. Yang, W., et al., *NFE2 induces miR-423-5p to promote gluconeogenesis and hyperglycemia by repressing the hepatic FAM3A-ATP-Akt pathway.* Diabetes, 2017. **66**(7): p. 1819-1832.

245. Patti, M.E., et al., *Coordinated reduction of genes of oxidative metabolism in humans with insulin resistance and diabetes: Potential role of PGC1 and NRF1.* Proceedings of the National Academy of Sciences, 2003. **100**(14): p. 8466-8471.

246. Riu, E., et al., *Overexpression of c-myc in the liver prevents obesity and insulin resistance.* The FASEB Journal, 2003. **17**(12): p. 1715-1717.

247. Peterson, C.W. and D.E. Ayer, *An extended Myc network contributes to glucose homeostasis in cancer and diabetes.* Front Biosci, 2011. **16**: p. 2206-2223.

248. Koh, J.-H., et al., *TFAM Enhances Fat Oxidation and Attenuates High-Fat Diet-Induced Insulin Resistance in Skeletal Muscle.* Diabetes, 2020. **68**(8): p. 1552-1564.

249. Jiang, B., et al., *The Flower Tea Coreopsis tinctoria Increases Insulin Sensitivity and Regulates Hepatic Metabolism in Rats Fed a High-Fat Diet.* Endocrinology, 2015. **156**(6): p. 2006-2018.

250. Friedrich, N., *Metabolomics in diabetes research.* Journal of Endocrinology, 2012. **215**(1): p. 29.

251. Nishikawa, T., et al., *Normalizing mitochondrial superoxide production blocks three pathways of hyperglycaemic damage.* Nature, 2000. **404**(6779): p. 787-790.

252. Wang, W., et al., *Mitochondrial fission triggered by hyperglycemia is mediated by ROCK1 activation in podocytes and endothelial cells.* Cell metabolism, 2012. **15**(2): p. 186-200.

253. Sharma, K., *Mitochondrial hormesis and diabetic complications.* Diabetes, 2015. **64**(3): p. 663-672.

254. Dugan, L.L., et al., *AMPK dysregulation promotes diabetes-related reduction of superoxide and mitochondrial function.* The Journal of clinical investigation, 2013. **123**(11).

255. Reddy, M.A. and R. Natarajan, *Epigenetics in diabetic kidney disease.* Journal of the American Society of Nephrology, 2011. **22**(12): p. 2182-2185.

256. Wang, Z. and H. Gleichmann, *GLUT2 in pancreatic islets: crucial target molecule in diabetes induced with multiple low doses of streptozotocin in mice.* Diabetes, 1998. **47**(1): p. 50-56.

257. Lenzen, S., *The mechanisms of alloxan-and streptozotocin-induced diabetes.* Diabetologia, 2008. **51**(2): p. 216-226.

258. Drury, R.A.B. and E.A. Wallington, *Preparation and fixation of tissues.* Carleton's histological technique, 1980. **5**: p. 41-54.

259. Drury, R.A.B., E.A. Wallington, and S.R. Cameron, *Carleton's histological technique*. 1967: London.

260. Kador, P.F., M. Wyman, and P.J. Oates, *Aldose reductase, ocular diabetic complications and the development of topical Kinostat®.* Progress in retinal and eye research, 2016. **54**: p. 1-29.

261. Warner, F.J., et al., *Angiotensin converting enzyme-2 (ACE2) and its possible roles in hypertension, diabetes and cardiac function.* Letters in Peptide Science, 2003. **10**(5-6): p. 377-385.

262. Yasuma, T., et al., *Amelioration of diabetes by protein S.* Diabetes, 2016. **65**(7): p. 1940-1951.

Thesis Summary

Methylglyoxal (MG) is produced as a minor by-product of various metabolic processes. However, in insulin-resistant states like obesity and type 2 diabetes, MG levels are known to increase due to altered glucose metabolism. The concentration of MG in the plasma of diabetic patients is associated with the level of blood glucose. MG is also a significant precursor of advanced glycation end products which are reported to be involved in the development of diabetes and diabetic complications. Therefore, various detoxification mechanisms are present in the body, one of them being the glyoxalase system. However, in diabetes, because of higher levels of MG, it can modify proteins from several tissues, including vascular endothelium and smooth muscles. MG induced modification in proteins may have adverse effects on cellular processes, and therefore such proteins are removed by exocytosis or secretion into the extracellular matrix. Skeletal muscle is the largest insulin-sensitive organ, accounts for up to 80% of insulin-stimulated glucose uptake. It is responsible for whole-body metabolism and energy homeostasis. Understanding the development of insulin resistance in response to methylglyoxal modified proteins can be useful in designing strategies for the management of diabetes. Therefore, in the present study, we focused on the effect of methylglyoxal on the secretome and proteome of muscle cells, clinical plasma, and animal plasma.

Secreted proteins comprise an important class of biomolecules that include a wide array of proteins such as serum proteins, matrix proteins as well as hormones, and growth factors. It is believed that approximately 10% of the human genome encodes for secreted proteins. Skeletal muscles have an endocrine function, producing a large number of proteins called myokines. Insulin resistance affects the secretion of myokines. Various factors, including oxidative stress, palmitic acid, TNF-α, are known to induce insulin resistance and affect the myokine secretion in muscle cells. Similarly, it has been shown that MG induces insulin resistance in muscle cells; however, MG induced changes in myokine secretion are not yet studied. Characterization of skeletal muscle secretome is still not complete even after the identification of numerous myokines in recent profiling studies, which is evident from the amount of overlap seen among

these studies. Type 2 diabetes's pathogenesis affects the functioning of all major organs that govern metabolic control, including skeletal muscles. Since myokines influence a number of different organs, any alteration of the skeletal muscle secretome can have vast and detrimental effects. Herein, we sought to identify the MG induced secretome of rat muscle cells to identify potential biomarkers for diabetes. We found that methylglyoxal does not affect cell viability up to 3 mM concentration**.** The IDA spectral library had 643 proteins, and 82 of those were upregulated while 99 were downregulated by more than 1.3-fold in MG-induced secretome in SWATH analysis**.** Of the total identified proteins, 180 proteins were identified with SignalP, and 113 proteins were identified with SecretomeP**.** In KEGG pathway analysis, differentially expressed proteins were found to be involved in various pathways like extracellular matrix (ECM)−receptor interaction, leukocyte transendothelial migration, fluid shear stress and atherosclerosis, complement and coagulation cascades, and lysosomal pathway. Apart from the above pathways, MG induced secretome had several proteins related to insulin resistance, obesity, and metabolic syndrome.

The usefulness of MG-induced secretome was studied in clinical plasma. Since MG levels increase in diabetes, it is expected that some of the secreted proteins observed in cell culture may also be found in clinical plasma. Therefore, to identify such proteins, SWATH-MS was performed to identify and quantify MG associated secreted proteins in the plasma. Hyperglycemic condition in diabetes promotes glycation and formation of reactive carbonyls such as glyoxal, methylglyoxal, which can, in turn, modify proteins leading to the formation of carboxyethyllysine (CEL) and Argpyrimidines (ARGPYR). In severe diabetes, due to elevated levels of MG, it is expected that MG associated modifications such as CEL and ARGPYR can be observed in plasma proteins. Human Serum albumin has been considered as a primary target for glycation due to its abundance, many lysine and arginine residues, and relatively long half-life. We, therefore, studied MG associated modification of HSA, which could reflect elevated levels of MG. A total of 238 proteins were identified in the spectral library obtained from IDA, out of which 37 proteins were upregulated, and 13 proteins were downregulated by more than 1.3 fold. Out of the total identified proteins, 189 proteins were identified with SignalP and 24 proteins with SecretomeP. The differentially expressed proteins were found to be involved in pathway Complement and coagulation cascades. CD44, an MG-induced secreted protein found

upregulated in muscle cells, which showed a similar trend as that of clinical proteomics data by ELISA too, and the protein was found to be 1.6 fold upregulated in diabetic plasma. To identify the MG-induced secreted proteins in the clinical plasma, the proteins identified in the plasma were compared with the MG induced secreted proteins in the muscle cells. CD44 was found to be a common protein between MG-induced secretome and clinical plasma proteome. It was found to be upregulated in the diabetic plasma as measured by ELISA and to have a role in the development of insulin resistance. The elevated levels of CD44 were accompanied by an increase in MG-induced CEL modifications of two HSA peptides, FKDLGEENFK and KVPQVSTPTLVEVSR, suggesting that the high levels of CD44 could be associated with an increase in the levels of MG in diabetes.

Insulin increases glucose uptake in muscle cells and adipocytes by stimulating the translocation of the glucose transporter GLUT4 from intracellular sites to the cell surface. Up to 75% of insulin-dependent glucose disposal occurs in skeletal muscle. Insulin resistance is a condition in which cells fail to respond appropriately to insulin. Molecular mechanisms known- Serine phosphorylation of IRS which weakens signal transduction and increased expression of P85α which decreases activity of PI3K. Insulin resistance is an essential hallmark of type 2 diabetes, where it is a driver of hyperglycemia. Since altered insulin signaling underlies the final manifestation of the syndrome, we have analyzed the effect of MG on total cell proteomics of skeletal muscles. We observed that methylglyoxal treatment reduces the glucose uptake in muscle cells and induces apoptosis. The IDA spectral library had 1963 proteins, and 214 of those were upregulated while 59 were downregulated by more than 1.3-fold in MG-induced secretome in SWATH analysis. Pathway analysis shows deregulation of various metabolic processes like Citrate cycle (TCA cycle), glycolysis/gluconeogenesis, Glyoxylate, and dicarboxylate metabolism. Transcription factors Nrf1, Atf4, Nfe2, myc were found to regulate many deregulated proteins, have a role in insulin resistance.

To check methylglyoxal induced proteins effects *in-vivo,* animal experiments were carried out. Since MG levels increase in diabetes, it is expected that some of the secreted proteins observed in cell culture or clinical plasma may also be found in animal plasma. Therefore, to identify such proteins, SWATH-MS was performed to identify and quantify MG induced proteins in the animal plasma. Hyperglycemic condition in diabetes promotes glycation and formation of

reactive carbonyls such as glyoxal, methylglyoxal, which can, in turn, modify proteins. We, therefore, studied MG associated modification of Rat serum albumin, which could reflect elevated levels of MG. Animal experiments were performed in 4 groups. Deregulated proteins of the MG-control group were found to be involved in the Proteasomal ubiquitin-independent protein catabolic process and collagen fibril organization. Deregulated proteins of the STZ-control group were found to be involved in positive regulation of reactive oxygen species metabolic process and positive regulation of receptor-mediated endocytosis. An increase in MG-induced modifications of two Rat Serum Albumin peptides, R(Argpyr)PCFSALTVDETYVPK and LVQEVTDFAK(CEL)TCVADENAENCDK, could be associated with an increase in the levels of MG in diabetes. Kidney histopathology studies showed moderate to severe changes in STZ and STZ-MG groups. Changes in Rat's eyes were observed, which can be associated with the onset of diabetic complications.

Appendix

Appendix 1 Clinical characteristics of diabetic and healthy subjects

	Sex (M/F)	Age (years)	On Medication	Weight (kg)	FBSL (mg/dL)	PP BSL (mg/dL)	HbA_{1c} (%)
Diabetic (n=10)	9M/1F	53.50 ± 10.81	Yes	77.39 ± 8.41	188.40 ± 95.28	230.20 ± 105.19	8.84 ± 2.16
Healthy (n=10)	8M/2F	33.50 ± 9.37	No	74.20 ± 12.96	104.20 ± 11.06	138.90 ± 15.06	5.23 ± 0.23

Appendix 2 List of identified proteins in Cell Secretome

N	Accession	Name	Peptides (95%)
1	P04937	Fibronectin	298
2	P30427-2	Isoform 2 of Plectin	209
3	P13941	Collagen alpha-1(III) chain	168
4	P02466	Collagen alpha-2(I) chain	162
5	P02454	Collagen alpha-1(I) chain	104
6	P60711	Actin, cytoplasmic 1	101
7	P63259	Actin, cytoplasmic 2	100
8	P31000	Vimentin	99
9	P33436	72 kDa type IV collagenase	92
10	O08628	Procollagen C-endopeptidase enhancer 1	76
11	P11883	Aldehyde dehydrogenase, dimeric NADP-preferring	71
12	Q9QXQ0	Alpha-actinin-4	68
13	P85972	Vinculin	61
14	Q62812	Myosin-9	56

15	O35763	Moesin	51
16	P12785	Fatty acid synthase	50
17	Q63083	Nucleobindin-1	50
18	P63018	Heat shock cognate 71 kDa protein	49
19	P48679	Prelamin-A/C	46
20	Q9Z1P2	Alpha-actinin-1	45
21	P04764	Alpha-enolase	44
22	P11980-2	Isoform M2 of Pyruvate kinase PKM	43
23	P34058	Heat shock protein HSP 90-beta	41
24	Q62894	Extracellular matrix protein 1	39
25	P47853	Biglycan	39
26	P82995	Heat shock protein HSP 90-alpha	38
27	O35142	Coatomer subunit beta'	38
28	P05065	Fructose-bisphosphate aldolase A	38
29	P05197	Elongation factor 2	37
30	P50137	Transketolase	35
31	P09495	Tropomyosin alpha-4 chain	34
32	P06761	Endoplasmic reticulum chaperone BiP	34
33	A2RUV9	Adipocyte enhancer-binding protein 1	33
34	P46462	Transitional endoplasmic reticulum ATPase	33
35	P04642	L-lactate dehydrogenase A chain	33
36	Q6Q0N0	Calsyntenin-1	33
37	P11762	Galectin-1	32
38	Q6P6T1	Complement C1s subcomponent	31
39	P30121	Metalloproteinase inhibitor 2	31
40	Q4TU93	C-type mannose receptor 2	30
41	P35053	Glypican-1	29
42	P63102	14-3-3 protein zeta/delta	29
43	P51886	Lumican	29
44	P16086	Spectrin alpha chain, non-erythrocytic 1	26

45	Q5U367	Multifunctional procollagen lysine hydroxylase and glycosyltransferase LH3	26
46	P62260	14-3-3 protein epsilon	26
47	P62630	Elongation factor 1-alpha 1	26
48	P31977	Ezrin	26
49	P02770	Serum albumin	26
50	P31044	Phosphatidylethanolamine-binding protein 1	25
51	Q66HD0	Endoplasmin	24
52	P04785	Protein disulfide-isomerase	24
53	Q9QZK5	Serine protease HTRA1	24
54	P16617	Phosphoglycerate kinase 1	24
55	Q63610	Tropomyosin alpha-3 chain	24
56	Q6P9V9	Tubulin alpha-1B chain	24
57	P68370	Tubulin alpha-1A chain	24
58	Q9ERB4	Versican core protein (Fragments)	23
59	Q9ERB4-3	Isoform Vint of Versican core protein	23
60	P10860	Glutamate dehydrogenase 1, mitochondrial	23
61	P13596	Neural cell adhesion molecule 1	23
62	P04636	Malate dehydrogenase, mitochondrial	23
63	P00787	Cathepsin B	23
64	P11598	Protein disulfide-isomerase A3	22
65	P29534	Vascular cell adhesion protein 1	22
66	Q63198	Contactin-1	21
67	Q3MIE4	Synaptic vesicle membrane protein VAT-1 homolog	21
68	P85845	Fascin	21
69	P20909	Collagen alpha-1(XI) chain	21
70	P20909-6	Isoform 6 of Collagen alpha-1(XI) chain	21
71	P20909-5	Isoform 5 of Collagen alpha-1(XI) chain	21
72	P20909-4	Isoform 4 of Collagen alpha-1(XI) chain	21
73	P20909-3	Isoform 3 of Collagen alpha-1(XI) chain	21

74	P20909-2	Isoform 2 of Collagen alpha-1(XI) chain	21
75	P16975	SPARC	21
76	P18418	Calreticulin	20
77	B5DFC9	Nidogen-2	20
78	Q9JI03	Collagen alpha-1(V) chain	20
79	B0BNI5	Olfactomedin-like protein 3	20
80	Q63716	Peroxiredoxin-1	20
81	P25113	Phosphoglycerate mutase 1	20
82	P10111	Peptidyl-prolyl cis-trans isomerase A	20
83	P11442	Clathrin heavy chain 1	19
84	Q68FP1-2	Isoform 2 of Gelsolin	19
85	Q68FP1	Gelsolin	19
86	P47942	Dihydropyrimidinase-related protein 2	19
87	P05371	Clusterin	19
88	P05982	NAD(P)H dehydrogenase [quinone] 1	19
89	P69897	Tubulin beta-5 chain	19
90	P07154	Cathepsin L1	19
91	Q6P9T8	Tubulin beta-4B chain	19
92	D3ZHA0	Filamin-C	18
93	P07943	Aldo-keto reductase family 1 member B1	18
94	P04797	Glyceraldehyde-3-phosphate dehydrogenase	18
95	P00507	Aspartate aminotransferase, mitochondrial	18
96	Q5XI73	Rho GDP-dissociation inhibitor 1	18
97	P04906	Glutathione S-transferase P	18
98	P50399	Rab GDP dissociation inhibitor beta	17
99	Q07936	Annexin A2	17
100	Q5RKI0	WD repeat-containing protein 1	17
101	P07150	Annexin A1	17
102	P16638-2	Isoform 2 of ATP-citrate synthase	17
103	P16638	ATP-citrate synthase	17

104	P29457	Serpin H1	17
105	O70513	Galectin-3-binding protein	17
106	P61983	14-3-3 protein gamma	17
107	P07151	Beta-2-microglobulin	17
108	Q07936-2	Isoform Long of Annexin A2	16
109	P24268	Cathepsin D	16
110	Q63598	Plastin-3	16
111	P48500	Triosephosphate isomerase	16
112	Q6P6V0	Glucose-6-phosphate isomerase	16
113	Q5XI22	Acetyl-CoA acetyltransferase, cytosolic	16
114	P68255	14-3-3 protein theta	16
115	Q3KRE8	Tubulin beta-2B chain	16
116	P85108	Tubulin beta-2A chain	16
117	P48500	Triosephosphate isomerase	16
118	P52944	PDZ and LIM domain protein 1	15
119	P45592	Cofilin-1	15
120	Q00918	Latent-transforming growth factor beta-binding protein 1	15
121	P62982	Ubiquitin-40S ribosomal protein S27a	15
122	Q63429	Polyubiquitin-C	15
123	P62986	Ubiquitin-60S ribosomal protein L40	15
124	P0CG51	Polyubiquitin-B	15
125	Q5XFX0	Transgelin-2	14
126	P08592	Amyloid-beta A4 protein	14
127	Q920A6	Retinoid-inducible serine carboxypeptidase	14
128	P0DP31	Calmodulin-3	14
129	P0DP30	Calmodulin-2	14
130	P0DP29	Calmodulin-1	14
131	Q4QQW8	Putative phospholipase B-like 2	14
132	P10960	Prosaposin	14
133	P68511	14-3-3 protein eta	14

134	P35213	14-3-3 protein beta/alpha	14
135	P35213-2	Isoform Short of 14-3-3 protein beta/alpha	14
136	P0DP30	Calmodulin-2	14
137	P0DP29	Calmodulin-1	14
138	Q6IRK9	Carboxypeptidase Q	13
139	Q9EPH8	Polyadenylate-binding protein 1	13
140	P08592-2	Isoform APP695 of Amyloid-beta A4 protein	13
141	P04256	Heterogeneous nuclear ribonucleoprotein A1	13
142	P85968	6-phosphogluconate dehydrogenase, decarboxylating	13
143	P24368	Peptidyl-prolyl cis-trans isomerase B	13
144	Q6AYC4	Macrophage-capping protein	13
145	P04961	Proliferating cell nuclear antigen	13
146	A7VJC2	Heterogeneous nuclear ribonucleoproteins A2/B1	13
147	A7VJC2-4	Isoform B1b of Heterogeneous nuclear ribonucleoproteins A2/B1	13
148	A7VJC2-3	Isoform A2b of Heterogeneous nuclear ribonucleoproteins A2/B1	13
149	A7VJC2-2	Isoform A2 of Heterogeneous nuclear ribonucleoproteins A2/B1	13
150	P04692-6	Isoform 6 of Tropomyosin alpha-1 chain	13
151	P04692-3	Isoform 3 of Tropomyosin alpha-1 chain	13
152	P04692	Tropomyosin alpha-1 chain	13
153	P58775-2	Isoform 2 of Tropomyosin beta chain	13
154	P70490	Lactadherin	12
155	O88600	Heat shock 70 kDa protein 4	12
156	Q62786	Prostaglandin F2 receptor negative regulator	12
157	O88989	Malate dehydrogenase, cytoplasmic	12
158	Q5M872	Dipeptidase 2	12
159	P01026	Complement C3	12
160	P41682	Alcohol dehydrogenase class 4 mu/sigma chain	12

161	P04692-7	Isoform 7 of Tropomyosin alpha-1 chain	12
162	P04692-5	Isoform 5 of Tropomyosin alpha-1 chain	12
163	P04692-4	Isoform 4 of Tropomyosin alpha-1 chain	12
164	P61980	Heterogeneous nuclear ribonucleoprotein K	11
165	Q9EQS0	Transaldolase	11
166	P10760	Adenosylhomocysteinase	11
167	P62804	Histone H4	11
168	P62963	Profilin-1	11
169	P38659	Protein disulfide-isomerase A4	11
170	P13697	NADP-dependent malic enzyme	11
171	P05369	Farnesyl pyrophosphate synthase	11
172	P63245	Receptor of activated protein C kinase 1	11
173	P35704	Peroxiredoxin-2	11
174	Q9EPB1	Dipeptidyl peptidase 2	11
175	P21744	Insulin-like growth factor-binding protein 4	11
176	O35814	Stress-induced-phosphoprotein 1	11
177	Q9ESW0	DNA damage-binding protein 1	11
178	P14841	Cystatin-C	11
179	Q08420	Extracellular superoxide dismutase [Cu-Zn]	11
180	P15429	Beta-enolase	11
181	P04692-8	Isoform 8 of Tropomyosin alpha-1 chain	11
182	Q68FR6	Elongation factor 1-gamma	10
183	O35276	Neuropilin-2	10
184	Q9QZA2	Programmed cell death 6-interacting protein	10
185	Q5U300	Ubiquitin-like modifier-activating enzyme 1	10
186	P42930	Heat shock protein beta-1	10
187	Q7TP47	Heterogeneous nuclear ribonucleoprotein Q	10
188	Q9R0D6	Transcobalamin-2	10
189	Q9EQV6	Tripeptidyl-peptidase 1	10
190	P07632	Superoxide dismutase [Cu-Zn]	10

191	O35567	Bifunctional purine biosynthesis protein PURH	10
192	P00786	Pro-cathepsin H	10
193	P05942	Protein S100-A4	10
194	P38983	40S ribosomal protein SA	10
195	Q62952-2	Isoform 2 of Dihydropyrimidinase-related protein 3	10
196	Q9JI92	Syntenin-1	10
197	Q5M7W5	Microtubule-associated protein 4	9
198	Q5M7W5-2	Isoform 2 of Microtubule-associated protein 4	9
199	Q5XI43	Matrix remodeling-associated protein 8	9
200	P23785	Progranulin	9
201	P13221	Aspartate aminotransferase, cytoplasmic	9
202	P14668	Annexin A5	9
203	Q63321	Procollagen-lysine,2-oxoglutarate 5-dioxygenase 1	9
204	P62909	40S ribosomal protein S3	9
205	Q63797	Proteasome activator complex subunit 1	9
206	Q4V7C7	Actin-related protein 3	9
207	Q64119	Myosin light polypeptide 6	9
208	P15087	Carboxypeptidase E	9
209	Q62952	Dihydropyrimidinase-related protein 3	9
210	Q00715	Histone H2B type 1	9
211	P35572	Insulin-like growth factor-binding protein 6	9
212	O35217	Multiple inositol polyphosphate phosphatase 1	9
213	P50398	Rab GDP dissociation inhibitor alpha	9
214	Q9JLJ3	4-trimethylaminobutyraldehyde dehydrogenase	8
215	Q66X93	Staphylococcal nuclease domain-containing protein 1	8
216	P41562	Isocitrate dehydrogenase [NADP] cytoplasmic	8
217	Q5XIM5	Protein CDV3 homolog	8
218	Q5I0D1	Glyoxalase domain-containing protein 4	8
219	O35783	Calumenin	8

220	Q91Y81	Septin-2	8
221	P62329	Thymosin beta-4	8
222	P85973	Purine nucleoside phosphorylase	8
223	P13832	Myosin regulatory light chain RLC-A	8
224	Q71UF4	Histone-binding protein RBBP7	8
225	O88767	Protein/nucleic acid deglycase DJ-1	8
226	P11030	Acyl-CoA-binding protein	8
227	Q66H12	Alpha-N-acetylgalactosaminidase	8
228	Q9JMJ4	Pre-mRNA-processing factor 19	8
229	Q62632	Follistatin-related protein 1	8
230	Q8CHN8-2	Isoform 2 of Mannan-binding lectin serine protease 1	8
231	P30349	Leukotriene A-4 hydrolase	7
232	P26772	10 kDa heat shock protein, mitochondrial	7
233	Q63081	Protein disulfide-isomerase A6	7
234	P62828	GTP-binding nuclear protein Ran	7
235	P13383	Nucleolin	7
236	P51635	Aldo-keto reductase family 1 member A1	7
237	P52296	Importin subunit beta-1	7
238	Q08163	Adenylyl cyclase-associated protein 1	7
239	Q9Z339	Glutathione S-transferase omega-1	7
240	Q8K4Y7	Soluble calcium-activated nucleotidase 1	7
241	P60901	Proteasome subunit alpha type-6	7
242	P13668	Stathmin	7
243	Q9Z0W7	Chloride intracellular channel protein 4	7
244	Q6AXR4	Beta-hexosaminidase subunit beta	7
245	O35244	Peroxiredoxin-6	7
246	Q6AYE5	Olfactomedin-like protein 3	7
247	P29315	Ribonuclease inhibitor	7
248	B3GNI6	Septin-11	7

249	B3GNI6-3	Isoform 3 of Septin-11	7
250	B3GNI6-2	Isoform 2 of Septin-11	7
251	Q6P7A9	Lysosomal alpha-glucosidase	7
252	Q9R063	Peroxiredoxin-5, mitochondrial	7
253	Q9R063-2	Isoform Cytoplasmic+peroxisomal of Peroxiredoxin-5, mitochondrial	7
254	P50503	Hsc70-interacting protein	7
255	Q01129	Decorin	7
256	O88656	Actin-related protein 2/3 complex subunit 1B	7
257	P01041	Cystatin-B	7
258	Q5RJP0	Aldose reductase-related protein 1	7
259	Q68FS4	Cytosol aminopeptidase	7
260	Q68FS4-2	Isoform 2 of Cytosol aminopeptidase	7
261	P07323	Gamma-enolase	7
262	Q9QZR6	Septin-9	7
263	Q9QZR6-2	Isoform 2 of Septin-9	7
264	Q9JLT0	Myosin-10	7
265	Q5U206	Calmodulin-like protein 3	7
266	P18666	Myosin regulatory light chain 12B	6
267	O35509	Ras-related protein Rab-11B	6
268	Q5U2U2	Crk-like protein	6
269	P02401	60S acidic ribosomal protein P2	6
270	Q9JLD2	Neuroserpin	6
271	Q4KM73	UMP-CMP kinase	6
272	P38650	Cytoplasmic dynein 1 heavy chain 1	6
273	Q9WV75	Spondin-2	6
274	P63039	60 kDa heat shock protein, mitochondrial	6
275	P06760	Beta-glucuronidase	6
276	P62944	AP-2 complex subunit beta	6
277	P62944-2	Isoform 2 of AP-2 complex subunit beta	6

278	Q6AYP5	Cell adhesion molecule 1	6
279	Q6AYP5-2	Isoform 2 of Cell adhesion molecule 1	6
280	B4F7E8	Niban-like protein 1	6
281	P19804	Nucleoside diphosphate kinase B	6
282	Q9JLZ1	Glutaredoxin-3	6
283	Q3T1K5	F-actin-capping protein subunit alpha-2	6
284	P84079	ADP-ribosylation factor 1	6
285	P61206	ADP-ribosylation factor 3	6
286	Q5XIM9	T-complex protein 1 subunit beta	6
287	Q6AYD3	Proliferation-associated protein 2G4	6
288	Q63413	Spliceosome RNA helicase Ddx39b	6
289	P63086	Mitogen-activated protein kinase 1	6
290	O35162	Heat shock 70 kDa protein 13	6
291	P62959	Histidine triad nucleotide-binding protein 1	6
292	P11232	Thioredoxin	6
293	Q9R0J8	Legumain	6
294	Q9WTT6	Guanine deaminase	6
295	P16391	RT1 class I histocompatibility antigen, AA alpha chain	6
296	Q9WVC0	Septin-7	6
297	P15865	Histone H1.4	6
298	Q794E4	Heterogeneous nuclear ribonucleoprotein F	6
299	Q91ZS3	45 kDa calcium-binding protein	6
300	Q91ZS3-2	Isoform 2 of 45 kDa calcium-binding protein	6
301	Q4V8H8	EH domain-containing protein 2	6
302	Q8CHN8	Mannan-binding lectin serine protease 1	6
303	Q9QZR6-3	Isoform 3 of Septin-9	6
304	P22062	Protein-L-isoaspartate(D-aspartate)	6
305	Q6LED0	Histone H3.1	6
306	P12711	Alcohol dehydrogenase class-3	6
307	Q6MG61	Chloride intracellular channel protein 1	6

308	P61589	Transforming protein RhoA	6
309	P14046	Alpha-1-inhibitor 3	6
310	P05539	Collagen alpha-1(II) chain	6
311	P62494	Ras-related protein Rab-11A	5
312	Q32KJ6	N-acetylgalactosamine-6-sulfatase	5
313	P50430	Arylsulfatase B	5
314	P84082	ADP-ribosylation factor 2	5
315	Q5M7U6	Actin-related protein 2	5
316	O54975	Xaa-Pro aminopeptidase 1	5
317	Q920J4	Thioredoxin-like protein 1	5
318	Q9WVH8	Fibulin-5	5
319	Q5FVF9	Biotinidase	5
320	Q64559	Cytosolic acyl coenzyme A thioester hydrolase	5
321	Q64559-1	Isoform 1 of Cytosolic acyl coenzyme A thioester hydrolase	5
322	Q9JI85	Nucleobindin-2	5
323	P18420	Proteasome subunit alpha type-1	5
324	P19945	60S acidic ribosomal protein P0	5
325	Q5XI32	F-actin-capping protein subunit beta	5
326	Q3T1J1	Eukaryotic translation initiation factor 5A-1	5
327	P17164	Tissue alpha-L-fucosidase	5
328	P20961	Plasminogen activator inhibitor 1	5
329	P45479	Palmitoyl-protein thioesterase 1	5
330	P04182	Ornithine aminotransferase, mitochondrial	5
331	P13084	Nucleophosmin	5
332	B2RYG6	Ubiquitin thioesterase	5
333	Q6P6T4	Echinoderm microtubule-associated protein-like 2	5
334	Q6P6T4-2	Isoform 2 of Echinoderm microtubule-associated protein-like 2	5
335	P28480	T-complex protein 1 subunit alpha	5

336	P09006	Serine protease inhibitor A3N	5
337	P17220	Proteasome subunit alpha type-2	5
338	P13852	Major prion protein	5
339	Q6P6R2	Dihydrolipoyl dehydrogenase, mitochondrial	5
340	Q63691	Monocyte differentiation antigen CD14	5
341	Q9QYV0	Disintegrin and metalloproteinase domain-containing protein 15	5
342	Q9QYV0-2	Isoform 2 of Disintegrin and metalloproteinase domain-containing protein 15	5
343	Q6B345	Protein S100-A11	5
344	P06238	Alpha-2-macroglobulin	5
345	P34064	Proteasome subunit alpha type-5	5
346	P18421	Proteasome subunit beta type-1	5
347	Q499S5	Stromelysin-3	5
348	Q641X3	Beta-hexosaminidase subunit alpha	5
349	P27867	Sorbitol dehydrogenase	5
350	P70615	Lamin-B1	5
351	P08699	Galectin-3	5
352	P85970	Actin-related protein 2/3 complex subunit 2	5
353	Q9QZR6-4	Isoform 4 of Septin-9	5
354	Q811A3	Procollagen-lysine,2-oxoglutarate 5-dioxygenase 2	5
355	Q811A3-2	Isoform 2 of Procollagen-lysine,2-oxoglutarate 5-dioxygenase 2	5
356	D3ZBN0	Histone H1.5	5
357	Q9EPC6	Profilin-2	5
358	Q6IE52	Murinoglobulin-2	5
359	Q8VHK7	Hepatoma-derived growth factor	4
360	P13676	Acylamino-acid-releasing enzyme	4
361	Q64598	Histone H2A type 1-F	4
362	Q4FZT6	Histone H2A type 3	4

363	Q00728	Histone H2A type 4	4
364	P0C170	Histone H2A type 1-E	4
365	P0C169	Histone H2A type 1-C	4
366	A9UMV8	Histone H2A.J	4
367	P05765	40S ribosomal protein S21	4
368	Q5XII0	Mammalian ependymin-related protein 1	4
369	Q9EQX9	Ubiquitin-conjugating enzyme E2 N	4
370	Q5RKI1	Eukaryotic initiation factor 4A-II	4
371	P63029	Translationally-controlled tumor protein	4
372	P38652	Phosphoglucomutase-1	4
373	P04762	Catalase	4
374	Q6PEC1	Tubulin-specific chaperone A	4
375	P97536	Cullin-associated NEDD8-dissociated protein 1	4
376	Q75WE7	von Willebrand factor A domain-containing protein 5A	4
377	Q6P502	T-complex protein 1 subunit gamma	4
378	P09895	60S ribosomal protein L5	4
379	Q5FVM4	Non-POU domain-containing octamer-binding protein	4
380	P06302	Prothymosin alpha	4
381	Q9Z2G8	Nucleosome assembly protein 1-like 1	4
382	P16636	Protein-lysine 6-oxidase	4
383	Q66HR2	Microtubule-associated protein RP/EB family member 1	4
384	P30904	Macrophage migration inhibitory factor	4
385	P01830	Thy-1 membrane glycoprotein	4
386	P85515	Alpha-centractin	4
387	Q9QZK8	Deoxyribonuclease-2-alpha	4
388	P62246	40S ribosomal protein S15a	4
389	P48037	Annexin A6	4
390	P84245	Histone H3.3	4
391	Q4KMA2	UV excision repair protein RAD23 homolog B	4
392	P29314	40S ribosomal protein S9	4

393	P26051	CD44 antigen	4
394	P26051-2	Isoform 1 of CD44 antigen	4
395	Q63548	Semaphorin-3A	4
396	Q6RUV5	Ras-related C3 botulinum toxin substrate 1	4
397	Q6P7Q4	Lactoylglutathione lyase	4
398	Q9WTV5	26S proteasome non-ATPase regulatory subunit 9	4
399	P05943	Protein S100-A10	4
400	P05964	Protein S100-A6	4
401	P30120	Metalloproteinase inhibitor 1	4
402	P63324	40S ribosomal protein S12	4
403	P47875	Cysteine and glycine-rich protein 1	4
404	P48004	Proteasome subunit alpha type-7	4
405	P48004-2	Isoform RC6-IS of Proteasome subunit alpha type-7	4
406	Q7M0E3	Destrin	4
407	B2GUZ5	F-actin-capping protein subunit alpha-1	4
408	Q03626	Murinoglobulin-1	4
409	Q03626-2	Isoform 2 of Murinoglobulin-1	4
410	P12928	Pyruvate kinase PKLR	4
411	P12928-2	Isoform L-type of Pyruvate kinase PKLR	4
412	Q63041	Alpha-1-macroglobulin	4
413	Q9Z0V5	Peroxiredoxin-4	4
414	Q5RJR2	Twinfilin-1	3
415	P62243	40S ribosomal protein S8	3
416	P41740	Atrial natriuretic peptide receptor 3	3
417	Q5I0D7	Xaa-Pro dipeptidase	3
418	Q76HN1	Hyaluronidase-1	3
419	Q6AY84	Secernin-1	3
420	Q63228	Glia maturation factor beta	3
421	P31232	Transgelin	3
422	Q68FR9	Elongation factor 1-delta	3

423	Q68FR9-2	Isoform 2 of Elongation factor 1-delta	3
424	P34067	Proteasome subunit beta type-4	3
425	Q63945	Protein SET	3
426	Q63945-2	Isoform 2 of Protein SET	3
427	P05370	Glucose-6-phosphate 1-dehydrogenase	3
428	P18422	Proteasome subunit alpha type-3	3
429	Q7TP54	Rho family-interacting cell polarization regulator 2	3
430	P02793	Ferritin light chain 1	3
431	Q4FZT9	26S proteasome non-ATPase regulatory subunit 2	3
432	Q63692	Hsp90 co-chaperone Cdc37	3
433	Q4FZY0	EF-hand domain-containing protein D2	3
434	Q9Z270	Vesicle-associated membrane protein-associated protein A	3
435	P27605	Hypoxanthine-guanine phosphoribosyltransferase	3
436	Q68FQ0	T-complex protein 1 subunit epsilon	3
437	P21670	Proteasome subunit alpha type-4	3
438	P85971	6-phosphogluconolactonase	3
439	P63159	High mobility group protein B1	3
440	P62898	Cytochrome c, somatic	3
441	P85125	Caveolae-associated protein 1	3
442	Q6AXS4	Renin receptor	3
443	P28073	Proteasome subunit beta type-6	3
444	P62250	40S ribosomal protein S16	3
445	P97697	Inositol monophosphatase 1	3
446	Q641W2	UPF0160 protein MYG1, mitochondrial	3
447	P61972	Nuclear transport factor 2	3
448	P39069	Adenylate kinase isoenzyme 1	3
449	Q5XIM7	Lysine--tRNA ligase	3
450	P24155	Thimet oligopeptidase	3
451	Q7M767	Ubiquitin-conjugating enzyme E2 variant 2	3

452	P19468	Glutamate--cysteine ligase catalytic subunit	3
453	O55096	Dipeptidyl peptidase 3	3
454	Q5RJL6	Meteorin-like protein	3
455	P18331	Inhibin beta A chain	3
456	P08081-2	Isoform Non-brain of Clathrin light chain A	3
457	P08081	Clathrin light chain A	3
458	Q5I0G4	Glycine--tRNA ligase (Fragment)	3
459	P62271	40S ribosomal protein S18	3
460	Q5M9G3	Caprin-1	3
461	Q6P7S1	Acid ceramidase	3
462	P27321	Calpastatin	3
463	P27321-3	Isoform 3 of Calpastatin	3
464	Q6AYH5	Dynactin subunit 2	3
465	O35806	Latent-transforming growth factor beta-binding protein 2	3
466	P08721	Osteopontin	3
467	B2GV06	Succinyl-CoA:3-ketoacid coenzyme A transferase 1, mitochondrial	3
468	P28576	Platelet-derived growth factor subunit A	3
469	P28576-2	Isoform Short of Platelet-derived growth factor subunit A	3
470	P0C5H9	Mesencephalic astrocyte-derived neurotrophic factor	3
471	Q62733	Lamina-associated polypeptide 2, isoform beta	3
472	Q6URK4	Heterogeneous nuclear ribonucleoprotein A3	3
473	Q6URK4-2	Isoform 2 of Heterogeneous nuclear ribonucleoprotein A3	3
474	P14562	Lysosome-associated membrane glycoprotein 1	3
475	Q62658	Peptidyl-prolyl cis-trans isomerase FKBP1A	3
476	Q4FZU2	Keratin, type II cytoskeletal 6A	3
477	Q10739	Matrix metalloproteinase-14	3
478	Q9JHW0	Proteasome subunit beta type-7	3
479	P17074	40S ribosomal protein S19	3

480	P28077	Proteasome subunit beta type-9	3
481	Q9JJ54	Heterogeneous nuclear ribonucleoprotein D0	3
482	Q9JJ54-4	Isoform 4 of Heterogeneous nuclear ribonucleoprotein D0	3
483	Q9JJ54-3	Isoform 3 of Heterogeneous nuclear ribonucleoprotein D0	3
484	Q9JJ54-2	Isoform 2 of Heterogeneous nuclear ribonucleoprotein D0	3
485	P30919	N(4)-(Beta-N-acetylglucosaminyl)-L-asparaginase	3
486	Q3B8Q2	Eukaryotic initiation factor 4A-III	3
487	P68101	Eukaryotic translation initiation factor 2 subunit 1	3
488	Q63148	Chordin	3
489	P49134	Integrin beta-1	3
490	Q07009	Calpain-2 catalytic subunit	3
491	Q64610	Ectonucleotide pyrophosphatase/phosphodiesterase family member 2	3
492	Q64610-2	Isoform 2 of Ectonucleotide pyrophosphatase/phosphodiesterase family member 2	3
493	Q9R1E9	Connective tissue growth factor	3
494	Q62611	Interleukin-1 receptor-like 1	3
495	Q62611-2	Isoform B of Interleukin-1 receptor-like 1	3
496	Q66H80	Coatomer subunit delta	3
497	Q8JZQ0	Macrophage colony-stimulating factor 1	3
498	Q63768	Adapter molecule crk	3
499	Q63768-2	Isoform Crk-I of Adapter molecule crk	3
500	P62628	Dynein light chain roadblock-type 1	3
501	P12346-2	Isoform 2 of Serotransferrin	3
502	P12346	Serotransferrin	3
503	Q4KM49	Tyrosine--tRNA ligase, cytoplasmic	3
504	Q32PX7	Far upstream element-binding protein 1	3

505	P21708	Mitogen-activated protein kinase 3	3
506	P21708-2	Isoform 2 of Mitogen-activated protein kinase 3	3
507	Q6IE64	Complement C1r subcomponent-like protein	3
508	P02773	Alpha-fetoprotein	3
509	Q99PP0	WNT1-inducible-signaling pathway protein 1	3
510	P17475	Alpha-1-antiproteinase	3
511	P23565	Alpha-internexin	3
512	Q00729	Histone H2B type 1-A	3
513	P08010	Glutathione S-transferase Mu 2	2
514	Q5XHY5	Threonine--tRNA ligase, cytoplasmic	2
515	P27321-7	Isoform 7 of Calpastatin	2
516	P27321-6	Isoform 6 of Calpastatin	2
517	P27321-5	Isoform 5 of Calpastatin	2
518	P27321-4	Isoform 4 of Calpastatin	2
519	P27321-2	Isoform 2 of Calpastatin	2
520	P07092	Glia-derived nexin	2
521	Q6AXS5	Plasminogen activator inhibitor 1 RNA-binding protein	2
522	Q6AXS5-2	Isoform 2 of Plasminogen activator inhibitor 1 RNA-binding protein	2
523	P35559	Insulin-degrading enzyme	2
524	P47727	Carbonyl reductase [NADPH] 1	2
525	Q00438	Polypyrimidine tract-binding protein 1	2
526	Q00438-2	Isoform PYBP1 of Polypyrimidine tract-binding protein 1	2
527	P10719	ATP synthase subunit beta, mitochondrial	2
528	P29598	Urokinase-type plasminogen activator	2
529	P21674	Follistatin	2
530	Q6P7C7	Transmembrane glycoprotein NMB	2
531	P84092	AP-2 complex subunit mu	2
532	Q63396	Activated RNA polymerase II transcriptional coactivator	2

		p15	
533	O89049	Thioredoxin reductase 1, cytoplasmic	2
534	P60868	40S ribosomal protein S20	2
535	P54313	Guanine nucleotide-binding protein G(I)/G(S)/G(T) subunit beta-2	2
536	O35353	Guanine nucleotide-binding protein subunit beta-4	2
537	P54311	Guanine nucleotide-binding protein G(I)/G(S)/G(T) subunit beta-1	2
538	P12001	60S ribosomal protein L18	2
539	Q6P6Q2	Keratin, type II cytoskeletal 5	2
540	Q6IG05	Keratin, type II cytoskeletal 75	2
541	Q06880	Neuroblastoma suppressor of tumorigenicity 1	2
542	Q6GMN2	Brain-specific angiogenesis inhibitor 1-associated protein 2	2
543	Q6GMN2-2	Isoform 2 of Brain-specific angiogenesis inhibitor 1-associated protein 2	2
544	Q5U318	Astrocytic phosphoprotein PEA-15	2
545	P62839	Ubiquitin-conjugating enzyme E2 D2	2
546	P61078	Ubiquitin-conjugating enzyme E2 D3	2
547	P37996	ADP-ribosylation factor-like protein 3	2
548	O35264	Platelet-activating factor acetylhydrolase IB subunit beta	2
549	Q9WUC4	Copper transport protein ATOX1	2
550	Q8R5M3	Leucine-rich repeat-containing protein 15	2
551	Q5FVH0	Complement C1q tumor necrosis factor-related protein 5	2
552	P62859	40S ribosomal protein S28	2
553	P41498	Low molecular weight phosphotyrosine protein phosphatase	2
554	P41498-2	Isoform 2 of Low molecular weight phosphotyrosine protein phosphatase	2
555	P11517	Hemoglobin subunit beta-2	2

556	P02091	Hemoglobin subunit beta-1	2
557	P07895	Superoxide dismutase [Mn], mitochondrial	2
558	P04550	Parathymosin	2
559	P16612	Vascular endothelial growth factor A	2
560	P16612-4	Isoform VEGF-A120 of Vascular endothelial growth factor A	2
561	P16612-3	Isoform VEGF-A144 of Vascular endothelial growth factor A	2
562	P16612-2	Isoform VEGF-A164 of Vascular endothelial growth factor A	2
563	Q9QVC8	Peptidyl-prolyl cis-trans isomerase FKBP4	2
564	P28075	Proteasome subunit beta type-5	2
565	Q10743	Disintegrin and metalloproteinase domain-containing protein 10	2
566	Q6AYS7	Aminoacylase-1A	2
567	O35987	NSFL1 cofactor p47	2
568	O55004	Ribonuclease 4	2
569	Q6QD51	Coiled-coil domain-containing protein 80	2
570	Q63663	Guanylate-binding protein 1	2
571	Q63009	Protein arginine N-methyltransferase 1	2
572	Q5M827	Pirin	2
573	O08629	Transcription intermediary factor 1-beta	2
574	Q8VHF5	Citrate synthase, mitochondrial	2
575	Q810F4	Protein FAM3C	2
576	Q05175	Brain acid soluble protein 1	2
577	Q6AY86	Vacuolar protein sorting-associated protein 26A	2
578	B2RZ78	Vacuolar protein sorting-associated protein 29	2
579	B2RZ78-2	Isoform 2 of Vacuolar protein sorting-associated protein 29	2
580	P36201	Cysteine-rich protein 2	2

581	P63004	Platelet-activating factor acetylhydrolase IB subunit alpha	2
582	Q6P799	Serine--tRNA ligase, cytoplasmic	2
583	P52796	Ephrin-B1	2
584	P14844	C-C motif chemokine 2	2
585	P40329	Arginine--tRNA ligase, cytoplasmic	2
586	P23358	60S ribosomal protein L12	2
587	Q63769	Sushi repeat-containing protein SRPX	2
588	Q63769-2	Isoform 2 of Sushi repeat-containing protein SRPX	2
589	Q63416	Inter-alpha-trypsin inhibitor heavy chain H3	2
590	P63326	40S ribosomal protein S10	2
591	P53812	Phosphatidylinositol transfer protein beta isoform	2
592	P53812-2	Isoform 2 of Phosphatidylinositol transfer protein beta isoform	2
593	P62775	Myotrophin	2
594	Q4KLF8	Actin-related protein 2/3 complex subunit 5	2
595	P97574	Stanniocalcin-1	2
596	P36972	Adenine phosphoribosyltransferase	2
597	P17046	Lysosome-associated membrane glycoprotein 2	2
598	Q5BJP3	Ubiquitin-fold modifier 1	2
599	P97546	Neuroplastin	2
600	P97546-3	Isoform 3 of Neuroplastin	2
601	P97546-1	Isoform 1 of Neuroplastin	2
602	P70645	Bleomycin hydrolase	2
603	Q6AYG5	Ethylmalonyl-CoA decarboxylase	2
604	Q99MZ8	LIM and SH3 domain protein 1	2
605	Q3KRD8	Eukaryotic translation initiation factor 6	2
606	P08649	Complement C4	2
607	P18484	AP-2 complex subunit alpha-2	2
608	Q1EHB3	A disintegrin and metalloproteinase with thrombospondin	2

		motifs 7	
609	Q1EHB3-2	Isoform 2 of A disintegrin and metalloproteinase with thrombospondin motifs 7	2
610	P01946	Hemoglobin subunit alpha-1/2	2
611	Q66HD3	Nuclear autoantigenic sperm protein	2
612	P43138	DNA-(apurinic or apyrimidinic site) lyase	2
613	P50475	Alanine--tRNA ligase, cytoplasmic	2
614	Q8CFN2	Cell division control protein 42 homolog	2
615	Q62920	PDZ and LIM domain protein 5	2
616	B0BN18	Prefoldin subunit 2	2
617	P16446	Phosphatidylinositol transfer protein alpha isoform	2
618	Q4V898	RNA-binding motif protein, X chromosome	2
619	P84586	RNA-binding motif protein, X chromosome retrogene-like	2
620	D4AE41	RNA binding motif protein, X-linked-like-1	2
621	Q68A21	Transcriptional activator protein Pur-beta	2
622	P0C6B8	Sushi, von Willebrand factor type A, EGF and pentraxin domain-containing protein 1	2
623	P42676	Neurolysin, mitochondrial	2
624	P0C0S7	Histone H2A.Z	2
625	Q5U2Z3	Nucleosome assembly protein 1-like 4	2
626	Q9R1T1	Barrier-to-autointegration factor	2
627	P22734	Catechol O-methyltransferase	2
628	P22734-2	Isoform 2 of Catechol O-methyltransferase	2
629	P04904	Glutathione S-transferase alpha-3	2
630	Q62638	Golgi apparatus protein 1	2
631	P81795	Eukaryotic translation initiation factor 2 subunit 3, X-linked	2
632	P49088	Asparagine synthetase [glutamine-hydrolyzing]	2
633	P54921	Alpha-soluble NSF attachment protein	2

634	P29524	Plasminogen activator inhibitor 2 type A	2
635	Q8VHV7	Heterogeneous nuclear ribonucleoprotein H	2
636	Q8VHV7-3	Isoform 3 of Heterogeneous nuclear ribonucleoprotein H	2
637	Q8VHV7-2	Isoform 2 of Heterogeneous nuclear ribonucleoprotein H	2
638	Q6AY09	Heterogeneous nuclear ribonucleoprotein H2	2
639	O89046	Coronin-1B	2
640	O70593	Small glutamine-rich tetratricopeptide repeat-containing protein alpha	2
641	O54800	Cadherin-8	2
642	O54800-2	Isoform 2 of Cadherin-8	2
643	Q4V885	Collectin-12	2

Appendix 3 Secretory proteins showing differential abundance in SWATH-MS analysis (Cell secretome)

N	Accession	Gene Name	Protein Name	p-value	Fold Change
1	Q68FP1-2	GELS	Isoform 2 of Gelsolin	4.00E-06	1.86908894
2	P29534	VCAM1	Vascular cell adhesion protein 1	7.1343E-07	10.8229924
3	Q5M872	DPEP2	Dipeptidase 2	5.2675E-11	9.2092774
4	Q4TU93	MRC2	C-type mannose receptor 2	1.224E-08	7.22024128
5	P26453	BASI	Basigin	0.00111	6.39639068
6	P35053	GPC1	Glypican-1	1.7074E-09	6.34773238
7	P26051	CD44	CD44 antigen	3.1474E-11	6.00200151

8	Q6AYP5	CADM1	Cell adhesion molecule 1	0.00059	5.7316863
9	P16391	HA12	RT1 class I histocompatibility antigen, AA alpha chain	2.3503E-09	5.24293594
10	P41740	ANPRC	Atrial natriuretic peptide receptor 3	8.5484E-07	5.06726704
11	P13596	NCAM1	Neural cell adhesion molecule 1	2.2197E-10	5.06502768
12	P01946	HBA	Hemoglobin subunit alpha-1/2	0.0006	4.96067887
13	M0RC99	RAB5A	Ras-related protein Rab-5A	0.00673	4.67892056
14	Q8VHF5	CISY	Citrate synthase, mitochondrial	0.00012	4.29120175
15	Q5XI43	MXRA8	Matrix remodeling-associated protein 8	4.1792E-08	3.70325912
16	P52796	EFNB1	Ephrin-B1	0.00178	3.70103209
17	P31232	TAGL	Transgelin	1.335E-08	3.42087427
18	P35952	LDLR	Low-density lipoprotein receptor	0.00105	3.41055366
19	P62703	RS4X	40S ribosomal protein S4, X isoform	0.0004	3.27725129
20	Q63691	CD14	Monocyte differentiation antigen CD14	0.00015	3.26398579
21	P06238	A2MG	Alpha-2-macroglobulin	0.00919	3.24208615
22	Q8R5M3	LRC15	Leucine-rich repeat-containing protein 15	0.00614	3.22055638
23	Q07936	ANXA2	Annexin A2	1.3829E-06	3.19770307
24	P13852	PRIO	Major prion protein	3.4245E-06	3.02894812
25	Q62636	RAP1B	Ras-related protein Rap-1b	5.6317E-08	2.94554471
26	Q08464	FZD2	Frizzled-2	0.00752	2.81123736
27	P24090	FETUA	Alpha-2-HS-glycoprotein	0.04601	2.65981332
28	Q80U96	XPO1	Exportin-1	0.01126	2.65457339
29	Q5U318	PEA15	Astrocytic phosphoprotein PEA-15	0.00755	2.64336

					838
30	P08649	CO4	Complement C4	0.00393	2.62898536
31	P62919	RL8	60S ribosomal protein L8	0.01303	2.5807924
32	O35276	NRP2	Neuropilin-2	3.6862E-06	2.5016858
33	P0C5H9	MANF	Mesencephalic astrocyte-derived neurotrophic factor	0.00685	2.46302343
34	P14046	A1I3	Alpha-1-inhibitor 3	0.01764	2.35593841
35	Q9QY17	PACN2	Protein kinase C and casein kinase substrate in neurons 2 protein	0.00491	2.33496188
36	Q7M767	UB2V2	Ubiquitin-conjugating enzyme E2 variant 2	0.00403	2.22558688
37	P18418	CALR	Calreticulin	0.000001451	2.21878805
38	P01026	CO3	Complement C3	0.02878	2.13471781
39	Q765I2	UTS2B	Urotensin-2B	0.04336	2.09964579
40	P38659	PDIA4	Protein disulfide-isomerase A4	0.00165	2.05852901
41	P29598	UROK	Urokinase-type plasminogen activator	0.00028	2.05602277
42	P0DP31	CALM3	Calmodulin-3	0.000093254	2.03264314
43	Q7M0E3	DEST	Destrin	0.000023676	1.99247417
44	P05942	S10A4	Protein S100-A4	0.00119	1.98159598
45	Q63416	ITIH3	Inter-alpha-trypsin inhibitor heavy chain H3	0.01321	1.9695794
46	P24368	PPIB	Peptidyl-prolyl cis-trans isomerase B	7.1696E-09	1.93145045
47	Q9ERB4	CSPG2	Versican core protein (Fragments)	5.1864E-08	1.92868241
48	Q00715	H2B1	Histone H2B type 1	0.0012	1.92296441
49	O70352	CD82	CD82 antigen	0.0255	1.91835657
50	P62250	RS16	40S ribosomal protein S16	0.00762	1.90856126

51	Q6LED0	H31	Histone H3.1	0.00421	1.87295594
52	Q498E0	TXD12	Thioredoxin domain-containing protein 12	0.00527	1.8655779
53	P08699	LEG3	Galectin-3	0.000039855	1.77134285
54	P23358	RL12	60S ribosomal protein L12	0.02724	1.76009304
55	Q5XI32	CAPZB	F-actin-capping protein subunit beta	0.00012	1.72466171
56	P13084	NPM	Nucleophosmin	0.04491	1.69724134
57	Q66HD0	ENPL	Endoplasmin	0.00979	1.68275838
58	P49134	ITB1	Integrin beta-1	0.03881	1.6389988
59	P04692-6	TPM1	Isoform 6 of Tropomyosin alpha-1 chain	0.02289	1.63641035
60	P47727	CBR1	Carbonyl reductase [NADPH] 1	0.02371	1.54390361
61	Q63081	PDIA6	Protein disulfide-isomerase A6	0.01115	1.53843746
62	P01830	THY1	Thy-1 membrane glycoprotein	0.00045	1.5215802
63	P04785	PDIA1	Protein disulfide-isomerase	0.00029	1.50012835
64	Q62786	FPRP	Prostaglandin F2 receptor negative regulator	0.00012	1.49503604
65	P62246	RS15A	40S ribosomal protein S15a	0.01439	1.4785654
66	P28073	PSB6	Proteasome subunit beta type-6	0.0185	1.46350712
67	P62963	PROF1	Profilin-1	0.000068562	1.4561384
68	P04937	FINC	Fibronectin	0.00071	1.42222756
69	P62944	AP2B1	AP-2 complex subunit beta	0.02688	1.41462659
70	O54975	XPP1	Xaa-Pro aminopeptidase 1	0.01224	1.40878104
71	P31977	EZRI	Ezrin	0.00901	1.39847983
72	P61589	RHOA	Transforming protein RhoA	0.0166	1.39429

					7
73	Q9R063	PRDX5	Peroxiredoxin-5, mitochondrial	0.000054696	1.38078223
74	Q5XI22	THIC	Acetyl-CoA acetyltransferase, cytosolic	0.01543	1.3633895
75	P30904	MIF	Macrophage migration inhibitory factor	0.03946	1.35704022
76	Q9Z0W7	CLIC4	Chloride intracellular channel protein 4	9.7974E-06	1.34114328
77	Q9EPC6	PROF2	Profilin-2	0.01173	1.33920426
78	P62959	HINT1	Histidine triad nucleotide-binding protein 1	0.00079	1.33006614
79	P05369	FPPS	Farnesyl pyrophosphate synthase	0.00184	1.32919972
80	P14562	LAMP1	Lysosome-associated membrane glycoprotein 1	0.03194	1.31799426
81	P26772	CH10	10 kDa heat shock protein, mitochondrial	0.01763	1.31643684
82	Q5I0D1	GLOD4	Glyoxalase domain-containing protein 4	0.02394	1.31150523
83	Q5U2U2	CRKL	Crk-like protein	0.00766	0.73721377
84	Q4KM73	KCY	UMP-CMP kinase	0.05407	0.71104147
85	P31000	VIME	Vimentin	0.000022298	0.70683156
86	P08592	A4	Amyloid-beta A4 protein	0.00059	0.69331501
87	P62628	DLRB1	Dynein light chain roadblock-type 1	0.03188	0.69055174
88	P17164	FUCO	Tissue alpha-L-fucosidase	0.00013	0.68588306
89	P48450	ERG7	Lanosterol synthase	0.03092	0.68029474
90	Q641X3	HEXA	Beta-hexosaminidase subunit alpha	0.0027	0.6785347
91	Q9EPB1	DPP2	Dipeptidyl peptidase 2	0.00898	0.65026358
92	Q32KJ6	GALNS	N-acetylgalactosamine-6-sulfatase	0.04292	0.64900357
93	P04961	PCNA	Proliferating cell nuclear antigen	0.01752	0.64532984

94	Q6AXR4	HEXB	Beta-hexosaminidase subunit beta	0.02352	0.63947601
95	P06760	BGLR	Beta-glucuronidase	0.0007	0.6378096
96	Q8K4Y7	CANT1	Soluble calcium-activated nucleotidase 1	0.00283	0.63170615
97	P30919	ASPG	N(4)-(Beta-N-acetylglucosaminyl)-L-asparaginase	0.01844	0.6271429
98	P16636	LYOX	Protein-lysine 6-oxidase	0.00933	0.62354014
99	Q9JI03	CO5A1	Collagen alpha-1(V) chain	0.00349	0.61980904
100	Q6P7S1	ASAH1	Acid ceramidase	0.0174	0.60301498
101	Q5XII0	EPDR1	Mammalian ependymin-related protein 1	0.02165	0.601679
102	P29315	RINI	Ribonuclease inhibitor	0.00018	0.60167554
103	Q6IRK9	CBPQ	Carboxypeptidase Q	4.1791E-06	0.5924145
104	P20961	PAI1	Plasminogen activator inhibitor 1	0.00214	0.58001324
105	P50609	FMOD	Fibromodulin	0.01921	0.57775043
106	Q9QZK5	HTRA1	Serine protease HTRA1	9.2936E-07	0.57197159
107	P00786	CATH	Pro-cathepsin H	0.01974	0.56923372
108	Q62894	ECM1	Extracellular matrix protein 1	7.5952E-07	0.53799067
109	P18331	INHBA	Inhibin beta A chain	0.000082876	0.51580379
110	Q6AYE5	OAF	Out at first protein homolog	0.00126	0.51003356
111	P24268	CATD	Cathepsin D	0.00269	0.5072663
112	P13941	CO3A1	Collagen alpha-1(III) chain	0.00013	0.50673228
113	P07154	CATL1	Cathepsin L1	0.000043806	0.50659473
114	P70490	MFGM	Lactadherin	0.00163	0.50080229
115	P15087	CBPE	Carboxypeptidase E	0.00004046	0.50072

					183
116	P33436	MMP2	72 kDa type IV collagenase	6.0276E-07	0.49759269
117	Q9JLD2	NEUS	Neuroserpin	0.00205	0.49449132
118	P02466	CO1A2	Collagen alpha-2(I) chain	0.000023951	0.49386468
119	Q9QZK8	DNS2A	Deoxyribonuclease-2-alpha	0.00181	0.48941647
120	Q6IE64	C1RL	Complement C1r subcomponent-like protein	0.00909	0.48869131
121	P00787	CATB	Cathepsin B	0.01178	0.48560997
122	P07151	B2MG	Beta-2-microglobulin	6.1138E-06	0.48238604
123	O70513	LG3BP	Galectin-3-binding protein	4.9459E-07	0.48097471
124	Q8JZQ0	CSF1	Macrophage colony-stimulating factor 1	0.00039	0.47927656
125	O55004	RNAS4	Ribonuclease 4	0.00195	0.47618562
126	Q00918	LTBP1	Latent-transforming growth factor beta-binding protein 1	1.2039E-08	0.47166258
127	Q6TUG0	DJB11	DnaJ homolog subfamily B member 11	0.00844	0.46579442
128	Q9R0D6	TCO2	Transcobalamin-2	4.1003E-06	0.44707541
129	Q8CHN8-2	MASP1	Isoform 2 of Mannan-binding lectin serine protease 1	0.00001526	0.44289632
130	Q8CHN8-2	MASP1	Isoform 2 of Mannan-binding lectin serine protease 1	0.00001526	0.44289632
131	Q9JLZ1	GLRX3	Glutaredoxin-3	0.000024785	0.44172622
132	Q63321	PLOD1	Procollagen-lysine,2-oxoglutarate 5-dioxygenase 1	9.1439E-06	0.43891847
133	P45479	PPT1	Palmitoyl-protein thioesterase 1	0.000022981	0.4328556
134	P28576	PDGFA	Platelet-derived growth factor subunit A	0.00035	0.42992513
135	Q01129	PGS2	Decorin	0.000086264	0.4275542
136	P30121	TIMP2	Metalloproteinase inhibitor 2	4.2128E-10	0.41618959

137	P23785	GRN	Progranulin	3.1343E-08	0.41481256
138	Q66H12	NAGAB	Alpha-N-acetylgalactosaminidase	5.82E-08	0.41199147
139	Q9EQV6	TPP1	Tripeptidyl-peptidase 1	1.2289E-06	0.40869591
140	Q9R0J8	LGMN	Legumain	3.5946E-07	0.4056788
141	Q5RJL6	METRL	Meteorin-like protein	1.4302E-06	0.40404912
142	Q5U367	PLOD3	Multifunctional procollagen lysine hydroxylase and glycosyltransferase LH3	9.5585E-09	0.4023236
143	A2RUV9	AEBP1	Adipocyte enhancer-binding protein 1	0.000023174	0.39877101
144	P16612	VEGFA	Vascular endothelial growth factor A	0.000058632	0.39550442
145	P10960	SAP	Prosaposin	0.000022862	0.39531947
146	O35806	LTBP2	Latent-transforming growth factor beta-binding protein 2	0.00069	0.39429347
147	P42930	HSPB1	Heat shock protein beta-1	4.7252E-07	0.37840836
148	Q62632	FSTL1	Follistatin-related protein 1	1.9333E-06	0.37763036
149	Q6Q0N0	CSTN1	Calsyntenin-1	2.318E-07	0.37444824
150	P14844	CCL2	C-C motif chemokine 2	1.4701E-07	0.35781369
151	P14841	CYTC	Cystatin-C	7.1331E-08	0.35084342
152	Q920A6	RISC	Retinoid-inducible serine carboxypeptidase	1.7141E-08	0.34157623
153	B0BNI5	OLFL3	Olfactomedin-like protein 3	4.6804E-09	0.33733751
154	P97546	NPTN	Neuroplastin	0.0008	0.33654418
155	Q9EQX6	PDGFC	Platelet-derived growth factor C	0.00172	0.33442601
156	P53813	PROS	Vitamin K-dependent protein S	0.00271	0.33441438
157	Q6AXS4	RENR	Renin receptor	0.00002216	0.33285667
158	Q6P6T1	C1S	Complement C1s subcomponent	1.3706E-06	0.33028

					446
159	Q64610	ENPP2	Ectonucleotide pyrophosphatase/phosphodiesterase family member 2	3.4221E-07	0.32946561
160	Q76HN1	HYAL1	Hyaluronidase-1	0.00946	0.32086081
161	O08628	PCOC1	Procollagen C-endopeptidase enhancer 1	1.2291E-09	0.31612478
162	Q9WV75	SPON2	Spondin-2	1.6063E-09	0.30275796
163	P51886	LUM	Lumican	0.000026818	0.29466987
164	P47853	PGS1	Biglycan	1.1716E-11	0.2942031
165	Q9R1E9	CTGF	Connective tissue growth factor	2.2758E-07	0.29318939
166	P30120	TIMP1	Metalloproteinase inhibitor 1	0.000069981	0.28856266
167	P05371	CLUS	Clusterin	4.8373E-09	0.28658307
168	P21744	IBP4	Insulin-like growth factor-binding protein 4	1.5362E-07	0.28620419
169	Q9WVH8	FBLN5	Fibulin-5	3.941E-10	0.28203447
170	O35217	MINP1	Multiple inositol polyphosphate phosphatase 1	4.8754E-06	0.27569844
171	Q499S5	MMP11	Stromelysin-3	8.7641E-10	0.26849417
172	Q5FVF9	BTD	Biotinidase	0.0003	0.25508352
173	Q10739	MMP14	Matrix metalloproteinase-14	1.3074E-06	0.25232487
174	Q08420	SODE	Extracellular superoxide dismutase [Cu-Zn]	0.000025617	0.24957251
175	Q06880	NBL1	Neuroblastoma suppressor of tumorigenicity 1	0.000030614	0.23605421
176	Q10743	ADA10	Disintegrin and metalloproteinase domain-containing protein 10	1.5379E-06	0.23410779
177	Q63083	NUCB1	Nucleobindin-1	0.000043829	0.22605262
178	Q5FVH0	C1QT5	Complement C1q tumor necrosis factor-related protein 5	8.4661E-06	0.22156149
179	Q62638	GSLG1	Golgi apparatus protein 1	0.04585	0.21066

					08
180	P35572	IBP6	Insulin-like growth factor-binding protein 6	1.6206E-06	0.19571197
181	O54715	VAS1	V-type proton ATPase subunit S1	3.7537E-07	0.12330781

Appendix 4 List of identified proteins in Clinical plasma proteome

N	Accession	Name	Species	Peptides (95%)
1	P02768	Serum albumin	HUMAN	534
2	P01024	Complement C3	HUMAN	178
3	P01023	Alpha-2-macroglobulin	HUMAN	158
4	P0DOX5	Immunoglobulin gamma-1 heavy chain	HUMAN	134
5	P02787	Serotransferrin	HUMAN	132
6	P04114	Apolipoprotein B-100	HUMAN	113
7	P0DOX7	Immunoglobulin kappa light chain	HUMAN	105
8	P02675	Fibrinogen beta chain	HUMAN	98
9	P01834	Immunoglobulin kappa constant	HUMAN	95
10	P01859	Immunoglobulin heavy constant gamma 2	HUMAN	93
11	P0C0L5	Complement C4-B	HUMAN	85
12	P0C0L4	Complement C4-A	HUMAN	85
13	P0C0L4-2	Isoform 2 of Complement C4-A	HUMAN	83
14	P01861	Immunoglobulin heavy constant gamma 4	HUMAN	81
15	P02671	Fibrinogen alpha chain	HUMAN	75
16	P02671-2	Isoform 2 of Fibrinogen alpha chain	HUMAN	75
17	P01860	Immunoglobulin heavy constant gamma 3	HUMAN	71
18	P01009	Alpha-1-antitrypsin	HUMAN	68
19	P00738	Haptoglobin	HUMAN	64
20	P00450	Ceruloplasmin	HUMAN	51

21	P02679	Fibrinogen gamma chain	HUMAN	51
22	P02679-2	Isoform Gamma-A of Fibrinogen gamma chain	HUMAN	51
23	P02647	Apolipoprotein A-I	HUMAN	48
24	P02790	Hemopexin	HUMAN	47
25	P08603	Complement factor H	HUMAN	38
26	P01876	Immunoglobulin heavy constant alpha 1	HUMAN	36
27	P04217	Alpha-1B-glycoprotein	HUMAN	34
28	P02765	Alpha-2-HS-glycoprotein	HUMAN	34
29	Q14624	Inter-alpha-trypsin inhibitor heavy chain H4	HUMAN	31
30	P00747	Plasminogen	HUMAN	31
31	Q14624-3	Isoform 3 of Inter-alpha-trypsin inhibitor heavy chain H4	HUMAN	30
32	Q14624-2	Isoform 2 of Inter-alpha-trypsin inhibitor heavy chain H4	HUMAN	30
33	P00739	Haptoglobin-related protein	HUMAN	28
34	P00739-2	Isoform 2 of Haptoglobin-related protein	HUMAN	28
35	P0DOX2	Immunoglobulin alpha-2 heavy chain	HUMAN	27
36	P00751	Complement factor B	HUMAN	26
37	P02774	Vitamin D-binding protein	HUMAN	25
38	P02774-3	Isoform 3 of Vitamin D-binding protein	HUMAN	25
39	P06727	Apolipoprotein A-IV	HUMAN	23
40	P19827	Inter-alpha-trypsin inhibitor heavy chain H1	HUMAN	23
41	P02751	Fibronectin	HUMAN	21
42	P02751-9	Isoform 9 of Fibronectin	HUMAN	21
43	P02751-8	Isoform 8 of Fibronectin	HUMAN	21
44	P02751-7	Isoform 7 of Fibronectin	HUMAN	21
45	P02751-5	Isoform 5 of Fibronectin	HUMAN	21
46	P02751-3	Isoform 3 of Fibronectin	HUMAN	21
47	P02751-17	Isoform 17 of Fibronectin	HUMAN	21

48	P02751-15	Isoform 15 of Fibronectin	HUMAN	21
49	P02751-14	Isoform 14 of Fibronectin	HUMAN	21
50	P02751-13	Isoform 13 of Fibronectin	HUMAN	21
51	P02751-10	Isoform 10 of Fibronectin	HUMAN	21
52	P01008	Antithrombin-III	HUMAN	21
53	P01871	Immunoglobulin heavy constant mu	HUMAN	21
54	P01871-2	Isoform 2 of Immunoglobulin heavy constant mu	HUMAN	21
55	P20742	Pregnancy zone protein	HUMAN	21
56	P02751-6	Isoform 6 of Fibronectin	HUMAN	20
57	P19823	Inter-alpha-trypsin inhibitor heavy chain H2	HUMAN	20
58	P04196	Histidine-rich glycoprotein	HUMAN	20
59	P20742-2	Isoform 2 of Pregnancy zone protein	HUMAN	20
60	P06396	Gelsolin	HUMAN	19
61	P01031	Complement C5	HUMAN	19
62	P02749	Beta-2-glycoprotein 1	HUMAN	19
63	P0DOX8	Immunoglobulin lambda-1 light chain	HUMAN	19
64	P06396-4	Isoform 4 of Gelsolin	HUMAN	18
65	P06396-3	Isoform 3 of Gelsolin	HUMAN	18
66	P06396-2	Isoform 2 of Gelsolin	HUMAN	18
67	P01011	Alpha-1-antichymotrypsin	HUMAN	18
68	B9A064	Immunoglobulin lambda-like polypeptide 5	HUMAN	18
69	P0DOX6	Immunoglobulin mu heavy chain	HUMAN	18
70	P01042-2	Isoform LMW of Kininogen-1	HUMAN	17
71	P0DOY3	Immunoglobulin lambda constant 3	HUMAN	17
72	P0DOY2	Immunoglobulin lambda constant 2	HUMAN	17
73	P10909	Clusterin	HUMAN	16

74	P10909-5	Isoform 5 of Clusterin	HUMAN	16
75	P10909-2	Isoform 2 of Clusterin	HUMAN	16
76	P01042	Kininogen-1	HUMAN	16
77	P02748	Complement component C9	HUMAN	16
78	P02763	Alpha-1-acid glycoprotein 1	HUMAN	16
79	A0M8Q6	Immunoglobulin lambda constant 7	HUMAN	16
80	P10909-4	Isoform 4 of Clusterin	HUMAN	15
81	Q96PD5	N-acetylmuramoyl-L-alanine amidase	HUMAN	14
82	P43652	Afamin	HUMAN	13
83	P04004	Vitronectin	HUMAN	13
84	Q96PD5-2	Isoform 2 of N-acetylmuramoyl-L-alanine amidase	HUMAN	13
85	P00734	Prothrombin	HUMAN	13
86	P01780	Immunoglobulin heavy variable 3-7	HUMAN	13
87	P0CF74	Immunoglobulin lambda constant 6	HUMAN	13
88	P25311	Zinc-alpha-2-glycoprotein	HUMAN	12
89	P36955	Pigment epithelium-derived factor	HUMAN	12
90	P05090	Apolipoprotein D	HUMAN	11
91	P04432	Immunoglobulin kappa variable 1D-39	HUMAN	11
92	P01597	Immunoglobulin kappa variable 1-39	HUMAN	11
93	P01019	Angiotensinogen	HUMAN	10
94	P02766	Transthyretin	HUMAN	10
95	P02750	Leucine-rich alpha-2-glycoprotein	HUMAN	10
96	P02760	Protein AMBP	HUMAN	10
97	P01764	Immunoglobulin heavy variable 3-23	HUMAN	10
98	A0A075B6S5	Immunoglobulin kappa variable 1-27	HUMAN	10
99	P01619	Immunoglobulin kappa variable 3-20	HUMAN	9
100	P19652	Alpha-1-acid glycoprotein 2	HUMAN	9
101	P01782	Immunoglobulin heavy variable 3-9	HUMAN	9
102	P01602	Immunoglobulin kappa variable 1-5	HUMAN	9

103	P01599	Immunoglobulin kappa variable 1-17	HUMAN	9
104	A0A0B4J1X5	Immunoglobulin heavy variable 3-74	HUMAN	9
105	P02743	Serum amyloid P-component	HUMAN	8
106	P07358	Complement component C8 beta chain	HUMAN	8
107	P02649	Apolipoprotein E	HUMAN	8
108	P27169	Serum paraoxonase/arylesterase 1	HUMAN	8
109	P02753	Retinol-binding protein 4	HUMAN	8
110	P05156	Complement factor I	HUMAN	8
111	P05155	Plasma protease C1 inhibitor	HUMAN	8
112	P05155-3	Isoform 3 of Plasma protease C1 inhibitor	HUMAN	8
113	P05155-2	Isoform 2 of Plasma protease C1 inhibitor	HUMAN	8
114	P01767	Immunoglobulin heavy variable 3-53	HUMAN	8
115	P03952	Plasma kallikrein	HUMAN	8
116	P0DP04	Immunoglobulin heavy variable 3-43D	HUMAN	8
117	P08697	Alpha-2-antiplasmin	HUMAN	7
118	P09871	Complement C1s subcomponent	HUMAN	7
119	A0A0C4DH38	Immunoglobulin heavy variable 5-51	HUMAN	7
120	P02652	Apolipoprotein A-II	HUMAN	7
121	A0A0B4J1Y9	Immunoglobulin heavy variable 3-72	HUMAN	7
122	P04430	Immunoglobulin kappa variable 1-16	HUMAN	7
123	P01594	Immunoglobulin kappa variable 1-33	HUMAN	7
124	P01593	Immunoglobulin kappa variable 1D-33	HUMAN	7
125	P08697-2	Isoform 2 of Alpha-2-antiplasmin	HUMAN	6
126	P07225	Vitamin K-dependent protein S	HUMAN	6
127	P05543	Thyroxine-binding globulin	HUMAN	6
128	P69905	Hemoglobin subunit alpha	HUMAN	6
129	P04003	C4b-binding protein alpha chain	HUMAN	6

130	P05546	Heparin cofactor 2	HUMAN	6
131	P00736	Complement C1r subcomponent	HUMAN	6
132	A0A0A0MS15	Immunoglobulin heavy variable 3-49	HUMAN	6
133	A0A0C4DH42	Immunoglobulin heavy variable 3-66	HUMAN	6
134	P0DP03	Immunoglobulin heavy variable 3-30-5	HUMAN	6
135	P01768	Immunoglobulin heavy variable 3-30	HUMAN	6
136	P01624	Immunoglobulin kappa variable 3-15	HUMAN	6
137	A0A0B4J1X8	Immunoglobulin heavy variable 3-43	HUMAN	6
138	A0A087WSY6	Immunoglobulin kappa variable 3D-15	HUMAN	6
139	Q06033	Inter-alpha-trypsin inhibitor heavy chain H3	HUMAN	5
140	Q06033-2	Isoform 2 of Inter-alpha-trypsin inhibitor heavy chain H3	HUMAN	5
141	P68871	Hemoglobin subunit beta	HUMAN	5
142	P08185	Corticosteroid-binding globulin	HUMAN	5
143	P13645	Keratin, type I cytoskeletal 10	HUMAN	5
144	P13671	Complement component C6	HUMAN	5
145	P0DOX3	Immunoglobulin delta heavy chain	HUMAN	5
146	A0A0B4J1V0	Immunoglobulin heavy variable 3-15	HUMAN	5
147	P0DP02	Immunoglobulin heavy variable 3-30-3	HUMAN	5
148	P01772	Immunoglobulin heavy variable 3-33	HUMAN	5
149	P01591	Immunoglobulin J chain	HUMAN	5
150	P04433	Immunoglobulin kappa variable 3-11	HUMAN	5
151	A0A0A0MRZ8	Immunoglobulin kappa variable 3D-11	HUMAN	5
152	A0A0J9Y	Immunoglobulin heavy variable 3-64D	HUMAN	5

	X35			
153	P07360	Complement component C8 gamma chain	HUMAN	4
154	P10643	Complement component C7	HUMAN	4
155	P01614	Immunoglobulin kappa variable 2D-40	HUMAN	4
156	A0A087WW87	Immunoglobulin kappa variable 2-40	HUMAN	4
157	P63261	Actin, cytoplasmic 2	HUMAN	4
158	P60709	Actin, cytoplasmic 1	HUMAN	4
159	P02656	Apolipoprotein C-III	HUMAN	4
160	A0A075B6K5	Immunoglobulin lambda variable 3-9	HUMAN	4
161	P80748	Immunoglobulin lambda variable 3-21	HUMAN	4
162	P01701	Immunoglobulin lambda variable 1-51	HUMAN	4
163	A0A0C4DH69	Immunoglobulin kappa variable 1-9	HUMAN	4
164	A0A0C4DH25	Immunoglobulin kappa variable 3D-20	HUMAN	4
165	P06312	Immunoglobulin kappa variable 4-1	HUMAN	4
166	P15814	Immunoglobulin lambda-like polypeptide 1	HUMAN	4
167	P04264	Keratin, type II cytoskeletal 1	HUMAN	3
168	P0DP08	Immunoglobulin heavy variable 4-38-2	HUMAN	3
169	P0DP06	Immunoglobulin heavy variable 4-30-4	HUMAN	3
170	P06331	Immunoglobulin heavy variable 4-34	HUMAN	3
171	P01825	Immunoglobulin heavy variable 4-59	HUMAN	3
172	P01824	Immunoglobulin heavy variable 4-39	HUMAN	3
173	A0A0C4DH41	Immunoglobulin heavy variable 4-61	HUMAN	3
174	P18428	Lipopolysaccharide-binding protein	HUMAN	3
175	P01700	Immunoglobulin lambda variable 1-47	HUMAN	3
176	P01615	Immunoglobulin kappa variable 2D-28	HUMAN	3

177	A0A075B6P5	Immunoglobulin kappa variable 2-28	HUMAN	3
178	P29622	Kallistatin	HUMAN	3
179	O95445	Apolipoprotein M	HUMAN	3
180	O95445-2	Isoform 2 of Apolipoprotein M	HUMAN	3
181	A0A0C4DH34	Immunoglobulin heavy variable 4-28	HUMAN	3
182	P01717	Immunoglobulin lambda variable 3-25	HUMAN	3
183	P07357	Complement component C8 alpha chain	HUMAN	3
184	A0A075B6R2	Immunoglobulin heavy variable 4-4	HUMAN	3
185	P23083	Immunoglobulin heavy variable 1-2	HUMAN	3
186	A2NJV5	Immunoglobulin kappa variable 2-29	HUMAN	3
187	A0A0A0MRZ7	Immunoglobulin kappa variable 2D-26	HUMAN	3
188	A0A075B6S2	Immunoglobulin kappa variable 2D-29	HUMAN	3
189	P0DP09	Immunoglobulin kappa variable 1-13	HUMAN	3
190	A0A0B4J2D9	Immunoglobulin kappa variable 1D-13	HUMAN	3
191	P05452	Tetranectin	HUMAN	3
192	A0A0C4DH67	Immunoglobulin kappa variable 1-8	HUMAN	3
193	A0A087WSZ0	Immunoglobulin kappa variable 1D-8	HUMAN	3
194	Q03591	Complement factor H-related protein 1	HUMAN	3
195	P0DP01	Immunoglobulin heavy variable 1-8	HUMAN	3
196	A0A0C4DH31	Immunoglobulin heavy variable 1-18	HUMAN	3
197	P06310	Immunoglobulin kappa variable 2-30	HUMAN	3

198	A0A075B6S6	Immunoglobulin kappa variable 2D-30	HUMAN	3
199	P68133	Actin, alpha skeletal muscle	HUMAN	3
200	P68032	Actin, alpha cardiac muscle 1	HUMAN	3
201	P63267	Actin, gamma-enteric smooth muscle	HUMAN	3
202	P62736	Actin, aortic smooth muscle	HUMAN	3
203	P01743	Immunoglobulin heavy variable 1-46	HUMAN	3
204	P01742	Immunoglobulin heavy variable 1-69	HUMAN	3
205	A0A0B4J2H0	Immunoglobulin heavy variable 1-69D	HUMAN	3
206	A0A0C4DH29	Immunoglobulin heavy variable 1-3	HUMAN	3
207	P0DOX4	Immunoglobulin epsilon heavy chain	HUMAN	3
208	P02042	Hemoglobin subunit delta	HUMAN	3
209	P0DP07	Immunoglobulin heavy variable 4-31	HUMAN	2
210	P01699	Immunoglobulin lambda variable 1-44	HUMAN	2
211	P51884	Lumican	HUMAN	2
212	A0A075B6K4	Immunoglobulin lambda variable 3-10	HUMAN	2
213	P35858	Insulin-like growth factor-binding protein complex acid labile subunit	HUMAN	2
214	P35858-2	Isoform 2 of Insulin-like growth factor-binding protein complex acid labile subunit	HUMAN	2
215	P04278-5	Isoform 5 of Sex hormone-binding globulin	HUMAN	2
216	P04278	Sex hormone-binding globulin	HUMAN	2
217	P35908	Keratin, type II cytoskeletal 2 epidermal	HUMAN	2
218	P04259	Keratin, type II cytoskeletal 6B	HUMAN	2
219	P35527	Keratin, type I cytoskeletal 9	HUMAN	2
220	A0A0C4DH68	Immunoglobulin kappa variable 2-24	HUMAN	2

221	P06681	Complement C2	HUMAN	2
222	P06681-3	Isoform 3 of Complement C2	HUMAN	2
223	P06681-2	Isoform 2 of Complement C2	HUMAN	2
224	P22352	Glutathione peroxidase 3	HUMAN	2
225	Q08380	Galectin-3-binding protein	HUMAN	2
226	O75636	Ficolin-3	HUMAN	2
227	O75636-2	Isoform 2 of Ficolin-3	HUMAN	2
228	A0A0C4DH24	Immunoglobulin kappa variable 6-21	HUMAN	2
229	O14791	Apolipoprotein L1	HUMAN	2
230	O14791-3	Isoform 3 of Apolipoprotein L1	HUMAN	2
231	O14791-2	Isoform 2 of Apolipoprotein L1	HUMAN	2
232	P11021	Endoplasmic reticulum chaperone BiP	HUMAN	2
233	P06276	Cholinesterase	HUMAN	2
234	A0A087WSY4	Immunoglobulin heavy variable 4-30-2	HUMAN	2
235	P00488	Coagulation factor XIII A chain	HUMAN	2
236	O43866	CD5 antigen-like	HUMAN	2
237	P35542	Serum amyloid A-4 protein	HUMAN	2

Appendix 5 Secretory proteins showing differential abundance in SWATH-MS analysis (Clinical plasma)

N	Accession	Gene Name	Protein Name	p-value	Fold Change
1	A0A075B6R2	HV404	Immunoglobulin heavy variable 4-4	0.03188	3.878650322
2	Q9HAP6	LIN7B	REVERSED Protein lin-7 homolog B	0.01103	3.613135688
3	P09871	C1S	Complement C1s subcomponent	0.02049	2.480894739
4	P0DJI8	SAA1	Serum amyloid A-1 protein	0.00068	2.442924017
5	P02775	CXCL7	Platelet basic protein	0.00729	2.313039014
6	P49908	SEPP1	Selenoprotein P	5.857E-05	2.100066959
7	P07225	PROS	Vitamin K-dependent protein S	0.00605	2.091797473
8	P00738	HPT	Haptoglobin	7.554E-05	2.018925514
9	P06276	CHLE	Cholinesterase	0.00965	1.993845587
10	A0A087WSY4	HV432	Immunoglobulin heavy variable 4-30-2	0.0073	1.908018439
11	P16070	CD44	CD44 antigen	0.01743	1.885991164
12	Q03591	FHR1	Complement factor H-related protein 1	0.02104	1.795934079
13	O75636	FCN3	Ficolin-3	0.00025	1.789138748
14	P01614	KVD40	Immunoglobulin kappa variable 2D-40	0.02051	1.750874587
15	P05154	IPSP	Plasma serine protease inhibitor	0.03586	1.705257793
16	P10643	CO7	Complement component C7	0.00123	1.67872379
17	P05090	APOD	Apolipoprotein D	0.00081	1.673927

					897
18	P04430	KV116	Immunoglobulin kappa variable 1-16	0.01288	1.624497371
19	P00736	C1R	Complement C1r subcomponent	0.00906	1.611392485
20	P04004	VTNC	Vitronectin	0.01057	1.582994474
21	O95445	APOM	Apolipoprotein M	0.01846	1.545240717
22	A0A075B6K5	LV39	Immunoglobulin lambda variable 3-9	0.01163	1.543517777
23	A0A0C4DH24	KV621	Immunoglobulin kappa variable 6-21	0.0043	1.538073399
24	P01591	IGJ	Immunoglobulin J chain	0.04957	1.499245854
25	A0A0C4DH34	HV428	Immunoglobulin heavy variable 4-28	0.05339	1.488702225
26	P02753	RET4	Retinol-binding protein 4	0.02217	1.453763438
27	P01031	CO5	Complement C5	0.00165	1.446834578
28	P02743	SAMP	Serum amyloid P-component	0.02021	1.429631606
29	P03952	KLKB1	Plasma kallikrein	0.00035	1.388052861
30	P06310	KV230	Immunoglobulin kappa variable 2-30	0.02613	1.335819726
31	P02671	FIBA	Fibrinogen alpha chain	0.00473	1.334528668
32	P01011	AACT	Alpha-1-antichymotrypsin	0.01859	1.301111101
33	P01042-2	KNG1	Isoform LMW of Kininogen-1	0.02075	0.711912892
34	P35858	ALS	Insulin-like growth factor-binding protein complex acid labile subunit	0.0247	0.711061872
35	P01876	IGHA1	Immunoglobulin heavy constant alpha 1	0.01556	0.654729766
36	P02656	APOC3	Apolipoprotein C-III	0.01601	0.647431648
37	P01008	ANT3	Antithrombin-III	0.00225	0.643591

					653
38	P05155	IC1	Plasma protease C1 inhibitor	0.00734	0.592932967
39	P01024	CO3	Complement C3	0.00997	0.584126594
40	P01871	IGHM	Immunoglobulin heavy constant mu	0.02	0.558561566
41	P0C0L4	CO4A	Complement C4-A	0.00252	0.435359121
42	P02790	HEMO	Hemopexin	0.0012	0.415327657
43	P20742	PZP	Pregnancy zone protein	0.00012	0.193417624

Curriculum vitae

Shakuntala Bai

Proteomics Facility, Biochemical sciences division
CSIR-National Chemical Laboratory, Pune: 411008
Email: s.bai@ncl.res.in
Contact no.: +919604439010

Education	
2013-Present	**Ph.D.in Biological Sciences**, AcSIR (CSIR-National Chemical Laboratory, Pune, India)
2010-2012	**Masters in Biotechnology**, Jiwaji University, Gwalior, India (73.8%)
2007-2010	**Bachelors in Biotechnology**, Jiwaji University, Gwalior, India (72.2%)
Research Experience	
Aug 2013-present	Doctoral fellow CSIR-National Chemical Laboratory, Pune, India Advisor: Dr. Mahesh J. Kulkarni Project: Study of methylglyoxal induced proteome in muscle cells
Jan 2012-June2012	Master's Project ICMR-National Institute of malaria research, New Delhi, India Advisor: Dr. Jyoti Das Project: To Study the Antimalarial Properties of Garlic Extract on *Plasmodium falciparum*
Skills and Techniques	
	Proficient in mass spectrometry, proteomics and cell culture techniques, animal experiments: • Growth and maintenance of cell lines • Handling of animals • Sample preparation- efficient protein extraction from mammalian cells • Gel electrophoresis analysis (1D and 2DE)

	• Western blot analysis, ELISA • Trypsin digestion and independent handling of mobile phases, nano LC, micro LC and HPLC columns; liquid chromatography (RP) • Data independent acquisition on NanoLC-synapt G1 HDMS, Micro LC-Triple TOF 5600, MALDI-TOF/TOF 5800 • Expression analysis using SWATH workflow, MRM HR, Data Dependent Acquisition • Data interpretation using various proteomic softwares- PLGS (Protein Lynx Global Server), Protein Pilot, PeakView, MarkerView, MultiQuant, Proteome Discoverer • Functional classification of identified proteome and Statistical Analysis (Bioinformatic tools like KAAS, DAVID, STRING, MetaboAnalyst, Cytoscape) • Basic molecular biology techniques: DNA and RNA isolation, agarose gel electrophoresis

Awards and Fellowship

- Lightening talk winner in International virtual symposium on functional and interaction proteomics: Application in food and health, 12th annual meeting of proteomics society, India 2020, organized by CSIR-NCL, Pune on 22nd - 24th december 2020
- Awarded UGC-RGNF JRF fellowship for 5 years in 2013
- Qualified Graduate Aptitude Test in Engineering (GATE), 2013
- Qualified Graduate Aptitude Test in Engineering (GATE), 2012

Workshops and Conferences

	• Participated in National seminar cum workshop on applications of bioinformatics in life sciences, held at DBT bioinformatics centre, Govt of india,school of studies in neuroscience, Jiwaji university, Gwalior during march 08-09, 2013 • Presented poster at International diabetes summit 2017,organized by Chellaram diabetes institute, from 10th to 12th march 2017

- Attended 2nd International diabetes summit 2018,organized by Chellaram diabetes institute, from 9th to 11th March 2018

- Participated in two-days hands-on workshop on metabolomics held on 09th-10th December, 2018, in NCCS Pune

- Participated in the training program on Shotgun proteomics with Q Exactive Orbitrap mass spectrometry 19-21, March 2014 at Thermo techinical centre, Powai

- Presented poster in 7th annual meeting of proteomics society, India 2015 conducted by centre for bioseparation technology, VIT university, Vellore on 3rd-6th december, 2015

- Presented poster in International conference on functional and interaction proteomics: Application in food and health, 8th annual meeting of proteomics society, India 2016, organized by NIPGR, new delhi on 14th - 17th december 2016

- Participated in 6th annual meeting of the proteomics society of India held at IIT Bomay during 7-9 December, 2014

- Participated and presented poster during 25-26 february, 2015, as a part of the national science day celebrations 2015, at Csir-National chemical laboratory,Pune,India

- Participated and presented poster during 23-24 february, 2017, as a part of the national science day celebrations-2017, at Csir-National chemical laboratory,Pune,India

- Trans-Proteomic Pipeline Workshop in the Targeted Proteomics Workshop and International Symposium, IIT Bombay, Mumbai, December 10-14, 2015

- Skyline Workshop in the Targeted Proteomics Workshop and International Symposium, IIT Bombay, Mumbai, February 24-27,

	2018 • Participated in International virtual symposium on functional and interaction proteomics: Application in food and health, 12th annual meeting of proteomics society, India 2020, organized by CSIR-NCL, Pune on 22nd - 24th december 2020

Publications

1. **Shakuntala Bai**, Arvindkumar H. Chaurasiya, Reema Banarjee, Prachi B. Walke, Faraz Rashid, Ambika G. Unnikrishnan, and Mahesh J. Kulkarni. "CD44, a Predominant Protein in Methylglyoxal-Induced Secretome 2 of Muscle Cells, is Elevated in Diabetic Plasma." *ACS Omega* 2020 https://doi.org/10.1021/acsomega.0c01318

2. Routaray, ChinmayeeBar, Renuka Bhor, **Shakuntala Bai**, Nitin Suryakant Kadam, Surabhi Jagtap, Pooja Jignesh Doshi, Shyam Sundar, Sangeeta Sawant, Mahesh J. Kulkarni, and Kalpana Pai. "SWATH-MS based quantitative proteomics analysis to evaluate the antileishmanial effect of Commiphora wightii "Guggul" and Amphotericin B on a clinical isolate of Leishmania donovani." *Journal of Proteomics* (2020): 103800.

3. Banarjee, Reema, Akshay Sharma, **Shakuntala Bai**, Arati Deshmukh, and Mahesh Kulkarni. "Proteomic study of endothelial dysfunction in response to homocysteinylated albumin." *Journal of Proteins and Proteomics* 10, no. 3 (2019): 167-178.

4. Banarjee, Reema, Akshay Sharma, **Shakuntala Bai**, Arati Deshmukh, and Mahesh Kulkarni. "Proteomic study of endothelial dysfunction induced by AGEs and its possible role in diabetic cardiovascular complications." *Journal of proteomics* 187 (2018): 69-79.

5. Deshmukh, Arati B., **Shakuntala Bai**, T. Aarthy, Rubina S. Kazi, Reema Banarjee, Rajeshwari Rathore, M. V. Vijayakumar, H. V. Thulasiram, Manoj Kumar Bhat, and M. J. Kulkarni. "Methylglyoxal attenuates insulin signaling and downregulates the enzymes involved in cholesterol biosynthesis." *Molecular BioSystems* 13, no. 11 (2017): 2338-2349.

ABSTRACT

Name of the Student: Shakuntala Bai **Registration No.:** 10BB13A26037

Faculty of Study: Biological Sciences **Year of Submission:** 2021

AcSIR academic center/CSIR Lab:CSIR-NCL**Name of the Supervisor(s):**Dr. Mahesh J. Kulkarni

Title of the thesis: Study of methylglyoxal induced proteome in muscle cells

---

Methylglyoxal (MG), a glycolytic intermediate and reactive dicarbonyl, is responsible for exacerbation of insulin resistance and diabetic complication. Skeletal muscle is the largest insulin-sensitive organ, accounts for up to 80% of insulin stimulated glucose uptake. Understanding the development of insulin resistance in response to methylglyoxal modified proteins can be useful in designing strategies for the management of diabetes. Therefore, in the present thesis, we have focused on the effect of methylglyoxal on the secretome and proteome of muscle cells, clinical plasma, and animal plasma.

In secretome analysis, differentially expressed proteins were found to be involved in various pathways like leukocyte transendothelial migration, fluid shear stress and atherosclerosis, and lysosomal pathway. MG induced secretome had several proteins related to insulin resistance, obesity, and metabolic syndrome. CD44 was found to be a common protein between MG induced secretome and clinical plasma proteome. The elevated levels of CD44 were accompanied by an increase in MG-induced CEL modifications of two HSA peptides, FKDLGEENFK and KVPQVSTPTLVEVSR, suggesting that the high levels of CD44 could be associated with an increase in the levels of MG in diabetes. Total cell proteome shows deregulation of various metabolic processes like Citrate cycle (TCA cycle), glycolysis/gluconeogenesis, glyoxylate and dicarboxylate metabolism. Transcription factors Nrf1, Atf4, Nfe2, and myc were found to regulate many deregulated proteins and lead to insulin resistance. In animal plasma proteomics, an increase in MG-induced modifications of two Rat Serum Albumin peptides, R(Argpyr)PCFSALTVDETYVPK and LVQEVTDFAK(CEL)TCVADENAENCDK, could be associated with an increase in the levels of MG in diabetes. Study of the effect of methylglyoxal on the secretome and proteome of muscle cells, clinical plasma, and animal plasma provided the groundwork for further studies and provided clues for designing strategies for the management of diabetes.

Details of publications, emanating from the thesis-work

1. **Bai, Shakuntala**, Arvindkumar H. Chaurasiya, Reema Banarjee, Prachi B. Walke, Faraz Rashid, Ambika G. Unnikrishnan, and Mahesh J. Kulkarni. "CD44, a Predominant Protein in Methylglyoxal-Induced Secretome of Muscle Cells, is Elevated in Diabetic Plasma." *ACS omega* 5, no. 39 (2020): 25016-25028. https://doi.org/10.1021/acsomega.0c01318

Poster/Lightening talk emanating from the thesis work

Lightening talk titled "**CD44, a predominant protein in methylglyoxal induced secretome of muscle cells, is elevated in diabetic plasma"** presented in International virtual symposium on functional and interaction proteomics: Application in food and health, 12th annual meeting of proteomics society, India 2020, organized by CSIR-NCL, Pune on 22nd - 24th december 2020.

Abstract

Methylglyoxal (MG), a glycolytic intermediate and reactive dicarbonyl, is responsible for exacerbation of insulin resistance and diabetic complication. In this study, MG induced secretome of rat muscle cells was identified and relatively quantified by SWATH-MS. A total of 643 proteins were identified in MG induced secretome, out of which 82 proteins were upregulated and 99 proteins were downregulated by more than 1.3 fold in SWATH analysis. Further, secretory proteins from the classical secretory pathway and non-classical secretory pathway were determined using SignalP and SecretomeP, respectively. A total of 180 proteins were identified with SignalP, and 113 proteins were identified with SecretomeP. The differentially expressed proteins were functionally annotated by KEGG Pathway analysis using Cytoscape software with plugin Clustermaker. The differentially expressed proteins were found to be involved in various pathways like, ECM-receptor interaction, leukocyte transendothelial migration, fluid shear stress and atherosclerosis, complement and coagulation cascades and

lysosomal pathway. Since the MG levels are high in diabetic conditions, the presence of MG induced secreted proteins was inspected by profiling human plasma of healthy and diabetic subjects (n=10 each). CD44, a predominant MG induced secreted protein, was found to be elevated in the diabetic plasma and has a role in the development of insulin resistance.

ACS OMEGA

http://pubs.acs.org/journal/acsodf

Article

CD44, a Predominant Protein in Methylglyoxal-Induced Secretome of Muscle Cells, is Elevated in Diabetic Plasma

Shakuntala Bai, Arvindkumar H. Chaurasiya, Reema Banarjee, Prachi B. Walke, Faraz Rashid, Ambika G. Unnikrishnan, and Mahesh J. Kulkarni*

Cite This: *ACS Omega* 2020, 5, 25016−25028

Read Online

ACCESS | Metrics & More | Article Recommendations | Supporting Information

ABSTRACT: Methylglyoxal (MG), a glycolytic intermediate and reactive dicarbonyl, is responsible for exacerbation of insulin resistance and diabetic complication. In this study, MG-induced secretome of rat muscle cells was identified and relatively quantified by SWATH-MS. A total of 643 proteins were identified in MG-induced secretome, of which 82 proteins were upregulated and 99 proteins were downregulated by more than 1.3-fold in SWATH analysis. Further, secretory proteins from the classical secretory pathway and nonclassical secretory pathway were identified using SignalP and SecretomeP, respectively. A total of 180 proteins were identified with SignalP, and 113 proteins were identified with SecretomeP. The differentially expressed proteins were functionally annotated by KEGG pathway analysis using Cytoscape software with plugin clusterMaker. The differentially expressed proteins were found to be involved in various pathways like extracellular matrix (ECM)−receptor interaction, leukocyte transendothelial migration, fluid shear stress and atherosclerosis, complement and coagulation cascades, and lysosomal pathway. Since the MG levels are high in diabetic conditions, the presence of MG-induced secreted proteins was inspected by profiling human plasma of healthy and diabetic subjects (n = 10 each). CD44, a predominant MG-induced secreted protein, was found to be elevated in the diabetic plasma and to have a role in the development of insulin resistance.

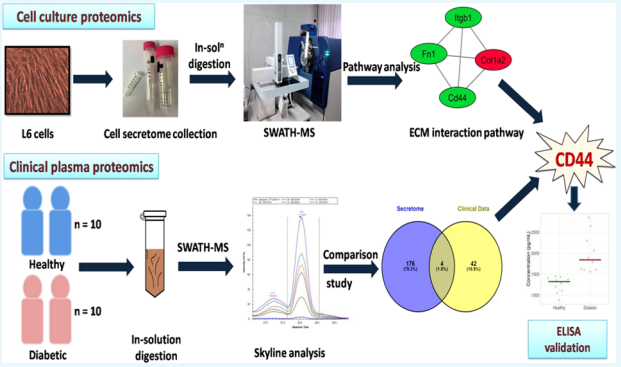

INTRODUCTION

Methylglyoxal (MG) is produced as a minor byproduct of various metabolic processes.[1] However, in insulin-resistant states like obesity and type 2 diabetes, MG levels are known to increase due to altered glucose metabolism. The concentration of MG in the plasma of diabetic patients is associated with the level of blood glucose.[2] The intracellularly produced MG can readily diffuse into the extracellular matrix. Since MG is highly reactive, it readily reacts with and modifies proteins, lipids, and DNA and can affect their normal structure and function.[3,4] It is also a major precursor of advanced glycation end products, which are reported to be involved in the development of diabetes and diabetic complications and whose detrimental effects have been widely reported.[5−8] Therefore, various detoxification mechanisms are present in the body, one of them being the glyoxalase system. This system comprises glutathione and two enzymes, viz., glyoxalase I and glyoxalase II. MG first reacts with glutathione to form a hemithioacetal, which is metabolized by glyoxalase I into S-D-lactoyl-glutathione. This intermediate is further metabolized into D-lactate by glyoxalase II, and glutathione is regenerated.[9] However, in diabetes, because of higher levels of MG, it can modify proteins from several tissues, including vascular endothelium and smooth muscles.[10,11] MG-induced modification in proteins may have adverse effects on cellular processes, and therefore, such proteins are removed by exocytosis or secretion into the extracellular matrix.[12]

Secreted proteins comprise an important class of biomolecules, that include a wide array of proteins such as serum proteins and matrix proteins as well as hormones and growth factors. It is believed that approximately 10% of the human genome encodes for secreted proteins.[13] Quintessential examples of secreted proteins include serum albumin, immunoglobulins, and enzymes of the digestive tract.[14] Even in the regulation of cell renewal and differentiation, proteins secreted in low abundance but that are highly bioactive, such as cytokines, and growth factors contribute significantly.[15]

Recent studies have indicated that apart from being the largest organ, skeletal muscles also have an endocrine function,

Received: March 24, 2020
Accepted: July 16, 2020
Published: September 23, 2020

https://dx.doi.org/10.1021/acsomega.0c01318
ACS Omega 2020, 5, 25016−25028

producing a large number of proteins called myokines. These proteins have been reported to have widespread action on different organs and tissues.[16] A number of tissues are reported to be regulated by myokines, and the synthesis and secretion of myokines are controlled by several factors including differentiation, exercise,[17] and in vitro electrical stimulation.[18] Apart from these factors, insulin resistance affects the secretion of myokines.[16] Various factors including oxidative stress, palmitic acid, and TNF-α are known to induce insulin resistance and affect the myokine secretion in muscle cells.[19−21] Similarly, it has been shown that MG induces insulin resistance in muscle cells;[22] however, MG-induced changes in myokine secretion are not yet studied. Characterization of skeletal muscle secretome is still not complete even after the identification of numerous myokines in recent profiling studies, which is evident from the amount of overlap seen among these studies. The pathogenesis of type 2 diabetes affects the functioning of all major organs that govern metabolic control including skeletal muscles. Since myokines influence a number of different organs, any alteration of the skeletal muscle secretome can have wide and detrimental effects. Herein, we sought to identify the MG-induced secretome of rat muscle cells and its validation in clinical plasma samples to identify potential biomarkers for diabetes.

METHODOLOGY

Chemicals. All fine chemicals and reagents were obtained from Sigma-Aldrich (St. Louis, MO). Dulbecco's modified Eagle's medium (DMEM) for cell culture was procured from HiMedia. Fetal bovine serum (FBS) (US origin) and trypsin were purchased from Invitrogen (Carlsbad, CAA). Plasticware for tissue culture was procured from Nunc (Rochester, NY). The Bradford protein estimation kit was purchased from Bio-Rad Laboratories. Centrifugal filters (3 kDa cutoff) and C18 Zip-Tip desalting columns were procured from Millipore (Millipore, Billerica, MA). Liquid chromatography columns, Eskigent C18-RP HPLC column (100 × 0.3 mm, 3 μm, 120 Å), were procured from Sciex (Sciex, Framingham, MA). The RapiGest SF surfactant was purchased from Waters (#186001860, Waters Corporation, MA). All solvents for liquid chromatography−mass spectrometry (LC−MS) were procured from J.T. Baker (J T. Baker, PA). The ELISA kit sCD44std Instant ELISA was procured from Thermo (#BMS209INST, eBioscience, Vienna, Austria).

Research Design. The schematic of the complete experimental design adopted in this study is depicted in Figure 1. The study was conducted to characterize methylglyoxal-induced secretome of muscle cells and identify the presence of methylglyoxal-induced secreted proteins in the diabetic plasma. The conditioned media from three individual experiments, each of control cells and methylglyoxal-treated cells were used for the identification of secretome by SWATH-MS. The mass spectrometric acquisition was performed for three different experiments in technical triplicates. The presence of methylglyoxal-induced secreted proteins was evaluated by performing proteomics analysis of 10 plasma samples each of healthy control and diabetic subjects by SWATH-MS in technical triplicates. CD44, one of the predominant methylglyoxal-induced secreted proteins, was evaluated for its presence in the same set of clinical samples in technical duplicates. Since this was a pilot study, the sample size was limited to a maximum of 20 samples.

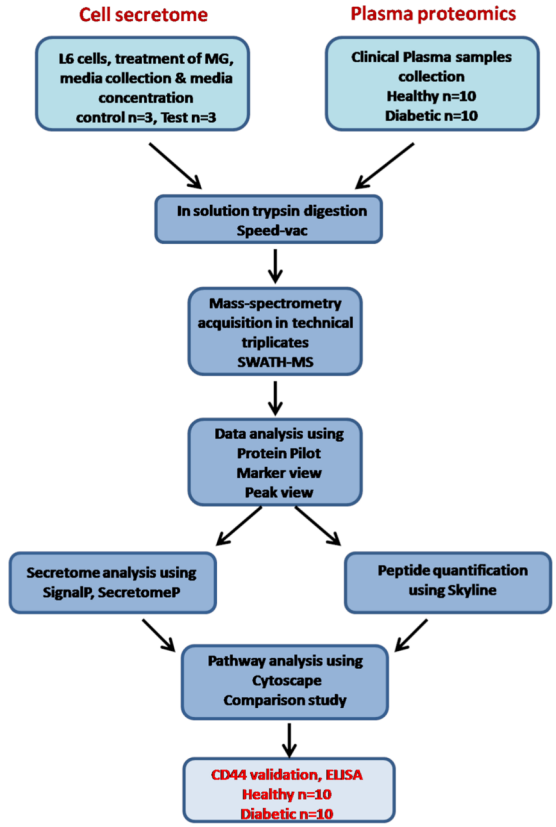

Figure 1. Overview of the complete experimental design.

Cell Culture and Differentiation. Rat L6 muscle cells were procured from the National Centre for Cell Sciences, Pune. They were grown in DMEM supplemented with 10% (v/v) heat-inactivated fetal bovine serum (FBS). The cells were maintained at 37 °C in a humidified atmosphere containing 5% (v/v) CO_2. Cells were differentiated in DMEM supplemented with 2% FBS for 6 days, and the progress of differentiation was monitored microscopically.

Cell Viability Assay. The cytotoxicity of methylglyoxal on L6 cells was assessed using the trypan blue (0.5%) dye exclusion test. Cells were seeded into 24-well culture plates and were grown for 24 h. Further, cells were serum-starved for 4 h in serum-free DMEM and treated with methylglyoxal at different concentrations for 3 h. After treatment, cells were washed twice with Dulbecco's phosphate-buffered saline, harvested using trypsin, and trypan blue staining was performed for assessing cell viability. Viable cells were counted using a hemocytometer.

Collection and Preparation of Conditioned Media. Differentiated and confluent cells were washed thrice with complete DMEM with no supplements, including phenol red, serum, or antibiotics, and were kept for serum starvation for 4 h. After treatment with methylglyoxal for 3 h, the conditioned media containing secretory proteins were collected and centrifuged twice at 4018g for 15 min at 4 °C to pellet down the detached cells and debris. The supernatant was collected and concentrated by passing through Amicon 15 mL 3 kDa cutoff filters (Millipore). The final secreted proteins were then dissolved in RapiGest. Protein concentration was estimated colorimetrically by Bradford's assay.

Clinical Sample Details. Clinical plasma proteomics was performed to validate the results of methylglyoxal-induced L6

https://dx.doi.org/10.1021/acsomega.0c01318
ACS Omega 2020, 5, 25016−25028

cell secretome. Clinical plasma samples were collected from the Chellaram Diabetes Institute, Pune, India, as per the guidelines of the Indian Council of Medical Research. The approval of the Institutional Ethics Committee was taken for the study, and informed consent was obtained from all of the subjects before blood collection. Only subjects with no history of other chronic clinical disorders, such as liver/kidney disease, thyroid disorders, or pregnancy, were included in the study. The proteomics study and enzyme-linked immunosorbent assay (ELISA) study both comprised healthy subjects (n = 10) and diabetic subjects (n = 10). Plasma preparation was done by collecting peripheral venous blood in ethylenediaminetetraacetic acid (EDTA) vacutainers (BD Biosciences). After the sample collection, biochemical parameters such as fasting blood glucose and glycated hemoglobin (HbA_{1c}) were analyzed immediately. Details of patients are given in Table S1. Erythrocytes were separated from plasma by centrifugation at 200g for 5 min. Next, the supernatant was centrifuged at 9300g for 15 min and plasma was carefully separated and stored at −80 °C until use.

In-Solution Trypsin Digestion. Total protein (100 μg) in 0.1% RapiGest for each plasma sample was used for digestion. Before reduction and alkylation, proteins were denatured by incubating at 80 °C for 15 min. Further, proteins were reduced using 100 mM dithiothreitol for 15 min at 60 °C and then alkylated by treating with 200 mM iodoacetamide for 30 min in the dark at room temperature. Trypsin was added at 1:25 (w/w) enzyme-to-protein ratio and incubated at 37 °C for 18 h; 2 μL of formic acid was added to inactivate trypsin and stop the digestion. For desalting of the digested peptides, C18 Zip-Tips were used, and the desalted peptides were concentrated using Speed Vac. For LC−MS analysis, peptides were reconstituted in 3% acetonitrile with 0.1% formic acid.

Liquid Chromatography−Mass Spectrometry Analysis. *SWATH-MS Analysis for Secretome.* SWATH analysis was performed on a Triple-TOF 5600 (AB Sciex; Concord, Canada) mass spectrometer coupled with Micro LC 200 (Eksigent; Dublin, CA) in high-sensitivity mode. A spectral library was generated by pooling equal amounts of peptide samples from each treatment and analyzing by information-dependent acquisition (IDA). Briefly, peptides were separated on a Eksigent C18-RP HPLC column (100 × 0.3 mm, 3 μm, 120 Å) using a 95 min gradient of 3% to 35% mobile phase B at a flow rate of 8 μL/min (mobile phase A: water with 0.1% formic acid; mobile phase B: acetonitrile with 0.1% formic acid). Accumulation time for MS was 250 ms and for MS/MS was 100 ms. Fragmentation was done using rolling collision energy. For SWATH-MS acquisition, the precursor mass range of 400−1250 m/z was divided into a set of 34 overlapping windows of 25 m/z each. For MS/MS, collision energy was optimized for each window and spectra were collected from 100 to 2000 m/z. Fragment ion scans were performed over an accumulation time of 70 ms, while for the precursor survey scan, it was 100 ms. All samples were acquired in biological and technical triplicates.

To get spectral library from IDA run, data was analyzed by ProteinPilot software version 5.0 using UniProt *Rattus norvegicus* database updated with Uniprot release 2019_02; 8,060 reviewed protein entries. The enzyme used for digestion was set to trypsin, and carbamidomethylation of cysteine residues was set as fixed modification. Search was performed using a false discovery rate (FDR) of 1%. The resultant spectral library was imported into PeakView v2.2 software, and SWATH runs for all samples were processed using 50 ppm mass error, 5 min RT window, 99% confidence, and 1% FDR. The peak areas thus generated in PeakView were imported into MarkerView v 1.2.1, wherein statistical analysis using the t-test was performed. Normalization across the runs was performed using total area sum. All of the raw mass spectrometric data have been deposited at the public repository PeptideAtlas (PASS01477).

SWATH-MS Analysis for Clinical Plasma. *LC−MS Conditions.* The trypsin-digested samples (healthy and diabetic) were desalted offline by Zip-Tip (Millipore) and loaded on to an EksigentTrap (ChromXP C-18-CL: 0.35 × 0.5 mm, 3 μm, 120 Å) and analytical Nano column (ChromXP3C-18-CL: 0.075 × 15 mm, 3 μm, 120 Å) fitted with an Eksigent nanoLC-Ultra 2D system, which was connected to a Triple-TOF 6600 mass spectrometer (Sciex, Ontario, Canada). Peptides were separated on nanoLC using the following mobile phase composition: water/acetonitrile/formic acid (A, 98/2/0.2%; B, 2/98/0.2%). The flow rate was kept at 300 nL/min, and 2000 ng of each sample was injected on the column. An overall 3.5 h gradient run was used for separation, which started with 5 min of 5% B, followed by a linear increase of B to 35% in 80 min and further increase to 50% B in 90 min. In the end, mobile phase B was increased to 90% in 1 min and maintained for 13 min, after which the gradient was brought back to the initial 5% B in 1 min and held for 6 min.

MS/MS Conditions. The sample data was acquired in information-dependent acquisition (IDA) mode using an ESI ion source. The ESI source was maintained at a voltage of 2300 V and a temperature of 130 °C, with curtain gas of 25 psi, nebulizer gas of 20 psi, and heater gas of 10 psi. For MS survey scan, mass range m/z 350−1250 was scanned with a resolution ≥30 000 full width at half-maxima (FWHM) with an accumulation time of 250 ms. For MS/MS, 35 product ion scans over the mass range m/z 100−1600 were collected in high-sensitivity mode. The criteria for precursor selection for MS/MS were set at a threshold of more than 120 counts per second and a charge state of 2+ to 5+. Also, the dynamic exclusion for precursor selection was set for 3 s. Collision energy (CE) for fragmentation was optimized for each precursor using an IDA CE parameter script, and collision energy spread (CES) was set at 5 eV. The total cycle time for the survey scan and product ion scan was set at 2.35 s.

Label-Free Quantitation. Label-free quantification was performed using SWATH-MS, wherein the mass range of 350−1250 Da was divided into a set of 75 overlapping windows of 12 Da each with 1 Da overlap between each window. The CE for each window was optimized, and a CES of 5 eV was set. MS/MS scans were acquired in high-sensitivity mode with a mass resolution of 15 000. The total duty cycle comprised one MS survey scan of 50 ms and 75 MS/MS scans of 50 ms each. Each sample was acquired in triplicate runs for quantification. The raw mass spectrometric data for all IDA and SWATH runs is deposited at the public repository PeptideAtlas (PASS01478).

SWATH Data Processing. The IDA runs were searched against the UniProt protein database (release 2018_04; 20,341 reviewed protein entries) limited to *Homo sapiens* taxonomy with ProteinPilot v5.0 software. For the analysis, cysteine alkylation was set to iodoacetamide and digestion to trypsin. The search was performed using biological modifications as ID focus and thorough ID as a search effort. FDR for peptide identification was set to 1%. Proteins having at least two

https://dx.doi.org/10.1021/acsomega.0c01318
ACS Omega 2020, 5, 25016−25028

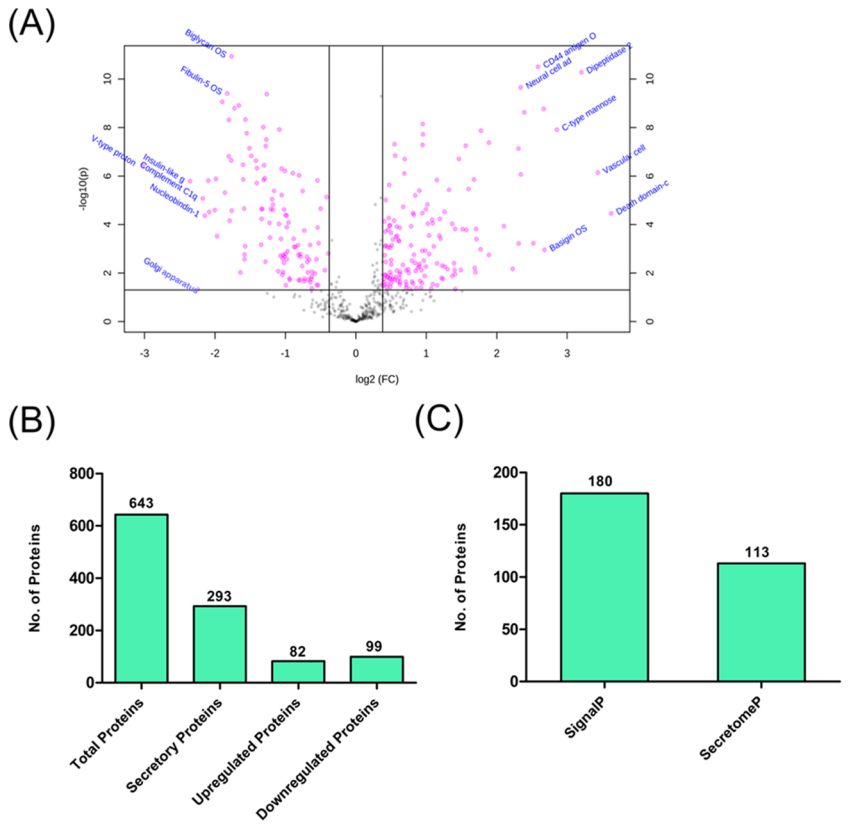

Figure 2. Proteomic analysis for secretome: differential proteomics analysis done by SWATH-MS. (A) Volcano plot, made using Metaboanalyst 4.0 online analytical tool, indicates the proteins with differential abundance >1.3-fold and p-value < 0.05 in pink. (B) Number of differentially expressed proteins in MG vs control. (C) Number of secretory proteins obtained through SignalP and SecretomeP.

unique peptides with a minimum 95% confidence and detected with less than 1% FDR were considered for relative quantitation analysis.

The result of the IDA analysis was used as a reference spectral library for SWATH processing using PeakView v2.2 software. The spectral library was imported and filtered by setting the mass tolerance to 50 ppm, peptide confidence to 99%, number of peptides to 5, and number of transitions to 6. Peptides shared between two or more protein families were excluded from quantitation. Further, the proteins whose peptides passed the 1% FDR criteria set in the SWATH 2.0 plugin of PeakView were exported to MarkerView v 1.2.1. Statistical analysis was performed in MarkerView using a t-test, and those proteins with a p-value ≤ 0.05 were considered for quantitation. The proteins having fold change ≥ 1.3 or ≤ 1.3 were considered as differentially expressed in our experiment.

Bioinformatic Analysis. The differentially secreted proteins were analyzed for protein−protein interactions and pathways using the STRING 11.0 database (Search Tool for the Retrieval of Interacting Genes), and the protein−protein interaction (PPI) network was imported into Cytoscape 3.2, an open-source network visualization software. The clustering of proteins was performed using the clusterMaker plugin in Cytoscape. The identification of secretory proteins was done using both classical and nonclassical secretion prediction tools. The web-based SignalP 5.0 server (http://www.cbs.dtu.dk/services/SignalP/) was used for predicting classically secreted proteins, and the data was processed using the "eukarya" option. For the prediction of nonclassically secreted proteins, SecretomeP 2.0 (http://www.cbs.dtu.dk/services/SecretomeP/) was used.

Data Analysis for Quantification of Methylglyoxal-Modified Peptides. Skyline (version 4.1.0, MacCoss Lab) was used for the quantification of peptides using SWATH.wiff files. The FASTA file of human serum albumin was used for theoretical mass spectral library generation. Unmodified peptides and corresponding carboxyethyl-modified peptides of albumin were specified for the targeted quantification of peptides. Retention times of precursors were manually corrected wherever required. Only intense and co-eluting fragment ions of a particular precursor were considered for quantification. The sum of the area under the curve (AUC) of these selected fragment ions was used for the quantification of the precursor. The digestion enzyme was specified as trypsin. The maximum missed cleavage was set to 1. Carbamidomethylation at cysteine (57.021464 Da), MG-H1 at arginine (54.01565 Da), and carboxyethyl modification at lysine and arginine (72.021126 Da) were specified as methylglyoxal-associated modifications. Precursor ion charge states were specified as +2 and +3, whereas fragment ion charge states were specified as +1 and +2. Fragment ion mass tolerance was set to 0.5 Da. The acquisition method was selected as DIA, and the product mass analyzer was set as TOF. The isolation scheme was selected as SWATH (15 m/z) at a resolving power of 15 000. The peak area of the modified peptide was normalized with the peak area of its corresponding unmodified peptide. The CEL-modified peptide content in diabetic plasma was expressed as a fold change ratio of the normalized peak area of the CEL-modified peptide of diabetic plasma to the

https://dx.doi.org/10.1021/acsomega.0c01318
ACS Omega 2020, 5, 25016−25028

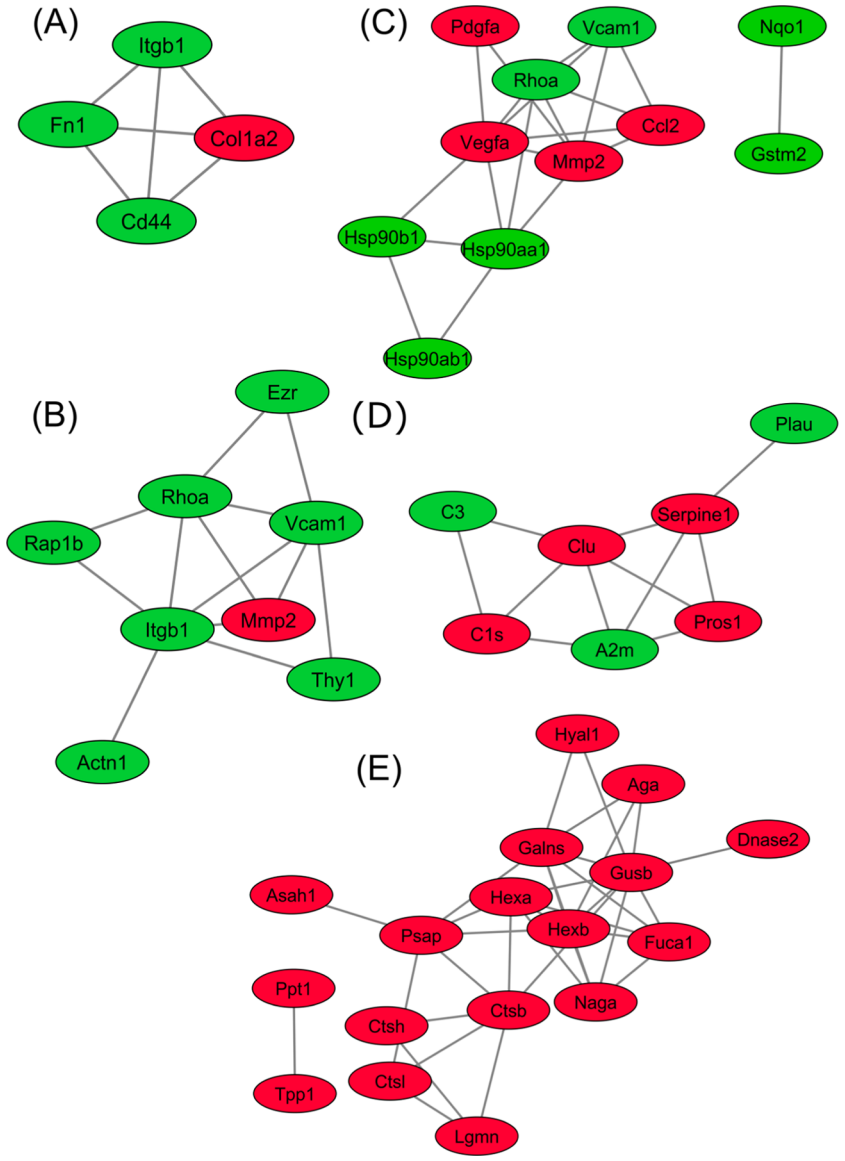

Figure 3. Bioinformatic analysis: PPI network clusters showing differentially abundant proteins involved in (A) ECM−receptor interactions, (B) leukocyte transendothelial migration, (C) fluid shear stress and atherosclerosis, (D) complement and coagulation cascades, and (E) lysosomal pathway; green indicates >1.3-fold higher abundance and red indicates >1.3-fold lesser abundance in MG-treated cells.

normalized peak area of CEL-modified peptide of healthy plasma.

ELISA. The prediluted human plasma samples (20 μL; 1:60) were added to each well, and the volume was made up with 130 μL of distilled water. The plate was covered and incubated for 3 h at room temperature with intermittent agitation on a microplate shaker. The plate was washed thrice with (400 μL per well) wash buffer. After the washes, the excess wash buffer was removed by tapping the plate on an absorbent pad. Then, 100 μL of TMB substrate solution was added to all wells, including the blank wells, and incubated at room temperature for about 10 min. The enzyme reaction was stopped by adding 100 μL of stop solution into each well, and the absorbance of each microwell was recorded at 450 nm. The standard curve of CD44 was plotted in the concentration range of 62.5−4000 pg/mL, and CD44 concentration in the plasma was calculated by elisaanalysis.com online software using the 4-parameter logistic regression algorithm. The box plot of CD44 concentration was plotted for healthy and diabetic subjects using the web app PlotsOfData.[23]

Statistical Analysis. Mass spectrometry acquisition for cell secretome experiments was performed for three individual cell culture experiments in technical triplicates. The clinical plasma proteomic analysis was performed for 10 plasma samples each of healthy control and diabetic subjects in technical triplicates for each sample, and ELISA was performed in duplicates for the same set of plasma samples. Statistical analysis was performed by Student's *t*-test for quantitation of both proteomic data, peptide quantification in clinical plasma and for ELISA, and one way analysis of variance (ANOVA) was performed for the cell viability assay. Data were expressed as mean ± SEM. A p-value ≤ 0.05 was considered as statistically significant. For proteomic analysis, the proteins with more than two matching peptides and fold change difference of $\geq$1.3 in protein expression were considered.

https://dx.doi.org/10.1021/acsomega.0c01318
ACS Omega 2020, 5, 25016−25028

Table 1. Differentially Expressed Secretory Proteins Involved in Insulin Resistance

accession number	gene name	protein name	p-value	fold change	reference
		Upregulated Proteins			
P29534	Vcam1	vascular cell adhesion protein 1	7.13×10^{-7}	10.82	50
P26051	Cd44	CD44 antigen	3.15×10^{-11}	6	48
Q6AYP5	Cadm1	cell adhesion molecule 1	0.00059	5.73	51
P41740	Npr3	atrial natriuretic peptide receptor 3	8.55×10^{-7}	5.06	52
P01946	Hba1	hemoglobin subunit α-1/2	0.0006	4.96	53
Q63691	Cd14	monocyte differentiation antigen CD14	0.00015	3.26	54
P06238	A2m	α-2-macroglobulin	0.00919	3.24	55
Q07936	Anxa2	annexin A2	1.38×10^{-6}	3.19	56
P24090	Ahsg	α-2-HS-glycoprotein	0.04601	2.65	57
P08649	C4	complement C4	0.00393	2.62	58
P0C5H9	Manf	mesencephalic astrocyte-derived neurotrophic factor	0.00685	2.46	59
P18418	Calr	calreticulin	1.45×10^{-6}	2.21	60
P01026	C3	complement C3	0.02878	2.13	61
Q765I2	Uts2b	urotensin-2B	0.04336	2.09	62
P38659	Pdia4	protein disulfide-isomerase A4	0.00165	2.05	63
P05942	S100a4	protein S100-A4	0.00119	1.98	64
P08699	Lgals3	galectin-3	3.99×10^{-5}	1.77	65
P13084	Npm1	nucleophosmin	0.04491	1.69	66
P62963	Pfn1	profilin-1	6.86×10^{-5}	1.45	67
		Downregulated Proteins			
P05371	Clu	clusterin	4.84×10^{-9}	3.48	68
P51886	Lum	lumican	2.68×10^{-5}	3.39	69
Q9WV75	Spon2	spondin-2	1.61×10^{-9}	3.3	70
P53813	Pros	vitamin K-dependent protein S	0.00271	2.99	71
P42930	Hspb1	heat shock protein β-1	4.73×10^{-7}	2.64	72
P16612	Vegfa	vascular endothelial growth factor A	5.86×10^{-5}	2.52	73
Q5RJL6	Metrnl	meteorin-like protein	1.43×10^{-6}	2.47	74
P30121	Timp2	metalloproteinase inhibitor 2	4.21×10^{-10}	2.4	75
P02466	Col1a2	collagen α-2(I) chain	2.4×10^{-5}	2.02	76
P15087	Cpe	carboxypeptidase E	4.05×10^{-5}	1.99	77
P07154	Ctsl	cathepsin L1	4.38×10^{-5}	1.97	78
P24268	Ctsd	cathepsin D	0.00269	1.97	79
Q6P7S1	Asah1	acid ceramidase	0.0174	1.65	80
P48450	Lss	lanosterol synthase	0.03092	1.46	38

RESULTS AND DISCUSSION

Methylglyoxal Does Not Affect Cell Viability up to 3 mM Concentration. Methylglyoxal, a highly reactive dicarbonyl compound, is reported to induce oxidative stress in cells.[6] Therefore, we have evaluated its cytotoxicity on L6 rat skeletal muscle cells. MG concentration above 3 mM reduced the cell viability, as observed by trypan blue staining (Figure S1) and, therefore, 3 mM MG treatment was used for all secretome experiments.

Methylglyoxal-Induced Secretome. Methylglyoxal-induced secretome was tryptically digested, and SWATH-MS analysis was carried out for three individual experiments in technical triplicates for identification and expression analysis. The volcano plot indicates the proteins with differential abundance >1.3-fold and p-value < 0.05 in pink (Figure 2A). The IDA spectral library had 643 proteins (Table S2), and 82 of those were upregulated while 99 were downregulated by more than 1.3-fold in MG-induced secretome in SWATH analysis (Figure 2B). All of the differentially expressed proteins (Table S3) were significant at p-value < 0.05. Secretory proteins from the classical secretory pathway and nonclassical secretory pathway were determined using SignalP and SecretomeP, respectively.[24,25] Of total identified proteins, 180 proteins were identified with SignalP and 113 proteins were identified with SecretomeP (Figure 2C). The KEGG pathway analysis was done using Cytoscape software with plugin clusterMaker.[26] Differentially expressed proteins were found to be involved in various pathways like extracellular matrix (ECM)−receptor interaction (Figure 3A), leukocyte transendothelial migration (Figure 3B), fluid shear stress and atherosclerosis (Figure 3C), complement and coagulation cascades (Figure 3D), and lysosomal pathway (Figure 3E). ECM−receptor interactions are known to contribute to histopathological lesions in diabetic nephropathy. Previously, methylglyoxal was found to inhibit endothelial cell adhesion to type IV collagen of renal glomerular cells, podocytes, and mesangial cells, leading to the development of diabetic nephropathy.[27] In this study, the extracellular matrix (ECM) proteins such as integrin β-1, fibronectin, and CD44 antigen were upregulated in methylglyoxal-induced secretome and may induce insulin resistance. Aberrant regulation of ECM components is observed in obesity associated with insulin resistance.[28] MG-induced upregulation of key proteins such as ezrin, integrin β-1, Ras-related protein Rap-1b, transforming protein RhoA, Thy-1 membrane glycoprotein, and vascular cell adhesion protein 1 and downregulation of 72 kDa type IV collagenase, which are involved in leukocyte transendothelial migration, form an important step in eliciting inflammatory

https://dx.doi.org/10.1021/acsomega.0c01318
ACS Omega 2020, 5, 25016−25028

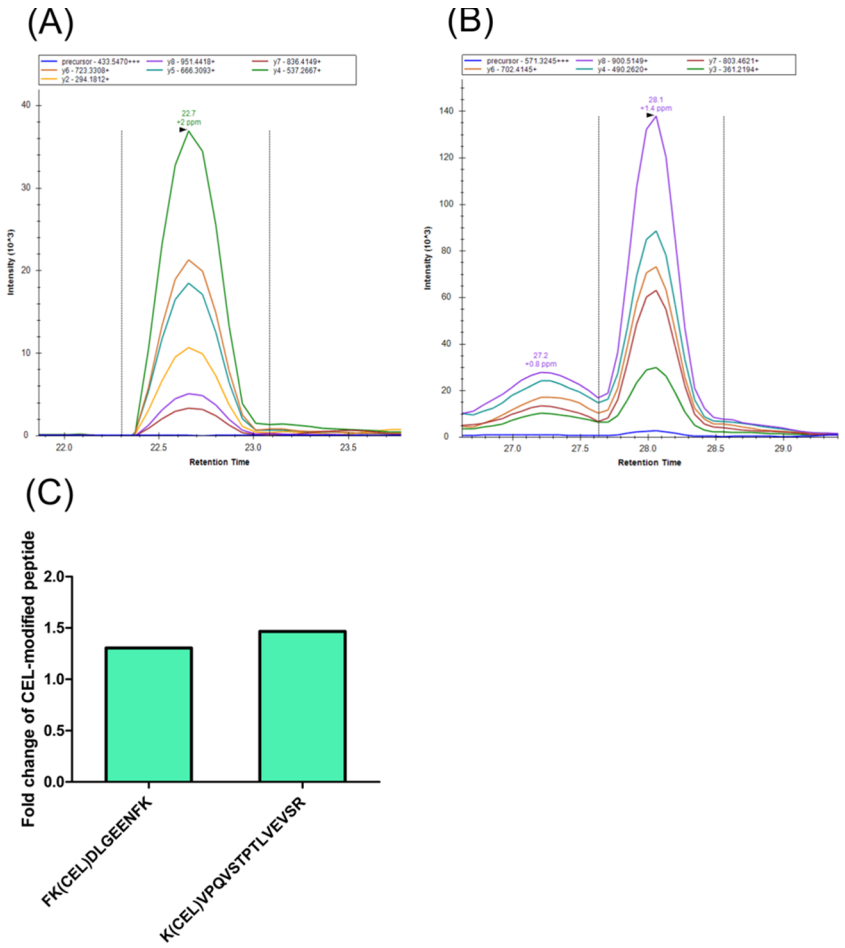

Figure 4. Quantification of CEL-modified peptides. Representative extracted ion chromatograms showing co-elution of *y* fragment ions of CEL-modified peptides (A) FK(*CEL*)DLGEENFK and (B) K(*CEL*)VPQVSTPTLVEVSR of human serum albumin in diabetic plasma. (C) Fold change in expression of CEL-modified albumin peptides FK(*CEL*)DLGEENFK and K(*CEL*)VPQVSTPTLVEVSR in plasma sample of diabetic subjects compared to healthy subjects.

immune response.[29] MT1-MMP-dependent shedding of CD44 plays a key role in regulation of leukocyte adhesion to the pancreatic blood vessels and the transendothelial migration of diabetogenic, cytotoxic T cells into the islet cells.[30] This was also associated with enrichment of proteins involved in complement and coagulation cascades such as complement C3, α-2-macroglobulin, and urokinase-type plasminogen activator that were upregulated and proteins such as complement C1s subcomponent, clusterin, vitamin K-dependent protein S, and plasminogen activator inhibitor 1 were downregulated in MG-induced secretome. A complement and coagulation system has been implicated in the pathogenesis of metabolic disorders, including insulin resistance, non-alcoholic fatty liver disease, and type 2 diabetes.[31] In obesity and type 2 diabetes, adipocytes are actively involved in production of complement components such as C3 factor. Higher levels of serum C3 are correlated with insulin resistance, endothelial dysfunction, and progression of diabetic nephropathy.[32] C3 is also associated with cardiovascular diseases, as it interacts with the coagulation system. Similarly, proteins involved in fluid shear stress and atherosclerosis such as endoplasmin, heat shock protein HSP 90-β, heat shock protein HSP 90-α, transforming protein RhoA, vascular cell adhesion protein 1, NAD(P)H dehydrogenase [quinone] 1, and glutathione S-transferase Mu 2 were upregulated, and proteins such as platelet-derived growth factor subunit A, vascular endothelial growth factor A, 72 kDa type IV collagenase, and C−C motif chemokine 2 were downregulated in response to MG treatment. People with diabetes tend to develop accelerated atherosclerosis.[33] Glycation of extracellular matrix proteins such as glycated collagen alters the endothelial cell function and could contribute to the development of atherosclerotic plaques. In this study, ECM proteins were differentially regulated in response to MG treatment. Proteins such as vascular cell adhesion protein 1 and transforming protein RhoA were upregulated.[34] NAD(P)H dehydrogenase [quinone] 1 and its homologue NADPH oxidase act downstream to the AGE-RAGE axis and are involved in the production of ROS and inflammatory response.[35] Another important pathway that was enriched in the MG-induced secretome was the lysosomal pathway. MG is a highly reactive dicarbonyl responsible for the formation of diverse AGEs, which are implicated in the pathogenesis of diabetes. Cells have evolved combat mechanisms to degrade AGEs via lysosome-mediated autophagy pathways. In a recent study, it has been demonstrated that modulation of lysosome biogenesis leading to autophagy was responsible for the degradation of AGEs in the diabetic kidney. In the case of autophagy-deficient mutant cells, lysosomal biogenesis was not observed, resulting in the accumulation of AGEs in the

https://dx.doi.org/10.1021/acsomega.0c01318
ACS Omega 2020, 5, 25016−25028

Table 2. Details of Precursors and Fragments Used in Quantification

sr. no.	modification site	peptide sequence	charge state	modification	monoisotopic m/z	fragment ion (m/z) used for quantification
1	K36	FKDLGEENFK	+3	unmodified	409.5399	$y2^+$ (294.1812)
						$y4^+$ (537.2667)
						$y5^+$ (666.3093)
						$y6^+$ (723.3308)
						$y7^+$ (836.4149)
						$y8^+$ (951.4418)
2	K36	FKDLGEENFK	+3	CEL	433.547	$y2^+$ (294.1812)
						$y4^+$ (537.2667)
						$y5^+$ (666.3093)
						$y6^+$ (723.3308)
						$y7^+$ (836.4149)
						$y8^+$ (951.4418)
3	K438	KVPQVSTPTLVEVSR	+3	unmodified	547.3174	$y3^+$ (361.2194)
						$y4^+$ (490.262)
						$y6^+$ (702.4145)
						$y7^+$ (803.4621)
						$y8^+$ (900.5149)
4	K438	KVPQVSTPTLVEVSR	+3	CEL	571.3245	$y3^+$ (361.2194)
						$y4^+$ (490.262)
						$y6^+$ (702.4145)
						$y7^+$ (803.4621)
						$y8^+$ (900.5149)

glomeruli and renal vasculature, which was associated with enhanced inflammation and fibrosis.[36] However, MG-induced secretome showed downregulation of various proteins such as *N*(4)-(*β*-*N*-acetylglucosaminyl)-L-asparaginase, acid ceramidase, V-type proton ATPase subunit S1, cathepsin B, cathepsin D, pro-cathepsin H, cathepsin L1, deoxyribonuclease-2-*α*, tissue *α*-L-fucosidase, *N*-acetylgalactosamine-6-sulfatase, *β*-glucuronidase, *β*-hexosaminidase subunit *α*, *β*-hexosaminidase subunit *β*, hyaluronidase-1, legumain, *α*-*N*-acetylgalactosaminidase, palmitoyl-protein thioesterase 1, prosaposin, and tripeptidyl-peptidase 1, which are involved in the lysosomal degradation pathway. The impaired lysosomal degradation system is associated with aging and diabetes. Accumulated AGEs exacerbate diabetes and diabetic complications.[37]

Apart from the above pathways, MG-induced secretome had several proteins related to insulin resistance, obesity, and metabolic syndrome. Table 1 provides information on these important proteins. Proteins such as vascular cell adhesion protein 1, cell adhesion molecule 1, CD44 antigen, atrial natriuretic peptide receptor 3, *α*-2-macroglobulin, monocyte differentiation antigen CD14, annexin A2, complement C3 and C4 proteins, calreticulin, urotensin-2B, protein S100-A4, and galectin-3 were upregulated, and similarly, some of the downregulated proteins included were lanosterol synthase, acid ceramidase, cathepsin D, cathepsin L1, carboxypeptidase E, metalloproteinase inhibitor 2, meteorin-like protein, etc. In our previous study, we have shown that MG downregulates enzymes such as lanosterol synthase involved in cholesterol biosynthesis.[38]

Elevated Levels of Methylglyoxal-Modified Serum Albumin Peptides in Diabetic Plasma. The hyperglycemic condition in diabetes promotes glycation and formation of reactive carbonyls such as glyoxal and methylglyoxal, which can, in turn, modify proteins leading to the formation of carboxyethyllysine (CEL) and argpyrimidines (ARGPYR).[39,40] In severe diabetes, due to elevated levels of MG, it is expected that MG-associated modifications such as CEL and ARGPYR can be observed in plasma proteins. Human serum albumin has been considered as a primary target for glycation due to its abundance, many lysine and arginine residues, and relatively long half-life.[41,42] We, therefore, studied MG-associated modification of HSA, which could reflect elevated levels of MG. A label-free SWATH-MS approach was used for the quantification of MG-modified peptides. The peptides and their fragments that are consistently observed in all of the samples were considered for analysis (Figure 4A,B). The *y* ions were considered for peptide quantification as they were more intense than *b* ions.[43] The sum of the area under the curve (AUC) of selected *y* ions was used for peptide quantification. Two peptides, F**K**DLGEENFK and **K**VPQVSTPTLVEVSR, showed CEL modification of lysine residues, and their intensities were found to be high in diabetic plasma. The peak area of CEL-modified peptides in healthy and diabetic plasma samples was normalized with the peak area of their corresponding unmodified peptide. The increase in CEL modification in diabetes was expressed as fold change over healthy control (Figure 4C). The level of CEL-modified peptide FK(*CEL*)DLGEENFK in diabetic subjects was 1.31-fold higher than in healthy subjects. Similarly, the level of CEL-modified albumin peptide K(*CEL*)VPQVSTPTLVEVSR in diabetic subjects was 1.47-fold higher than in healthy subjects. Details of precursor and fragment ions used for quantification are summarized in Table 2. The retention time of quantified peptides has been shown in Figure S2. Normalized CEL-modified areas for both peptides are shown in Figure S3.

Proteomic Analysis of Clinical Plasma. The usefulness of MG-induced secretome was studied in clinical plasma. Since MG levels increase in diabetes, it is expected that some of the secreted proteins observed in cell culture may also be found in clinical plasma. Therefore, to identify such proteins, SWATH-MS was performed to identify and quantify MG-associated secreted proteins in the plasma. Tryptic digest of clinical plasma was subjected to expression analysis using SWATH-MS workflow. A total of 238 proteins were identified in the spectral

https://dx.doi.org/10.1021/acsomega.0c01318
ACS Omega 2020, 5, 25016−25028

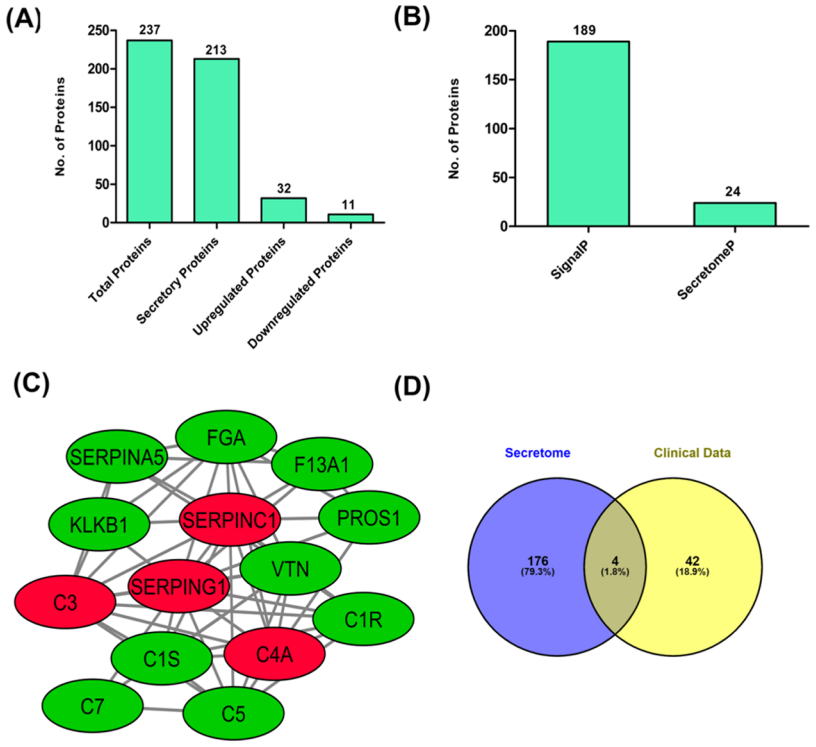

Figure 5. Proteomic analysis for clinical plasma: differential proteomics analysis done by SWATH-MS. (A) Number of differentially expressed proteins in diabetic healthy control. (B) Number of secretory proteins obtained through SignalP and SecretomeP. (C) PPI network cluster showing proteins involved in complement and coagulation cascades; green indicates >1.3-fold higher abundance and red indicates >1.3-fold lesser abundance in diabetic subjects. (D) Venn diagram showing the common proteins in secretome and clinical data.

library obtained from IDA (Table S4), of which 37 proteins were upregulated and 13 proteins were downregulated by more than 1.3-fold (Figure 5A). All of the differentially expressed proteins (Table S5) were significant at p-value < 0.05. Of the total identified proteins, 189 proteins were identified with SignalP and 24 proteins with SecretomeP (Figure 5B). The KEGG pathway analysis was done using Cytoscape software with a plugin clusterMaker. The differentially expressed proteins were found to be involved in pathway complement and coagulation cascades (Figure 5C). Among differentially expressed proteins, upregulated proteins were complement C1r subcomponent, complement C1s subcomponent, vitronectin, complement C5, complement component C7, fibrinogen α chain, coagulation factor XIII A chain, vitamin K-dependent protein S, plasma kallikrein, and plasma serine protease inhibitor, while downregulated proteins included complement C3, antithrombin-III, plasma protease C1 inhibitor, and complement C4-A. Interestingly, two pathways, mainly the complement system and ECM−receptor interaction, were shared between MG-induced secretome and diabetic plasma.

CD44 Antigen Protein Was Found to be Common among Secretome and Clinical Data. To identify MG-induced secreted proteins in the clinical plasma, the differentially expressed proteins from secretome and clinical plasma were analyzed for the presence of common proteins. There was a scarce overlap between MG-induced secretome and plasma proteins since plasma is a heterogeneous matrix that represents proteins secreted from various tissues including muscle cells, liver, adipose, and nervous tissue. Among 189 proteins identified, only four proteins were observed to be common between MG-induced secretome and clinical plasma (Figure 5D); however, only one protein, particularly CD44 antigen protein, showed a common trend in both the groups (Table 3). CD44 antigen protein was found to be upregulated with a 6-fold change in MG-induced secretome and 1.88-fold in diabetic plasma.

Table 3. Common Proteins between Cell Secretome and Clinical Plasma Proteome

sr. no.	protein name	fold change (secretome)	fold change (clinical plasma proteomics)
1	complement C1s subcomponent	3.02 down	2.48 up
2	vitamin K-dependent protein S	2.99 down	2.09 up
3	**CD44 antigen**	**6** up	**1.88** up
4	complement C3	2.13 up	1.71 down

Validation of CD44 Antigen Protein by ELISA in Clinical Subjects. To validate CD44, an MG-induced secreted protein upregulated in diabetes, ELISA was performed in duplicate in the plasma from healthy and diabetic subjects (n = 10 from each group). The CD44 median for healthy and diabetic subjects was 1321 and 1840 pg/mL, respectively (Figure 6A). The fold change was calculated, which showed a similar trend as that of proteomics data, and the protein was found to be 1.6-fold upregulated in diabetic plasma (Figure 6B).

CD44 is a multifunctional cell surface receptor molecule. It interacts with hyaluronan and osteopontin and regulates inflammatory and proinflammatory responses. It exists in several isoforms due to alternate splicing mechanisms.[44] The protein is expressed in several cell types and is involved in various disease conditions, including insulin resistance, obesity,

https://dx.doi.org/10.1021/acsomega.0c01318
ACS Omega 2020, 5, 25016−25028

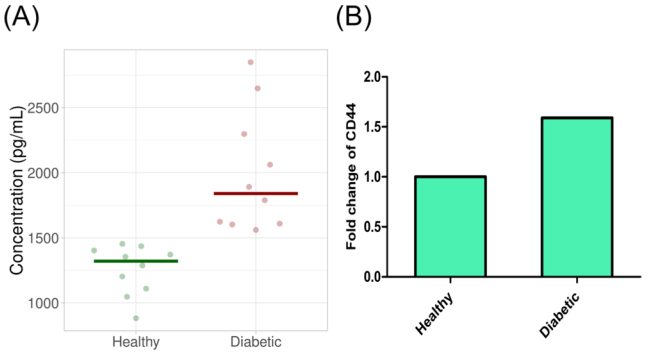

Figure 6. Validation of CD44 antigen protein by ELISA in clinical plasma: (A) Box plot of CD44 concentration plotted for healthy and diabetic subjects (n = 10 each group). The CD44 median for healthy and diabetic subjects was 1321 and 1840 pg/mL, respectively. (B) Fold change bar graph showing higher abundance of CD44 in diabetic subjects (p-value < 0.0002).

metabolic syndrome, diabetes, and cancer.[45−47] The levels of CD44 were found to be significantly increased in insulin-resistance conditions (IR) in a study involving 58 healthy, overweight, and moderately obese white adult participants. The elevated level of the CD44 gene was accompanied with increased expression of OPN, CD68, and IL6.[48] In another study, CD44 protein levels were positively correlated with insulin resistance as measured by HbA_{1c} (n = 55, r = 0.49, p-value < 0.001) and HOMA-IR (n = 55, r = 0.29, p-value < 0.03). Similarly, genome-wide association studies, as well as computational biology studies, involving analysis of microarray data suggested that CD44 plays an important role in the pathogenesis of adipose tissue inflammation and insulin resistance.[49] Further studies are required to develop CD44 as a molecular marker for dysregulated methylglyoxal metabolism.

CONCLUSIONS

This is the first study that describes the secretome of muscle cells in response to methylglyoxal treatment in muscle cells. About 180 proteins were identified to be secretory proteins either with SignalP or SecretomeP. The differentially expressed secretory proteins were involved in various pathways like ECM−receptor interaction, leukocyte transendothelial migration, fluid shear stress and atherosclerosis, complement and coagulation cascades, and lysosomal pathway. To identify the MG-induced secreted proteins in the clinical plasma, the proteins identified in the plasma were compared with the MG-induced secreted proteins in the muscle cells. CD44 was found to be a common protein between MG-induced secretome and clinical plasma proteome. It was found to be upregulated in the diabetic plasma as measured by ELISA and to have a role in the development of insulin resistance. The elevated levels of CD44 were accompanied by an increase in MG-induced CEL modifications of two HSA peptides, FKDLGEENFK and KVPQVSTPTLVEVSR, suggesting that the high levels of CD44 could be associated with an increase in the levels of MG in diabetes.

ASSOCIATED CONTENT

Supporting Information

The Supporting Information is available free of charge at https://pubs.acs.org/doi/10.1021/acsomega.0c01318.

Effect of methylglyoxal (MG) on cell viability (Figure S1), retention time of quantified peptides (Figure S2), normalized CEL-modified peptide area (Figure S3) (PDF)

Clinical characteristics of diabetic and healthy subjects (Table S1); list of identified proteins in cell secretome (Table S2); secretory proteins showing differential abundance in SWATH-MS analysis (cell secretome) (Table S3); list of identified proteins in clinical plasma (Table S4); secretory proteins showing differential abundance in SWATH-MS analysis (clinical plasma) (Table S5) (XLSX)

AUTHOR INFORMATION

Corresponding Author

Mahesh J. Kulkarni − *Proteomics Facility, Biochemical Sciences Division, CSIR-National Chemical Laboratory, Pune 411008, India; Academy of Scientific and Innovative Research (AcSIR), Ghaziabad 201 002, India;* orcid.org/0000-0003-3932-9092; Phone: +912025902541; Email: mj.kulkarni@ncl.res.in

Authors

Shakuntala Bai − *Proteomics Facility, Biochemical Sciences Division, CSIR-National Chemical Laboratory, Pune 411008, India; Academy of Scientific and Innovative Research (AcSIR), Ghaziabad 201 002, India*

Arvindkumar H. Chaurasiya − *Proteomics Facility, Biochemical Sciences Division, CSIR-National Chemical Laboratory, Pune 411008, India; Academy of Scientific and Innovative Research (AcSIR), Ghaziabad 201 002, India*

Reema Banarjee − *Proteomics Facility, Biochemical Sciences Division, CSIR-National Chemical Laboratory, Pune 411008, India*

Prachi B. Walke − *Proteomics Facility, Biochemical Sciences Division, CSIR-National Chemical Laboratory, Pune 411008, India; Academy of Scientific and Innovative Research (AcSIR), Ghaziabad 201 002, India*

Faraz Rashid − *Sciex, Gurugram 122015, Haryana, India*

Ambika G. Unnikrishnan − *Chellaram Diabetes Institute, Pune 411021, India*

Complete contact information is available at: https://pubs.acs.org/10.1021/acsomega.0c01318

Notes

The authors declare no competing financial interest.

ACKNOWLEDGMENTS

S.B., A.H.C., P.B.W., and R.B. thank the University Grants Commission and the Council of Scientific and Industrial Research, India, for research fellowship. This work was supported by CSIR, India.

REFERENCES

(1) Thornalley, P. J. The glyoxalase system in health and disease. *Mol. Aspects Med.* **1993**, *14*, 287−371.

(2) McLellan, A. C.; Thornalley, P. J.; Benn, J.; Sonksen, P. H. Glyoxalase system in clinical diabetes mellitus and correlation with diabetic complications. *Clin. Sci.* **1994**, *87*, 21−29.

(3) Maessen, D. E. M.; Stehouwer, C. D. A.; Schalkwijk, C. G. The role of methylglyoxal and the glyoxalase system in diabetes and other age-related diseases. *Clin. Sci.* **2015**, *128*, 839−861.

(4) Rabbani, N.; Thornalley, P. J. Dicarbonyl proteome and genome damage in metabolic and vascular disease. *Biochem. Soc. Trans.* **2014**, *42*, 425−432.
(5) Jang, J. H.; Kim, E. A.; Park, H. J.; Sung, E. G.; Song, I. H.; Kim, J. Y.; Woo, C. H.; Doh, K. O.; Kim, K. H.; Lee, T. J. Methylglyoxal-induced apoptosis is dependent on the suppression of c-FLIPL expression via down-regulation of p65 in endothelial cells. *J. Cell. Mol. Med.* **2017**, *21*, 2720−2731.
(6) Miyazawa, N.; Abe, M.; Souma, T.; Tanemoto, M.; Abe, T.; Nakayama, M.; Ito, S. Methylglyoxal augments intracellular oxidative stress in human aortic endothelial cells. *Free Radical Res.* **2010**, *44*, 101−107.
(7) Schalkwijk, C. G. Vascular AGE-ing by methylglyoxal: the past, the present and the future. *Diabetologia* **2015**, *58*, 1715−1719.
(8) Yamawaki, H.; Saito, K.; Okada, M.; Hara, Y. Methylglyoxal mediates vascular inflammation via JNK and p38 in human endothelial cells. *Am. J. Physiol. Cell Physiol.* **2008**, *295*, C1510−C1517.
(9) Thornalley, P. J. The glyoxalase system: new developments towards functional characterization of a metabolic pathway fundamental to biological life. *Biochem. J.* **1990**, *269*, 1.
(10) Dhar, A.; Dhar, I.; Desai, K. M.; Wu, L. Methylglyoxal scavengers attenuate endothelial dysfunction induced by methylglyoxal and high concentrations of glucose. *Br. J. Pharmacol.* **2010**, *161*, 1843−1856.
(11) Chang, T.; Wang, R.; Wu, L. Methylglyoxal-induced nitric oxide and peroxynitrite production in vascular smooth muscle cells. *Free Radical Biol. Med.* **2005**, *38*, 286−293.
(12) Thornalley, P. J. Cell activation by glycated proteins. AGE receptors, receptor recognition factors and functional classification of AGEs. *Cell. Mol. Biol.* **1998**, *44*, 1013−1023.
(13) Pavlou, M. P.; Diamandis, E. P. The cancer cell secretome: a good source for discovering biomarkers? *J. Proteomics* **2010**, *73*, 1896−1906.
(14) Lodish, H.; Berk, A.; Zipursky, S. L.; Matsudaira, P.; Baltimore, D.; Darnell, J. *Molecular Cell Biology*, 4th ed.; National Center for Biotechnology Information: Bookshelf, 2000.
(15) Skalnikova, H.; Motlik, J.; Gadher, S. J.; Kovarova, H. Mapping of the secretome of primary isolates of mammalian cells, stem cells and derived cell lines. *Proteomics* **2011**, *11*, 691−708.
(16) Eckardt, K.; Görgens, S. W.; Raschke, S.; Eckel, J. Myokines in insulin resistance and type 2 diabetes. *Diabetologia* **2014**, *57*, 1087−1099.
(17) Norheim, F.; Raastad, T.; Thiede, B.; Rustan, A. C.; Drevon, C. A.; Haugen, F. Proteomic identification of secreted proteins from human skeletal muscle cells and expression in response to strength training. *Am. J. Physiol. Endocrinol. Metab.* **2011**, *301*, E1013−E1021.
(18) Nikolić, N.; Bakke, S. S.; Kase, E. T.; Rudberg, I.; Halle, I. F.; Rustan, A. C.; Thoresen, G. H.; Aas, V. Electrical pulse stimulation of cultured human skeletal muscle cells as an in vitro model of exercise. *PLoS One* **2012**, *7*, No. e33203.
(19) Giacco, F.; Brownlee, M. Oxidative stress and diabetic complications. *Circ. Res.* **2010**, *107*, 1058−1070.
(20) Deshmukh, A. S.; Cox, J.; Jensen, L. J.; Meissner, F.; Mann, M. Secretome analysis of lipid-induced insulin resistance in skeletal muscle cells by a combined experimental and bioinformatics workflow. *J. Proteome Res.* **2015**, *14*, 4885−4895.
(21) Yoon, J. H.; Song, P.; Jang, J.-H.; Kim, D.-K.; Choi, S.; Kim, J.; Ghim, J.; Kim, D.; Park, S.; Lee, H. Proteomic analysis of tumor necrosis factor-alpha (TNF-α)-induced L6 myotube secretome reveals novel TNF-α-dependent myokines in diabetic skeletal muscle. *J. Proteome Res.* **2011**, *10*, 5315−5325.
(22) Ahmad, K.; Shaikh, S.; Lee, E. J.; Lee, Y. H.; Choi, I. Consequences of dicarbonyl stress on skeletal muscle proteins and in Type 2 diabetes. *Curr. Protein Pept. Sci.* **2019**, DOI: 10.2174/1389203720666191119100759.
(23) Postma, M.; Goedhart, J. PlotsOfData—A web app for visualizing data together with their summaries. *PLoS Biol.* **2019**, *17*, No. e3000202.
(24) Armenteros, J. J. A.; Tsirigos, K. D.; Sønderby, C. K.; Petersen, T. N.; Winther, O.; Brunak, S.; von Heijne, G.; Nielsen, H. SignalP 5.0 improves signal peptide predictions using deep neural networks. *Nat. Biotechnol.* **2019**, *37*, 420.
(25) Bendtsen, J. D. v.; Jensen, L. J.; Blom, N.; Von Heijne, G.; Brunak, Sr. Feature-based prediction of non-classical and leaderless protein secretion. *Protein Eng. Des. Sel.* **2004**, *17*, 349−356.
(26) Morris, J. H.; Apeltsin, L.; Newman, A. M.; Baumbach, J.; Wittkop, T.; Su, G.; Bader, G. D.; Ferrin, T. E. clusterMaker: a multi-algorithm clustering plugin for Cytoscape. *BMC Bioinf.* **2011**, *12*, 436.
(27) Pedchenko, V. K.; Chetyrkin, S. V.; Chuang, P.; Ham, A.-J. L.; Saleem, M. A.; Mathieson, P. W.; Hudson, B. G.; Voziyan, P. A. Mechanism of perturbation of integrin-mediated cell-matrix interactions by reactive carbonyl compounds and its implication for pathogenesis of diabetic nephropathy. *Diabetes* **2005**, *54*, 2952−2960.
(28) Lin, D.; Chun, T.-H.; Kang, L. Adipose extracellular matrix remodelling in obesity and insulin resistance. *Biochem. Pharmacol.* **2016**, *119*, 8−16.
(29) Getter, T.; Margalit, R.; Kahremany, S.; Levy, L.; Blum, E.; Khazanov, N.; Keshet-Levy, N. Y.; Tamir, T. Y.; Major, M. B.; Lahav, R. Novel inhibitors of leukocyte transendothelial migration. *Bioorg. Chem.* **2019**, *92*, No. 103250.
(30) Savinov, A. Y.; Strongin, A. Y. Defining the roles of T cell membrane proteinase and CD44 in type 1 diabetes. *IUBMB Life* **2007**, *59*, 6−13.
(31) Phieler, J.; Garcia-Martin, R.; Lambris, J. D.; Chavakis, T. The role of the complement system in metabolic organs and metabolic diseases. *Semin. Immunol.* **2013**, 47−53.
(32) Morinaga, H.; Talukdar, S.; Bae, E. J.; Olefsky, J. M. Increased macrophage migration into adipose tissue in obese mice. *Diabetes* **2012**, *61*, 346−354.
(33) Cantero, A.-V.; Portero-Otín, M.; Ayala, V.; Auge, N.; Sanson, M.; Elbaz, M.; Thiers, J.-C.; Pamplona, R.; Salvayre, R. Nègre-Salvayre, A., Methylglyoxal induces advanced glycation end product (AGEs) formation and dysfunction of PDGF receptor-β: implications for diabetic atherosclerosis. *FASEB J.* **2007**, *21*, 3096−3106.
(34) Kemeny, S. F.; Figueroa, D. S.; Andrews, A. M.; Barbee, K. A.; Clyne, A. M. Glycated collagen alters endothelial cell actin alignment and nitric oxide release in response to fluid shear stress. *J. Biomech.* **2011**, *44*, 1927−1935.
(35) Papadaki, M.; Eskin, S. G.; Ruef, J.; Runge, M. S.; McIntire, L. V. Fluid shear stress as a regulator of gene expression in vascular cells: possible correlations with diabetic abnormalities. *Diabetes Res. Clin. Prac.* **1999**, *45*, 89−99.
(36) Takahashi, A.; Takabatake, Y.; Kimura, T.; Maejima, I.; Namba, T.; Yamamoto, T.; Matsuda, J.; Minami, S.; Kaimori, J.-y.; Matsui, I. Autophagy inhibits the accumulation of advanced glycation end products by promoting lysosomal biogenesis and function in the kidney proximal tubules. *Diabetes* **2017**, *66*, 1359−1372.
(37) Grimm, S.; Horlacher, M.; Catalgol, B.; Hoehn, A.; Reinheckel, T.; Grune, T. Cathepsins D and L reduce the toxicity of advanced glycation end products. *Free Radical Biol. Med.* **2012**, *52*, 1011−1023.
(38) Deshmukh, A. B.; Bai, S.; Aarthy, T.; Kazi, R. S.; Banarjee, R.; Rathore, R.; Vijayakumar, M.; Thulasiram, H.; Bhat, M. K.; Kulkarni, M. Methylglyoxal attenuates insulin signaling and downregulates the enzymes involved in cholesterol biosynthesis. *Mol. BioSyst.* **2017**, *13*, 2338−2349.
(39) Mir, A. R.; Habib, S.; Khan, F.; Alam, K.; Ali, A. Structural changes in histone H2A by methylglyoxal generate highly immunogenic amorphous aggregates with implications in autoimmune response in cancer. *Glycobiology* **2015**, *26*, 129−141.
(40) Ahmed, N.; Battah, S.; Karachalias, N.; Babaei-Jadidi, R.; Horányi, M.; Baróti, K.; Hollan, S.; Thornalley, P. J. Increased formation of methylglyoxal and protein glycation, oxidation and nitrosation in triosephosphate isomerase deficiency. *Biochim. Biophys. Acta, Mol. Basis Dis.* **2003**, *1639*, 121−132.
(41) Bhat, S.; Jagadeeshaprasad, M. G.; Venkatasubramani, V.; Kulkarni, M. J. Abundance matters: role of albumin in diabetes, a proteomics perspective. *Expert Rev. Proteomics* **2017**, *14*, 677−689.

(42) Jagadeeshaprasad, M. G.; Venkatasubramani, V.; Unnikrishnan, A. G.; Kulkarni, M. J. Albumin Abundance and Its Glycation Status Determine Hemoglobin Glycation. *ACS Omega* **2018**, *3*, 12999−13008.
(43) Rathore, R.; Sonwane, B. P.; Jagadeeshaprasad, M. G.; Kahar, S.; Santhakumari, B.; Unnikrishnan, A. G.; Kulkarni, M. J. Glycation of glucose sensitive lysine residues K36, K438 and K549 of albumin is associated with prediabetes. *J. Proteomics* **2019**, *208*, No. 103481.
(44) Nagano, O.; Saya, H. Mechanism and biological significance of CD44 cleavage. *Cancer Sci.* **2004**, *95*, 930−935.
(45) Hasib, A.; Hennayake, C. K.; Bracy, D. P.; Bugler-Lamb, A. e. R.; Lantier, L.; Khan, F.; Ashford, M. L. J.; McCrimmon, R. J.; Wasserman, D. H.; Kang, L. CD44 contributes to hyaluronan-mediated insulin resistance in skeletal muscle of high-fat-fed C57BL/6 mice. *Am. J. Physiol. Endocrinol. Metab.* **2019**, *317*, E973−E983.
(46) Nomiyama, T.; Perez-Tilve, D.; Ogawa, D.; Gizard, F.; Zhao, Y.; Heywood, E. B.; Jones, K. L.; Kawamori, R.; Cassis, L. A.; Tschöp, M. H. Osteopontin mediates obesity-induced adipose tissue macrophage infiltration and insulin resistance in mice. *J. Clin. Invest.* **2007**, *117*, 2877−2888.
(47) Mattheolabakis, G.; Milane, L.; Singh, A.; Amiji, M. M. Hyaluronic acid targeting of CD44 for cancer therapy: from receptor biology to nanomedicine. *J. Drug Targeting* **2015**, *23*, 605−618.
(48) Liu, L. F.; Kodama, K.; Wei, K.; Tolentino, L. L.; Choi, O.; Engleman, E. G.; Butte, A. J.; McLaughlin, T. The receptor CD44 is associated with systemic insulin resistance and proinflammatory macrophages in human adipose tissue. *Diabetologia* **2015**, *58*, 1579−1586.
(49) Kodama, K.; Horikoshi, M.; Toda, K.; Yamada, S.; Hara, K.; Irie, J.; Sirota, M.; Morgan, A. A.; Chen, R.; Ohtsu, H. Expression-based genome-wide association study links the receptor CD44 in adipose tissue with type 2 diabetes. *Proc. Natl. Acad. Sci. U.S.A.* **2012**, *109*, 7049−7054.
(50) Indulekha, K.; Surendar, J.; Mohan, V. High sensitivity C-reactive protein, tumor necrosis factor-α, interleukin-6, and vascular cell adhesion molecule-1 levels in Asian Indians with metabolic syndrome and insulin resistance (CURES-105). *J. Diabetes Sci. Technol.* **2011**, *5*, 982−988.
(51) Wang, T.-T.; Wang, X.-M.; Zhang, X.-L. Circulating Vascular Cell Adhesion Molecule-1 (VCAM-1) and Intercellular Adhesion Molecule-1 (ICAM-1): Relationship with carotid artery elasticity in patients with impaired glucose regulation (IGR). *Ann. Endocrinol.* **2019**, 72−76.
(52) Pivovarova, O.; Gögebakan, Ö.; Klöting, N.; Sparwasser, A.; Weickert, M. O.; Haddad, I.; Nikiforova, V. J.; Bergmann, A.; Kruse, M.; Seltmann, A.-C. Insulin up-regulates natriuretic peptide clearance receptor expression in the subcutaneous fat depot in obese subjects: a missing link between CVD risk and obesity? *J. Clin. Endocrinol.* **2012**, *97*, E731−E739.
(53) Zhang, R.; Barker, L.; Pinchev, D.; Marshall, J.; Rasamoelisolo, M. l.; Smith, C.; Kupchak, P.; Kireeva, I.; Ingratta, L.; Jackowski, G. Mining biomarkers in human sera using proteomic tools. *Proteomics* **2004**, *4*, 244−256.
(54) Lim, P. S.; Chang, Y.-K.; Wu, T.-K. Serum Lipopolysaccharide-Binding Protein is Associated with Chronic Inflammation and Metabolic Syndrome in Hemodialysis Patients. *Blood Purif.* **2019**, *47*, 28−36.
(55) Cura-Esquivel, I.; Cordero-Pérez, P.; Torres-González, L.; Muñoz-Espinosa, L. E. Acute phase markers in obese children and adolescents with metabolic disorders. *Arch. Argent. Pediatr.* **2018**, *116*, 275−282.
(56) Liu, B.; Xu, Y.; Voss, C.; Qiu, F.-h.; Zhao, M.-z.; Liu, Y.-d.; Nie, J.; Wang, Z.-l. Altered protein expression in gestational diabetes mellitus placentas provides insight into insulin resistance and coagulation/fibrinolysis pathways. *PLoS One* **2012**, *7*, No. e44701.
(57) Wang, Y.; Koh, W.-P.; Jensen, M. K.; Yuan, J.-M.; Pan, A. Plasma Fetuin-A Levels and Risk of Type 2 Diabetes Mellitus in A Chinese Population: A Nested Case-Control Study. *Diabetes Metab. J.* **2019**, *43*, No. 474.
(58) Copenhaver, M.; Yu, C.-Y.; Hoffman, R. P. Complement Components, C3 and C4, and the Metabolic Syndrome. *Curr. Diabetes Rev.* **2019**, *15*, 44−48.
(59) Wu, T.; Zhang, F.; Yang, Q.; Zhang, Y.; Liu, Q.; Jiang, W.; Cao, H.; Li, D.; Xie, S.; Tong, N. Circulating mesencephalic astrocyte-derived neurotrophic factor is increased in newly diagnosed prediabetic and diabetic patients, and is associated with insulin resistance. *Endocr. J.* **2017**, EJ16−0472.
(60) Srinivasan, V.; Tatu, U.; Mohan, V.; Balasubramanyam, M. Molecular convergence of hexosamine biosynthetic pathway and ER stress leading to insulin resistance in L6 skeletal muscle cells. *Mol. Cell. Biochem.* **2009**, *328*, 217−224.
(61) Xin, Y.; Hertle, E.; van der Kallen, C. J. H.; Schalkwijk, C. G.; Stehouwer, C. D. A.; van Greevenbroek, M. M. J. Complement C3 and C4, but not their regulators or activated products, are associated with incident metabolic syndrome: the CODAM study. *Endocrine* **2018**, *62*, 617−627.
(62) Calan, M.; Arkan, T.; Kume, T.; Bayraktar, Fr. The relationship between urotensin II and insulin resistance in women with gestational diabetes mellitus. *Hormones* **2019**, *18*, 91−97.
(63) Chien, C.-Y.; Hung, Y.-J.; Shieh, Y.-S.; Hsieh, C.-H.; Lu, C.-H.; Lin, F.-H.; Su, S.-C.; Lee, C.-H. A novel potential biomarker for metabolic syndrome in Chinese adults: Circulating protein disulfide isomerase family A, member 4. *PLoS One* **2017**, *12*, No. e0179963.
(64) Arner, P.; Petrus, P.; Esteve, D.; Boulomié, A.; Näslund, E.; Thorell, A.; Gao, H.; Dahlman, I.; Rydén, M. Screening of potential adipokines identifies S100A4 as a marker of pernicious adipose tissue and insulin resistance. *Int. J. Obes.* **2018**, *42*, 2047.
(65) Atalar, M. N.; Abuşoğlu, S.; Ünlü, A.; Tok, O.; İpekçi, S. H.; Baldane, S.; Kebapcılar, L. Assessment of serum galectin-3, methylated arginine and Hs-CRP levels in type 2 diabetes and prediabetes. *Life Sci.* **2019**, *231*, No. 116577.
(66) Wang, X.; Ma, H.; Wang, X. Nucleophosmin/B23 contributes to hepatic insulin resistance through the modulation of NF-κB pathway. *Biochem. Biophys. Res. Commun.* **2019**, *511*, 214−220.
(67) Romeo, G. R.; Pae, M.; Eberlé, D.; Lee, J.; Shoelson, S. E. Profilin-1 haploinsufficiency protects against obesity-associated glucose intolerance and preserves adipose tissue immune homeostasis. *Diabetes* **2013**, *62*, 3718−3726.
(68) Hoofnagle, A. N.; Wu, M.; Gosmanova, A. K.; Becker, J. O.; Wijsman, E. M.; Brunzell, J. D.; Kahn, S. E.; Knopp, R. H.; Lyons, T. J.; Heinecke, J. W. Low clusterin levels in high-density lipoprotein associate with insulin resistance, obesity, and dyslipoproteinemia. *Arterioscler., Thromb., Vasc. Biol.* **2010**, *30*, 2528−2534.
(69) Wolff, G.; Taranko, A. E.; Meln, I.; Weinmann, J.; Sijmonsma, T.; Lerch, S.; Heide, D.; Billeter, A. T.; Tews, D.; Krunic, D. Diet-dependent function of the extracellular matrix proteoglycan Lumican in obesity and glucose homeostasis. *Mol. Metab.* **2019**, *19*, 97−106.
(70) Zhu, L.-H.; Wang, A.; Luo, P.; Wang, X.; Jiang, D.-S.; Deng, W.; Zhang, X.; Wang, T.; Liu, Y.; Gao, L. Mindin/Spondin 2 inhibits hepatic steatosis, insulin resistance, and obesity via interaction with peroxisome proliferator-activated receptor α in mice. *J. Hepatol.* **2014**, *60*, 1046−1054.
(71) Yasuma, T.; Yano, Y.; D'Alessandro-Gabazza, C. N.; Toda, M.; Gil-Bernabe, P.; Kobayashi, T.; Nishihama, K.; Hinneh, J. A.; Mifuji-Moroka, R.; Roeen, Z. Amelioration of diabetes by protein S. *Diabetes* **2016**, *65*, 1940−1951.
(72) Yuan, H.; Wang, T.; Niu, Y.; Liu, X.; Fu, L. AMP-activated protein kinase-mediated expression of heat shock protein beta 1 enhanced insulin sensitivity in the skeletal muscle. *FEBS Lett.* **2017**, *591*, 97−108.
(73) Wagner, H.; Fischer, H.; Degerblad, M.; Alvarsson, M.; Gustafsson, T. Improvement of insulin sensitivity in response to exercise training in type 2 diabetes mellitus is associated with vascular endothelial growth factor A expression. *Diabetes Vasc. Dis. Res.* **2016**, *13*, 361−366.
(74) Jung, T. W.; Lee, S. H.; Kim, H.-C.; Bang, J. S.; El-Aty, A. M. A.; Hacımüftüoğlu, A.; Shin, Y. K.; Jeong, J. H. METRNL attenuates lipid-induced inflammation and insulin resistance via AMPK or

https://dx.doi.org/10.1021/acsomega.0c01318
ACS Omega 2020, 5, 25016−25028

PPARδ-dependent pathways in skeletal muscle of mice. *Exp. Mol. Med.* **2018**, *50*, 122.
(75) Nagareddy, P. R.; Rajput, P. S.; Vasudevan, H.; McClure, B.; Kumar, U.; Macleod, K. M.; McNeill, J. H. Inhibition of matrix metalloproteinase-2 improves endothelial function and prevents hypertension in insulin-resistant rats. *Br. J. Pharmacol.* **2012**, *165*, 705−715.
(76) Kang, L.; Ayala, J. E.; Lee-Young, R. S.; Zhang, Z.; James, F. D.; Neufer, P. D.; Pozzi, A.; Zutter, M. M.; Wasserman, D. H. Diet-induced muscle insulin resistance is associated with extracellular matrix remodeling and interaction with integrin $\alpha 2\beta 1$ in mice. *Diabetes* **2011**, *60*, 416−426.
(77) Liew, C. W.; Assmann, A.; Templin, A. T.; Raum, J. C.; Lipson, K. L.; Rajan, S.; Qiang, G.; Hu, J.; Kawamori, D.; Lindberg, I. Insulin regulates carboxypeptidase E by modulating translation initiation scaffolding protein eIF4G1 in pancreatic β cells. *Proc. Natl. Acad. Sci. U.S.A.* **2014**, *111*, E2319−E2328.
(78) Huang, X.; Vaag, A.; Carlsson, E.; Hansson, M.; Ahrén, B.; Groop, L. Impaired cathepsin L gene expression in skeletal muscle is associated with type 2 diabetes. *Diabetes* **2003**, *52*, 2411−2418.
(79) Liu, L.; Chen, B.; Zhang, X.; Tan, L.; Wang, D. W. Increased cathepsin D correlates with clinical parameters in newly diagnosed type 2 diabetes. *Dis. Markers* **2017**, *2017*, No. 5286408.
(80) Chavez, J. A.; Holland, W. L.; Bär, J.; Sandhoff, K.; Summers, S. A. Acid ceramidase overexpression prevents the inhibitory effects of saturated fatty acids on insulin signaling. *J. Biol. Chem.* **2005**, *280*, 20148−20153.

https://dx.doi.org/10.1021/acsomega.0c01318
ACS Omega 2020, 5, 25016−25028